Development of an advanced passive solar still with separate condenser

A thesis submitted in fulfilment of the requirements for the degree of Doctor of Philosophy in Mechanical Engineering

Amos Madhlopa

Energy Systems Research Unit
Department of Mechanical Engineering
University of Strathclyde
Glasgow
United Kingdom

2009

Copyright declaration

Acknowledgements

The present work was made possible through support from many people. I acknowledge the contribution from everyone. In particular, I would like to thank Cameron Johnstone for his proper supervision and guidance, and for reading and correcting all the manuscripts.

I am very grateful to the Commonwealth Scholarship Commission and the British Council for the financial support. The centre for WASHTED at the Malawi Polytechnic, and Universities of Strathclyde and Malawi are also acknowledged for the various forms of support. My sincere gratitude is also conveyed to the Department of Meteorological Services in Malawi for allowing me to use their Stevenson screen, and Kipp & Zonen pyranometer and shadow ring during data collection at the Malawi Polytechnic.

Special thanks go to my wife and daughters for their love, care and moral support. I also acknowledge my father, mother, elder brother and sisters for their support during my academic progression. All friends and relatives are thanked for their contribution to this work.

Table of contents

List of acronyms

AFNOR	Association Française de Normalisation
ANSI	American National Standards Institute
ASHRAE	American Society of Heating, Refrigerating and Air-Conditioning Engineers
ASME	American Society of Mechanical Engineers
ASS	Advanced solar still
ASTM	American Society for Testing and Materials
BSI	British Standards Institution
CEN	Comité Européen de Normalisation
CSS	conventional solar still
EC	electric conductivity
ED	electrodialysis
EPMG2	European Modelling Group 2
EU	European Union
GHG	Greenhouse gas
IAPWS	International Association for the Properties of Water and Steam
IPCC	Intergovernmental Panel on Climate Change
ISO	International Organization for Standardization
MED	multi-effect distillate
MK	Malawi Kwacha (local currency in Malawi)
MSF	multi-stage flash
NF	nanofiltration
RBD	randomized block design
RO	reverse osmosis
TDS	total dissolved solids
TRNSYS	Transient Simulation Program
UK	United Kingdom
UN	United Nations

UNEP	United Nations Environment Programme
VCD	vapour compression distillation
WASHTED	Water, Sanitation, Health and Technology Development
WHO	World Health Organization
WRC	World Radiation Centre
WMO	World Meteorological Organization

Nomenclature

A	area (m^2)
A_{ec}	area across the entrance from the evaporator to condenser chamber (m^2)
A′	projected area (m^2)
AR	aspect ratio (dimensionless)
b	parameter in Eqs.(2.44), (2.47) and (2.48), (dimensionless)
B	breadth (m)
Bi	Biot number (dimensionless)
C_p	specific heat capacity at constant pressure ($J\ kg^{-1}\ K^{-1}$)
d	parameter in Eqs.(2.44), (2.47) and (2.48), (dimensionless)
D	coefficient of diffusion mass transfer ($m^2\ s^{-1}$)
e	parameter in Eq.(2.48), (dimensionless)
E	equation of time (hour)
É	emissive power ($W\ m^{-2}$)
g	acceleration due to gravity ($m\ s^{-2}$)
F	solar radiation absorption factor (dimensionless)
G	irradiance (Wm^{-2})
Gr	Grashof number (dimensionless)
h	coefficient of heat transfer ($W\ m^{-2}\ K^{-1}$)
H	daily insolation (Jm^{-2})
Ĥ	mean monthly daily insolation (Jm^{-2})
I	hourly insolation (Jm^{-2})
K	coefficient of extinction (m^{-1})
k	thermal conductivity ($W\ m^{-1}\ K^{-1}$)
L	length (m)
L'	specific latent heat of vaporization ($J\ kg^{-1}$)
$\dot{L}$	factor level (dimensionless)
m	mass (kg)
M	molecular mass (kg/kmole)

$\dot{m}$	rate of vapour diffusion/flow (kg s^{-1})
$\dot{m}'$	mass flux (kg m^{-2} s^{-1})
n	refractive index (dimensionless)
N	day of a year (with N=1 on 1 January)
N'	number of experimental runs (dimensionless)
Nu	Nusselt number (dimensionless)
P	pressure (Nm^{-2})
Pr	Prandtl number (dimensionless)
q	heat flux (W m^{-2})
$\dot{q}$	heat source (W m^{-3})
$\vec{q}$	heat flux with direction and magnitude (W m^{-2})
Q	power or rate of energy flow (W)
r_n	reflectance of the perpendicular component of unpolarized light (dimensionless)
r_{pr}	reflectance of the parallel component of unpolarized light (dimensionless)
r^2	coefficient of determination (dimensionless)
R	thermal resistance (K W^{-1})
$\dot{R}$	ratio of evaporator to condenser chamber volume (dimensionless)
Ra	Rayleigh number (dimensionless)
R_{ai}	air gas constant (J $kg^{-1}K^{-1}$)
R_v	vapour gas constant (J $kg^{-1}K^{-1}$)
S	characteristic length or equivalent spacing (m)
S_o	extraterrestrial duration of sunshine (hour)
$\hat{S}$	mean monthly daily duration of sunshine (hour)
t	time (s)
t_{ct}	civil time (hour)
t_{dy}	daylight saving time (hour)
t_s	solar time (hour)
t_{sn}	solar noon time (hour)
T	temperature (K)
U	coefficient of heat loss (W m^{-2} K^{-1})

V	velocity (m s^{-1})
V'	volume (m^3)
W	view factor (dimensionless)
x	distance/thickness (m)
x_{ec}	gap crossed by water vapour from evaporator to condenser (m)
Y	distillate yield (kg m^{-2})
y	distance (m)
$\hat{Y}$	mean daily distillate yield (kg m^{-2})
z	distance (m)
Z	height (m)

Greek symbols

α	absorptance
α'	thermal diffusivity (m^2 s^{-1})
β	angle of inclination to the horizontal plane (degree)
β'	coefficient of thermal expansivity (K^{-1})
ε	emittance (dimensionless)
ϕ	latitude (degree)
Φ	relative humidity (dimensionless)
Γ	angle defined in Eqs.(2.3) and (2.12), (degree)
γ	azimuth angle (degree)
Δ	change in
∇^2	Laplacian (a scalar differential operator)
η	efficiency (dimensionless, %)
μ	dynamic viscosity (kg m^{-1} s^{-1})
θ	angle of incidence (degree)
Θ	longitude of a site (degree)
Θ_{sd}	standard longitude (degree)
λ	wavelength (m)

ρ	reflectance (dimensionless)
τ	transmittance (dimensionless)
φ	density (kg m^{-3})
σ	Stefan-Boltzman constant (W m^{-2} K^{-4})
ν	kinematic viscosity (m^2 s^{-1})
ω	hour angle (degree)
ψ	solar altitude (degree)

Subscripts

1	initial/first
2	final/second
3	third
a	air/ambient
b	beam
bb	black body
bo	bottom
bh	beam on horizontal surface
bp	beam on tilted plane
bw	back wall of evaporator chamber
c	convective
cc	condenser chamber
cd	conduction
co	condensing cover
cs	condensing surface (glass cover, basin liner 2 and condensing cover)
d	diffuse
dd	daily distillate
df	diffusion
di	directly received/intercepted
dh	diffuse on horizontal surface

dp	diffuse on tilted plane
ds	distillation/desalination
dw	distilled water
dy	day light saving
e	evaporative/evaporation
ec	evaporator chamber
ef	effective
er	external reflector
es	external source
ew	east wall
fc	front surface of condenser
fw	front wall of evaporator chamber
g	global or total
gc	glass cover
gh	global on horizontal surface
gr	ground
gp	global on tilted plane
ig	internally generated
in	indirectly receive/intercepted
iw	inner surface of the walls of the evaporator
i-j	from the i^{th} to the j^{th} surface
lo	local
n	normal/perpendicular
o	extraterrestrial
ov	overall
p	plane/inclined plane
pr	parallel
ps	polystyrene
pu	purging
pw	plywood

r	radiative
rt	ground-reflected radiation on a tilted surface
s	solar/sun
sc	solar constant
sk	sky
sr	surface
ss	sunset
st	still
sw	side wall
sl	side wall around basin 1
s2	side wall around basin 2
s3	side wall around basin 3
td	temperature difference between i^{th} and (i+1) iteration
to	total
u	upper layer
v	vapour
vc	vapour in condenser chamber
ve	vapour in evaporator chamber
w	water
wa	wall
wd	wind
wl	water in basin 1
ws	water surface
ww	west wall
z	zenith
λ	monochromatic radiation

Abstract

Clean water is essential for socio-economic development. Nevertheless, there is limited access to water that meets standard limits of water quality, especially in the African region. The quality of water can be improved through desalination. Conventional techniques for desalination are available but they require a large input of energy, mostly from fossil fuels that contribute to environmental degradation. Consequently, there is need to use sustainable energy sources, with solar energy being one of the most promising alternatives.

A conventional solar still (CSS) is widely exploited but it has low efficiency. Thus, numerous modelling and design attempts have been made to improve its performance. For modelling, it is necessary to know the distribution of solar radiation inside the still. However, previous models excluded view factors of surfaces exchanging radiation. These models would therefore have limited accuracy. For still design, different modifications that included the use of a reflector and external condenser were proposed hitherto but the external condenser was not shielded against solar radiation. Consequently, the condenser unit would be relatively hot, thereby curtailing distillate yield. The objective of this investigation was to overcome these limitations.

A new model that incorporates view factors and calculates the distribution of solar radiation in a single-slope solar still has been developed. This model was applied to a CSS and an advanced solar still (ASS) with a separate condenser. Numerical results were then used to design and fabricate prototype stills which were tested outdoors at the University of Strathclyde and the Malawi Polytechnic. It is found that the new model is more accurate than the previous models at both test sites. It appears therefore that the proposed model can be applied universally. Empirically, the solar shield was effective in keeping the condenser unit relatively cool and the ASS produced more distilled water than the CSS.

Chapter 1

Introduction

1.0 Water, environment and economy

Clean water is essential for good health which influences the social and economic development of any nation. People who use contaminated water are prone to waterborne diseases (WHO, 2006), and they cannot effectively engage themselves in economic activities. Moreover, financial resources that could have been allocated to developmental projects are channelled to disease-curing efforts. Consequently, ill health contributes to the retardation of economic growth.

However, there is limited access to drinking water that meets acceptable standard levels of biological, chemical and physical constituents. Over 97 % of water available on the earth's surface is salty (Tiwari et al., 2003), and environmental pollution caused predominantly by anthropogenic activities is also contributing to the degradation of fresh water resources. The WHO (2008) reported that 78 % and 96 % of the rural and urban populations used clean drinking water in 2006 on a global scale respectively. So, 4 billion cases of diarrhoea are reported annually, with 88 % of them being ascribed to the use of unclean water, and insufficient sanitation and hygiene (WHO, 2007). This indicates the need for interventions that aim at providing clean water. In view of this, the millennium development goals incorporate a target to halve the percentage of the population without access to safe water by 2015 (UN, 2007). Indeed, this goal can be achieved through a multi-faceted approach which includes the development of appropriate technologies for water desalination. Nevertheless, a sustainable source of energy is required to provide fresh water to a larger proportion of the world population.

Recently, there have been concerns about environmental degradation arising predominantly from the exploitation of non-renewable energy resources. Anthropogenic activities are generating greenhouse gasses (GHG) that account for most of the ambient air temperature rise (Saikku et al., 2008). In particular, the burning of fossil fuels is significantly contributing to climate change through the emission of carbon dioxide (major GHG) and other substances (UNEP, 1988; IPCC, 1995; UN, 2007). Parry et al. (2008) reported that the impacts of climate change are currently observable. Consequently, application of renewable energy technologies in the provision of fresh water can assist in alleviating environmental degradation.

1.1 Water desalination

Conventional techniques for desalting water can broadly be classified into thermal and membrane based categories (Fritzmann et al., 2007). The former class of techniques includes multi-stage flash (MSF), multi-effect distillation (MED) and vapour compression distillation (VCD) while the latter class comprises reverse osmosis (RO), nanofiltration (NF) and electrodialysis (ED). In thermal desalination, salts are removed from water by evaporation-condensation processes. Membrane based techniques employ a membrane through which water diffuses with a high proportion of the salts being retained. However, these techniques require a large input of energy and are not cost-effective for low demands of clean water (Mowla and Karimi, 1995). According to Bouchekima et al. (1998), improvements in solar distillation technology makes it ideal for desalinating water in remote areas with water demands below 50 m^3 per day. Nevertheless, there is still need to increase the productivity of solar stills at an affordable cost especially in developing parts of the world.

UN (2008) reported that regions with developing economies were: a) Africa, b) Asia and Pacific (excluding Australia, Japan, New Zealand, and the member states of the Commonwealth Independent States in Asia) and c) Latin America. Amongst these regional groupings, access to clean water was most limited in the African region (46 % in rural areas and 82 % in urban areas in 2006), (WHO, 2008). Moreover, many African countries receive relatively high levels of solar radiation (Diabaté et al., 2004). Thus, solar distillation can be a potential method of providing fresh water in the region.

One of the developing African countries with limited access to clean water is Malawi. So, it is used as a representative of the developing parts of the world where solar desalination systems can possibly be exploited to improve the quality of water. In this country, the major sources of water in remote areas are shallow wells, boreholes, gravity-fed piped systems, springs, rivers and lakes. However, these water sources are threatened by depletion and degradation mainly due to population increase, improper disposal of wastes and poor agricultural practices (Mumba et al., 1999; Lakudzala et al., 1999). Pritchard et al. (2007) studied 21 protected and 5 unprotected shallow wells during four different times of the year. They found that drinking water was significantly polluted with faecal waste. Over 50 % of 176 boreholes studied by Msonda et al. (2007) had fluoride concentrations exceeding the limit of 1.5×10^{-6} kg/ litre set by the WHO. Several other authors have reported on the low quality of drinking water, especially in rural areas of Malawi. The WHO (2008) reported that 72 % and 96 % of the population in rural and urban areas respectively have access to improved drinking water sources. So, there is need to find sustainable ways of improving the quality of water, especially in remote areas.

Fuel wood is the major source of energy in Malawi. Unfortunately, the heavy and inefficient consumption of fuel wood is contributing to deforestation and other environmental problems (Hyde and Seve, 1993). Moreover, grid electricity is not available in most rural areas of the country. Consequently, a sustainable source of energy is needed to produce clean water in such areas. It appears that solar energy is a potential source of energy for powering thermal and photovoltaic systems because the country has a suitable solar climate for exploiting solar technologies (Diabaté et al., 2004; Madhlopa, 2006a).

In Malawi, distilled water is mostly produced by using electrical heaters, and it is generally used in industries and laboratories where water of analytical grade is required. In addition, distilled water is needed in rechargeable accumulators for automobiles and electronic appliances that are used even in rural areas. Nevertheless, this commodity is hardly found in such areas of the country. One potential technique for providing clean water to communities in these areas is to use solar energy. Nevertheless, very limited work has been done on solar distillation in Malawi. Madhlopa (2006b) studied the diurnal performance of a single-slope conventional solar still under outdoor weather conditions in Malawi. Distillate data was captured over a period of 32400 s, with symmetry at solar noon (starting from 16200 s before local solar noon) on each test day (Chang et al., 2002). It was found that the solar distillation system produced 0.820 to 3.454 kg m^{-2} during the daily test period, depending on the prevailing weather conditions. Madhlopa and Johnstone (2008) used solar radiation data captured at 19 different weather sites (spread all over Malawi) to estimate mean monthly daily yield of distilled water from a conventional solar still. They found that there was great potential for solar desalination in the country. So, there is need to do more work in the field of solar distillation, especially in modelling, designing, construction and evaluation of solar stills.

1.2 Research objectives

A conventional solar still (CSS) has a thin layer of water in a horizontal basin, transparent cover over the water with one or two slopes (Fig.1.1). Saline water in the basin is heated by solar radiation passing through the transparent cover and absorbed by the water and bottom part of the still basin. Vapour flows upwards from the hot water and condenses when it comes into contact with the cooler inner surface of the transparent cover. The evaporation and condensation processes take place within the same chamber in a conventional solar still. The condensate (clean water) is collected in a channel fitted along the lower edge of the transparent cover. For a given set of design parameters, the productivity of the system is influenced by climatic and operational factors, and a single-slope solar still intercepts a higher proportion of solar radiation than a double-sloped solar still at both low and high latitude locations (Garg and Mann, 1976). These findings are consistent with the fact that the back wall of a single-slope solar still is significantly higher than the front wall. So, it reflects part of the incoming solar radiation onto the surface of water, which augments the amount of solar energy for driving the evaporation process in a single-slope solar still. Thus, the back wall of this variety of solar stills acts as an internal reflector. In contrast, the back wall of a double-slope solar still is practically short and therefore, it reflects a negligible amount of solar radiation onto the surface of saline water. In view of this, the present investigation focused on solar stills with one slope.

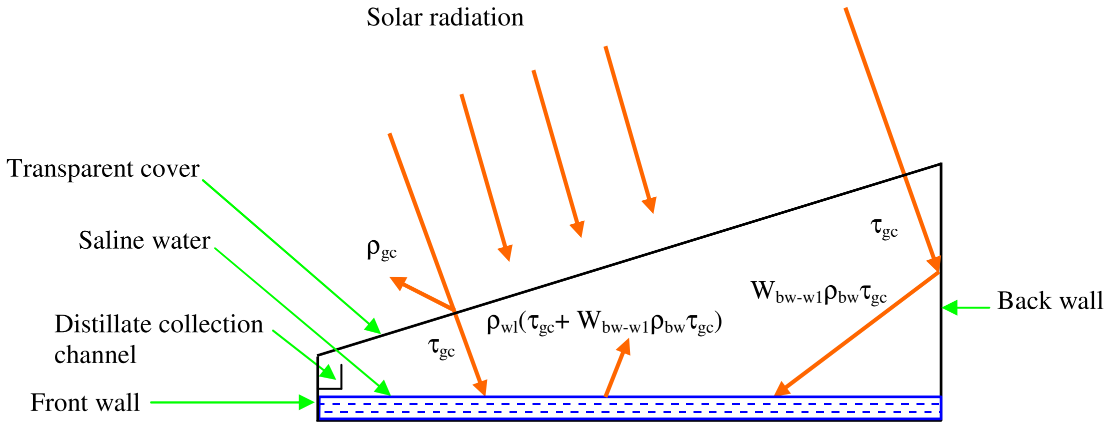

(a)

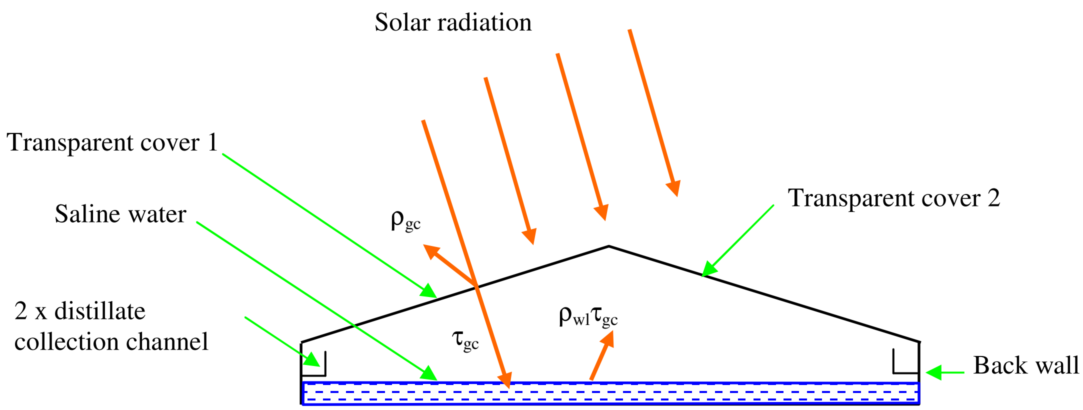

(b)

Fig.1.1: Cross-section of a basic solar still with a) single slope and b) double slope.

The rates of water evaporation and condensation increase with the difference between the temperatures of saline water and transparent cover. Nevertheless, the transparent cover absorbs part of the incoming solar radiation and it also receives heat from the hot saline water (through convection, condensation and radiation). Consequently, the temperature of the transparent cover is elevated which reduces the rate of distillate production. In view of this drawback, various researchers have sought to improve the performance of a CSS through modelling and experimental studies. It should be mentioned that the advantages of solar system modelling include economic and time factors (Duffie and Beckman, 2006). For instance, the sensitivity of the output variable to changes in the input parameters can quickly be established before conducting costly experiments.

Incoming solar radiation is the most important meteorological input variable in solar distillation (Nafey et al., 2000). It comprises beam and diffuse components that have different optical properties when incident on a surface (Reindl et al., 1990; Foster et al., 2009). Beam radiation travels directly from the sun's disc to a receiver surface, and its rays can be traced from the sun's position and used in determining the solar altitude and azimuth angles. These angles influence the amount of beam radiation directly reaching a given surface. In contrast, diffuse radiation comes from the whole sky vault and its rays are not traceable from the sun's position. In addition, the amount of diffuse solar energy directly received by a given surface depends on the proportion of the sky viewed by the surface (Dave, 1977; Markvart., 1994). Further, solar radiation reflected from a reflector to a receiver is influenced by both the reflectance and view factor of the reflector relative to the receiver (Jansen, 1985). However, previous models on the distribution of solar radiation inside a solar still ignored view factors, and so, their accuracy would be limited (Cooper, 1973; Tanaka and Nakatake, 2006, 2007; Tiwari and Tiwari, 2007; Tripathi and Tiwari, 2004, 2006). As for solar still design, improvements have included the use of a) reflectors to increase the intensity of solar radiation falling on the surface of saline water in the evaporator basin, and b) separate condenser to keep the condensing surface relatively cool and therefore augment the rate of evaporation-condensation. Nevertheless, the separate condenser used in previous work was not shielded from solar radiation (Fath and Elsherbiny, 1993; El-Bahi and Inan, 1999a, b; Fath and Hosny, 2002). A bare condenser would absorb part of the incoming solar radiation, thereby raising its temperature and curtailing distillate productivity. The aim of the present investigation was therefore to develop an advanced solar still with shielded separate condenser and higher efficiency than a conventional solar still. This design would assist in increasing the availability of clean water in remote and isolated areas. To achieve this goal, the following specific objectives of the research were set out: a) to model the performance of conventional and advanced solar stills, b) to design, construct and test prototype solar stills, and c) to verify the accuracy of the proposed model for predicting the performance of the solar stills.

1.3 Research procedure

Initially, a conceptual ASS with separate evaporator and condenser units was developed and modelled. The ASS comprised separate evaporator and condenser chambers (Fig.1.2). One basin of saline water (first effect) was fitted in the evaporator chamber. The condenser chamber housed basin 2 with saline water (second effect) and basin 3 with saline water (third effect) with a metallic condensing cover over the third effect and an opaque insulation shield over the condensing cover. Basins 2 and 3 were stepped to minimise thermal inertia. The performance of the ASS was theoretically evaluated and compared with that of a CSS under the same meteorological conditions. Irradiance, ambient air temperature and wind speed were the input meteorological variables to the model. Further, the model was calibrated and the sensitivity of distillate production to changes in the design and operational parameters of the ASS was determined. It was found that distillate productivity of the ASS was higher than that of the CSS, and the productivity of the ASS was most sensitive to the absorptance of basin liner 1, ratio of the volume of the evaporator to that of the condenser unit, mass of water in basins 1 and 2, and the coefficient of heat loss from the bottom of the still. These results were employed to design and construct prototype solar stills for experimentation. The geometry of the CSS was the same as that of the evaporator unit of the ASS for meaningful comparison of the two systems.

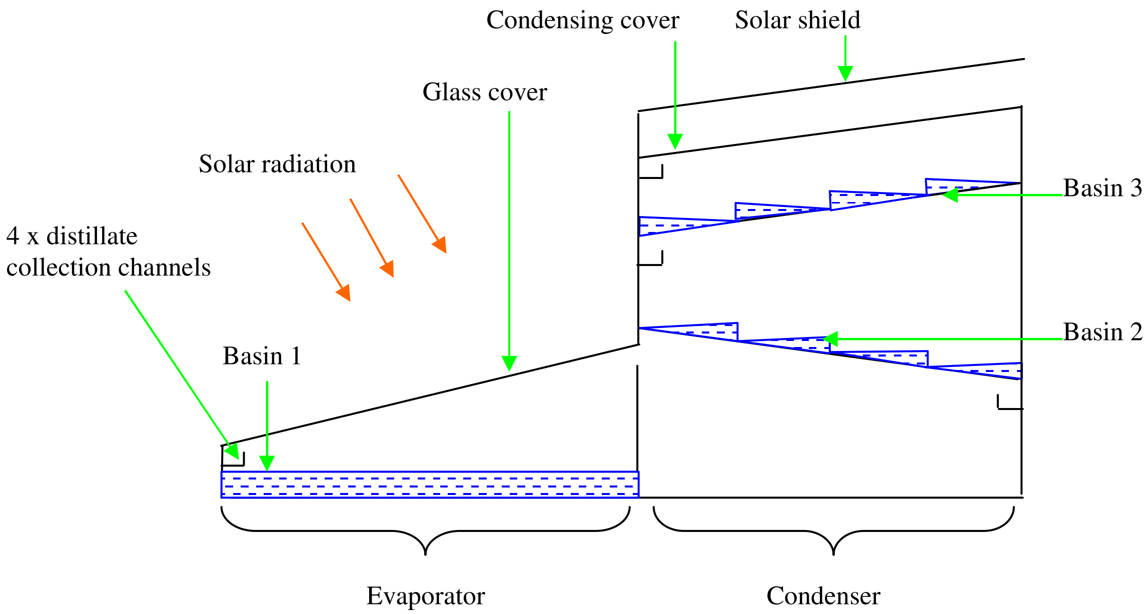

Fig.1.2: Cross-section of an advanced solar still.

A randomised block experimental design was formulated to collect empirical data for model verification and system evaluation. In this experimental design, the CSS and ASS would be tested at two locations (the University of Strathclyde and Malawi Polytechnic). The choice of these locations was based on astronomical, meteorological and logistical factors. So, the two solar stills were initially tested outdoors at the former location before being shipped to the latter test site.

At each test site, measurements were taken by using accurate instruments that conformed to standard specifications. Kipp & Zonen pyranometers (models CM 6B and CM 11) were used to measure global and diffuse irradiance on a horizontal surface, while the temperature of water and other components was sensed by T-type thermocouples. The sensors for wind speed were Vector Instruments cup anemometer (model A100L2) and Delta-T Devices cup anemometer (model AN4). All pyranometers, thermocouples and anemometer were connected to a Delta-T Devices Ltd data logger (model DL2e). In addition, the mass of distilled water was determined by using digital analytical balances (Jadever Scale Ltd balance model JB-6000 and Ohaus balance model B500A). In addition, the quality of distillate output was monitored by Jenway conductivity/TDS meter (model 470) and Orion pH meter (model 601A). The acquired data was analyzed to establish the statistical validity of the observed trends. Detailed results from modelling and experimentation of the CSS and ASS are presented and discussed in this thesis.

1.4 Contribution to knowledge

This investigation has made the following contributions to knowledge:

a) Solar still modelling is important for the development of this type of technology. In this investigation, a new model for calculating the distribution of solar radiation in a single-slope conventional solar still (CSS) has been proposed. Incoming global solar radiation is divided into beam and diffuse components, and the view factors of surfaces that exchange radiation are taken into account in the new model. The model was verified by using empirical data. It was found that the accuracy of modelling a single-slope solar still improved (Madhlopa and Johnstone, 2009a).

b) A model for predicting the performance of a solar still with separate condenser and reflecting surfaces has been developed. This model incorporates the optical properties of beam and diffuse solar radiation, and view factors of the receiving and reflecting surfaces. Again, empirical data was used to verify the numerical scheme. It was found that the new model is more accurate in predicting the yield of distilled water than previous models at high and low latitudes. So, it can be applied in any part of the world.

c) An advanced solar still (ASS) with shielded separate condenser has been developed. The CSS and ASS were studied theoretically under the same meteorological conditions. Simulation results showed that the ASS produced more distilled water than the CSS (Madhlopa and Johnstone, 2009b). Prototype stills were then designed, constructed and tested to verify the proposed model and compare the performance of the two designs of solar stills under outdoor environmental conditions. It was experimentally observed that the solar shield fitted on the top part of the condenser unit was effective in keeping the temperature of the condenser cover relatively cool. In addition, the ASS was more efficient than the CSS under the same meteorological conditions. Consequently, a solar still with higher distillate output has been developed in this investigation.

1.5 Thesis organization

This thesis contains eight chapters. In Chapter 1, the limitation of access to clean water and associated socio-economic problems are discussed. It is shown that solar desalination can contribute to the sustainable provision of clean water, especially in tropical countries. Thus, research to improve the performance of the solar desalination technology is important. An outline of the research objectives is also given, and the chapter ends with a brief description of the research procedure followed in this work. Chapter 2 examines the fundamentals of solar radiation, and heat and mass transfer as they relate to the current theory and practice of solar distillation. The process of developing and verifying a mathematical model for solar stills is described in Chapter 3 while the experimental design is presented in Chapter 4. Materials and methods for testing of the solar stills are given in Chapter 5, with Chapter 6 focusing on results for model verification. Detailed empirical results are presented and discussed in Chapter 7. Finally, the main conclusions drawn from this investigation and recommendations for future research are presented in Chapter 8.

1.6 References

Bouchekima, B., Gros, B., Oahes, R. and Diboun, M., 1998. Performance study of the capillary film solar distiller. *Desalination,*116, pp.185-192.

Chang, J.M., Shen, M.C. and Huang, B.J., 2002. A criterion study of solar irradiation patterns for the performance testing of thermosyphon solar water heaters. *Solar Energy*, 73, pp.287-292.

Cooper, P.I., 1973. The maximum efficiency of single-effect solar stills. *Solar Energy*, 15, pp.205-217.

Dave, J.V., 1977. Validity of the isotropic-distribution approximation in solar energy estimations. *Solar Eenrgy*, 19, pp.331-333.

Diabaté, L., Blanc, Ph and Wald, L., 2004. Solar climate in Africa. *Solar Energy*, 76, pp.733-744.

Duffie, J.A. and Beckman, W.A., 2006. *Solar Engineering of Thermal Processes*. 3rd ed. New York: Wiley Interscience, pp.658-659.

El-Bahi, A. and Inan, D., 1999a. Analysis of a parallel double glass solar still with separate condenser. *Renewable Energy*, 17, pp.509-521.

El-Bahi, A. and Inan, D., 1999b. A solar still with minimum inclination, coupled to an outside condenser. *Desalination*, 123, pp.79-83.

Fath, H.E.S. and Elsherbiny, S.M., 1993. Effect of adding a passive condenser on solar still performance. *Energy Conversion and Management,* 34, pp.63-72.

Fath, H.E.S. and Hosny, H.M., 2002. Thermal performance of a single-sloped basin still with an inherent built-in additional condenser. *Desalination*, 142, pp.19-27.

Foster, R., Ghassemi, M. and Cota, A., 2009. *Solar energy: Renewable energy and the environment*. Boca: CRC Press, pp.7-52.

Fritzmann, C., Löwenberg, J., Wintgens, T. and Melin, T., 2007. State-of-the-art of reverse osmosis desalination. *Desalination*, 216, pp.1-76.

Garg, H.P. and Mann, H.S., 1976. Effect of climatic, operational and design parameters on the year round performance of single-sloped and double-sloped solar still under Indian arid zone conditions. *Solar Energy*, 18, pp.159-164.

Hyde, W.F. and Seve, J.E., 1993. The economic role of wood production in tropical deforestation: The severe example of Malawi. *Forest Ecology and Management*, 57, pp.283-300.

IPCC, 1995. *Climate Change 1994*. Cambridge: Cambridge Press.

Jansen, T.J., 1985. *Solar engineering technology*. Eaglewood Cliffs: Prentice-Hall Inc., pp.13-33.

Lakudzala, D.D., Tembo, K.C. and Manda, I.K., 1999. An investigation of chemical pollutants in Lower Shire River, Malawi. *Malawi Journal of Science and Technology*, 5, pp.87-94.

Madhlopa, A., 2006a. Solar climate in Malawi. *Solar Energy*, 80, pp.1055-1057.

Madhlopa, A., 2006b. Study of diurnal production of distilled water by using solar irradiation distribution about solar noon. *Eurosun 2006 International Conference*. Glasgow, United Kingdom 27-30 June 2006.

Madhlopa, A. and Jonstone, C., 2008. Potential for water distillation by using solar energy in Malawi. En*vironment and Health International Magazine*, 10, pp.51-53.

Madhlopa, A. and Johnstone, C., 2009a. Model for computation of solar fraction in a single-slope solar still. *Solar Energy*, 83, pp.873-882.

Madhlopa, A. and Johnstone, C., 2009b. Numerical study of a passive solar still with separate condenser. *Renewable Energy*, 34, pp.1668-1677.

Markvart, T. ed., 1994. *Solar electricity*. Chichester: John Wiley & Sons, pp.6-18.

Mowla, D. and Karimi, G., 1995. Mathematical modelling of solar stills in Iran. *Solar Energy*, 55, pp.389-393.

Msonda, K.W.M., Masamba, W.R.L. and Fabiano, E., 2007. A study of fluoride groundwater occurrence in Nathenje, Lilongwe, Malawi. *Physics and Chemistry of the Earth*, 32, pp.1178–1184

Mumba, P.P., Banda, J.W. and Kaunda, E., 1999. Chemical Pollution in Selected Reservoirs and Rivers in Lilongwe District, Malawi. *Malawi Journal of Science and Technology*, 5, pp.74-86.

Nafey, A.S., Abdelkader, M., Abdelmotalip, A. and Mabrouk, A.A., 2000. Parameters affecting solar still productivity. *Energy Conversion and Management*, 41, pp.1797-1809.

Parry, M., Canziani, O. and Palutikof, J., 2008. Key IPCC conclusions on climate change impacts and adaptations. *WMO Bulletin*, 57(2), pp.77-85.

Pritchard, M., Mkandawire, T. and O'neill, J.G., 2007. Biological, chemical and physical drinking water quality from shallow wells in Malawi: Case study of Blantyre, Chiradzulu and Mulanje. *Physics and Chemistry of the Earth*, 32, pp.1167-1177.

Reindl, D.T., Beckman, W.A. and Duffie, J.A., 1990. Evaluation of hourly tilted surface radiation models. *Solar Energy*, 45, pp.9-17.

Saikku, L., Rautiainen, A. and Kauppi, P.E., 2008. The sustainability challenge of meeting carbon dioxide targets in Europe by 2020. *Energy Policy*, 36, pp.730-742.

Tanaka, H., and Nakatake, Y., 2006. Theoretical analysis of a basin type solar still with internal and external reflectors. *Desalination*, 197, pp.205-216.

Tanaka, H. and Nakatake, Y., 2007. Effect of inclination of external flat plate reflector of basin type still in winter. *Solar Energy*, 81, pp.1035-1042.

Tiwari, G.N., Singh, H.N. and Tripathi, R., 2003. Present status of solar distillation. *Solar Energy*, 75, pp.367-373.

Tiwari, A.K. and Tiwari, G.N., 2007. Thermal modelling based on solar fraction and experimental study of the annual performance of a single slope passive solar still: The effect of water depths. *Desalination*, 207, pp.184-204.

Tripathi, R. and Tiwari, G.N., 2004. Performance evaluation of solar still by using the concept of solar fraction. *Desalination*, 169, pp.69-80.

Tripathi, R. and Tiwari, G.N., 2006. Thermal modelling of passive and active solar stills for different depths of water by using the concept of solar fraction. *Solar Energy*, 80, pp.956-967.

UN, 2007. *Development goals report 2007*. New York: United Nations.

UN, 2008. *World economic situation and prospects 2008*. New York: United Nations.

UNEP, 1988. *Environmental Perspective to the Year 2000 and Beyond*. Kent: Penshurst Press Ltd, pp.13-16.

WHO, 2006. *Guidelines for drinking-water*. Geneva: World Health Organization.

WHO, 2007. *Combating waterborne disease at household level*. Geneva: World Health Organization.

WHO, 2008. *World Health Statistics 2008*. Geneva: World Health Organization.

Chapter 2

Current state of the art

2.0 Introduction

The present investigation was aimed at developing a solar still with improved distillate yield per unit area of the evaporator basin. To achieve this aim, three specific objectives were set out on modelling, experimentation and evaluation of the solar still performance in Section 1.2. In addition, it has been shown in the same section that a solar distillation system converts solar radiation to heat which is transferred from the solar absorber to other components of the system through convection, conduction, evaporation and radiation. Part of the heat is lost to the environment. Thus, the physics of solar radiation and basic principles of heat and mass transfer were required to model conceptual solar stills. Simulation results were used to design and fabricate prototype solar stills which were tested outdoors to verify the accuracy of the proposed model and evaluate the performance of the stills under real meteorological conditions.

Solar radiation is a free and renewable source of energy and the most influential environmental factor that affects solar energy systems (Nafey et al., 2000). Consequently, knowledge about its characteristics is vital in modelling, designing, testing and application of solar technologies which fall into photovoltaic and thermal categories. The former group of solar energy systems directly converts solar radiation into electrical energy through the photoelectric effect (Rappaport, 1959; García-Rodrígue, 2003) while the latter generates heat from solar radiation. This heat is transferred from the solar absorber to different components of the system through various modes of heat transfer that also affect the performance of solar thermal systems, including solar stills which operate on the principles of heat and mass transfer. So, the present work is within the theme of solar thermal applications.

In this chapter, fundamentals of solar radiation, and heat and mass transfer are discussed and applied to the process of solar desalination. Then, some limitations to previous work in modelling and designing of solar stills are identified. In particular, well-known characteristics of solar radiation are used to establish the limitation of previous models on the distribution of solar radiation inside a solar still with reflectors. In addition, it is shown that the efficiency of a CSS is low. Consequently, some modifications to the design of the CSS have been proposed by various researchers in the past. Nevertheless, the performance of solar stills remains limited. The current state of the art is described and some limitations to previous work are outlined in this chapter.

2.1 Solar radiation

2.1.1 Solar constant and components

The sun is the primary source of solar radiation. It emits radiation at an equivalent black body temperature of about 6000 K with a constant intensity outside the earth's atmosphere (Kane, 2005). Irradiance on a surface which is at right angles to the direction of propagation of solar energy at an average distance between the earth and the sun outside the atmosphere is the solar constant (G_{sc}). This constant is required in solar radiation analysis, as shown in Section 2.1.4. So, several authors have attempted to establish its accurate value for application in solar engineering and science. Johnson (1954) found G_{sc} =1395 Wm^{-2} while Frohlich (1977), as cited in Duffie and Beckman (2006), advocated a value of 1373 Wm^{-2}. Darula et al. (2005) recommended 1366.1 Wm^{-2} as a more accurate value of G_{sc} but the World Radiation Centre (WRC) adopted a value of 1367 Wm^{-2} (Gueymard, 2004). Therefore, the WRC value of G_{sc} is used in the computation of irradiance on an inclined glass cover in this investigation (Chapter 3).

Outside the earth's atmosphere, there is only direct (beam) radiation. However, as solar radiation propagates through the atmospheric matter, it undergoes scattering, absorption and transmission (Sharma and Pal, 1965). The scattering process produces the diffuse component of global solar radiation (Ineichen, 2008). So, the global solar radiation that reaches the earth's surface comprises beam and diffuse components (Liu and Jordan, 1960; Yang et al., 2001). The two components of solar radiation have different optical properties when incident on a surface (Reindl et al., 1990). Beam radiation travels directly from the sun's disc to a receiver surface, and its rays are traceable from the sun's position and used in determining solar angles. This component of radiation can also be focused to increase the amount of solar energy intercepted per unit area of an absorber surface. The intensity of beam radiation increases with the clearness of the sky. It may be as high as 900 Wm^{-2} on a clear day but as low as 10 Wm^{-2} on a cloudy day around solar noon, depending on location. On the other hand, diffuse radiation comes from the whole sky vault and it cannot be focused. Moreover, its rays are not traceable from the sun's position, and the amount of diffuse solar energy directly received by a given surface depends on the proportion of the sky viewed by the surface (Duffie and Beckman, 2006). The intensity of diffuse radiation decreases with increasing the clearness of the sky. It may be as high as 180 Wm^{-2} on a cloudy day but as low as 50 Wm^{-2} on a clear day around solar noon, depending on location. In addition, the efficiency of most solar collectors decreases with increasing the percentage of diffuse irradiance (ISO, 1994).

2.1.2 Solar time

Knowledge about solar time (t_s) is required in the computation of solar angles, which influence the amount of beam radiation reaching a surface on the earth. Solar time depends on the apparent angular motion of the sun as it traverses the sky. In view of this, clock time (t_{ct}) is converted to t_s in studies on the availability of solar radiation (Garg, 1982). At a given locality, t_s can be given by (Foster et al., 2009):

$$t_s = t_{ct} + E + (\Theta_{sd} - \Theta)/15 - t_{dy} \tag{2.1}$$

$$E = 229.2\{0.000075 + 0.001868 \cos \Gamma - 0.032077 \sin \Gamma - 0.014615 \cos (2\Gamma) - 0.04089 \sin (2\Gamma)\}/60 \tag{2.2}$$

$$\Gamma = 360(N-1)/365 \tag{2.3}$$

It should be mentioned that there is an additional correction for day light saving (t_{dy}) depending on the season of the year and location (ASHRAE, 1991). For instance, t_{dy}=1 hour from the last Sunday of March to the last Saturday of October and t_{dy}=0 on other days at the University of Strathclyde. On the other hand, t_{dy}=0 throughout the year at the Malawi Polytechnic.

At solar noon, the sun passes over the local meridian of an observer and beam rays make the minimum angle with the zenith. The local solar noon (t_{sn}) is given by (Garg and Datta, 1993):

$$t_{sn}=12-E \pm (\Theta_{sd}- \Theta)/15 \tag{2.4}$$

A plus sign is used in Eq.(2.4) if the observer is in the eastern hemisphere, with a minus sign for an observer in the western hemisphere. The length of time between sunrise and sunset indicates the potential duration of sunshine and level of global radiation. Jain (1988) reported that the extraterrestrial sunshine duration S_o for a given day is given by:

$$S_o = (2/15) \cos^{-1} (-\tan \phi \tan \delta) \tag{2.5}$$

However, the measured sunshine duration is less than the extraterrestrial hours of sunshine for a particular day and location due to atmospheric turbidity, and shading effect from hills and other structures on the earth's surface.

2.1.3 Sun position and direction of beam radiation

At any given time and place, knowledge about the position of the sun is required for calculation of the beam component of the solar radiation incident on a tilted surface, and for determination of the angular-dependent optical properties of transparent materials (Jansen, 1985; Tesfamichael and Wäckelgård, 2000). The position of the sun can be specified by the zenith (θ_z), declination (δ), azimuth (γ_s) and hour (ω) angles (Braun and Mitchell, 1983). Beam radiation makes an angle θ_z with the normal to a horizontal plane (zenith) and angle θ_p with the normal to an inclined plane. It should also be mentioned that δ is the angle between the sun's rays and the equatorial plane, and this parameter is positive in the northern hemisphere and negative in the southern hemisphere. In addition, the solar azimuth angle is measured from south to the horizontal projection of the sun's rays on a horizontal plane, and it is negative in the east of south and positive in the west of south (Duffie and Beckman, 2006). The earth has to turn through ω to bring the meridian of an observer at a specific point directly in line with the rays of the sun, and ω is negative in the morning, zero at solar noon and positive in the afternoon (Garg, 1982). The various solar and surface angles are shown in Fig.2.1.

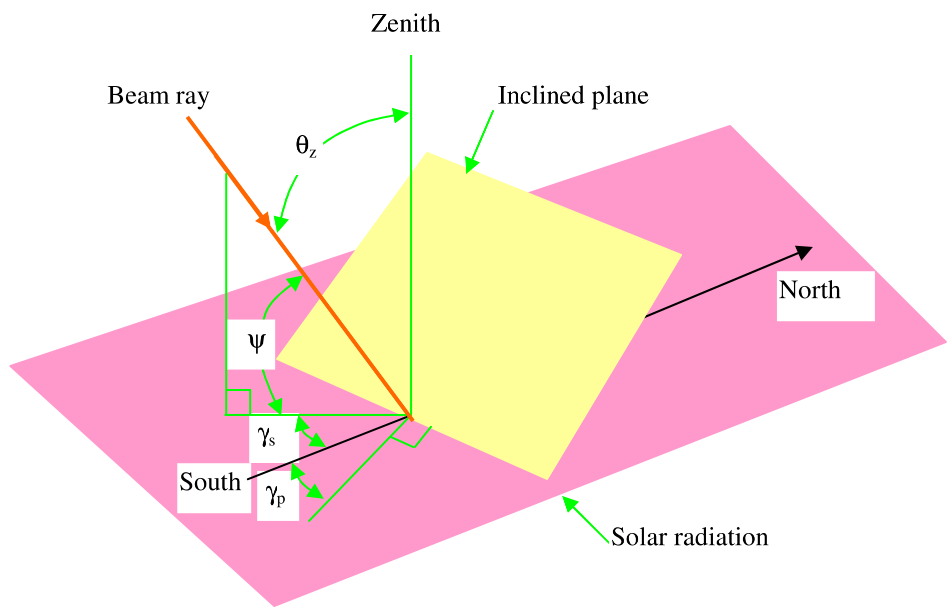

Fig.2.1: Diagram showing a beam ray from the sun onto an inclined surface, and solar and surface angles (in the northern hemisphere).

The angle of incidence (θ_p) of solar radiation on a surface inclined at angle β to the horizontal plane influences the proportions of solar radiation absorbed and transmitted by the receiving surface. ISO (1994) reported that angles of incidence less than 30^o from the normal have negligible effect on the absorptance-transmitance product

($\alpha'\tau$). At solar noon, the angle of incidence is zero or close to zero while the intensity of solar radiation is optimum. An expression for θ_p is given by (Howell et al., 1982):

$$\cos\theta_p = \cos\theta_z \cos\beta + \sin\theta_z \sin\beta \cos(\gamma_s - \gamma_p) \quad (2.6)$$

$$\cos\theta_z = \sin\delta \sin\phi + \cos\delta \cos\phi \cos\omega \quad (2.7)$$

$$\cos\gamma_s = (\sin\phi \cos\delta \cos\omega - \cos\phi \sin\delta)/\cos\alpha \quad (2.8)$$

$$\omega = 15(t_s - 12) \quad (2.9)$$

$$\psi = 90^o - \theta_z \quad (2.10)$$

It is noted that Eqs.(2.7) and (2.8) also involve the declination angle (δ). Jain (1988) reported the following expression for computation of this angle:

$$\delta = 0.006918 - 0.399912 \cos\Gamma + 0.07257 \sin\Gamma - 0.006758 \cos 2\Gamma + 0.000907 \sin 2\Gamma - 0.002697 \cos 3\Gamma + 0.00148 \sin 3\Gamma \quad (2.11)$$

$$\Gamma = 360\,(N-1)/365 \quad (2.12)$$

When the sun is directly overhead on a horizontal surface ($\psi=90^o$ and $\theta_z=0$), solar radiation transmittance through the atmosphere is a maximum at a given location on the earth's surface. The zenith angle is equal to zero during some time in the year at sites within the tropical region, and it is always greater than zero at sites outside this region. The magnitude of the zenith angle is smallest and the potential for stable meteorological conditions is highest around solar noon (ISO, 1994). So, irradiance on the earth's surface is a maximum around solar noon on a clear day. Eqs. (2.6 to 2.12) were used in the computation of solar distribution in a single slope solar still in Chapter 3.

2.1.4 Extraterrestrial radiation and solar radiation on inclined surfaces

Extraterrestrial radiation is a theoretical amount of solar energy that would be available on a horizontal plane on the earth's surface if the earth was not surrounded by an atmosphere. In reality, solar radiation is attenuated as it passes through the particulate matter surrounding the earth, resulting in a decrease of its intensity when measured on a plane on the earth's surface. At any specific time within the day, extraterrestrial irradiance is given by (Suehrcke, 1994; Sailor et al., 2006):

$$\mathrm{G_o} = \mathrm{G_{sc}}\left(1 + 0.033\cos\frac{360N}{365}\right)\cos\theta_z \tag{2.13}$$

where G_{sc} is the solar constant (=1367 Wm^{-2}).

In modelling and experimental studies of solar energy systems, hourly (I) and daily (H) solar radiation data is sometimes required. So, integrated values of hourly (I_o) and daily (H_o) extraterrestrial radiation on a horizontal plane are used in such computations (Anderson, 1983; Duffie and Beckman, 2006):

$$I_o = \frac{43200}{\pi} G_{sc}\left(1 + 0.033\cos\frac{360N}{365}\right)\left[\cos\phi\cos\delta(\sin\omega_2 - \sin\omega_1) + \frac{\pi(\omega_2 - \omega_1)}{180}\sin\phi\sin\delta\right] \tag{2.14}$$

$$H_o = \frac{86400 G_{sc}}{\pi}\left(1 + 0.033\cos\frac{360N}{365}\right)\left(\cos\phi\cos\delta\sin\omega_{ss} + \frac{\pi\omega_{ss}}{180}\sin\phi\sin\delta\right) \tag{2.15}$$

It should be noted that the solar constant (G_{sc}) appears in both Eqs. (2.14) and (2.15). In addition, the hourly and daily extraterrestrial radiation is influenced by the day of the year and solar angles at a given location. Extraterrestrial radiation can be used to compute available solar radiation on a horizontal plane on the earth's surface. However, solar radiation on a tilted surface is needed in the design and performance studies of solar collectors.

Reindl et al. (1990) and Quaschning and Hanitsch (1998) reported that the total irradiance on a tilted plane consists of the beam, diffuse and ground-reflected components, and it can be given by:

$$G_{gp} = G_{bp} + G_{dp} + G_{gr} \tag{2.16}$$

In practice, global irradiance is commonly measured on a horizontal surface (Thekaekara, 1976). Models are therefore employed to generate a data base of solar radiation received by inclined surfaces. For beam radiation, a geometric factor (R_b) is used to compute beam irradiance on a tilted surface from horizontal beam irradiance (Duffie and Beckman, 2006):

$$R_b=G_{bp}/G_{bh} = \cos \theta_p/\cos \theta_z \tag{2.17}$$

From Eqs.(2.6) and (2.17), R_b can also be expressed in the form:

$$R_b=\cos \beta+ \tan \theta_z \sin \beta \cos (\gamma_s-\gamma_p) \tag{2.18}$$

Using Eqs.(2.8) and (2.18), R_b for a vertical surface (β=90^o) can therefore be simplified to:

$$R_b=\cos (\gamma_s-\gamma_p)/\tan \psi \tag{2.19}$$

So, beam irradiance on a vertical surface can be computed from:

$$G_{bp} = \frac{\cos(\gamma_s - \gamma_p)G_{bh}}{\tan\psi} \tag{2.20}$$

It is seen from Eq.(2.20) that G_{bp} depends on the solar azimuth and altitude angles for a given value of the surface orientation and beam irradiance intercepted by a horizontal surface. It should also be mentioned that $\gamma_p=0$ and $\gamma_p=180^o$ for south-facing and north-facing surfaces, respectively. In addition, ψ is maximum at solar noon.

For diffuse radiation, solar energy received by an inclined surface depends on its view of the sky. This component of global radiation comprises the isotropic, circumsolar and horizon brightening parts (Puri et al., 1980; Gueymard, 2001). Isotropic diffuse radiation is emitted uniformly from the entire sky vault while circumsolar diffuse radiation originates from forward scattering and it is around the sun in the sky. Horizon brightening diffuse radiation is intense near the horizon and it is most conspicuous in a clear sky. Based on the different parts of diffuse radiation, various models have been developed to estimate diffuse radiation on a tilted surface. Liu and Jordan (1963) derived an isotropic diffuse model. In this model, all the diffuse radiation was assumed to be isotropic. So, the amount of diffuse solar energy intercepted by a surface depends on its view of the sky (Dave, 1977):

$$I_{dp}=W_{p\text{-}sk}I_{dh} \tag{2.21}$$

If the surface is not obstructed by other structures, its view factor relative to the sky can be given by:

$$W_{p\text{-}sk}=0.5(1+\cos\beta) \tag{2.22}$$

Eq.(2.22) shows that an unobstructed horizontal surface ($\beta=0$) views 100 % of the sky, and so it receives more diffuse solar radiation than an unobstructed surface inclined at $\beta>0$. Hay and Davies (1980), as cited in Duffie and Beckman (2006), took into account the circumsolar diffuse part to derive the following model for calculating diffuse radiation on a surface:

$$I_{dp}=I_{dh}\{(1-r)\,W_{p\text{-}sk}+rR_b\} \tag{2.23}$$

where $r=I_{bh}/I_o$.

Later, Reindl et al. (1990) modified Eq.(2.23) by taking into account the horizon brightening component:

$$I_{dp}=I_{dh}\{(1-r)\, W_{p\text{-}sk}\, (1+f \sin^3(0.5\beta)) + rR_b\} \tag{2.24}$$

where $f=(I_{bh}/I_{gh})^{0.5}$

The influence of $W_{p\text{-}sk}$ is depicted in all the three aforementioned common models for estimating diffuse solar energy on a given surface. It should be mentioned that the isotropic model is the simplest and most widely used model, and it yields the most conservative estimates (Duffie and Beckman, 2006).

Again, the ground-reflected component depends on the view factor of the ground with respect to the tilted surface (Quaschning and Hanitsch, 1998):

$$G_{gr}= w_{gr\text{-}p}\, \rho_{gr} G_{gh} \tag{2.25}$$

$$w_{gr\text{-}p} =0.5\ (1-\cos\beta) \tag{2.26}$$

Eqs.(2.25) and (2.26) show that G_{gr} would decrease with β and ρ_{gr}. Thus, $G_{gr}=0$ for a horizontal surface. In addition, the effect of the ground-reflected component on the performance of a solar collector can be ignored depending on the physical features surrounding the collector (ISO, 1994). The principles of solar radiation on an inclined plane were applied in the computation of solar radiation intercepted by the glass cover and walls of a solar still with one slope in Chapter 3.

2.1.5 Solar radiation measurement

Solar radiation that reaches the earth's surface is lower than the extraterrestrial radiation. In addition, commonly available solar data is measured on a horizontal surface. Thus, solar data on an inclined plane is mostly computed from solar radiation on a horizontal plane. Consequently, solar radiation received by a horizontal surface at a given site needs to be measured for radiation analysis and other applications.

Available global solar radiation on a horizontal surface can be directly measured by using a pyranometer (Thekaekara, 1976). According to the ISO 9060 classification standard, there are three classes of pyranometers: secondary standard, first and second classes, with the secondary standard class being the best (Kipp & Zonen, 2006). First class pyranometers are also recommended for measuring irradiance for performance evaluation of solar collectors (ISO, 1994). Nevertheless, it is often desirable to know the individual levels of beam and diffuse radiation for purposes of solar energy system modelling, design, testing and application. So, these components of global radiation are measured on a given plane.

Beam radiation can be measured by using direct or indirect methods. In the direct approach, a pyrheliometer is used to measure beam radiation at normal incidence but this instrument is costly (Kudish and Evseev, 2008). So, only limited meteorological sites have pyrheliometers. In the indirect method, beam radiation is determined by subtracting diffuse radiation from global radiation. In this case, concurrent measurements of global and diffuse radiation are taken in the same plane.

Diffuse radiation can be measured by using a pyranometer fitted with an occulting disk or shadow ring, with the occulting disk yielding more accurate data. However, the disk requires an expensive sun-tracking system. In view of this, diffuse radiation is commonly measured by using a pyranometer with a stationary ring in the east-west axis. The ring blocks off beam radiation and a small amount of diffuse radiation from reaching the sensor (Fig.2.2), which results in slightly lower readings of diffuse irradiance. A correction factor is therefore applied to the data to take care of this error. In this investigation, diffuse irradiance on a horizontal surface was therefore measured by using a pyranometer fitted with a shadow ring. The difference between global and diffuse irradiance yielded beam irradiance. Beam and diffuse radiation data captured on a horizontal surface was then used to compute irradiance on the glass cover and walls of a single slope solar still.

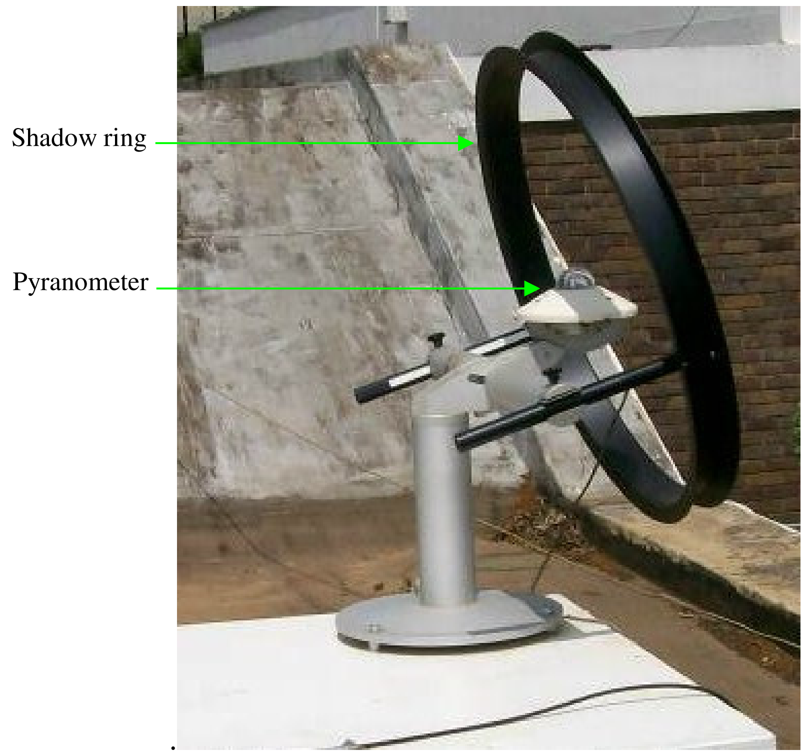

Fig.2.2: A Kipp & Zonen pyranometer with a shadow ring mounted on roof top at Malawi Polytechnic.

2.1.6 Attenuation of solar radiation through glazing

Solar radiation travels through air before it reaches a transparent cover (such as glass). The cover reflects (ρ), absorbs (α) and transmits (τ) part of the radiation. The sum of the proportions of reflected, absorbed and transmitted radiation is equal to one and these fractions are influenced by the optical properties of incoming solar radiation (Edlin, 1958; Lorenz, 1998; ASHRAE, 2001). In particular, the wavelength (λ) and direction (θ) of radiation influence the magnitude of attenuation. So, α, ρ and τ can be expressed as:

$$\alpha(\lambda,\theta) + \rho(\lambda,\theta) + \tau(\lambda,\theta) = 1 \qquad (2.27)$$

Most of the solar radiation received by the earth's surface is within a wavelength range of 0.29 to 3 x10^{-6} m (Thekaekara, 1976). Nevertheless, many types of window glazing have a weak spectral selectivity in the solar spectrum (ASHRAE, 2001). In view of this, only their angular dependence can be taken into account as shown in Fig.2.3.

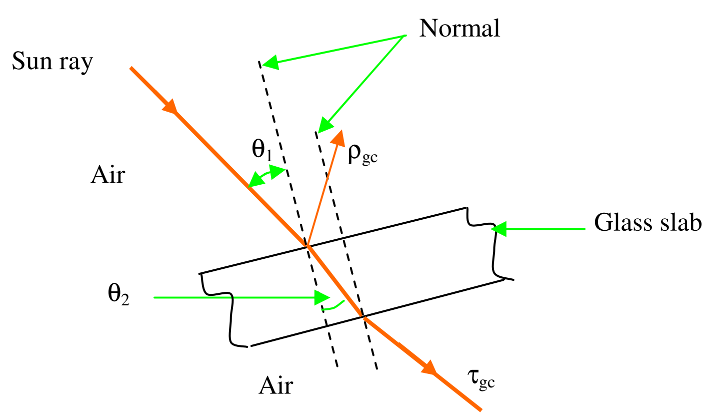

Fig.2.3: Propagation of solar radiation through air and a glass cover.

Incoming solar radiation is polarized when it propagates through a transparent material (Tekelioglu and Wood, 2009). Perpendicular and parallel components of unpolarized radiation are polarized differently by the transparent material. This results in differences in the reflectance, absorptance and transmittance of the cover material for the two components. The transmittance of the cover can be computed by including the angular dependence of solar attenuation (Briscoe and Galvin, 1991).

For the perpendicular component of unpolarized radiation, the reflectance (ρ_n), absorptance (α_n) and transmittance (τ_n) are calculated as follows (Duffie and Beckman, 2006):

$$\tau_{ab} = e^{\left(-Kx_{gc}/\cos\theta_2\right)} \tag{2.28}$$

$$\alpha_\mathrm{n} = (1 - \tau_{ab})\left(\frac{1-r_n}{1-r_n\tau_{ab}}\right) \tag{2.29}$$

$$r_n = \frac{\sin^2(\theta_2-\theta_1)}{\sin^2(\theta_2+\theta_1)} \tag{2.30}$$

$$\tau_n = \frac{\tau_{ab}(1-r_n)^2}{1-(r_n\tau_{ab})} \tag{2.31}$$

Similar equations are used to calculate the corresponding values of the absorptance, transmittance and reflectance for the parallel component of unpolarized solar radiation, with r_n replaced by r_{pr}:

$$r_{pr} = \frac{\tan^2(\theta_2-\theta_1)}{\tan^2(\theta_2+\theta_1)} \tag{2.32}$$

The required angular-dependent optical properties of a single transparent cover are obtained from:

$$\alpha = (\alpha_n+\alpha_{pr})/2 \tag{2.33}$$

$$\tau = (\tau_n+\tau_{pr})/2 \tag{2.34}$$

$$\rho=(\rho_n+\rho_{pr})/2 \tag{2.35}$$

The reflectance of a single cover can be given by:

$$\rho \cong \tau_{ab} - \tau \tag{2.36}$$

It should be mentioned that the values of ρ and τ at normal incidence ($\theta_1=0$) are commonly available for different transparent materials with specified thicknesses. So, Eqs.(2.28) and (2.36) were used to compute the value of K (at normal incidence) for a glass cover fitted over a solar still in Chapter 3. This parameter was then used to determine the values of α, τ and ρ at different angles of incidence.

2.2 Heat and mass transfer

Heat transfer is the flow of energy from one point to another due to temperature differences between the points, and it can take place through conduction, convection and radiation. In a solar thermal system, heat is distributed from the absorber to other components of the system through one or a combination of these modes of heat transfer. Heat transmission in solar collectors may also lead to a loss of useful energy and a reduction in the system efficiency. Consequently, the design, construction, testing and operation of heat exchangers require knowledge about heat transmission mechanisms.

2.2.1 Conduction

Heat conduction is the rate of energy transfer between two points in a medium whereby kinetic energy is transferred between particles or groups of particles (ASHRAE, 2001). This mode of heat transfer can take place in gaseous, liquid and solid phases of a substance. In addition, heat is conducted in the direction of decreasing temperature. The temperatures in question may vary (transient) or remain constant (steady-state) with time.

For transient heat conduction in three dimensions, heat flow is based on the theory proposed by Fourier (1822) as cited in Gruber and Lesne (2005) and Lienhard and Lienhard (2006):

$$\nabla^2 T + \frac{\dot{q}}{k} = \frac{1}{\alpha'}\frac{\partial T}{\partial t} \tag{2.37}$$

where ∇^2 is the Laplacian.

In Cartesian coordinates, Eq.(2.37) is given as:

$$\frac{\partial^2 T}{\partial x^2} + \frac{\partial^2 T}{\partial y^2} + \frac{\partial^2 T}{\partial z^2} + \frac{\dot{q}}{k} = \frac{1}{\alpha'}\frac{\partial T}{\partial t} \tag{2.38}$$

Eq.(2.37) can also be expressed in cylindrical or spherical coordinates, depending on the geometry of the conductor. It is possible to solve this equation analytically to obtain an accurate spatial distribution of temperature at a given time. Nevertheless, some mathematical models involve systems of differential equations which cannot be solved analytically. In such cases, numerical methods can be used to obtain an approximate solution. In one dimension, Eq.(2.38) reduces to:

$$\frac{\partial^2 T}{\partial x^2} + \frac{\dot{q}}{k} = \frac{1}{\alpha'}\frac{\partial T}{\partial t} \tag{2.39}$$

The heat flux in three dimensions can be given by:

$$\vec{\mathrm{q}} = -k\nabla \mathrm{T} \tag{2.40}$$

where ∇T is the temperature gradient (a vector quantity).

In one dimension, heat flux (q) can be calculated from:

$$q = -k\frac{dT}{dx} \tag{2.41}$$

It is noted from Eq.(2.41) that the rate of heat transfer increases with the coefficient of heat conduction (k) and temperature gradient. Thus, materials with relatively high values of k (such as copper; aluminium, stainless steel and galvanized steel) are suitable for the fabrication of solar absorber plates while those with low values of k (such as plywood, polystyrene, sawdust and cork) are appropriate for insulation to reduce heat loss from a given system to the environment. In addition, k varies with the direction of heat flow and temperature of the conductor (Lienhard and Lienhard, 2006). The rate of heat flow (Q) across the slab without heat source (Fig.2.4) can be given by (ASHRAE, 2001):

$$Q = kA(\Delta T)/x \tag{2.42}$$

$$\Delta T = T_1 - T_2 \tag{2.43}$$

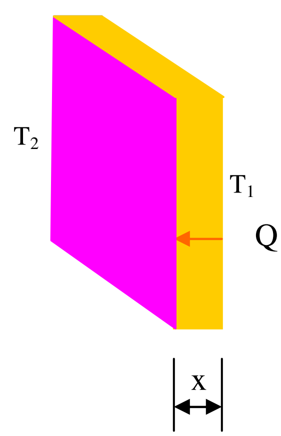

Fig.2.4: One dimensional heat conduction across a slab at $T_1 > T_2$.

2.2.2 Convection

Heat convection is the rate of energy transfer between two points in a fluid which involves mixing of the fluid by natural or forced mechanisms. In natural convection, the fluid moves due to the density gradient arising from temperature differences. Forced convection occurs when a moving fluid absorbs heat and transports it away by means of an external pump such as a fan. At the fluid-solid boundary, heat is transferred by means of conduction. Heat may be transferred from a hot solid surface to a cold fluid or from a hot fluid to a cold surface. The rate of heat transfer by natural convection can be given by (Jacob, 1949 cited in Tsilingiris, 2009; Hollands et al., 1976):

$$q = h_c (T_2 - T_1) \tag{2.44}$$

where h_c=Nu k/S, Nu = b(Gr Pr)^d, and b and d are dimensionless parameters.

It should be noted that the Nusselt number (Nu) is a ratio of convective (h_c) to conductive (k/S) heat transfer coefficients within a fluid. This parameter is dimensionless and it can be calculated from the product of the Grashof (Gr) and Prandtl (Pr) numbers. The former parameter is a ratio of buoyancy to viscous force in a fluid while the latter is a ratio of kinematic viscosity (ν) to thermal diffusivity (α'). Both of these parameters are also dimensionless and they can be given by (Sanders and Holman, 1972; ASHRAE, 2001):

$$\mathrm{Pr} = \nu/\alpha' \tag{2.45}$$

$$\mathrm{Gr} = \frac{gS^3\beta'\varphi^2(\Delta T)}{\mu^2} \tag{2.46}$$

Eqs.(2.45) and (2.46) show that the product (GrPr) is influenced by fluid properties, the difference between the surface and fluid temperatures, and the geometry of the surface in contact with the fluid. Consequently, the coefficient of convective heat transfer is also affected by the same factors.

Natural convection can be divided into three regions, depending on the value of the dimensionless parameter d (ASHRAE, 2001): a) turbulent natural convection (d=1/3), b) laminar natural convection (d=1/4), and c) a region with d<1/4. When a fluid flows under forced convention, a boundary layer is created between the fluid and the surface (say a flat surface) in contact with the fluid (Fig.2.5). Flow within the boundary layer close to the leading edge of the surface is laminar forced convection. As flow continues along the surface, there is a rise in the thickness of the boundary layer to a critical level. Thereafter, turbulent forced convection sets in. So, forced convection can be laminar or turbulent. At a very low fluid velocity, flow remains laminar in long tubes or channels with small hydraulic diameter and it is said to be fully developed laminar flow. At a high fluid velocity or in a tube with large diameter, transition to turbulent flow takes place and flow is fully developed turbulent. These flow regions are employed in the computation of the coefficient of convective heat transfer (h_c), and ASHRAE (2001) and Incropera et al. (2007) provide a summary of models used for this computation. For instance, h_c for natural convection can be given by:

$$h_c = b\frac{k}{S}\left(\frac{S^3\varphi^2\beta' g\Delta T}{\mu^2}\right)^d\left(\frac{\mu C_p}{k}\right)^d \tag{2.47}$$

where S=height, length, diameter and 0.5x diameter for vertical plates or pipes, horizontal plates, horizontal pipes and spheres respectively.

For forced convection, h_c can be calculated from:

$$h_c = b\frac{k}{S}\left(\frac{S\dot{m}'}{\mu}\right)^e\left(\frac{\mu C_p}{k}\right)^d \tag{2.48}$$

It is noted from Eq.(2.47) that the coefficient of natural convection is independent of the characteristic length (S) when d=1/3. For forced convection, h_c is independent of the geometry of a cavity when the exponent e=1 in Eq.(2.48).

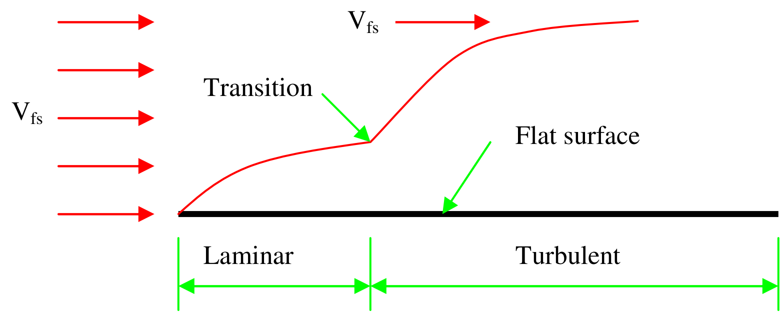

Fig.2.5: Formation of laminar and turbulent boundary layers when a fluid flows over a flat surface. The velocity of the fluid increases with the distance from the surface and the edge. V_{fs} is the free stream flow velocity.

2.2.3 Radiation

a) Optical view factor

An optical view factor influences the exchange of radiation between two given surfaces, and it depends on the geometries of the surfaces in question. For isothermal and diffuse surfaces, the view factor ($W_{i\text{-}j}$) is defined as the proportion of energy leaving surface (i) that is incident on surface (j), (Mishra et al., 2008). Moreover, the energy leaving surface (i) may reach other surfaces surrounding it. So, using the law of conservation of energy, this yields:

$$W_{i\text{-}i} + W_{i\text{-}2} + W_{i\text{-}3} + \ldots + W_{i\text{-}j} = 1 \qquad (2.49)$$

where (2), (3), (4)…(j) are surfaces that surround surface (i).

If a surface views itself, then $W_{i\text{-}i} > 0$, as shown in Fig.2.6

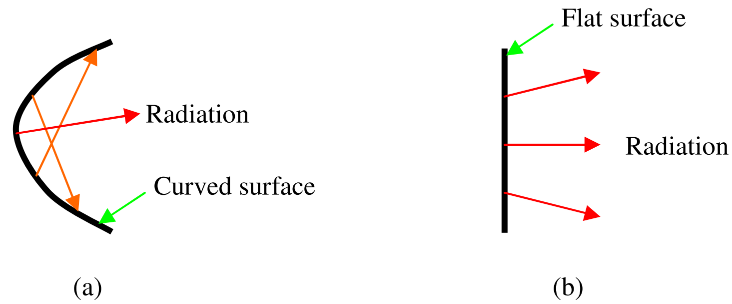

Fig.2.6: a) A curved surface exchanges radiation with itself and other surfaces.
b) A flat surface exchanges radiation with other surfaces only.

In addition, the following relationships are also useful for calculation of radiation exchange amongst surfaces (Incropera et al., 2007):

$$W_{1\text{-}(2,3)} = W_{1\text{-}2} + W_{1\text{-}3} \tag{2.50}$$

$$W_{(2,3)\text{-}1} = (A_2W_{2\text{-}1} + A_3W_{3\text{-}1})/(A_2 + A_3) \tag{2.51}$$

$$A_1W_{1\text{-}2} = A_2W_{2\text{-}1} \tag{2.52}$$

It should be noted that surface (1) views a combination of surfaces (2) and (3) in Eq.(2.50) while surfaces (2) and (3) jointly view surface (1) in Eq.(2.51). Eq.(2.52) expresses the reciprocity of view factors, which is particularly necessary for computation of radiation exchange between surfaces with finite and infinite areas. This equation is required in the calculation of radiation exchange between a solar collector (with finite area) and the sky (with infinite area).

b) Radiative heat transfer

Heat radiation is the transfer of thermal energy through electromagnetic waves (Sabbagh, 1977; Lienhard and Lienhard, 2006). This mode of heat transfer does not require a medium for propagation, unlike heat conduction and convection. Consequently, the use of a vacuum to reduce heat loss only eliminates convective and conductive heat losses. In fact, the presence of a medium between a radiator and receiver provides impedance to radiative heat transfer. The amount of energy emitted by a radiator depends on the nature of the material, microscopic structure and temperature of the radiator and its surroundings. A blackbody, for instance, absorbs all the radiation incident on it. Its emissive power to a hemispherical region above it is given by (Boltzmann, 1884 cited in Crepeau, 2007; MacIntyre, 1974):

$$\acute{E}_{bb}=\sigma T^4 \tag{2.53}$$

$$E'_{bb,\lambda} = \frac{c_1 \lambda^{-5}}{e^{c_2/(\lambda T)} - 1} \tag{2.54}$$

where $c_1 = 3.742 \times 10^{-16}$ Wm^2 and $c_2 = 0.014388$ m K are respectively the first and second Planck's constants.

A real surface absorbs part of the radiant energy which it receives. So, its emissive power to a hemispherical surface above it is given by:

$$\acute{E} = \varepsilon\sigma\left(T_i^4 - T_j^4\right) \tag{2.55}$$

$$\acute{E}_\lambda = \varepsilon_\lambda \acute{E}_{bb,\lambda} \tag{2.56}$$

$$\varepsilon = \frac{1}{\sigma T^4} \int_0^\infty \varepsilon_\lambda E'_{bb,\lambda} d\lambda \tag{2.57}$$

If ε_λ is independent of λ, then $\varepsilon = \varepsilon_\lambda$, and a surface with such a characteristic is known as a gray body. In practical calculations, surfaces are usually assumed to be gray because of the unavailability of information about the relationship between ε_λ and λ. It should also be mentioned that the energy from a non-black surface comprises the radiant and reflected components, and this energy may leave the surface specularly or diffusely. The reflected radiation follows one direction from a specular reflector but it goes in different directions from a diffuse reflector (Fig.2.7).

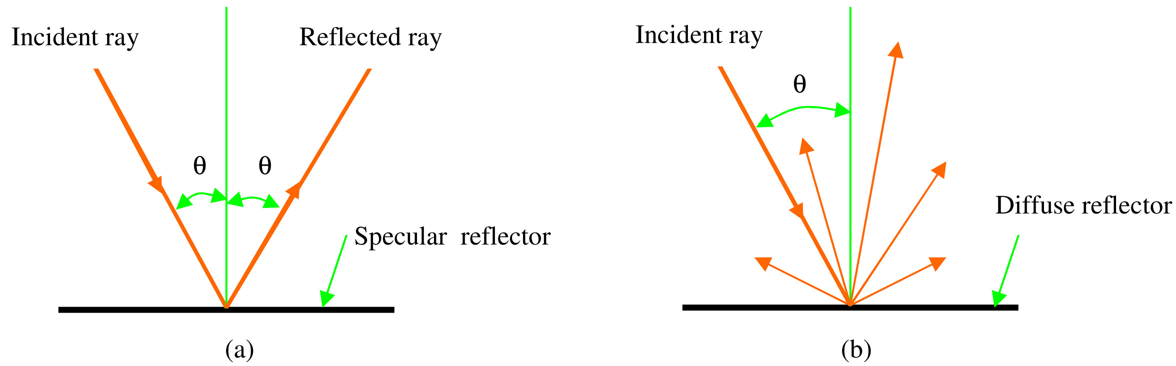

Fig.2.7: Reflection of radiation on a) specular and b) diffuse surfaces.

If solar irradiance on surface (i) is G_{gp}, then the amount of solar power reflected diffusely from surface (i) to surface (j) can be given by (Duffie and Beckman, 2006):

$$G_{i-j} = W_{i-j}\,\rho_i G_{gp} \tag{2.58}$$

Eq.(2.58) shows that the amount of solar radiation reflected to a receiver is influenced by both the reflectance and view factor of the surfaces. To calculate the amount of radiation energy transferred between two surface, the following assumptions are often made (ASHRAE, 2001): a) surfaces are gray or black, b) radiation and reflection are diffuse, c) α=ε, and α does not depend on the temperature of the source of the incident radiation and d) surfaces are separated by a non-absorbing medium. For two given surfaces, the net radiative heat transfer can be given by (Hewitt et al., 1994):

$$Q = \frac{\sigma\left(T_i^4 - T_j^4\right)}{\dfrac{1-\varepsilon_i}{A_i\varepsilon_i} + \dfrac{1-\varepsilon_j}{A_j\varepsilon_j} + \dfrac{1}{A_i W_{i,j}}} \tag{2.59}$$

The net radiative heat transfer between two surfaces can also be expressed in a linear form by defining a coefficient of radiative heat transfer:

$$Q = A_i h_{r,i-j}\left(T_i - T_j\right) \tag{2.60}$$

$$h_{r,i-j} = \frac{\sigma\left(T_i^2 + T_j^2\right)\left(T_i + T_j\right)}{\frac{1-\varepsilon_i}{\varepsilon_i} + \frac{A_i(1-\varepsilon_j)}{A_j\varepsilon_j} + \frac{1}{W_{i,j}}} \tag{2.61}$$

If the two surfaces are rectangular and parallel to each other, then $W_{i-j} \approx 1$ and $A_i = A_j$. Consequently, Eq.(2.61) reduces to:

$$h_{r,i-j} = \sigma\varepsilon_{i,j}\left(T_i^2 + T_j^2\right)\left(T_i + T_j\right) \tag{2.62}$$

$$\varepsilon_{i,j} = \frac{1}{\varepsilon_i} + \frac{1}{\varepsilon_j} - 1 \tag{2.63}$$

2.2.4 Thermal resistance

The flow of heat is analogous to that of an electric current. Thermal energy flows from a point at higher temperature to another point at lower temperature, encountering resistance in the process. For conductive, convective and radiative heat transfers, the corresponding resistances are given by (Sebald et al., 1979; Hsieh, 1981; ASHRAE, 2001):

$$R_{cd} = \frac{x}{kA} \tag{2.64}$$

$$R_c = \frac{1}{h_c A} \tag{2.65}$$

$$R_r = \frac{1}{h_r A} \tag{2.66}$$

It is observed that R_{cd} increases with decreasing k for given values of A and x, which is useful in thermal insulation. Often, a material with a low value of k is used as an insulator to curtail heat loss from a thermal system. Similarly, convective and radiative resistances increase with decreasing their corresponding coefficients of heat transfer for a constant value of A. Thermal resistance due to evaporative heat transfer (R_e) is computed by replacing h_c with h_e in Eq.(2.65).

The effective resistance for a given thermal network is found by using laws similar to those of electrical resistance for series or parallel connections (Sebald et al., 1979; Hsieh, 1981; ASHRAE, 2001).

$$R_{ef} = R_1+R_2+...+R_r\text{, for series connection} \tag{2.67}$$

$$\frac{1}{R_{ef}} = \frac{1}{R_1} + \frac{1}{R_2} + ... + \frac{1}{R_r}\text{, for parallel connection} \tag{2.68}$$

Eqs.(2.67) and (2.68) are useful in the analysis of a real thermal system with multiple resistances. For instance, a solar still has composite resistances. Consequently, this system can also be analyzed by using the resistance method.

2.2.5 Mass transfer

Mass transfer takes place through molecular diffusion or convection. In molecular diffusion, molecules of a fluid diffuse into the matrix of another fluid or solid (Incropera et al., 2007). For instance, water vapour from a water surface may diffuse into the surrounding air to form a binary mixture over the surface. The transfer of mass in a binary mixture is initiated by a density gradient and diffusion stops when the gradient is zero. Molecular diffusion in one dimension for a binary mixture (of substances A and B, where substance B is dilute) can be described by Fick's law (Bird et al., 1960 cited in ASHRAE, 2001):

$$\dot{m}' = \varphi_B V - D\varphi \frac{d(\varphi_B / v)}{dx} \tag{2.69}$$

$$\varphi=\varphi_A+\varphi_B \tag{2.70}$$

For a solid or stagnant fluid (V=0) with $\varphi_B << \varphi$, Eq. (2.69) can be expressed in the form:

$$\dot{m}' = -D\frac{d\varphi_B}{dx} \qquad (2.71)$$

The mass diffusivity of water vapour (D_v) in air can be taken as 2.55x10^{-5} m^{2}s^{-1} at T=298 K and P= 101325 N m^{-2}. It is also calculated according to Sherwood and Pigford (1952), as cited in ASHRAE (2001):

$$D_v = \frac{9.26x10^{-10}}{P}\left(\frac{T^{2.5}}{T+245}\right) \qquad (2.72)$$

The fundamental principles of solar radiation, and heat and mass transfer discussed in the preceding sections of this chapter are related to the solar distillation process in Section 2.3.

2.3 Heat and mass transfer as applied to solar distillation process

Saline water in the basin of a solar still is heated by solar radiation that passes through the transparent cover and is absorbed by the water and bottom part of the basin liner. Vapour rises from the hot water and condenses when it gets into contact with the inner surface of the transparent cover at or below dew point. The condensate is collected through a channel fitted along the lower edge of the transparent cover.

The solar distillation process involves all the three modes of heat transfer (Fig.2.9a). There is heat conduction through the transparent cover, bottom and side walls, which results in a loss of heat from the still. This loss can be reduced by using a thick insulation layer with a relatively low k-value. Heat from the basin liner is transferred to the saline water by convection while thermal energy from the hot water is transferred by vaporization, convection and radiation, onto the condensing cover. Water vapour condenses on the cover, yielding latent heat of condensation and distilled water.

In turn, the cover dissipates heat to the environment by convective and radiative heat transfer modes. It should be noted that internal heat transfer in a solar still also includes mass transfer. Consequently, special correlations are used to estimate the coefficients of convective and evaporative heat transfers from hot water to the transparent cover surface. A resistance network for a conventional solar distillation system is shown in Fig.2.9(b).

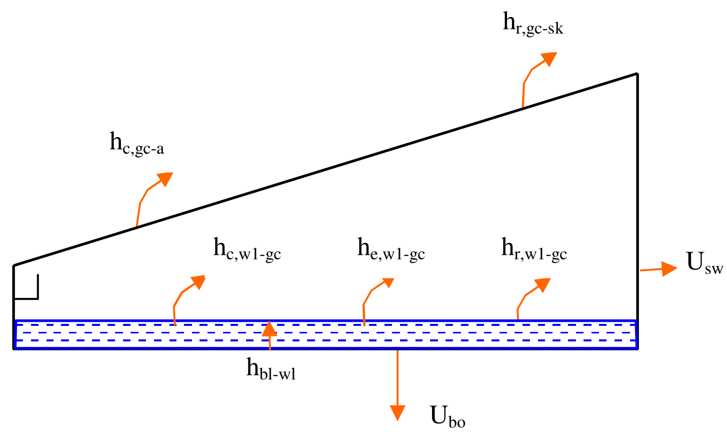

Fig.2.9(a): Heat transfer modes in a conventional solar still.

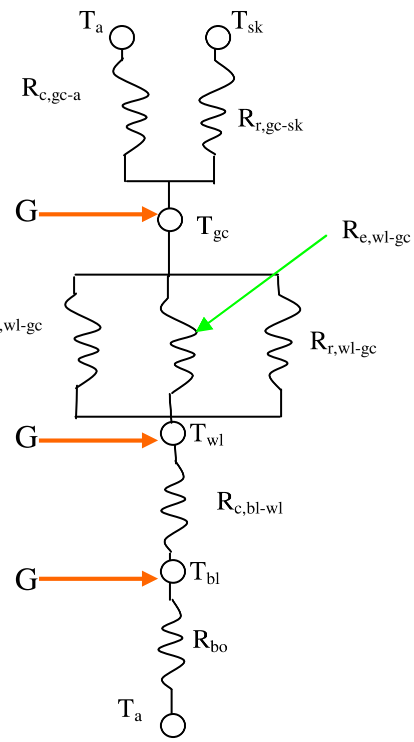

Fig.2.9(b): A thermal resistance network corresponding to the heat transfer modes in a conventional solar still.

Dunkle (1961) proposed the first correlation of the heat and mass transfer inside a solar still, with b=0.075 and d=1/3 in Eq.(2.47). Some limitations of this correlation have been reported in literature. Cooper (1970), as cited in Kumar and Tiwari (1996), observed that the correlation is appropriate for upward heat transfer across a horizontal air space. Rheinlander (1982) developed an alternative model for estimating heat and mass transfer in a basin type solar still. It was found that there was good agreement between theoretical and experimental data. Clark (1990) pointed out that Dunkle's correlation overestimated the evaporative coefficient of heat transfer at temperatures exceeding 328 K, and he therefore formulated a suitable model for calculating the convective and evaporative coefficients of heat transfer in solar stills operating at higher average temperatures (>328 K). Kumar and Tiwari (1996) reported that the correlation did not take into account the volume of the air space between the hot water and the condensing cover. So, they included the mean height of the air space between the saline water and the cover in their model, and found that b=0.0322 and d=0.4114 for a passive solar still, and b=0.0538 and d=0.383 for an active solar distiller. Tsilingiris (2007) studied the influence of using the thermophysical properties of the mixture of moisture and dry air in the derivation of the coefficients of heat and mass transfer in solar stills. It was found that the accuracy of modelling the transfer of heat and mass in solar stills improved when the thermophysical properties of a binary mixture were used instead of the thermophysical properties of dry air. Recently, Tsilingiris (2009) reported the following general equations for calculating coefficients of heat transfer by natural convection and evaporation from the surface of hot water to a condensing cover:

$$h_{c,w-cs} = bk_a S^{3d-1}\left(\frac{g\varphi_a\beta'_a}{\mu_a\alpha'_a}\right)^d\left[\left(T_w - T_{cs}\right) + \frac{T_w\left(P_w - P_{cs}\right)\left(M_a - M_v\right)}{M_a P_{to} - P_w\left(M_a - M_v\right)}\right]^d \quad (2.73)$$

$$h_{e,w-cs} = \frac{1000L'_w h_{c,w-cs} R_{ai}}{C_{p,a} R_v}\frac{P_{to}}{\left(P_{to} - P_w\right)\left(P_{to} - P_{cs}\right)} \quad (2.74)$$

Thermophysical properties of a binary mixture were used in the study. It was found that d=1/3 can be used in a wide range of operating temperatures for a practical solar still, and b=0.075 when the rate of distillation is lower than $1\text{x}10^{-4}$ kg m^{-2} s^{-1} and b=0.05 at higher distillate outputs. In addition, there was good agreement between theoretical and experimental rate of distillate production.

Heat loss from the top of the glass cover to the environment is predominantly by convection (to ambient air) and radiation (to sky). Wind influences the convective heat transfer from the top part of the cover and the wind coefficient of heat transfer can be calculated from (Wattmuf et al., 1977):

$$h_{c,gc-a} = \begin{cases} 2.8 + 3V_{wd}, V_{wd} \le 5ms^{-1} \\ 6.15V_{wd}^{0.8}, V_{wd} > 5ms^{-1} \end{cases} \quad (2.75)$$

Eq.(2.62) is commonly used to compute the coefficient of radiative heat transfer inside a basin-type solar still, and radiative heat loss from the top can be referenced to the sky and computed from:

$$h_{r,gc-sk} = \sigma\varepsilon_{gc}(T_{gc}^2 + T_{sk}^2)(T_{gc} + T_{sk}) \tag{2.76}$$

The sky temperature can be computed from (Sharma and Mullick, 1991):

$$T_{sk} = 0.0552 T_a^{1.5} \tag{2.77}$$

Heat is also lost from the bottom part of the still. The coefficient of bottom heat loss can be calculated from (Anderson, 1983):

$$\mathrm{U}_{\mathrm{bo}} = k / x \tag{2.78}$$

The distillate yield (Y) in a time interval of (t_2-t_1) can be calculated as follows:

$$Y = \int_{t_1}^{t_2} \left[\frac{h_{e,w-sc}(T_w - T_{sc})}{L'_w} \right] dt \tag{2.79}$$

The specific latent heat of water vaporization (L′) can be calculated using a correlation reported by Belessiotis et al. (1995) while the saturation vapour pressure (P) can be computed according to ASHRAE (2001) and the total pressure can be taken to be approximately equal to the standard atmospheric pressure (Tsilingiris, 2009).

2.4 Some limitations to previous work

2.4.1 Distribution of solar radiation in a single slope solar still

Mathematical modelling plays a vital role in the development of different types of technologies. Consequently, it also finds application in the design and simulation experiments of solar energy systems, including solar stills.

Modelling of the solar distillation process requires input variables that may be climatic or non-climatic. Climatic variables include solar radiation, ambient temperature, wind speed and atmospheric pressure. Fortunately, long-term primary data for most of these climatic variables is available at many sites in the world. This data can directly be used in predicting the output from a solar still, yielding relatively accurate results. Non-climatic variables include design and operating parameters. For a given set of system design parameters (basin area, insulation thickness, aperture size, colour of absorber surface and others), the distillate output from the system is influenced by climatic and operational factors (Garg and Mann, 1976). In particular, solar radiation is the most influential environmental parameter (Nafey et al., 2000). It is therefore necessary to know its distribution inside the solar still in order to accurately establish the actual amount of solar energy absorbed by saline water.

Some attempts have been made to determine the proportion of incident solar radiation that contributes to the heat and mass transfer processes in a conventional solar still (CSS). Cooper (1973) studied the factors that affect the efficiency of a single-slope solar still with a horizontal basin, taking into consideration the proportion of solar radiation reflected from the walls onto the surface of saline water. It was estimated that irradiance on the water increased by 10 %. Nevertheless, a model was not established for calculating the reported fraction. Tripathi and Tiwari (2004) proposed a model for computing the distribution of solar radiation inside a single-slope solar still. In their model, they also took into account the part of solar radiation reflected from the walls onto the water surface, and calculated the solar fraction for the back wall. They found that the effect of solar fraction was significant at low solar altitudes. Later, Tripathi and Tiwari (2006) used the same model to study passive and active solar stills with a single slope. Again, they found that solar fraction was significantly influential at low solar altitudes. More recently, Tiwari and Tiwari (2007) studied the annual and seasonal performance of a conventional solar distiller with one slope by using the idea of solar fraction. Their results were in close conformity with findings from other studies.

The model proposed by Tripathi and Tiwari (2004) and used in subsequent studies, is realistic because it attempts to quantify the actual amount of solar energy that contributes to the heat and mass transfer processes in a solar still. In their analysis, the solar fraction on the back wall is computed from the azimuth and altitude angles of the sun, and the latitude and longitude of the site for a given geometry of the still. This indicates that the solar fraction provided by their model is derived based on the properties of beam radiation only. However, they applied the computed values of solar fraction to global irradiance, to obtain effective irradiance, which comprises both beam and diffuse components. Moreover, their model did not take into account the view factor of surfaces exchanging radiation, and it yielded a root mean square error of 32.13 %. Thus, models based on these findings would have limited accuracy.

El-Swify and Metias (2002) used plane reflectors to augment solar radiation falling on the water surface in a solar still with single slope. It was found that reflectors increased distillate output. Tanaka and Nakatake (2006) performed a theoretical analysis of a solar still with internal and external reflectors. They found that the reflectors raised the productivity of the solar distiller. Later, Tanaka and Nakatake (2007a) numerically studied the performance of a solar still with an internal vertical reflector and inclined external reflector. They found that a tilted external reflector increased the distillate yield. Madhlopa and Johnstone (2009a) proposed a model for calculating solar fraction in a single-slope solar still of the conventional variety. They found that the beam solar fraction was affected by both the geometry of the solar still and position of the sun in the sky but the diffuse solar fraction was only dependent on the geometry of the solar distillation system. Their model exhibited a lower root mean square error than that of the previous model. It was concluded that splitting global radiation into its beam and diffuse components and applying view factors to surfaces that exchange radiation improved the accuracy of distillate yield prediction. Again, Madhlopa and Johnstone (2009b) theoretically studied a solar still with separate condenser. Simulation results showed that this still produced more distilled water than a CSS under the same meteorological conditions. Nevertheless, previous studies on solar stills with internal and external reflectors did not take into consideration the view factors of receiving and reflecting surfaces. Consequently, the accuracy of the previous models for predicting the distillate production of this variety of solar stills would be limited.

2.4.2 Solar still design

In a solar still, the difference between the temperature of water and cover is the driving force of the distillation process (Eq. 2.79). It influences the rate of evaporation from the surface of water in the basin to the condensing cover. However, the heat transferred from hot water to the transparent cover elevates the temperature of the cover as well, thereby reducing the driving force and rate of distillation in a CSS. Consequently, the CSS suffers from low efficiency (Al-Kharabsheh and Goswami, 2003). In view of this, many researchers have attempted to improve its performance through different modifications, including: reduction of heat loss from the bottom to increase useful energy (Cooper, 1969), use of a dye with a high absorptance in saline water to augment solar absorption by the water (Garg and Mann, 1976; Tamini, 1987), use of reflectors to increase solar radiation incident on saline water (Tamini, 1987), decreasing the depth of saline water in the basin (Lawrence et al., 1990), cooling the condensing cover (Tiwari et al., 1985; Lawrence et al., 1990), use of internal (Ahmed, 1988) and external condensers (El-Bahi and Inan, 1999a), suspending a baffle in the basin (El-Sebaii et al., 2000), inclusion of storage elements in the still (Naim and Kawi 2002a), use of charcoal (Naim and Kawi 2002b) and sponge cubes in the basin (Bassam et al., 2003), and integration of an asymmetric compound parabolic concentrator and extra vessel that acted as a heat sink to a single-slope solar still (Smyth et al., 2005).

Based on the various modifications, solar stills are broadly classified into active and passive systems (Tiwari et al., 2003). The active variety is supplied with additional thermal energy from an external source (such as a flat plate or concentrator collector) to augment the temperature of the saline water in the basin, and this class of stills is suitable for commercial production of distilled water. The passive variety does not employ an outside source of energy but water vapour flows from the evaporator to the condensing cover by natural (convection, diffusion and purging) or forced circulation in both classes of stills. Natural circulation does not require a blower, thereby reducing costs associated with forced circulation.

Different types of solar stills have been reported in literature, including basin (Löf et al., 1968; Sodha et la., 1980; El-Bassuoni and Tayeb, 1994) and wick stills (Tiwari, 1984; Minasian and Al-Karaghouri, 1995; Tanaka and Nakatake, 2007b). In a basin type solar still, saline water is fed into a basin where it is heated by incoming solar radiation. Then, vapour from the hot saline water is condensed to produce distilled water (Figs.1.1 (a) and (b)). A conventional solar still has one basin with no heat recovery from the transparent cover which results in a low efficiency (Al-Kharabsheh and Goswami, 2003). Nevertheless, multiple basins may be stacked to recover heat (Mahdi, 1992; Tiwari et al., 1993; Al-Hinai, 2002). In this case, the lowest basin liner is blackened while the other basin liners are made of a transparent sheet (such as glass) to allow incoming solar radiation reach the bottom part of the still (Fig.2.10 (a)). In a wick type solar still, a blackened wick is soaked with saline water and heated by incoming solar radiation (Fig.2.10 (b)). Again, vapour from the hot wet wick is condensed to produce distilled water. Basin type solar stills are common and they have been exploited in supplying clean water in areas that cannot be easily accessed (Varun, 2009). So, this study examines this type of stills with separate condensers.

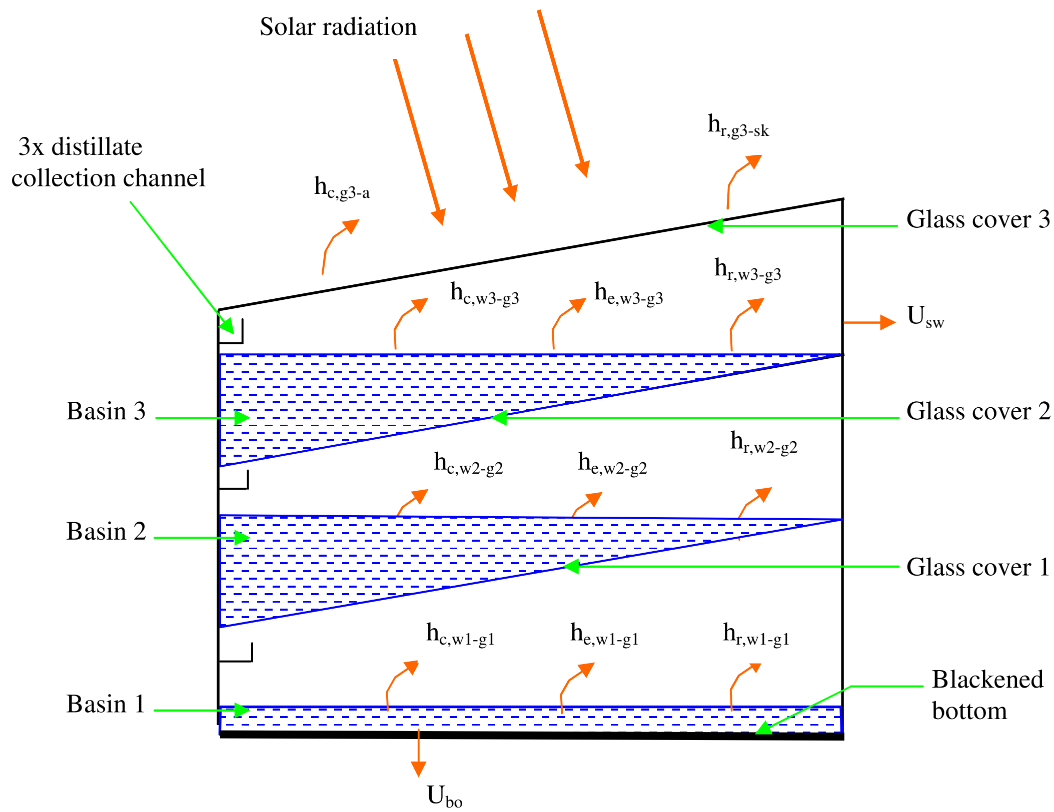

(a)

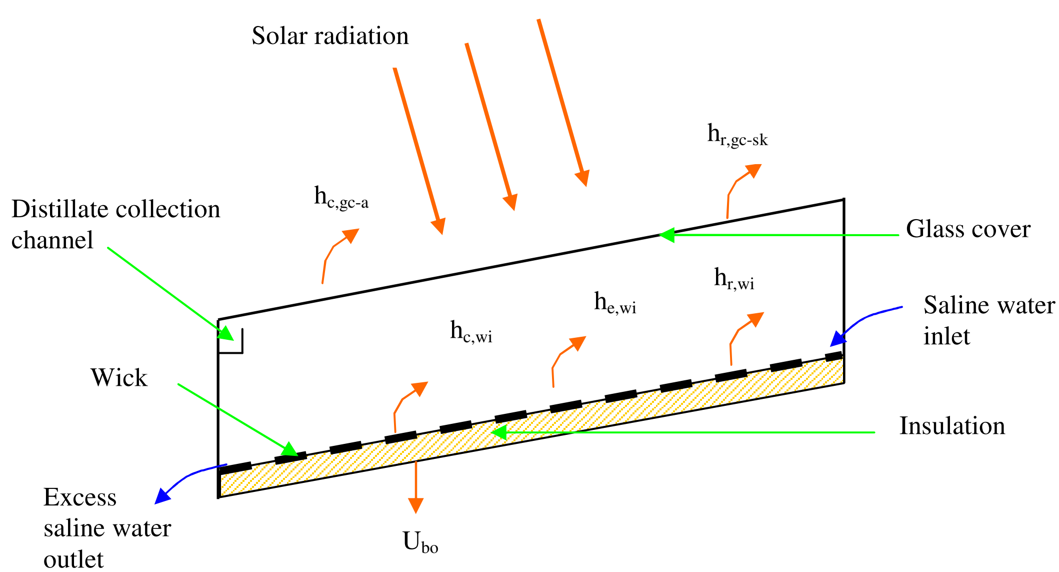

(b)

Fig.2.10: Examples of a) multi-basin and b) wick type solar stills.

Several researchers have suggested design improvements to the passive solar still with separate condenser and natural circulation of water vapour. Fath and Elsherbiny (1993) added an external condenser to a single-slope solar still. The condenser was located in the shadow zone of the still. A reflecting mirror was fitted on the back wall to augment the amount of solar radiation reflected from the wall onto the surface of saline water. They found that there was an increase in the still efficiency. El-Bahi and Inan (1999a) developed a solar still with double-glazing and a separate condenser. The condenser, with a vertical reflector in its front part, was located on the shaded side of the evaporator. This still design enabled the saline water to receive direct and reflected solar radiation. Results showed that the distillate productivity conformed to findings from previous work and it increased when the condenser was cooled by running cold water over the glass cover. Again, El-Bahi and Inan (1999b) studied a solar still with one glass cover, and a separate condenser. A vertical steel reflector was fitted on the front part of the condenser to increase the proportion of solar radiation falling on the water surface. The reflector cast a shadow over the condenser system. It was found that the solar still with separate condenser performed better than the solar distillation system without a separate condenser. Later, Fath and Hosny (2002) studied the thermal performance of a single sloped solar still with an additional condenser. They found that distillate yield was influenced by the intensity of solar radiation, bottom insulation, mass of basin, area of evaporation surface and reflectance of the inner surface of the condenser.

The designs of a solar still with separate condenser examined in all these previous studies can be fabricated using locally-available skills and materials in developing countries. However, the condenser unit is located in the shadow zone of the still (without a solar shield), which exposes the unit to diffuse and ground-reflected components of solar radiation. Consequently, the temperature of an unshielded separate condensing cover would rise significantly during day time.

2.5 Summary

In this chapter, fundamentals of solar radiation, and heat and mass transfer have been presented. Outside the earth's atmosphere, all solar radiation is direct and it is known as extraterrestrial radiation. As the radiation propagates through the atmosphere, it is attenuated, resulting in beam and diffuse components. These components of solar radiation have different optical characteristics. View factors influence exchange of radiation between two surfaces with given thermophysical properties. Heat is transferred by conduction, convection or radiation while mass transfer is by convection and diffusion. These basic principles are related to a solar still which intercepts solar radiation and converts it to thermal energy. It is highlighted that solar radiation intensity is the most influential environmental factor in this distillation process. Thus, it is necessary to know its distribution inside a solar still for accurate modelling of the distillation process. Nevertheless, previous models on the distribution of solar radiation in a solar still ignored view factors, and so, their accuracy would be limited. Solar distillation involves heat and mass transfer, with all the three modes of heat transfer existing in the distillation process. It is noted that a CSS has limited efficiency. In view of this, various improvements including the use of reflectors and separate condenser have been made. It is argued that exposing a separate condenser to solar radiation would curtail distillate productivity. Finally, it appears that there is paucity of information on a) modelling a solar still with separate condenser and reflectors by splitting global radiation into its beam and diffuse components and taking into consideration the optical view factors of the reflecting and receiving surfaces, and b) a solar distillation system with a shielded separate condensing cover. This investigation attempts to overcome these limitations as shown in the next chapters.

2.6 References

Ahmed, S.T., 1988. Study of a single effect solar still with an internal condenser. *Solar & Wind Technology*, 5, pp.637-643.

Al-Hinai, H., Al-Nassri, M.S. and Jubran, B.A., 2002. Parametric investigation of a double-effect solar still in comparison with a single-effect solar still. *Desalination*, 150, pp.75-83.

Al-Kharabsheh, S. and Goswami, D.Y., 2003. Experimental study of an innovative solar water desalination system utilizing a passive vacuum technique. *Solar Energy*, 75, pp.pp.395-401.

Andesron, E.E., 1983. *Fundamentals of solar energy conversion*. Reading: Addison-Wesley Publishing Company, pp.52-53, 193-195.

ASHRAE, 1991. *ANSI/ASHRAE Standard 93: Methods of testing to determine the thermal performance of solar collectors*. Atlanta: American Society of Heating, Refrigerating and Air-Conditioning Engineers.

ASHRAE, 2001. *ASHRAE Handbook Fundamentals, SI ed*. Atlanta:American Society of Heating, Refrigerating and Air-Conditioning Engineers.

Bassam, A., Abu-Hijley, K. and Rababa'h, H.M., 2003. Experimental study of a solar still with sponge cubes in basin. *Energy Conversion and Management*, 44, pp.1411-1418.

Belessiotis, V., Voropoulos, E. and Delyannis, E., 1995. Experimental and theoretical method for determination of the daily output of a still: input-output method. *Desalination*, 100, pp.99-104.

Bird, R.B., Stuart, W.E. and Lightfoot, E.N., 1960. Transport phenomena. New York: John Wiley and Sons.

Boltzmann, L., 1884. Ableitung des Stefan'schen Gesetzes betreffend die Abhängigkeit der Wärmestrahlung von der Temperatur aus der electromagnetischen Lichttheorie. *Annalen der Physik und Chemie*, 22, pp.291-294.

Braun, J.E. and Mitchell, J.C., 1983. Solar geometry for fixed and tracking surfaces. *Solar Energy*, 31, pp.439-444.

Briscoe, B.J. and Galvin, K.P., 1991. The effect of surface fog on the transmittance of light. *Solar Energy*, 46, pp.191-197.

Clark, J. A., 1990. The steady state performance of a solar still. *Solar Energy*, 44, pp.43-49.

Cooper, P.I., 1969. The absorption of radiation in solar stills. *Solar Energy*, 12, pp.333-346.

Cooper, P. I., 1970. *The transient analysis of glass cover solar still*. Ph.D. Thesis: University of Western Australia.

Cooper, P.I., 1973. The maximum efficiency of single-effect solar stills. *Solar Energy*, 15, pp.205-217.

Crepeau, J., 2007. Joseph Stefan: His life and legacy in the thermal sciences. *Experimental Thermal and Fluid Science*, 31, pp.795-803.

Darula, S., Kittler, R. and Gueymard, C.A., 2005. Reference luminous solar constant and solar luminance for luminance calculations. *Solar Energy*, 79, pp.559-565.

Dave, J.V., 1977. Validity of the isotropic-distribution approximation in solar energy estimations. *Solar Eenrgy*, 19, pp.331-333.

Duffie, J.A. and Beckman, W.A., 2006. *Solar Engineering of Thermal Processes*. 3rd ed. New York:Wiley Interscience, pp.5-41, 85-103.

Dunkle, R.V., 1961. Solar water distillation: the roof type still and a multiple effect diffusion still. *International Development in Heat Transfer: International Heat Transfer Conference*. University of Colorado, 895-902 (part 5).

Edlin, F.E., 1958. Plastic glazings for solar energy collectors. *Solar Energy*, 2, pp.3-6.

El-Bahi, A. and Inan, D., 1999a. Analysis of a parallel double glass solar still with separate condenser. *Renewable Energy*, 17, pp.509-521.

El-Bahi, A. and Inan, D., 1999b. A solar still with minimum inclination, coupled to an outside condenser. *Desalination*, 123, pp.79-83.

El-Bassuoni, A.A. and Tayeb, A.M., 1994. Factors influencing basin-type solar desalination units. *Energy Conversion and Management*, 38, pp.693-698.

El-Sebaii, A.A., Aboul-Enein, S. and El-Bialy, E., 2000. Single basin still with baffle suspended absorber. *Energy Conversion and Management*, 41, pp.661-675.

El-Swify, M.E. and Metias, M.Z., 2002. Performance of double exposure solar still. *Renewable Energy*, 26, pp.531-547.

Fath, H.E.S. and Elsherbiny, S.M., 1993. Effect of adding a passive condenser on solar still performance. *Energy Conversion and Management*, 34, pp.63-72.

Fath, H.E.S. and Hosny, H.M., 2002. Thermal performance of a single-sloped basin still with an inherent built-in additional condenser. *Desalination*, 142, pp.19-27.

Foster, R., Ghassemi, M. and Cota, A., 2009. *Solar energy: Renewable energy and the environment*. Boca Raton: CRC Press, pp.7-52.

Fourier, J., 1822. Théorie analytique de la chaleur. Gauthiers – Villars, Paris, 1888.

Frohlich, C., 1977. Contemporary measures of the solar constant. In: O.R.White, ed. 1977. *The Solar Output and its variation*. Boulder: Colorado Associated Press.

García-Rodrígue, L., 2003. Renewable energy applications in desalination: state of the art. *Solar Energy*, 75, pp.381-393.

Garg, H.P., 1982. *Treatise on Solar Energy, vol. 1: Fundamentals of Solar Energy*. New York: John Wiley & Sons.

Garg, H.P. and Datta, G., 1993. Fundamentals and characteristics of solar radiation. *Renewable Energy*, 3, pp.305-319.

Garg, H.P. and Mann, H.S., 1976. Effect of climatic, operational and design parameters on the year round performance of single-sloped and double-sloped solar still under Indian arid zone conditions. *Solar Energy*, 18, pp.159-164.

Gruber, C. and Lesne, A., 2005. Hamiltonian model of heat conductivity and Fourier law. *Physica A*, 351, pp.358-372.

Gueymard, C.A., 2001. Parameterized transmittance model for direct beam and circumsolar spectral irradiance. *Solar Energy*, 71, pp.325-346.

Gueymard, C.A., 2004. The sun's total and spectral irradiance for solar energy applications and solar radiation models. *Solar Energy*, 76, pp.423-453.

Hay, J.E. and Davies, J.A., 1980. Calculation of the solar radiation incident on an inclined surface. In: J.E.Hay and T.K. Won, eds. 1980. *The first Canadian Solar Radiation Data Workshop*. Canada 59: Ministry of Supply and Services

Hewitt, G.F., Shires, G.L. and Bott, T.R., 1994. *Process heat transfer*. Boca Raton: CRC Press, pp.120-150.

Hollands, K.G.T., Unny, T.E., Raithby, G.D. and Konicek, L., 1976. Free convective heat transfer across inclined air layers. *Transactions of the ASME Journal of Heat Transfer*, 98, pp.189-193.

Howell, J.R., Bannerot, R.B. and Vliet, G.C., 1982. *Solar-thermal energy systems: A Analysis and design*. New York: McGraw_hill Book Company, pp.46-62.

Hsieh, C.K., 1981. Thermal analysis of CPC collectors. *Solar Energy*, 27, pp.19-29.

Incropera, F.P., DeWitt, D.P., Bergman, T.L. and Lavine, A.S., 2007. *Fundamentals of heat and mass transfer*. 6th ed. New Jersey: John Wiley & Sons, pp.880-915.

Ineichen, P., 2008. A broadband simplified version of the Solis clear sky model. *Solar Energy*, 82, pp.758-762.

ISO, 1994. *ISO 9806-1:1994(E): Test Methods for Solar Collectors –Part 1: Thermal Performance of Glazed Liquid Heating Collectors Including Pressure Drop*.Geneva: ISO.

Jacob, M., 1949. *Heat transfer*. first ed., vol.1. New York:John Wiley & Sons.

Jain, P.C., 1988. Accurate computations of monthly average daily extraterrestrial irradiation and the maximum possible sunshine duration. *Solar & Wind Energy Technology*, 5, pp.41-53.

Jansen, T.J., 1985. *Solar Engineering Technology*. New Jersey: Prentice-Hall Inc..

Johnson, F.S., 1954. The solar constant. *Meteorology*, 11, p.431.

Kane, R.P., 2005. Sun-earth relation: Historical development and present status – a brief review. *Advences in Space Research*, 35, 866-881.

Kipp & Zonen, 2006. *Instruction manual: CMP series 11/CMA series pyranometers / albedometer*. Delft: Kipp & Zonen.

Kudish, A.I. and Evseev, E.G., 2008. Assessment of four different correction models applied to the diffuse radiation measured with a shadow ring using global and and normal beam radiation measurements for Beer Sheva, Israel. *Solar Energy*, 82, pp.144-156.

Kumar, S. and Tiwari, G.N., 1996. Estimation of convective mass transfer in solar distillation systems. *Solar Energy*, 57, pp.459-464.

Lawrence, S.A., Gupta, S.P. and Tiwari, G.N., 1990. Effect of heat capacity on the performance of solar still with water flow over the glass. *Energy Conversion and Management*, 30, pp.277-285.

Lienhard IV, J.H., and Lienhard V, J.H., 2006. *A heat transfer textbook*. 3rd ed. Cambridge Massachusetts: Phlogiston Press.

Liu, B.Y.H. and Jordan, R.C., 1960. The interrelationship and characteristic distribution of direct, diffuse and total radiation. *Solar Energy*, 4, pp.1-19.

Liu, B.Y.H. and Jordan, R.C., 1963. The long-term average performance of flat-plate solar energy collectors. *Solar Energy*, 7, pp.53-74.

Löf, G.O.G., Close, D.J. and Duffie, J.A., 1968. A philosophy for solar energy development. *Solar Energy*, 12, pp.243-250.

Lorenz, W., 1998. Design guidelines for a glazing with a seasonally dependent solar transmittance. *Solar Energy*, 63, pp.79-96.

MacIntyre, D.A., 1974. The thermal radiation field. *Building Science*, 9, pp.247-262.

Madhlopa, A. and Johnstone, C., 2009a. Model for computation of solar fraction in a single-slope solar still. *Solar Energy*, 83, pp.873-882.

Madhlopa, A. and Johnstone, C., 2009b. Numerical study of a passive solar still with separate condenser. *Renewable Energy*, 34, pp.1668-1677.

Mahdi, N.A., 1992. Performance prediction of a multi-basin solar still. *Energy*, 17, pp.87-93.

Minasian, A.N. and Al-Karaghouri, A.A., 1995. An improved solar still: The wick-basin type. *Energy Conversion and Management*, 36, pp.213-217.

Mishra, S.C., Shukla, A. and Yadav, V., 2008. View factor calculation in the 2-D geometries using the collapsed dimension method. *International Communications in Heat and Mass Transfer*, 35, pp.630-636.

Nafey, A.S., Abdelkader, M., Abdelmotalip, A. and Mabrouk,A.A., 2000. Parameters affecting solar still productivity. *Energy Conversion and Management*, 41, pp.1797-1809.

Naim, M.M. and Kawi, M.A.A.E., 2002a. Non-conventional solar stills with energy storage element. *Desalination*, 153, pp.71-80.

Naim, M.M. and Kawi, M.A.A.E., 2002b. Non-conventional solar stills with charcoal particles as absorber medium. *Desalination*, 153, pp.55-64.

Puri, V.M., Jimenez, R., Menzer, M. and Costello, F.A., 1980. Total and non-isotropic diffuse insolation on tilted surfaces. *Solar Energy*, 25, pp.85-90.

Quaschning, V. and Hanitsch, R., 1998. Irradiance calculation on shaded surfaces. *Solar Energy*, 62, pp.369-375.

Rappaport, P., 1959. The photovoltaic effect and its utilization. *Solar Energy*, 3, pp.8-18.

Rheinlander, J., 1982. Numerical calculation of heat and mass transfer in solar stills. *Solar Energy*, 28, pp.173-178.

Reindl, D.T., Beckman, W.A. and Duffie, J.A., 1990. Evaluation of hourly tilted surface radiation models. *Solar Energy*, 45, pp.9-17.

Sabbagh, J.A., 1977. Heat transfer for solar energy utilization. In: A.A.M. Sayigh, ed. 1977. *Solar energy engineering*. New York: Academic Press, pp.83-103

Sanders, C.J. and Holman, J.P., 1972. Franz Grashof and the Grashof number. *Heat and Mass Transfer*, 15, pp.562-563.

Sailor, D.J., Resh, K. and Segura, D., 2006. Field measurement of albedo for limited extent test surfaces. *Solar Energy*, 80, pp.589-599.

Sebald, A.V., Clinton, J.R. and Langenbacher, F., 1979. Performance effects of Trombe wall control strategies. *Solar Energy*, 23, pp.479-487.

Sharma, M.R. and Pal, R.S., 1965. Total, direct and diffuse solar radiation in the Tropics. *Solar Energy*, 9, pp.183-192.

Sharma, V.B. and Mullick, S.C., 1991. Estimation of heat-transfer coefficients, the upward heat flow, and evaporation in a solar still. *ASME Journal of Solar Engineering*, 113, pp.36-41.

Sherwood,T.K. and Pigford, R.L., 1952. *Absorption and extraction*. New York: MacGraw-Hill.

Smyth, M., Norton, B. and Byres, W., 2005. Measured effect of reflector augmentation of simple basin type solar stills. *Ambient Energy*, 26, pp.59-70.

Sodha, M.S., Nayak, J.K., Tiwari, G.N. and Kumar, A., 1980. Double basin solar still. *Energy Conversion and Management*, 20, pp.23-32.

Suehrcke, H., 1994. The effect of time errors on the accuracy of solar radiation measuerement. *Solar Energy*, 53, pp.353-357.

Tamini, A., 1987. Performance of a solar still with reflectors and black dye. *Solar & Wind Technology*, 4, pp.443-446.

Tanaka, H. and Nakatake, Y., 2006. Theoretical analysis of a basin type solar still with internal and external reflectors. *Desalination*, 197, pp.205-216.

Tanaka, H. and Nakatake, Y., 2007a. Effect of inclination of external flat plate reflector of basin type still in winter. *Solar Energy*, 81, pp.1035-1042.

Tanaka, H. and Nakatake, Y., 2007b. Improvement of the tilted wick solar still by using a flat plate reflector. *Desalination*, 216, pp.139-146.

Tekelioglu, M., and Wood, B.D., 2009. Solar light transmission of polymer optical fibres. *Solar Energy*, 83, pp.2039-2049.

Tesfamichael, T. and Wäckelgård, E., 2000. Angular solar absorptance and incident angle modifier of selective absorbers for solar thermal collectors. *Solar Energy*, 68, pp.335-341.

Thekaekara, M.P., 1976. Solar radiation measurement: Techniques and instrumentation. *Solar Energy*, 18, pp.309-325.

Tiwari, G.N., 1984. Demonstration plant of a multi-wick solar still. *Enegry Conversion and Management*, 24, pp.313-317.

Tiwari, G.N., Madhuri and Garg, H.P., 1985. Effect of water flow over the glass cover of a single basin solar still with an intermittent flow of waste hot water in the basin. *Energy Conversion and Management*, 25, pp.315-322.

Tiwari, G.N., Singh, S.K. and Bhatnagar, V.P., 1993. Analytical thermal modelling of multi-basin solar still. *Energy Conversion and Management*, 34, pp.1261-1266.

Tiwari, G.N., Singh, H.N. and Tripathi, R., 2003. Present status of solar distillation. *Solar Energy*, 75, pp.367-373.

Tiwari, A.K. and Tiwari, G.N., 2007. Thermal modelling based on solar fraction and experimental study of the annual performance of a single slope passive solar still: The effect of water depths. *Desalination*, 207, pp.184-204.

Tripathi, R. and Tiwari, G.N., 2004. Performance evaluation of solar still by using the concept of solar fraction. *Desalination*, 169, pp.69-80.

Tripathi, R. and Tiwari, G.N., 2006. Thermal modelling of passive and active solar stills for different depths of water by using the concept of solar fraction. *Solar Energy*, 80, pp.956-967.

Tsilingiris, P.T., 2007. The influence of binary mixture thermophysical properties in the analysis of heat and mass transfer processes in solar distillation systems. *Solar Energy*, 81, pp.1482-1491.

Tsilingiris, P.T., 2009. Analysis of the heat and mass transfer processes in solar stills. *Solar Energy*, 83, pp.420-431.

Varun, A.K., 2009. Solar stills: A review. *Renewable and Sustainable Energy Reviews*, doi:10.1016/j.rser.2009.05.011.

Wattmuf, J.H., Charters, W.W.S. and Proctor, D., 1977. Solar and wind induced external coefficients for solar collectors. *Compless*, 2, p.56.

Yang, K., Huang, G.W. and Tamai, N., 2001. A hybrid model for estimating global solar radiation. *Solar Energy*, 70, pp.13-22.

Chapter 3

Development of a mathematical model

3.0 Introduction

Advances in solar distillation have been presented in chapter 2. It has been shown that a solar distillation system converts solar radiation into heat which is transferred from the absorber to different components of the system through convection, evaporation, conduction and radiation. Based on well-established fundamentals of solar radiation and heat and mass transfer, limitations to previous work were identified in solar still modelling and designing. As a step toward overcoming the former limitation, a mathematical model was developed in order to appraise the design and operational parameters of solar stills and to establish the sensitivity of these parameters through simulation.

Knowledge about design factors that influence the performance of a solar still is required in solar still simulation. These factors can broadly be classified into optical, heat transfer and heat loss characteristics (Cooper and Read, 1974). Optical characteristics comprise absorption, reflection and transmission of solar radiation when incident on the still. Once the radiation is absorbed by the still, it is converted to heat which is transferred from the absorber to other components of the still and the environment.

Internally, heat is transferred from the surface of hot saline water to the condensing cover through convection, evaporation and radiation. These modes of heat transfer are affected by the still geometry (Eqs.2.61, 2.73 and 2.74). Purging of vapour depends on the pressure difference inside the hot chamber (evaporator) and the cool chamber (condenser). Decreasing the volume of the evaporator relative to that of the condenser increases the pressure difference and therefore augments the rate of purging. Consequently, the ratio of the volume of the evaporator to that of the condenser affects the rate of heat transfer between the two spaces.

Heat is lost to the environment through the top, bottom and sides of the system. Heat loss through the top is desirable because it helps to keep the transparent cover temperature low, thereby increasing the rate of condensation and distillate production (Eq.2.79). On the other hand, heat loss through the bottom and side walls reduces useful thermal energy for the distillation process, and the productivity of the still. The various design factors that influence distillate productivity can be incorporated into a mathematical model that can be employed as a design tool for appraising the performance of the still. Some advantages of modelling have been mentioned in Chapter 2.

In this chapter, a mathematical model for simulating single slope solar stills is developed. This model takes into account the characteristics of solar radiation and optical view factors of surfaces that exchange radiation, and it is used to simulate a conventional solar still (CSS) and an advanced solar still (ASS) with separate condenser under the same meteorological conditions. Simulation results are presented and discussed in detail.

3.1 Energy system modelling

Advances in energy systems are resulting in complex configurations and processes which require appropriate computational tools for designing and performance appraisal. In this regard, simulation of energy systems is gaining acceptance as a suitable tool. It involves four tasks: a) building a physical model (such as a drawing) of the actual system, b) formulating a mathematical model from the physical model, c) applying a numerical method to obtain a solution, and d) putting into operation the numerical model to obtain results (Houbak, 1995). Each step in the simulation process is vital with regard to finding accurate results.

In building a physical model, it is necessary to draw the diagram of a system that is being modelled. Details of the major components of the system need to be captured in the drawing, with boundaries amongst the components clearly defined. In addition, assumptions are often made about processes that take place in a given system. Some of these processes are taken into account while others are neglected depending on reality. The next step, after building a physical model, is to formulate an appropriate mathematical model.

Basic principles (which include fundamental laws of heat and mass transfer such as those discussed in Chapter 2) are applied in formulating a suitable mathematical model. In practical thermal systems, heat may be transferred between a solid structure and its environment as shown in Fig.3.1. For transient transfer, the distribution of temperature inside the structure varies with time and space. If temperature gradients inside the solid are neglected, a lumped capacitance method may be used to find the variation of temperature with time (Incropera et al., 2007). So, the heat equation for solid structure with convective and radiative heat loss from its surface can be expressed as:

$$\rho V' C \frac{dT}{dt} = Q_{es} + Q_{ig} - \left[h_c (T - T_a) + \varepsilon\sigma\left(T^4 - T_{sr}^4\right)\right] \tag{3.1}$$

If the structure does not generate heat internally (Q_{ig}=0) with no heat flow from an external source (Q_{es}=0), then Eq.(3.1) reduces to:

$$\rho V' C \frac{dT}{dt} = -\left[h_c (T - T_a) + \varepsilon\sigma\left(T^4 - T_{sr}^4\right)\right] \tag{3.2}$$

The application of the lumped capacitance method depends on the Biot number (Bi), given by (Lienhard and Lienhard, 2006; Incropera et al., 2007):

$$Bi = \frac{T_1 - T_2}{T_2 - T_a} = \frac{h_c L}{k} \tag{3.3}$$

$$L = V'/A \tag{3.4}$$

The condition for use of the lumped capacitance method is (Shaw, 1993; Tan et al., 2009):

$$\mathrm{Bi} \le 0.1 \tag{3.5}$$

This method is important and preferred for finding solutions to heat-transfer problems of the transient variety (Incropera et al., 2007). Consequently, it is applied in the present mathematical model.

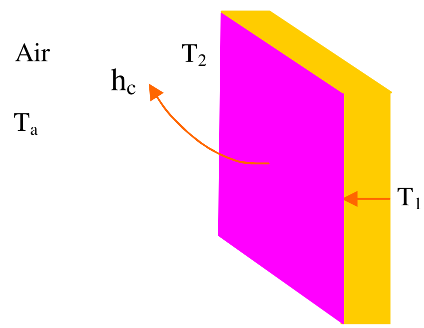

Fig.3.1: Heat transfer between a solid slab and ambient air ($T_a<T_2<T_1$).

In formulating a mathematical model, input variables to each major unit of an energy system are used to compute outputs from that unit. This often leads to a system of differential equations that can be solved analytically or numerically. However, Incropera et al. (2007) reported that analytical solutions to differential equations for transient systems are confined to simple geometries and boundary conditions. So, other differential equations can only be solved by numerical methods which yield approximate solutions.

Numerical techniques include finite element and finite difference methods. The former category of computational techniques is usually used to solve partial differential equations with boundary conditions that cannot be handled by finite difference methods (Burden and Faires, 1985). However, efficient error theorems for finite element methods are difficult to formulate and apply. On the other hand, finite difference methods have good stability but they require more effort to achieve a required accuracy. It is difficult to use finite difference methods on problems that involve derivatives and irregular regions. However, these methods exhibit an easier minimization procedure than finite element methods when applied to parabolic (such as the heat equation) and hyperbolic (such as the wave equation) partial derivatives. Moreover, finite difference methods are easier to apply (Incropera et al., 2007), and several authors have applied these techniques to solve a system of differential equations for solar distillation (Cooper, 1969; Abu-Qudais et al., 1996; Tchinda et al., 1999; Al-Hinai et al., 2002; Zurigat and Abu-Arabi, 2004). A finite difference scheme is therefore used in the present study.

A finite difference equation is written for each node in the nodal network, reducing the system to a set of linear algebraic equations. The system of algebraic equations can then be solved directly or iteratively. Direct methods include backward substitution, Gaussian elimination and matrix inversion, and are suitable for a small number of equations. In addition, they need a large computer memory and time. So, the iterative methods may be more efficient than the direct ones. Burden and Faires (1985) reported that iterative schemes are required to solve a non-linear system of differential equations. These schemes include the Jacobi and Gauss-Seidel methods. Generally, the Gauss-Seidel iterative method is superior to the Jacobi method. The former iterative method is therefore used in this investigation.

It should also be mentioned that a finite difference equation can be expressed in an explicit or implicit form. One drawback of the explicit method is its conditional stability (Incropera et al., 2007). As the time step increases, the solution may oscillate significantly from the steady-state conditions resulting in huge errors. In contrast, the convergence of a solution is unconditional in an implicit approach. For instance, the one-dimensional heat equation (Eq.2.39, assuming $\dot{q}=0$) can explicitly be discretized to:

$$\frac{1}{\alpha'}\frac{T_i^{j}-T_i^{j-1}}{\Delta t}=\frac{T_{i+1}^{j-1}+T_{i-1}^{j-1}-2T_i^{j-1}}{(\Delta x)^2} \tag{3.6}$$

where i=1, 2, 3… and j=1, 2, 3…

Solving for the interior ith nodal temperature at the jth time step yields:

$$T_i^{j}=F'\left(T_{i+1}^{j-1}+T_{i-1}^{j-1}\right)+\left(1-2F'\right)T_i^{j-1} \tag{3.7}$$

$$F'=\frac{\alpha'\Delta t}{(\Delta x)^2} \tag{3.8}$$

The accuracy of the finite difference method can be improved by decreasing the sizes of Δx and Δt. This increases the number of interior nodes and time steps and the computational time. So, the choice of mesh size is based on the accuracy and computational demands. In addition, stability constraints may be used to select the right values of Δx and Δt. For one dimensional interior node, the stability requirement is (Incropera et al., 2007):

$$F' \leq 1/2 \tag{3.9}$$

Consequently, Δt can be determined for fixed values of Δx and α′. It should also be mentioned that the one-dimensional heat equation can implicitly be discretized to:

$$\frac{1}{\alpha'}\frac{T_i^{j}-T_i^{j-1}}{\Delta t}=\frac{T_{i+1}^{j}+T_{i-1}^{j}-2T_i^{j}}{(\Delta x)^2} \tag{3.10}$$

Solving the implicit finite difference equation for the ith interior nodal temperature at the jth time step gives:

$$T_i^j = \frac{T_i^{j-1} + F_o\left(T_{i+1}^j + T_{i-1}^j\right)}{1 + 2F'} \tag{3.11}$$

Fortunately, there is no stability criterion for the implicit scheme because the solution is unconditionally stable. Lager values of Δx and Δt can be used with this method, thereby reducing the computational time. The final task in the simulation process is to solve the system of discretized equations which requires an appropriate computational platform.

Numerous simulation programs are in use by engineers and scientists around the world. These programs basically fall into: a) special purpose and b) general purpose categories (Nafey, 2005). A special purpose program is developed to simulate a specific process, with no flexibility. Any change to the process may demand extensive modifications to the program. Nevertheless, the advantage of a special purpose program is the simplicity of developing a mathematical model that adequately describes a real system. Consequently, several authors including Norton and Probert (1987), El-Nashar (1990), Zurigat and Abu-Arabi (2004) and Madhlopa and Ngwalo (2007) have developed special purpose programs or codes to simulate energy systems. These programs or codes are commonly written using programming languages such as BASIC, FORTRAN, Pascal and MATLAB (Burden and Faires, 1985; Vestlund et al., 2009). It should be mentioned that MATLAB is one of the powerful and popular generic programming languages for computations in engineering and science (Hoffbeck et al., 2001).

In contrast, a general purpose program is developed for simulation of different system configurations and operating conditions (Nafey, 2005). The model, in this case, comprises a set of equations for a given unit of the system. Each set of equations constitutes a module that may stand alone, and used in any process where it is required. Hence, a general purpose program comprises different modules, and it may be irrelevant to other computational problems due to its generality. Examples of well-known general purpose programs for simulating energy systems include EMPG2, EnergyPlus and TRNSYS. EMPG2 has features and capabilities for simulating a range of thermal systems, system control strategies and load types (Nafey, 2005) while TRNSYS is a modular program for simulating solar thermal systems (Klein et al., 1975; Duffie and Beckman, 2006). EnergyPlus is mainly suitable for building simulation (Loutzenhiser et al., 2007). Nevertheless, the choice to use a specific program depends on factors such as cost and computational capabilities of the program.

Both ESP-r and MATALAB computational platforms were available at the University of Strathclyde where the two solar stills were developed in this investigation. In addition, these solar energy systems were laboratory-scale units. However, the former computational tool is suitable for simulating the energy and environment of a building (with complex units and processes), (Clarke and Strachan, 1994). Thus, it was felt that a more specific code would be more suitable for the computational problem at hand. This would allow the development of a mathematical model that sufficiently described a physical system. Moreover, MATLAB software (with a high computational capability) was available. So, a special purpose code was written in this software to simulate the solar distillation process in the present study.

3.2 Model for solar distillation process

Different aspects of solar distillation have been theoretically examined in previous work. Tleimat and Howe (1966) correlated the rate of distillate production with brine flow rate and temperature difference between inlet and ambient air temperature. They found that distillate productivity could be augmented through constant supplement of warm water to the still. Malik and Van Tran (1973) studied nocturnal production of water using a simple mathematical model. Their model showed that distillate productivity was influenced by the initial temperature, drop in temperature and depth of the saline water. El-Nashar (1992) developed a simulation program for performance prediction of solar desalination plants. The program was used to optimize the operating parameters of the Abu Dhabi solar desalination plant. It was found that the observed and analytical results were in close conformity. The author was able to establish the maximum daily production based on the optimum operating parameters. Gandhidasan and Abualhamayel (1994) formulated a simple expression for estimating the mass of distillate from seawater. They obtained an expression of distillate as a function of climatic and initial conditions through a vapour pressure correlation. Porta et al. (1997) examined the thermal inertia of shallow solar stills using a lumped-parameter mathematical model. They found that distillate productivity was affected by sensitivity to thermal inertia. Nafey et al. (2000) developed an equation for predicting the daily productivity of a single-sloped solar still. They found that their equation could predict the daily productivity of distilled water with a relatively high degree of confidence. Various aspects of solar distillation have been modelled by other researchers, including Zurigat and Abu-Arabi (2002), Abu-Arabi et al. (2002), Radhwan (2004) and Tiwari and Tiwari (2007).

A common approach to modelling solar stills is the use of energy balance equations in which the input solar energy is balanced against the useful output energy and various losses from the system. It should be noted that the law of conservation of energy is vital in the analysis of heat transfer to and from a system. Tiwari et al. (2003) reported that correlations for the internal heat and mass transfer in a conventional solar developed by Dunkle (1961) are used in most studies on solar still modelling.

In Chapter 2, it was shown that previous models for computing the distribution of solar radiation inside a solar still did not incorporate optical view factors of surfaces that exchange radiation. In addition, the condenser unit of the previous design of a solar still with separate condenser was not shielded against solar radiation. Consequently, the condenser would be relatively hot, thereby limiting the performance of the still. The present investigation attempts to overcome these limitations. In this vein, a model for calculating the distribution of solar radiation inside a single-slope solar still is proposed. This model is applied to appraise the development of an ASS with shielded separate condenser.

3.2.1 New model for calculating effective irradiance

Fig.3.2 shows a schematic representation of the ASS. Incoming solar radiation is incident on the glass cover and part of it is directly transmitted onto the surface of saline water in the evaporator basin of the ASS. In addition, the walls of the evaporator chamber and the external reflector reflect solar radiation onto the water surface, and they cast shadows over the water surface during certain times of the day. It should nevertheless be mentioned that solar radiation reflected from the front wall onto the surface of saline water is negligible (Tripathi and Tiwari, 2004). In view of this, only the solar contributions from the back and side walls and external reflector were included in the computation of effective solar irradiance ($G_{g,ef}$) inside the solar still. In this study, global irradiance is split into its components and view factors of the receiving or reflecting surfaces are taken into consideration in the new model. Beam and diffuse irradiance on the walls and external reflector are computed and then used to calculate the required effective irradiance on the surface of saline water (Madhlopa and Johnstone, 2009).

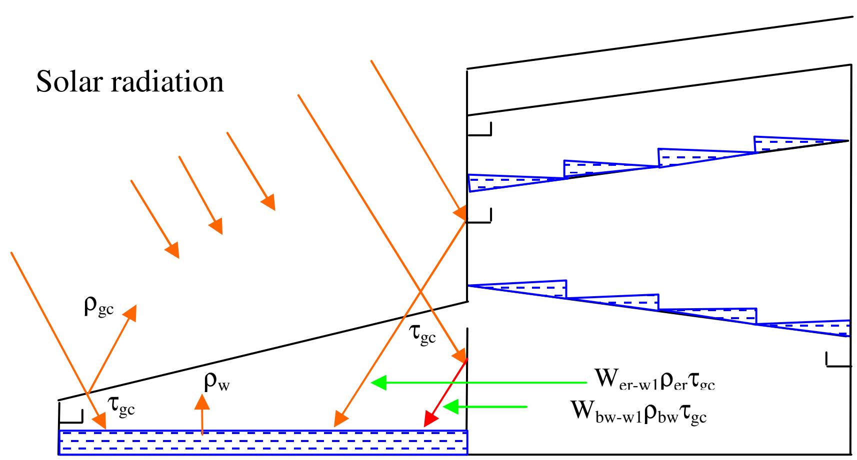

Fig.3.2: Distribution of solar radiation inside the advanced solar still.

For beam radiation, solar energy received directly by the water surface ($G_{b,di}$) and that intercepted by the walls ($G_{b,iw}$) and the external reflector ($G_{b,er}$) depend on the geometry of the solar still, beam irradiance on a horizontal surface and the position of the sun in the sky. So, $G_{b,di}$, $G_{b,iw}$ and $G_{b,er}$ can be given by (Tripathi and Tiwari, 2004; Madhlopa and Johnstone, 2009):

$$G_{b,di} = A_{di}G_{bh}/A_{w1} \tag{3.12}$$

$$G_{b,iw} = \left(A'_{bw} + A'_{ew} + A'_{ww}\right)G_{bh} / A_{w1} \tag{3.13}$$

$$G_{b,er} = A'_{er}G_{bh} / A_{w1} \tag{3.14}$$

Using a geometric analysis as in Fig.3.3 for the ASS, the area of saline water receiving beam radiation directly and the projected areas of the evaporator walls and external reflector are computed from the solar altitude and azimuth angles, and the latitude and longitude of the site (Tripathi and Tiwari, 2004; Tanaka and Nakatake, 2006; Madhlopa and Johnstone, 2009):

$$A_{di} = \begin{cases} L_{bl}\left[B_{bl} - \dfrac{Z_{fw}\cos\left(\gamma_s - \gamma_p\right)}{\tan\psi}\right], if\left|\gamma_s\right| < 90^o \\ L_{bl}\left[B_{bl} - \dfrac{Z_{fc}\cos\left(\gamma_s - \gamma_p\right)}{\tan\psi}\right], if\left|\gamma_s\right| \geq 90^o \end{cases} \tag{3.15}$$

$$A'_{bw} = \begin{cases} \dfrac{L_{b1}Z_{bw}\cos\left(\gamma_s - \gamma_p\right)}{\tan\psi}, for\left|\gamma_s\right| < 90^o \\ 0, for\left|\gamma_s\right| \geq 90^o \end{cases} \tag{3.16}$$

It should be mentioned that the sun is in front of the solar still when $|\gamma_s| < 90^o$ for a south-facing system (such as a solar energy system mounted facing the Equator at the University of Strathclyde). Otherwise, the sun is behind the system at this site. Thus, Eqs.(3.15) and (3.16) take into account the effects of shading for any position of the sun relative to a south-facing system. Similar equations are used for a north-facing system (such as a solar energy system mounted facing the Equator at the Malawi Polytechnic) but $|\gamma_s|>90^o$ when the sun is in front of the system at this location.

In the morning ($\omega<0$), rays of the sun are incident on the outer surface of the east wall and on the inner surface of the west wall. At solar noon ($\omega=0$), both the east and west walls receive equal amounts of solar energy. In the afternoon ($\omega>0$), the trend in the distribution of solar energy on the east and west walls is reversed. In view of the symmetry about solar noon, the projected areas of the two walls can be given by:

$$\mathrm{A}'_{\mathrm{ew}} = \begin{cases} B_{b1}\left[\dfrac{Z_{fw}\sin\left(\left|\gamma_s-\gamma_p\right|\right)}{\tan\psi}+0.5y\sin r\right], \omega \geq 0 \\ 0, \omega<0 \end{cases} \tag{3.17}$$

$$\mathrm{A}'_{\mathrm{ww}} = \begin{cases} B_{b1}\left[\dfrac{Z_{fw}\sin\left(\left|\gamma_s-\gamma_p\right|\right)}{\tan\psi}+0.5y\sin r\right], \omega \leq 0 \\ 0, \omega>0 \end{cases} \tag{3.18}$$

$$\sin r = \frac{\left(Z_{bw}-Z_{fe}\right)\sin\left(\left|\gamma_s-\gamma\right|\right)}{[\left(B_{b1}\tan\psi\right)^2+\left(Z_{bw}-Z_{fe}\right)^2+2B_{b1}\left(Z_{bw}-Z_{fe}\right)\tan\psi\cos\left(\gamma_s-\gamma\right)]^{0.5}} \tag{3.19a}$$

$$\mathrm{y} = \left[B_{b1}^2+\left(\frac{Z_{bw}}{\tan\psi}-\frac{Z_{fw}}{\tan\psi}\right)^2+2B_{b1}\left(\frac{Z_{bw}}{\tan\psi}-\frac{Z_{fw}}{\tan\psi}\right)\cos\left(\gamma_s-\gamma_p\right)\right]^{0.5} \tag{3.19b}$$

Saline water also receives solar energy from the external reflector. The projected area of the external reflector is given by (for a south facing surface):

$$\mathrm{A}'_{\mathrm{er}} = \begin{cases} \dfrac{L_{b1}Z_{er}\cos\left(\gamma_s-\gamma_p\right)}{\tan\psi}, for\left|\gamma_s\right|<90^o \\ 0, for\left|\gamma_s\right|\geq 90^o \end{cases} \tag{3.20}$$

A similar equation is used for a north-facing surface with the inequality signs in Eq.(3.20) reversed.

It is observed that the surface area of saline water that directly receives solar radiation, and the projected areas of the walls and external reflector are dependent on solar angles for a given set of still design and site parameters. This indicates that these areas and the amount of solar energy intercepted by them vary with the time of the day.

For diffuse radiation, solar energy received directly by the water surface ($G_{d,di}$) and that intercepted by the walls ($G_{d,iw}$) and the external reflector ($G_{d,er}$) can be calculated from (Duffie and Beckman, 2006):

$$G_{d,di}=W_{wl-sk}G_{dh} \tag{3.21}$$

$$G_{d,iw}= (A_{bw}W_{bw-sk}G_{dh}+ A_{ew}W_{ew-sk}G_{dh}+A_{ww}W_{ww-sk}G_{dh})/A_{w1} \tag{3.22}$$

$$G_{d,er}= A_{er}W_{er-sk}G_{dh}/A_{w1} \tag{3.23}$$

It is observed that the diffuse irradiance on the receiving surfaces depends on view factors for a given set of design parameters, which indicates that the diffuse irradiance on these surfaces is not affected by the position of the sun. The two components of solar energy received by the various surfaces are used to derive equations for calculating effective irradiance on the surface of saline water inside the solar still.

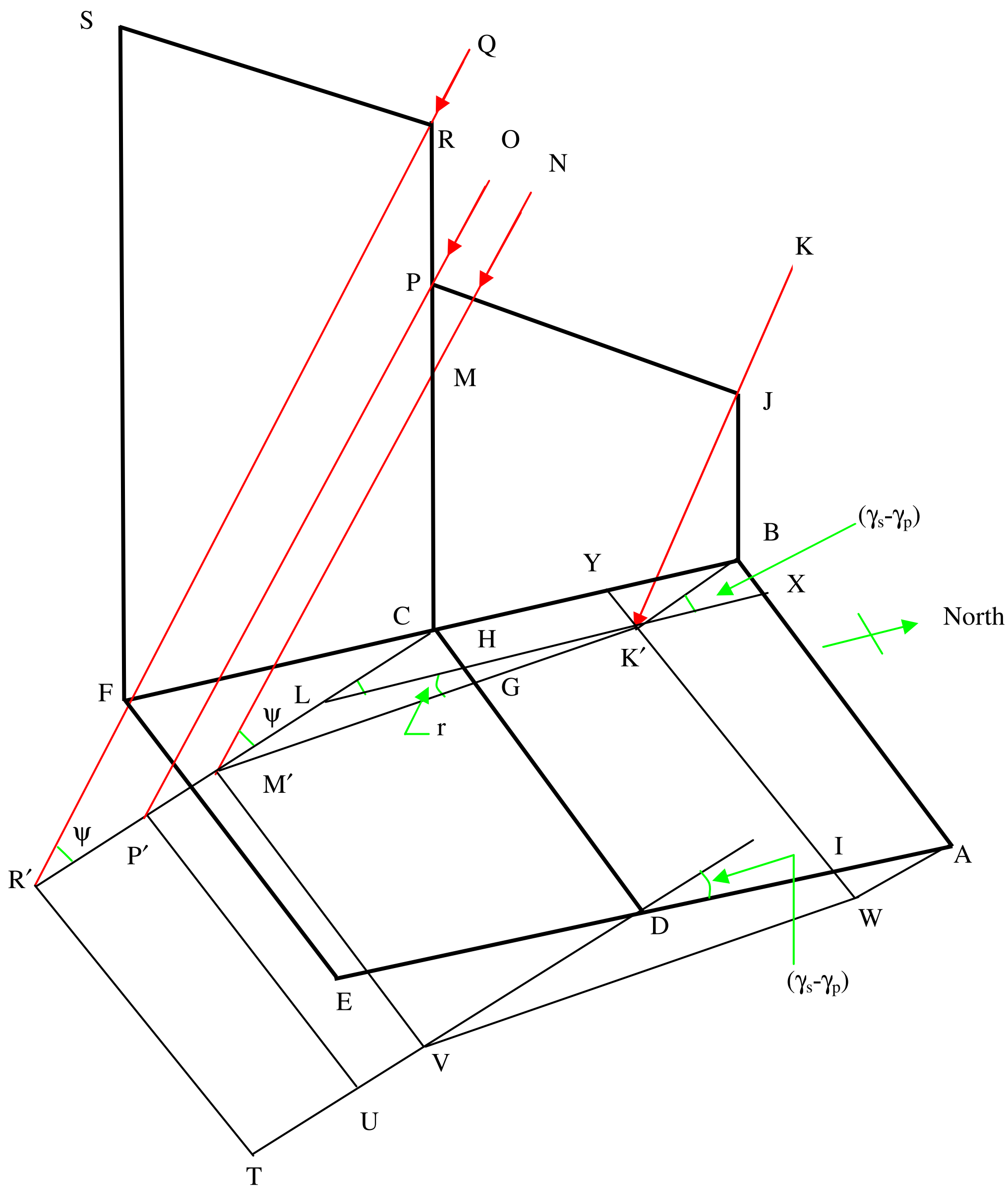

Fig.3.3: The geometry of a north-facing advanced solar still and rays (KK′, NM′, OP′and QR′) from the sun.

Saline water receives solar energy directly from the sun and indirectly from the walls and external reflector of the still. The amount of solar energy reflected by a particular wall is also influenced by the view factor of the wall with respect to the water surface. The beam solar energy received by the water can be given by:

$$A_{wl} G_{b,ef} = A_{di} G_{bh} + \rho_{iw} \left(W_{bw-w1} A'_{bw} + W_{ew-w1} A'_{ew} + W_{ww-w1} A'_{ww} \right) G_{bh} + \rho_{er} W_{er-w1} A'_{er} G_{bh} \tag{3.24}$$

Using Eq.(3.24), the effective beam irradiance inside the solar still can be calculated from:

$$G_{b,ef} = \left[A_{di} + \rho_{iw} \left(W_{bw-w1} A'_{bw} + W_{ew-w1} A'_{ew} + W_{ww-w1} A'_{ww} \right) + \rho_{er} W_{er-w1} A'_{er} \right] G_{bh} / A_{wl} \tag{3.25}$$

Similarly, diffuse solar energy intercepted by the water is given by:

$$A_{wl} G_{d,ef} = A_{wl} W_{wl\text{-}sk} G_{dh} + \rho_{iw} Q_{d,iw} + \rho_{er} A_{er} W_{er\text{-}wl} W_{er\text{-}sk} G_{dh} \tag{3.26}$$

$$Q_{d,iw} = \left(A_{bw} W_{bw\text{-}wl} W_{bw\text{-}sk} + A_{ew} W_{ew\text{-}wl} W_{ew\text{-}sk} + A_{ww} W_{ww\text{-}wl} W_{ww\text{-}sk} \right) G_{dh} \tag{3.27}$$

From Eq.(3.26) , the effective diffuse irradiance can be calculated as follows:

$$G_{d,ef} = \left(A_{wl} W_{wl\text{-}sk} G_{dh} + \rho_{iw} Q_{d,iw} + \rho_{er} A_{er} W_{er\text{-}wl} W_{er\text{-}sk} G_{dh} \right) / A_{wl} \tag{3.28}$$

The total effective solar irradiance inside the ASS can be calculated from:

$$G_{g,ef} = G_{b,ef} + G_{d,ef} \tag{3.29}$$

In this study, effective irradiance in a CSS is computed using a similar approach but without an external condenser and reflector.

All view factors for pairs of the internal surfaces of the still are computed in three dimensions according to Incropera et al.(2007). It is assumed that the two trapezoidal surfaces on the eastern and western sides of the solar still are rectangular in shape with breadth B_{bl} and length $0.5(Z_{bw}+Z_{fw})$. In addition, all the surfaces are treated as diffuse reflectors. Duffie and Beckman (2006) reported that the proportion of the sky viewed by a tilted surface is $0.5(1+\cos\beta)$, in the absence of any other obstruction. Based on this, W_{bw-sk}, W_{er-sk} and W_{wl-sk} are calculated as follows:

$$W_{bw-sk}=0.5(1+\cos\beta_{bw})-(W_{bw-ew}+W_{bw-fw}+W_{bw-ww}+W_{bw-er}) \tag{3.30}$$

$$W_{er-sk}=0.5(1+\cos\beta_{er}) \tag{3.31}$$

$$W_{wl-sk}=1-(W_{wl-bw}+W_{wl-ew}+W_{wl-fw}+W_{wl-ww}+W_{wl-er}) \tag{3.32}$$

It should be mentioned that $W_{bw-ew}=W_{bw-ww}$ (by symmetry) and the surface of saline water is horizontal ($\beta_{wl}=0$) with the back wall and external reflector being vertical ($\beta_{bw}=\beta_{er}=90^o$)**.** In addition, $W_{bw-er}=0$ because both the back wall and the external reflector are flat in the same plane. So, these two surfaces cannot view each other. The computed effective irradiance is used in the energy balance equations for the CSS and ASS.

3.2.2 Energy balance equations

The proposed model for calculating the distribution of solar energy inside a solar still was applied to the CSS and ASS. These solar stills were simulated under the same meteorological conditions. In this simulation, it was assumed that:

a) the two solar stills were air-tight,

b) purging and diffusion stopped when the temperature of water in basin 2 was greater or equal to that of water in the basin 1 ($T_{w2} \geq T_{w1}$),

c) ground-reflected solar radiation did not reach saline water in basin1,

d) solar radiation intercepted by the exterior surfaces of the walls was neglected,

e) there was no leakage of vapour and distilled water from the systems, and

f) there was negligible change (with time, t) in the mass of saline water in the basins.

With these assumptions, the energy balance equations for the present solar still components were formulated as follows:

Glass cover (gc)

$$m_{gc}C_{p,gc}\frac{dT_{gc}}{dt} = A_{gc}F_{gc}G_{g,ef} + A_{w1}h_{gc}\left(T_{w1} - T_{gc}\right) - A_{gc}h_{c,gc-a}\left(T_{gc} - T_{a}\right) - A_{gc}h_{r,gc-sk}\left(T_{gc} - T_{sk}\right) \tag{3.33}$$

$$h_{gc} = \left(\frac{R'h_{c,w1-gc}}{1+R'} + \frac{R'h_{e,w1-gc}}{1+R'} + h_{r,w1-gc}\right) \tag{3.34}$$

Basin liner 1 (bl)

$$m_{b1}C_{p,b1}\frac{dT_{b1}}{dt} = A_{w1}\left[F_{b1}G_{g,ef} - h_{c,b1-w1}\left(T_{b1} - T_{w1}\right) - U_{bo}\left(T_{b1} - T_{a}\right)\right] \tag{3.35}$$

Water in basin 1 (wl)

$$m_{w1}C_{P,w1}\frac{dT_{w1}}{dt} = A_{w1}\left[F_{w1}G_{g,ef} + h_{c,b1-w1}\left(T_{b1} - T_{w1}\right)\right] - \dot{m}_{d}L'_{w1} - A_{w1}h_{w1}\left(T_{w1} - T_{gc}\right) - A_{s1}U_{sw}\left(T_{w1} - T_{a}\right) \tag{3.36}$$

$$h_{w1} = h_{c,w1-gc} + h_{e,w1-gc} + h_{r,w1-gc} \tag{3.37}$$

$$\dot{m}_{d} = D\left(\mathrm{A}_{\mathrm{ec}} / x_{ec}\right)\left(\varphi_{ve} - \varphi_{vc}\right) \tag{3.38}$$

Basin liner 2 (b2)

$$m_{b2}C_{p,b2}\frac{dT_{b2}}{dt} = A_{w1}h_{pu}\left(T_{w1} - T_{gc}\right) + \dot{m}_{d}L'_{w1} - A_{b2}h_{c,b2-w2}\left(T_{b2} - T_{w2}\right) \tag{3.39}$$

$$h_{pu} = \frac{h_{c,w1-gc}}{1+R'} + \frac{h_{e,w1-gc}}{1+R'} \tag{3.40}$$

Water in basin 2 (w2)

$$m_{w2}C_{p,w2}\frac{dT_{w2}}{dt} = A_{b2}h_{c,b2-w2}\left(T_{b2}-T_{w2}\right) - A_{w2}h_{w2}\left(T_{w2}-T_{b3}\right) - A_{s2}U_{sw}\left(T_{w2}-T_{a}\right) \tag{3.41}$$

$$h_{w2} = h_{c,w2-b3} + h_{e,w2-b3} + h_{r,w2-b3} \tag{3.42}$$

Basin liner 3 (b3)

$$m_{w3}C_{p,b3}\frac{dT_{b3}}{dt} = A_{w2}h_{w2}\left(T_{w2}-T_{b3}\right) - A_{b3}h_{c,b3-w3}\left(T_{b3}-T_{w3}\right) \tag{3.43}$$

Water in basin 3 (w3)

$$m_{b3}C_{p,w3}\frac{dT_{w3}}{dt} = A_{b3}h_{c,b3-w3}\left(T_{b3}-T_{w3}\right) - A_{w3}h_{w3}\left(T_{w3}-T_{co}\right) - A_{s3}U_{sw}\left(T_{w3}-T_{a}\right) \tag{3.44}$$

$$h_{w3} = h_{c,w3-co} + h_{e,w3-co} + h_{r,w3-co} \tag{3.45}$$

Rate of evaporation ($\dot{m}_e$)

$$\dot{m}_e = \frac{A_{w1}h_{e,w1-gc}\left(T_{w1}-T_{gc}\right)}{L'_{w1}} + \frac{A_{w2}h_{e,w2-b3}\left(T_{w2}-T_{b3}\right)}{L'_{w2}} + \frac{A_{w3}h_{e,w3-co}\left(T_{w3}-T_{co}\right)}{L'_{w3}} + \dot{m}_d \tag{3.46}$$

The heat flux (Q_e) due to evaporation can be written as:

$$Q_e = h_{e,w1-gc}\left(T_{w1}-T_{gc}\right) + \frac{A_{w2}h_{e,w2-b3}\left(T_{w2}-T_{b2}\right)}{A_{w1}} + \frac{A_{w3}h_{e,w3-co}\left(T_{w3}-T_{co}\right)}{A_{w1}} + \frac{\dot{m}_d L'_{w1}}{A_{w1}} \tag{3.47}$$

The distillate yield (Y) and still efficiency of the system (η_{st}) in a time interval of (t_2-t_1) are calculated from:

$$Y = \frac{1}{A_{w1}} \int_{t_1}^{t_2} \dot{m}_e dt \qquad (3.48)$$

$$\eta_{st} = \frac{100 A_{w1} \int_{t_1}^{t_2} Q_e dt}{A_{gc} \int_{t_1}^{t_2} G_{gc} dt} \qquad (3.49)$$

It should be mentioned that the heat balance equations for the CSS are similar to those of the components of the evaporator unit of the ASS with the following modifications:

Glass cover (gc)

$$h_{gc} = h_{c,w1-gc} + h_{e,w1-gc} + h_{r,w1-gc} \qquad (3.50)$$

Water in basin (w1)

$$\dot{m}_d = 0 \qquad (3.51)$$

Rate of evaporation ($\dot{m}_e$):

$$\dot{m}_e = h_{e,w1-gc} (T_{w1} - T_{gc}) / L'_{w1} \qquad (3.52)$$

The various coefficients of heat transfer are shown in Fig.3.4 (a), with the corresponding thermal network in Fig.3.4 (b). The radiative heat transfer from the saline water in basin 1 to the liner of basin 2 was neglected due to the insignificant view factor of the surface of saline water with respect to this liner. For a similar reason, the radiative heat transfer from the condenser cover to the sky was neglected. It should also be noted that the glass cover, saline water and liner of basin 1 absorbed some proportions of solar radiation, as shown later in this section. Solar radiation absorbed by the cover reduces the temperature gradient between saline water and the cover, thereby reducing distillate productivity. The heat sink for the entire network is ambient air to ease the computation of the total thermal resistance of the network.

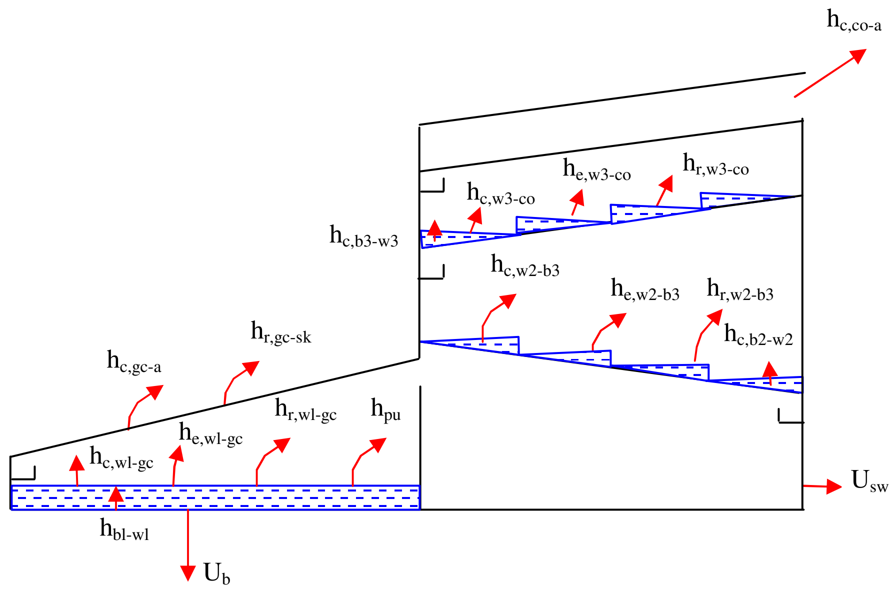

Fig.3.4(a): Heat transfer modes in the ASS.

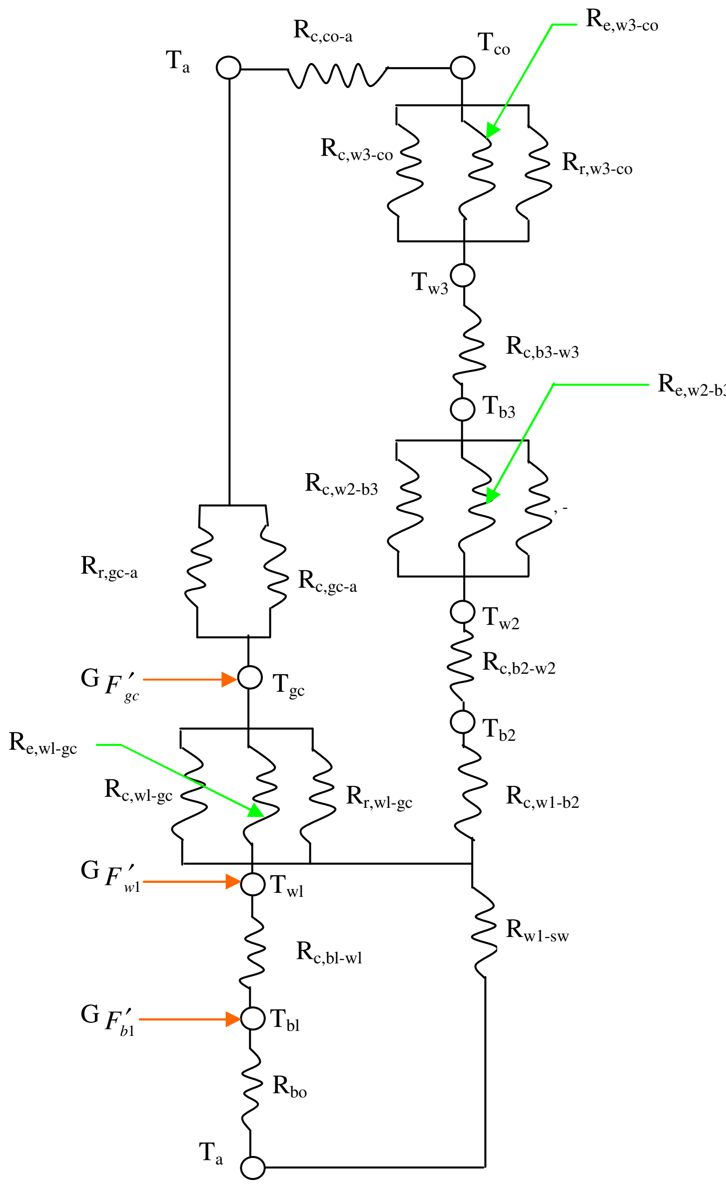

Fig.3.4 (b): A network of thermal resistance for the heat transfer modes in the ASS shown in Fig.3.4(a).

Solar radiation is attenuated as it propagates through the glass cover and saline water to reach the basin liner. These still components absorb part of the radiation, and the values of the solar absorption factors are computed by taking into account the angular dependence of solar transmission and absorption through a glass cover (Howell et al., 1982; Zurigat and Abu-Arabi, 2004):

$$F_{gc} = \alpha_{gc} \tag{3.53}$$

$$F_{w1} = \alpha_{w1}\, \tau_{gc} \tag{3.54}$$

$$F_{b1} = \alpha_{bl}\tau_{gc}\tau_{w1} \tag{3.55}$$

It should be noted from Eq.(3.54) that saline water in basin 1 absorbs ($\alpha_{wl}\tau_{gc}$) of the solar radiation that reaches its surface ($G_{g,ef}$). In practice, the fraction ($\alpha_{wl}\tau_{gc}$) can be increased by using a transparent cover with high transmittance and adding a dye to the saline water to raise the value of α_w (Cooper, 1973; Garg and Mann, 1976; Tiwari et al., 2003). Eq.(3.55) shows that basin liner 1 absorbs ($\alpha_{bl}\tau_{gc}\tau_{w1}$) of $G_{g,ef}$. Thus, using a transparent cover with high transmittance and a black liner (with high absorptance) practically augments the proportion of solar radiation absorbed by the basin liner (Lenel and Mudd, 1984). Solar radiation absorbed by the saline water and basin liner drives the heat and mass transfer processes within a still.

The distillation process involves transfer of heat by convection, evaporation and radiation within the still. In view of this, Eqs.(2.73) and (2.74) were used to estimate the coefficients of internal convective and evaporative heat transfers, respectively, from hot saline water to each of the condensing surfaces (glass cover, basin liner 2, basin liner 3 and condensing cover). In addition, the coefficient of internal radiative heat transfer was computed from Eq.(2.62). It should also be noted that basins 2 and 3 were inclined to the horizontal. In view of this, the coefficients of convective heat transfer from these basin liners to saline water were calculated according to Incropera et al. (2007):

$$h_c = Nu\, k_w / S \tag{3.56}$$

$$Nu = \left\{ \frac{0.825 + 0.387\, Ra^{1/6}}{[1 + (0.492 / \Pr)^{9/6}]^{8/27}} \right\}^2 \tag{3.57}$$

$$\Pr = C_{p,w}\, \nu_w / k_w \tag{3.58}$$

$$Ra = \frac{g \beta'_w S^3 (\Delta T) \sin\beta}{\alpha'_w \nu_w} \tag{3.59}$$

$$S = A/(2L + 2B) \tag{3.60}$$

Heat is lost from the distillation system to the environment through the top part, bottom and side walls of the solar still. Top heat loss takes place through convection ($h_{c,gc\text{-}a}$) and radiation ($h_{r,gc\text{-}sk}$). The values of $h_{c,gc\text{-}a}$ and $h_{r,gc\text{-}sk}$ were calculated from Eqs.(2.75) and (2.76) respectively. The coefficient of bottom heat loss was calculated from (Anderson, 1983):

$$U_{bo} = \left(\frac{x_{ps}}{k_{ps}} + \frac{x_{pw}}{k_{pw}} \right)^{-1} \tag{3.61}$$

The coefficient of heat loss from the sides was taken as 0.5 $Wm^{-2}K^{-1}$ (Klein, 1975) while the effective irradiance used in the energy balance equations was computed using a model presented in Section 3.1.1.

3.3 Numerical solution procedure

The system of differential equations in this study is transient and non-linear. In view of this, a finite difference method was used to discretize the equations implicitly to obtain a system of linear algebraic equations for the jth time step (Incropera et al., 2007):

Glass cover (gc)

$$T_{gc}^{j} = a_{10} + a_{11}T_{gc}^{j-1} + a_{12}T_{wl}^{j} \tag{3.62}$$

where $a_{10} = \dfrac{\Delta t\left(A_{gc}F_{gc}G_{g,ef} + A_{gc}h_{c,gc\text{-}a}T_a + A_{gc}h_{r,gc\text{-}sk}T_{sk}\right)}{\Delta t\left(A_{wl}h_{gc} + A_{gc}h_{c,gc\text{-}a} + A_{gc}h_{r,gc\text{-}sk}\right) + m_{gc}C_{p,gc}}$,

$$a_{11} = \frac{m_{gc}C_{p,gc}}{\Delta t\left(A_{wl}h_{gc} + A_{gc}h_{c,gc\text{-}a} + A_{gc}h_{r,gc\text{-}sk}\right) + m_{gc}C_{p,gc}}, \text{ and}$$

$$a_{12} = \frac{\Delta t A_{wl}h_{gc}}{\Delta t\left(A_{w1}h_{gc} + A_{gc}h_{c,gc\text{-}a} + A_{gc}h_{r,gc\text{-}sk}\right) + m_{gc}C_{p,gc}}$$

Basin liner 1 (bl)

$$T_{bl}^{j} = a_{20} + a_{21}T_{bl}^{j-1} + a_{22}T_{wl2}^{j} \tag{3.63}$$

where $a_{20} = \dfrac{\Delta t A_{w1}\left(F_{bl}G_{g,ef} + U_{bo}T_a\right)}{\Delta t A_{w1}\left(h_{c,bl\text{-}w1} + U_{bo}\right) + m_{bl}C_{p,bl}}$,

$$a_{21} = \frac{m_{bl}C_{p,bl}}{\Delta t A_{wl}\left(h_{c,bl\text{-}w1} + U_{bo}\right) + m_{bl}C_{p,bl}}, \text{ and}$$

$$a_{22} = \frac{\Delta t A_{wl}h_{c,bl\text{-}wl}}{\Delta t A_{wl}\left(h_{c,bl\text{-}w1} + U_{bo}\right) + m_{bl}C_{p,bl}}$$

Water in basin 1 (wl)

$$T_{w1}^{j} = a_{30} + a_{31}T_{w1}^{j-1} + a_{32}T_{gc}^{j} + a_{33}T_{b1}^{j} \tag{3.64}$$

where $a_{30} = \dfrac{\Delta t\left(A_{wl}F_{wl}G_{g,ef} - m_{df,m}L' + A_{s1}U_{sw}T_a\right)}{\Delta t A_{wl}(h_{c,bl\text{-}wl} + h_{w1}) + \Delta t A_{s1}U_{sw} + m_{wl}C_{p,wl}}$,

$$a_{31} = \frac{m_{wl} C_{p,wl}}{\Delta t A_{wl}(h_{c,bl\text{-}wl} + h_{w1}) + \Delta t A_{s1} U_{sw} + m_{wl} C_{p,wl}},$$

$$a_{32} = \frac{\Delta t A_{wl} h_{wl}}{\Delta t A_{wl}(h_{c,bl\text{-}wl} + h_{w1}) + \Delta t A_{s1} U_{sw} + m_{wl} C_{p,wl}}, \text{ and}$$

$$a_{33} = \frac{\Delta t A_{wl} h_{c,b1\text{-}wl}}{\Delta t A_{wl}(h_{c,bl\text{-}wl} + h_{w1}) + \Delta t A_{s1} U_{sw} + m_{wl} C_{p,wl}}$$

Basin liner 2 (b2)

$$T_{b2}^{j} = a_{40} + a_{41} T_{b2}^{j\text{-}1} + a_{42} T_{gc}^{j} + a_{43} T_{w1}^{j} + a_{44} T_{w2}^{j} \tag{3.65}$$

where $a_{40} = \dfrac{m_{df,o} L'}{\Delta t A_{b2} h_{c,b2\text{-}w2} + m_{b2} C_{p,b2}}$

$$a_{41} = \frac{m_{b2} C_{p,b2}}{\Delta t A_{b2} h_{c,b2\text{-}w2} + m_{b2} C_{p,b2}},$$

$$a_{42} = \frac{-\Delta t\, A_{wl} h_{pu}}{\Delta t A_{b2} h_{c,b2\text{-}w2} + m_{b2} C_{p,b2}},$$

$$a_{43} = \frac{\Delta t\, A_{wl} h_{pu}}{\Delta t A_{b2} h_{c,b2\text{-}w2} + m_{b2} C_{p,b2}}, \text{ and}$$

$$a_{44} = \frac{\Delta t\, A_{b2} h_{c,b2\text{-}w2}}{\Delta t A_{b2} h_{c,b2\text{-}w2} + m_{b2} C_{p,b2}}$$

Water in basin 2 (w2)

$$T_{w2}^{j} = a_{50} + a_{51} T_{w2}^{j\text{-}1} + a_{52} T_{b2}^{j} + a_{53} T_{b3}^{j} \tag{3.66}$$

where $a_{50} = \dfrac{\Delta t A_{s2} U_{sw} T_a}{\Delta t\left(A_{w2} h_{w2} + A_{b2} h_{c,b2\text{-}w2} + A_{s2} U_{sw}\right) + m_{w2} C_{p,w2}}$,

$$a_{51} = \frac{m_{w2} C_{p,w2}}{\Delta t\left(A_{w2} h_{w2} + A_{b2} h_{c,b2\text{-}w2} + A_{s2} U_{sw}\right) + m_{w2} C_{p,w2}},$$

$$a_{52} = \frac{\Delta t A_{b2}\, h_{c,b2\text{-}w2}}{\Delta t\left(A_{w2} h_{w2} + A_{b2} h_{c,b2\text{-}w2} + A_{s2} U_{sw}\right) + m_{w2} C_{p,w2}}, \text{ and}$$

$$a_{53} = \frac{\Delta t A_{b2} A_{w2} h_{w2}}{\Delta t\left(A_{w2} h_{w2} + A_{b2} h_{c,b2\text{-}w2} + A_{s2} U_{sw}\right) + m_{w2} C_{p,w2}}$$

Basin liner 3 (b3)

$$T_{b3}^{j} = a_{60} + a_{61} T_{b3}^{j\text{-}1} + a_{62} T_{w2}^{j} + a_{63} T_{w3}^{j} \qquad (3.67)$$

where $a_{60} = 0$,

$$a_{61} = \frac{m_{b3} C_{p,b3}}{\Delta t\left(A_{w2} h_{w2} + A_{b3} h_{c,b3\text{-}w3}\right) + m_{b3} C_{p,b3}},$$

$$a_{62} = \frac{\Delta t A_{w2} h_{w2}}{\Delta t\left(A_{w2} h_{w2} + A_{b3} h_{c,b3\text{-}w3}\right) + m_{b3} C_{p,b3}}, \text{ and}$$

$$a_{63} = \frac{\Delta t A_{b3} h_{c,b3\text{-}w3}}{\Delta t\left(A_{w2} h_{w2} + A_{b3} h_{c,b3\text{-}w3}\right) + m_{b3} C_{p,b3}}$$

Water in basin 3 (w3)

$$T_{w3}^{j} = a_{70} + a_{71} T_{w3}^{j\text{-}1} + a_{72} T_{b3}^{j} \qquad (3.68)$$

where $a_{70} = \dfrac{\Delta t\left(A_{w3} h_{w3} T_{co} + A_{s3} U_{ws} T_{a}\right)}{\Delta t\left(A_{b3} h_{c,b3\text{-}w3} + A_{w3} h_{w3} + A_{s3} U_{ws}\right) + m_{w3} C_{p,w3}}$,

$$a_{71} = \frac{m_{w3} C_{p,w3}}{\Delta t\left(A_{b3} h_{c,b3\text{-}w3} + A_{w3} h_{w3} + A_{s3} U_{ws}\right) + m_{w3} C_{p,w3}}, \text{ and}$$

$$a_{72} = \frac{\Delta t A_{b3} h_{c,b3\text{-}w3}}{\Delta t\left(A_{b3} h_{c,b3\text{-}w3} + A_{w3} h_{w3} + A_{s3} U_{ws}\right) + m_{w3} C_{p,w3}}$$

Distillate yield (Y_j) in the jth time step was calculated from the first ($Y_{1,j}$), second ($Y_{2,j}$) and third ($Y_{3,j}$) effects:

$$Y_{1,j} = \frac{(\Delta t) h_{e,w1-gc}\left(T_{w1}^{j} - T_{gc}^{j}\right)}{L'_{w1}} + \frac{(\Delta t)\dot{m}_{d}}{A_{w1}} \qquad (3.69)$$

$$Y_{2,j} = \frac{(\Delta t) A_{w2} h_{e,w2-b3} \left(T_{w2}^{j} - T_{b3}^{j}\right)}{A_{w1} L'_{w2}} \tag{3.70}$$

$$Y_{3,j} = \frac{(\Delta t) A_{w3} h_{e,w3-co} \left(T_{w3}^{j} - T_{co}\right)}{A_{w1} L'_{w3}} \tag{3.71}$$

$$Y_{j} = Y_{1,j} + Y_{2,j} + Y_{3,j} \tag{3.72}$$

In a given period of time, the cumulative distillate yield (Y) was calculated from:

$$Y = \sum_{i=0}^{i=j} Y_{i} \tag{3.73}$$

It should be noted that coefficients in the discretized equations are temperature dependent. So, the discrete algebraic equations can be solved by using the Gauss-Seidel iterative method because this method is efficient in handling linear and non-linear systems of equations and requires less computer memory (Burden and Faires, 1985). In this computational scheme, new temperature estimates are used in subsequent iterations. Thus, it was possible to perform the present computations on a Dell Inspiron laptop (model 6000 with microprocessor speed of 1.70 GHz, 504 MB of RAM and 55.8 GB of total space on hard disc).

A computer program was written in MATLAB (version 7.0) to solve the system of equations. A typical dialog box showing part of the program is presented in (Fig.3.5). Comment statements, in green font, are non-executable, and the condition for convergence of the solution was that the absolute difference between temperatures in the current and previous iterations should not exceed 0.5 K. This tolerance was chosen based on the accuracy of thermocouples used to measure the temperature of various system components reported in Chapter 5. In addition, a time step of 20 s was employed in this iterative scheme, and the temperature of the condensing cover (T_{co}) was assumed equal to ambient air temperature (T_a), (Fath and Elsherbiny, 1993). Initial values of the temperatures of the system components were assumed to be approximately equal to T_a, then solar altitude (ψ) and azimuth (γ_s) angles in the middle of a given time step were computed using Eqs.(2.8) and (2.10), respectively. The values of ψ and γ_s were used to calculate the areas of water receiving beam solar radiation directly and the projected areas of the walls and the external reflector. Effective beam radiation ($G_{b,ef}$) was determined from Eq.(3.25). Similarly, diffuse solar radiation intercepted by the saline water directly and indirectly was computed from the geometric parameters of the solar still (Eqs.3.21 to 3.23), with effective diffuse irradiance ($G_{d,ef}$) being determined from Eq.(3.28). Effective beam and diffuse irradiances were added to find the total effective irradiance ($G_{g,ef}$) on the water surface. In addition, the values ψ and azimuth γ_s were used to calculate angular-dependent optical properties of a single transparent cover (Eqs.2.28 to 2.36) and solar absorption factors (Eqs.3.53 to 3.55). Then, temperature dependent properties of fluids were determined and used to calculate appropriate coefficients of heat transfer (assumed constant in a given time step) for estimating temperatures in the next time step. The values of design and operating parameters used in this investigation are presented in Table 3.1. With these data, the system of equations was solved iteratively until a solution was found as shown in Fig.3.6.

Table 3.1: Reference design and operational parameters for the conventional and advanced solar stills.

Parameter	System CSS	System ASS	Range studied
Design parameters			
A_{b1} (m^2)	0.720	0.720	One level*
A_{b2} (m^2)	-	0.730	One level
A_{b3} (m^2)	-	0.730	One level
A_{ec} (m^2)	-	0.045	One level
A_{ev} (m^2)	1.091	2.114	One level
A_{gc} (m^2)	0.750	0.750	One level
A_{s2} (m^2)	-	1.313	One level
A_{s3} (m^2)	-	0.680	One level
A_{w2} (m^2)	-	0.730	One level
A_{w3} (m^2)	-	0.730	One level
B_{bl} (m)	0.800	0.800	One level
$h_{c,b1\text{-}w1}$ (W m^{-2} K^{-1})	100	100	100-140
L_{bl} (m)	0.900	0.900	One level
m_{b1} (kg)	5.0	5.0	One level
m_{b2} (kg)	-	6.0	One level
m_{b3} (kg)	-	6.0	One level
m_{gc} (kg)	10.0	10.0	One level
R' (dimensionless)	-	0.65	0.10-0.90
U_{bo} (W m^{-2} K^{-1})	1.203	1.203	1-9
U_{sw} (W m^{-2} K^{-1})	0.500	0.500	One level
$W_{bw\text{-}sk}$ (dimensionless)	0.23	0.23	One level
$W_{bw\text{-}wl}$ (dimensionless)	0.29	0.30	One level
$W_{ew\text{-}sk}$ (dimensionless)	0.18	0.14	One level
$W_{er\text{-}wl}$ (dimensionless)	-	0.09	One level
$W_{er\text{-}sk}$ (dimensionless)	-	0.50	One level
$W_{wl\text{-}sk}$ (dimensionless)	0.53	0.39	One level
x_{ps} (m)	0.023	0.023	One level
x_{pw} (m)	0.020	0.020	One level
x_{ec} (m)	-	0.020	One level
Z_{bw} (m)	0.425	0.418	One level
Z_{er} (m)	-	0.632	One level
Z_{fc} (m)	-	1.057	One level
Z_{fw} (m)	0.195	0.195	One level
α_{bl} (dimensionless)	0.90	0.90	0.90-1.00
β_{co} (degree)	-	10	One level
β_{gc} (degree)	16	16	One level
Operational parameters			
m_{w1} (kg)	20	20	10-30
m_{w2} (kg)	-	13	10-30
m_{w3} (kg)	-	13	10-30

*One level indicates that the value of the variable was not changed.

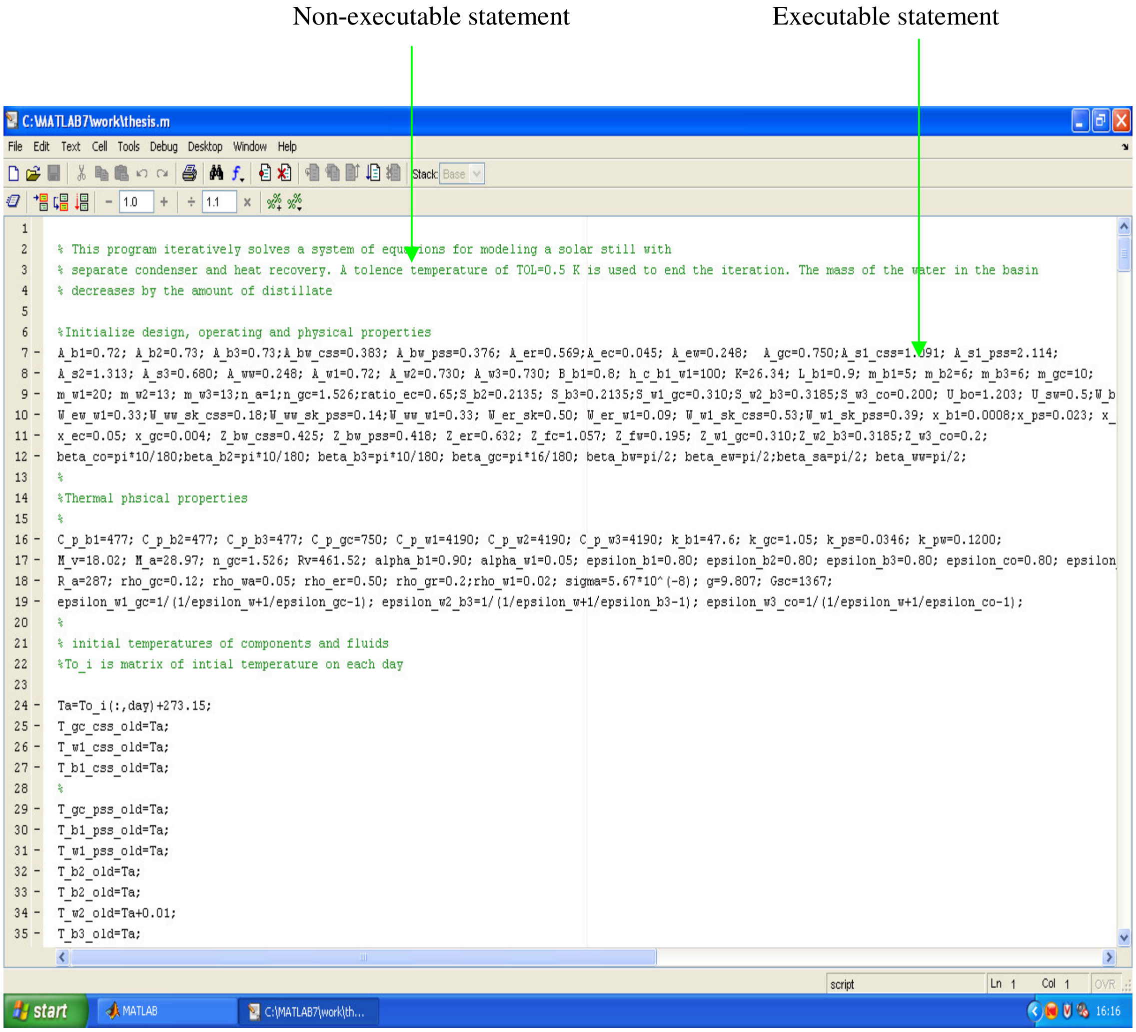

Fig.3.5: Dialog box showing part of the computational code in MATLAB.

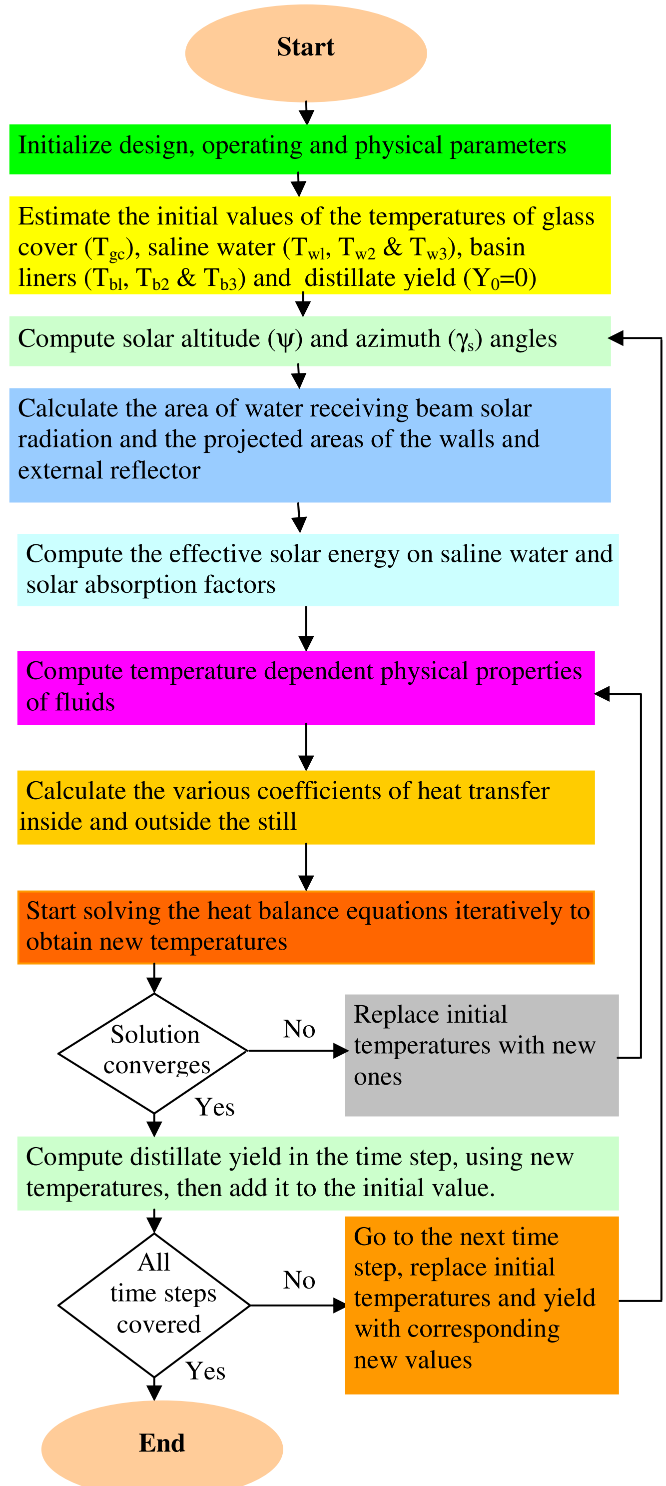

Fig.3.6: Flow chart for computation of the effective irradiance, temperatures of the system components and distillate yield in MATLAB software.

Various thermophysical properties were used in the present study (Table 3.2). The choice of these values was based on the materials used in the construction of the stills and the data reported in literature (Zurigat and Abu-Arabi, 2004; Tripathi and Tiwari, 2004; Duffie and Beckman, 2006; Incropera et al., 2007). The specific latent heat of water vaporization was calculated using a correlation reported by Belessiotis et al. (1995) while the saturation vapour pressure (P) was calculated according to ASHRAE (2001). Other physical properties of water (k, α', β', ν and φ) were calculated from temperature-dependent correlations (IAPWS, 1996). The densities of water vapour in the evaporator and condenser chambers were calculated using Eq.(3.74), at $0.5(T_{wl}+T_{gc})$ and $0.5(T_{b2}+T_a)$ respectively.

$$\varphi=P/(R_vT) \tag{3.74}$$

Table 3.2: Thermophysical properties and constants

Material	Physical property	Value
Galvanized steel	$C_{p,bl}$ ($Jkg^{-1}K^{-1}$)	477
Glass	$C_{p,gc}$ ($Jkg^{-1}K^{-1}$)	750
Water	$C_{p,w}$	4179
Galvanized steel	k_{bl} ($W\ m^{-1}\ K^{-1}$)	47.6
Glass	k_{gc} ($W\ m^{-1}\ K^{-1}$)	1.05
Polystyrene	k_{PS} ($W\ m^{-1}\ K^{-1}$)	0.0346
Plywood	k_{pw} ($W\ m^{-1}\ K^{-1}$)	0.1200
Glass	n_{gc} (dimensionless)	1.526
Water vapour	R_v ($Jkg^{-1}K^{-1}$)	461.52
Black paint	α_{bl} (dimensionless)	0.90
Water	α_{wl} (dimensionless)	0.05
Galvanized steel	ε_{co} (dimensionless)	0.80
Glass	ε_{gc} (dimensionless)	0.88
Water	ε_w (dimensionless)	0.96
Glass	ρ_{gc} (dimensionless)	0.10
Ground	ρ_{gr} (dimensionless)	0.20
Black paint	ρ_{wa} (dimensionless)	0.05
Pastel paint	ρ_{er} (dimensionless)	0.50
Water	ρ_w (dimensionless)	0.02
	σ ($Wm^{-2}K^{-4}$)	5.67×10^{-8}
Glass	τ_{gc} (dimensionless)	0.78

The performance of the present still was simulated together with a conventional system (with the same corresponding design parameters) under similar operating and meteorological conditions, and using hourly horizontal global and diffuse solar radiation data from Chileka weather site (15^{o} 40′ S, 34^{o} 58′ E) in Malawi. Hourly beam radiation was computed as the difference between global and diffuse radiation on a horizontal plane. Then, the hourly beam and diffuse insolation values were used to calculate the level of insolation on the glass cover (Eqs.2.17 and 2.24). Radiation data at intervals shorter than one hour is not available in Malawi and, therefore, mean values were calculated from the hourly insolation (I) to obtain irradiance (G) on a given surface.

$$G=I/3600 \tag{3.75}$$

The beam and diffuse irradiance on a horizontal surface on a typical date are presented in Fig.3.7. It is observed that beam irradiance was higher than diffuse irradiance during most of the day. This indicates that it was sunny, consistent with the climate of Malawi (Diabate´et al., 2004; Madhlopa, 2006). Effective irradiance was calculated at the midpoint of any given time interval. It should also be mentioned that data on daily minimum, average and maximum ambient air temperature was available for Chileka weather station. So, hourly ambient temperature was computed from daily minimum and maximum values (Muneer, 1997). A mean daily wind speed (2.0 m s^{-1}) was used, again, due to unavailability of hourly wind data at this weather station. In simulating the hourly performance of a single slope solar still, Tripathi and Tiwari (2004) assumed a constant wind speed (V_{wd}=0). They found close conformity between estimated and experimental data. Consequently, the use of an average wind speed in the present simulation is reasonable.

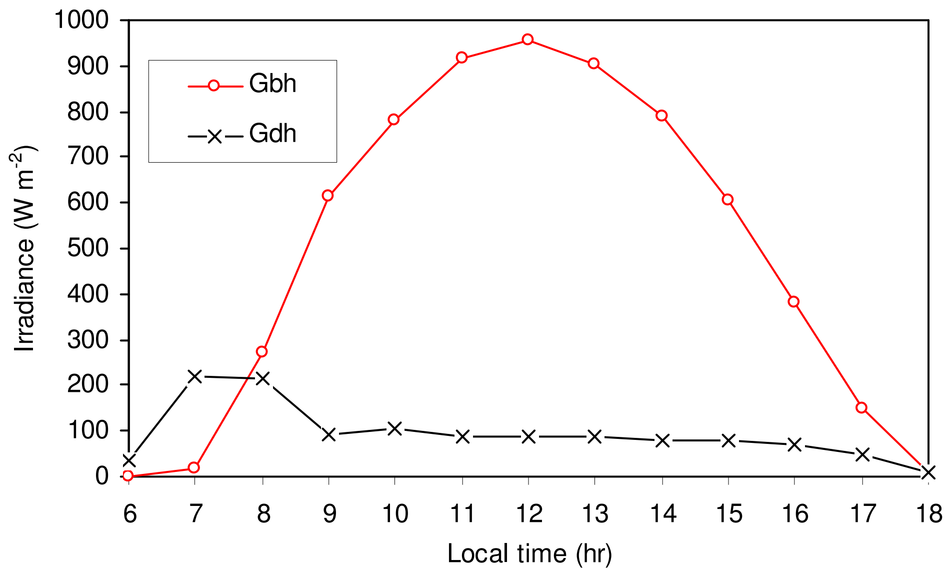

Fig.3.7: Beam (G_{bh}) and diffuse (G_{dh}) on a horizontal surface on 13 October 1989 at Chileka weather station in Malawi.

3.4 Simulation results

3.4.1 Variation of Biot numbers for solar still components

Initially, differential equations for the glass cover and basin liners were checked against the criterion for using the lumped capacitance method. Biot numbers for these system components were calculated, assuming that there was heat convection (h_c) from the glass cover to ambient air and from the basin liners to saline water. The coefficient of wind convection was applied to the glass cover. Similarly, the coefficient of heat convection from a given basin liner to saline water was used to compute its corresponding Biot number (Bi).

Maximum calculated values of Bi on a typical date are given in Table 3.3. It is observed that all the values of Bi are within the acceptable limit ($Bi \leq 0.1$) for using the lumped capacitance method. Similarly, Biot numbers for all other data used in model calibration and verification were within the stipulated range for application of the lumped capacitance method. In addition, it should be pointed out that the relatively high value of Bi for the transparent cover is attributed to the wind speed which influences heat convection to the environment. There is negligible temperature gradient within the layers of saline water in the basins because each layer is heated from the bottom. Consequently, the use of a lumped capacitance approach in this system of differential equations was reasonable.

Table 3.3: Maximum values of Biot numbers (Bi) for system components on 13 October 1989 at Chileka weather station in Malawi.

Component	Bi
Glass cover	0.034
Basin liner 1	0.002
Basin liner 2	0.001
Basin liner 3	0.001

3.4.2 Effective irradiance

Fig.3.8 shows the variation of observed and effective global irradiance with time. It is seen that the observed irradiance is higher than the effective irradiance, probably because some of the solar radiation intercepted by the glass cover is attenuated before it reaches the surface of saline water. Moreover, solar radiation is the most important environmental factor in distillate production (Nafey et al., 2000). So, this attenuation reduces the efficiency of the still. The observed trend in the variation of irradiance inside and outside the still indicates that the direct use of G_{gh} in the energy balance equations would lead to erroneous estimation of the distillate yield.

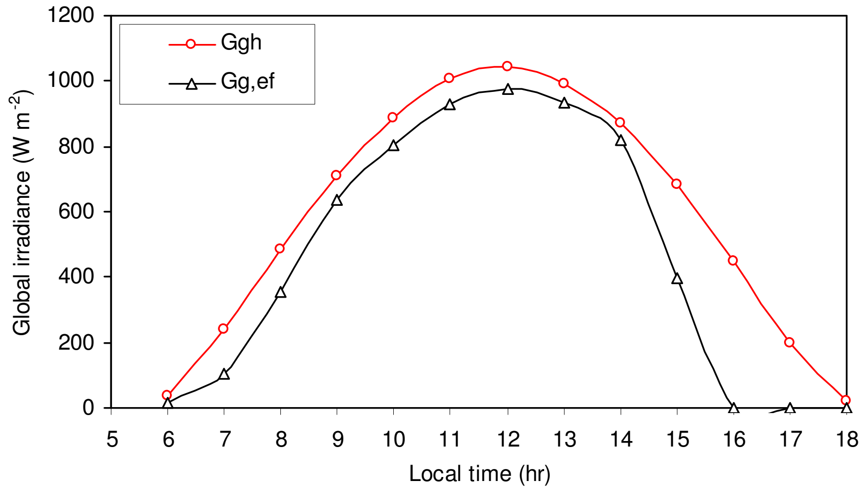

Fig.3.8: Observed (G_{gh}) and effective ($G_{g,ef}$) global irradiance

3.4.3 Temperature of ambient air and system components

Fig.3.9 shows the variation of the temperature of the ambient air (T_a), glass cover (T_{gc}), and saline water at reference values of the design and operating parameters. It is observed that $T_{gc,css}$ is higher than $T_{gc.Ass}$, with ($T_{wl,css}$-$T_{gc,css}$)=11 K and ($T_{wl,Ass}$-$T_{gc,Ass}$)=14 K at 12:00. This is probably due to the flow of part of the heat from the evaporator basin into the condenser chamber which tends to lower the glazing temperature, thereby increasing (T_{wl}-T_{gc}) in the ASS. These observations are consistent with findings from previous work (Fath and Elsherbiny, 1993; El-Bahi and Inan, 1999a, 1999b).

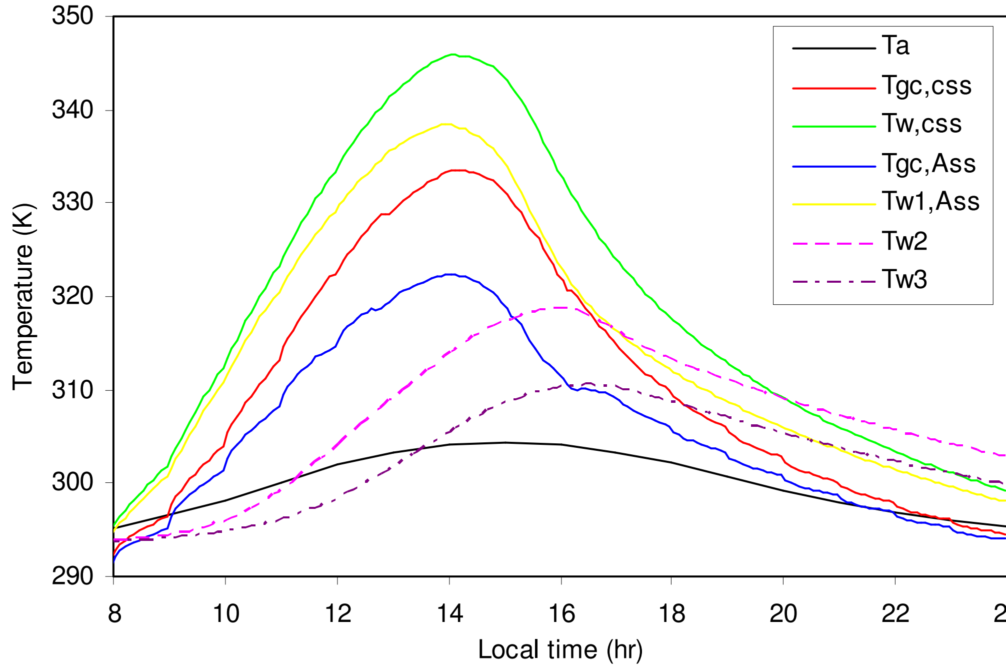

Fig.3.9: Variation of a) the temperature of ambient air (T_a), and simulated glass cover (T_{gc}), and water in basin 1 (T_{w1}), basin 2 (T_{w2}), and basin 3 (T_{w3}).

The temperature of saline water in the basin of the CSS (T_{wl},css) is higher than that in the evaporator basin of the ASS (T_{wl},Ass) during most of the day, with the difference (10 K) being maximum around 15:30 hr. This trend is attributed to the heat transfer modes from water in the evaporator basins (first effect) of the systems. In the conventional solar still, heat is lost to the ambient environment through the glass cover, bottom and side walls while heat is transferred by purging (predominantly) and diffusion from the evaporator basin to the condenser unit of the ASS, in addition to heat loses through the glass cover, bottom and side walls. It is nevertheless pleasing to note that the values of T_{wl} are comparable with experimental data reported in literature (Porta et al., 1997; Banat et al., 2002).

It is also seen that the temperature of water (T_{w2}) in basin 2 (second effect) is below that of basin 1 (T_{w1}) of the ASS from about 8:00 hr to 17:00 hr, with a maximum difference of 27 K around 13:00. This indicates that water vapour from the evaporator would be able to condense on the underside of basin 2 during most of the day, thereby augmenting the rate of productivity. After 17:00 hr, T_{w2} is higher than T_{w1} probably due to a lower rate of top heat loss from basin 3 than that from the glazing cover. The glass cover loses heat to the environment through convection and radiation while water in the upper basin loses heat to the condenser cover which has an insulation shield over it. So, top heat loss from the condenser cover is mainly by natural convection which would account for the lower rates of water cooling in basins 2 and 3.

The temperature of water in basin 3 (T_{w3}) is lower than T_{w2} from about 8:00 hr to later than 24:00 hr (maximum difference of 9 K around 15:00 hr), which again shows that vapour from water in basin 2 would be able to condense on the underside of basin 3 during the most part of the day. In addition, T_{w3} is slightly higher than T_a from 13:30 hr until after 24:00 hr, but the difference (T_{w3}-T_a) is relatively small (a maximum of 7 K around 17:00 hr). This indicates that distillate production from the third effect would be comparably low. The computed temperatures were used to predict distillate production under the prevailing meteorological conditions.

3.4.4 Distillate yield

In this section, the reported distillate productivity for the ASS is the total of contributions from water in basin1 (first effect), basin 2 (second effect) and basin 3 (third effect). Fig.3.10 shows the variation of cumulative distillate productivity of the CSS and ASS at reference values of the design and operating parameters. It is seen that in the morning (up to about 9:00 hr), distillate production is low for both stills. This is expected because production starts when air inside a still is saturated with water vapour. From about 10:00 hr, the productivity of the CSS is lower than that of the ASS.

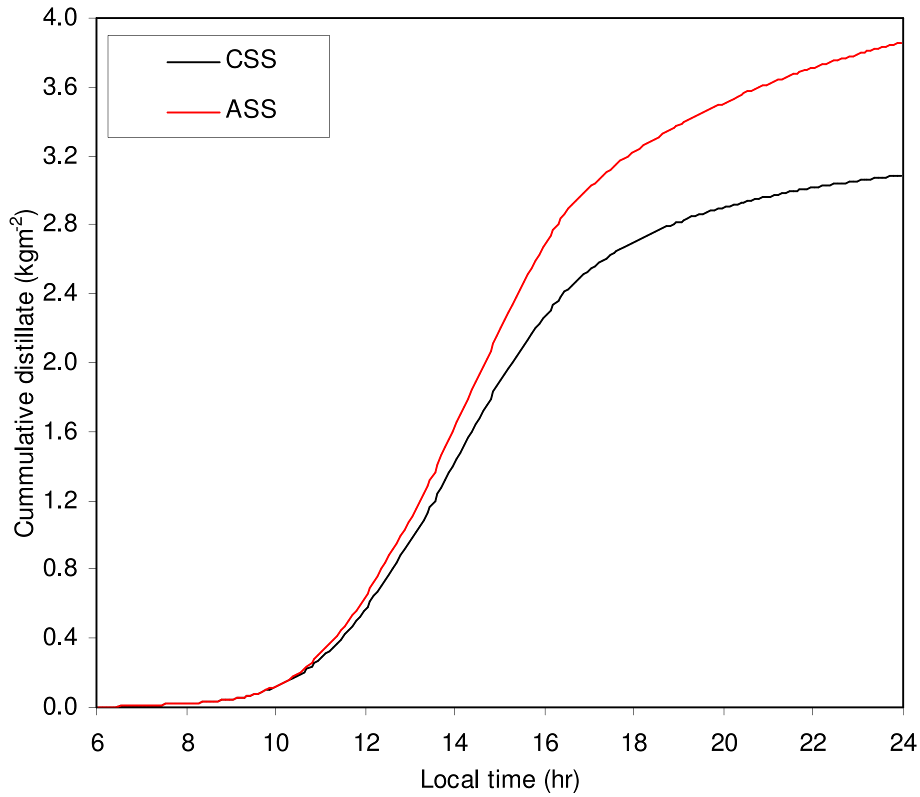

Fig.3.10: Simulated distillate production for a conventional still (CSS) and advanced solar still (ASS) on 13 October 1989 at Chileka weather station Malawi.

On a daily basis, the cumulative productivity of the CSS is 3.196 kg m^{-2} (with η=32 %) while that of the ASS is 4.101 kg m^{-2} (with η= 42 % and an improvement of 28 % over the productivity of the CSS). For the ASS, distillate contributions from the first, second and third effects are 70, 16 and 14% respectively. Purging contributes 99 % of the water vapour that condenses on the under side of basin 2 while diffusion accounts for the remaining proportion. The daily productivity of a CSS is about 3-4 kg m^{-2}, with a maximum thermal efficiency of 35 % (Kalogirou, 1997; Al-Kharabsheh and Goswami, 2003), which agree with the present observations. Results for the ASS also conform very well to experimental findings of Fath and Elsherbiny (1993) and El-Bahi and Inan (1999a). Nevertheless, there was need to calibrate the model in order to establish its accuracy.

3.4.5 Model calibration

The proposed model requires data on the design and operating factors of a solar still, and meteorological conditions (input variables) to compute distillate yield (output variable). Thus, empirical data on both input and output variables is needed for model calibration. Beam and diffuse radiation, ambient air temperature and wind speed are input weather variables to the model. Data on these input variables should be at short time intervals such as an hour or less for accurate simulation results. Moreover, the performance of a solar still is influenced by meteorological conditions for a given set of design and operating variables (Garg and Mann, 1976), and solar radiation is the most influential environmental factor. However, concurrent data on these input and output variables is scarce in literature. Many authors including Kumar and Tiwari (1996), El-Bahi and Inan (1999b), Voropoulos et al. (2003), Abdallah et al. (2008) reported data that was relevant to the objectives of their studies. Tripathi and Tiwari (2004) evaluated the performance of a solar still with a single slope by using the concept of solar fraction in New Delhi. They reported data on design, operating and meteorological parameters, and distillate output from experimental work. The hourly weather data comprised global solar irradiance (G_{gh}), ambient temperature and a constant value of wind speed over the glass cover (V_{wd}=0). This database appeared to be close to the requirements of the present model. Consequently, it was used in the calibration process.

It should be noted that G_{gh} in the Tripathi and Tiwari (2004) database was measured at the specified hours, so there was need to interpolate the values of irradiance between hours. This was done by correlating G_{gh} with time (t) from sunrise (r^2=0.96):

$$G_{gh} = \begin{cases} -133.514 + 0.075t - 1.832t^2, \text{ for } 1866 \le t \le 3973 \\ 0, \text{ for } t \le 1866 \text{ or } t \ge 3973 \end{cases} \qquad (3.76)$$

Eq.(3.76) was developed specifically for interpolation of missing values of global irradiance between adjacent hours. It is not a universal correlation for application to other data sets. The equation was then used to find hourly global radiation on a horizontal surface (I_{gh}):

$$I_{gh} = \int_{t_1}^{t_2} G_{gh}\,dt \tag{3.77}$$

Hourly diffuse radiation was estimated from the computed levels of hourly global radiation by using a piecewise polynomial correlation recommended for New Delhi location (Muneer et al., 1984):

$$\frac{I_{dh}}{I_{gh}} = \begin{cases} 0.95, & \text{for} \quad K_t < 0.175 \\ 0.9698 + 0.4353K_t - 3.4499K_t^2, & \text{for } 0.175 \le K_t \le 0.775 \\ 0.26, & \text{for} \quad K_t > 0.775 \end{cases} \tag{3.78}$$

where $K_t = I_{gh}/I_o$ is the clearness index of the sky.

Computed values of I_{gh} were used to determine the average irradiance in a given hour, in a similar way to that applied to the data for Chileka weather station in Section 3.3. The estimated irradiance is presented in Fig.3.11. It is observed that there is close conformity between estimated and experimental levels of global solar irradiance. The estimated irradiance was used in the simulation of a solar still reported by Tripathi and Tiwari (2004). Then, the root mean square error of simulation was calculated, and hourly simulated and experimental distillate values were statistically compared by using a *t*-test at 0.1 % significance level (Stone, 1993; Tripathi and Tiwari, 2004).

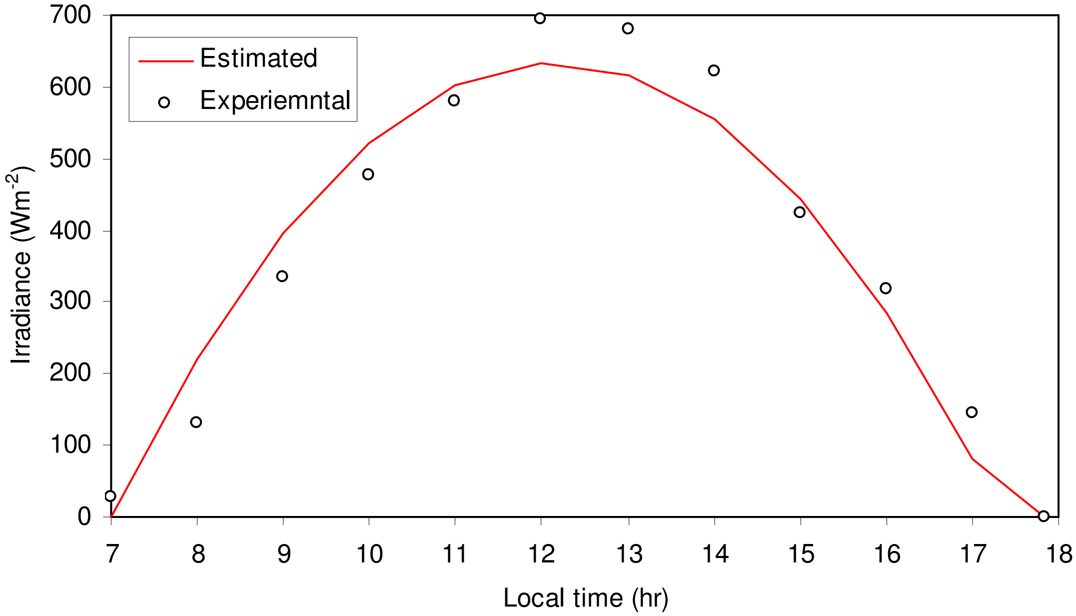

Fig.3.11: Estimated and experimental global irradiance on 27th March 2002 at New Delhi.

Fig.3.12 shows the variation of cumulative simulated and experimental distillate output. It is observed that there is close conformity between the two sets of data but simulated values are slightly higher than experimental data after 18:00. This is probably due to vapour and distillate leakage from a practical solar still. In the simulation process, it was assumed that there is no leakage of vapour and distilled water. Nevertheless, the root mean square error of simulation was 15 %, which is better than 32.13 % reported by Tripathi and Tiwari (2004) when they used their model on the same data. In addition, a statistical comparison between simulated and experimental distillate output yielded a computed *t*-value of 1.58 while the cut-off point for the *t*-statistic is 3.768 at 23 degrees of freedom. This indicates that the present model provides estimates that are not significantly different from empirical values (Stone, 1993). With this level of confidence, a sensitivity analysis of the proposed model was performed on the ASS.

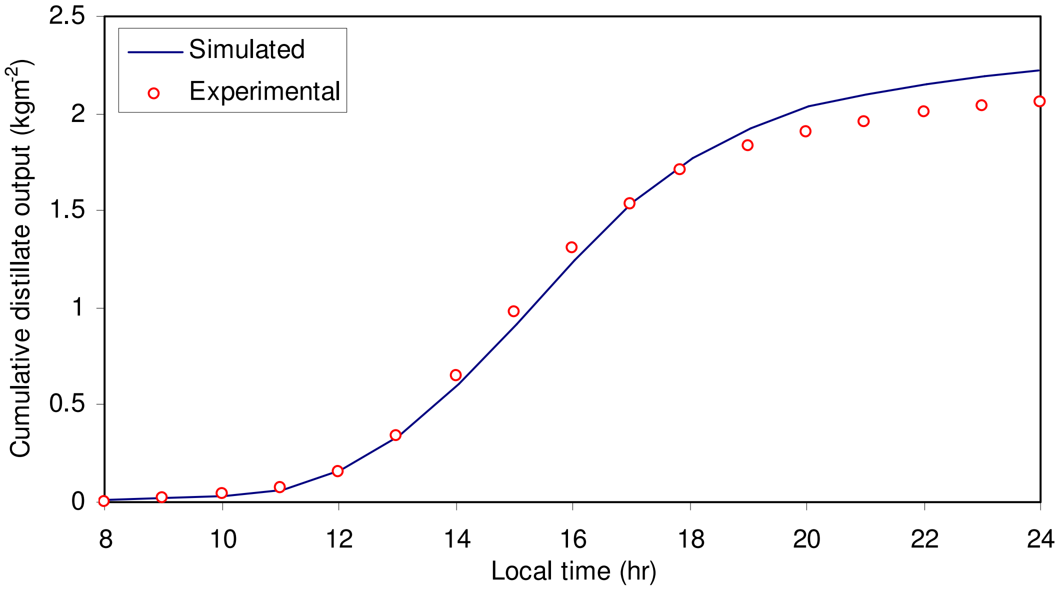

Fig.3.12: Simulated and experimental cumulative distillate yield.

3.4.6 Sensitivity analysis

A sensitivity analysis of the advanced solar still with a separate condenser was carried out (A parameter was varied while all the others were fixed at their respective reference levels). Fig.3.13 shows the variation of distillate productivity with the absorptance of the basin liner in the evaporator basin (α_{bl}). It is seen that productivity significantly increases with the magnitude of α_{bl}, consistent with Eq.(3.55) and results commonly reported in literature. For this reason, still basin liners (and other solar absorbing surfaces) are often painted black (or other black thin film used) on the absorber surface to enhance absorption of incoming solar radiation, which increases the water temperature and distillate yield.

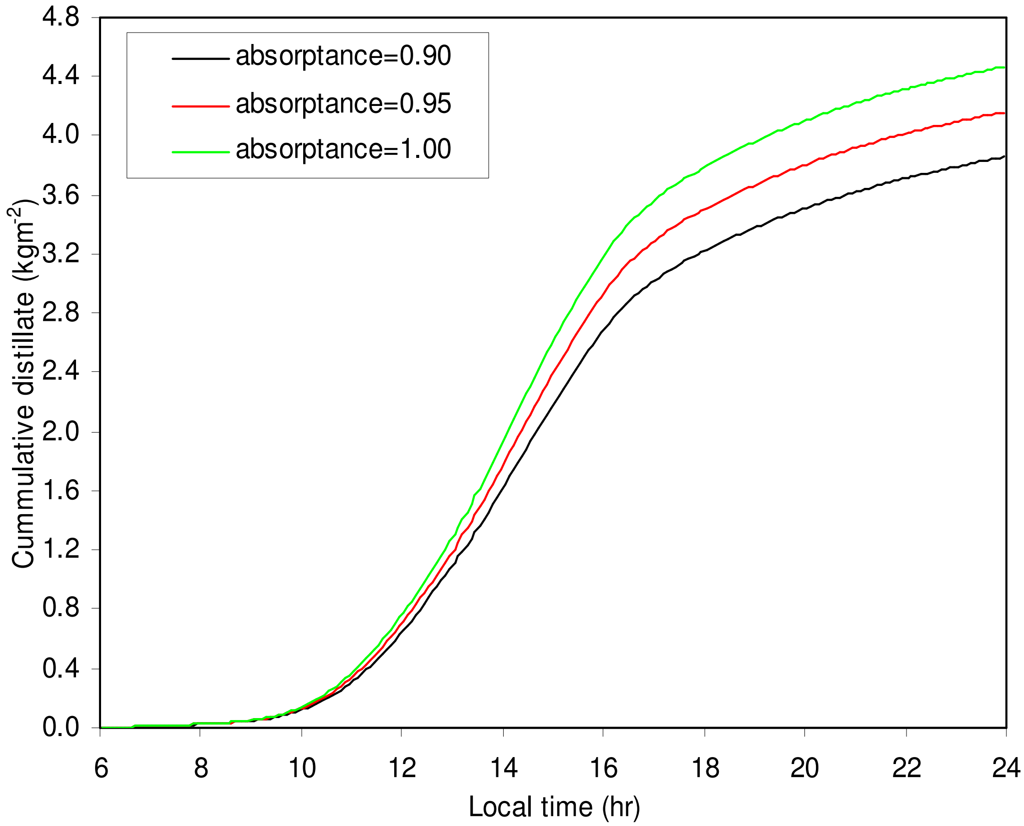

Fig.3.13: Effect of absorptance of the evaporator basin liner on distillate yield (for $h_{c,b1-w1}$=100 $Wm^{-2}K^{-1}$, m_{w1}=20 kg, m_{w2}=13 kg, m_{w3}=13 kg, R′=0.65 and U_{bo}=1.203 $Wm^{-2}K^{-1}$).

Fig.3.14 shows the effect of the ratio of the volume of the evaporator chamber to that of the condenser chamber (R′). It is observed that the distillate production decreases with increasing values of R′. This observation is attributed to the fact that R′ increases with the volume of the evaporator. Nevertheless, the pressure of air decreases with increasing its volume. So, as the volume of the evaporator increases, the pressure in this chamber decreases, which results in a decrease in the rate of purging. These results are consistent with findings of Fath (1996).

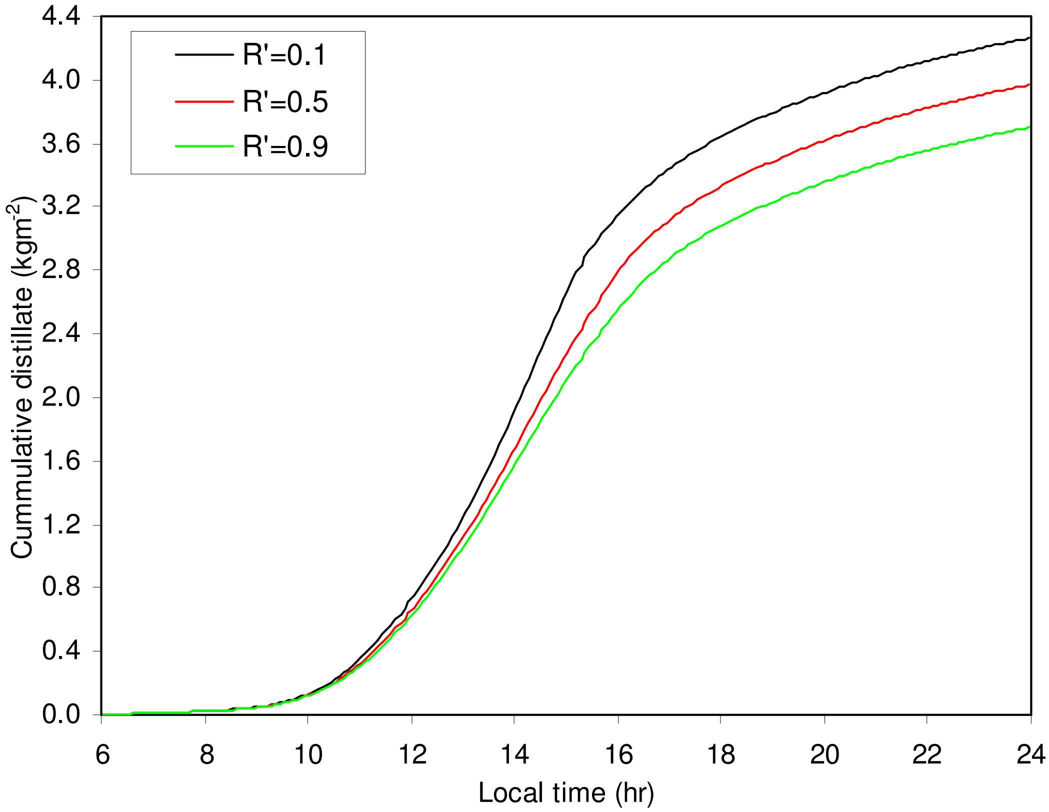

Fig.3.14: Effect of the ratio of the volume of the evaporator to condenser (R′) on distillate yield (for $h_{c,b1-w1}$=100 $Wm^{-2}K^{-1}$, m_{w1}=20 kg, m_{w2}=13 kg, m_{w3}=13 kg, U_{bo}=1.203 $Wm^{-2}K^{-1}$ and α_{bl}=0.90).

Fig.3.15 shows the effect of changing the values of the coefficient of convective heat transfer from the evaporator basin liner to saline water ($h_{c,b1-w1}$) on the level of distillate production. It is observed that the yield of distilled water is not affected by the variation of $h_{c,b1-w1}$ within the range considered in this study. These findings conform to the previous work. Mowla and Karimi (1995) used a value of 130 W m^{-2} K^{-1} while Zurigat and Abu-Arabi (2004) chose a value of 135 W m^{-2} K^{-1}. Tripathi and Tiwari (2006) reported $h_{c,b1-w1}$ = 100 Wm^{-2} K^{-1}. In all these studies, the authors found realistic simulation results.

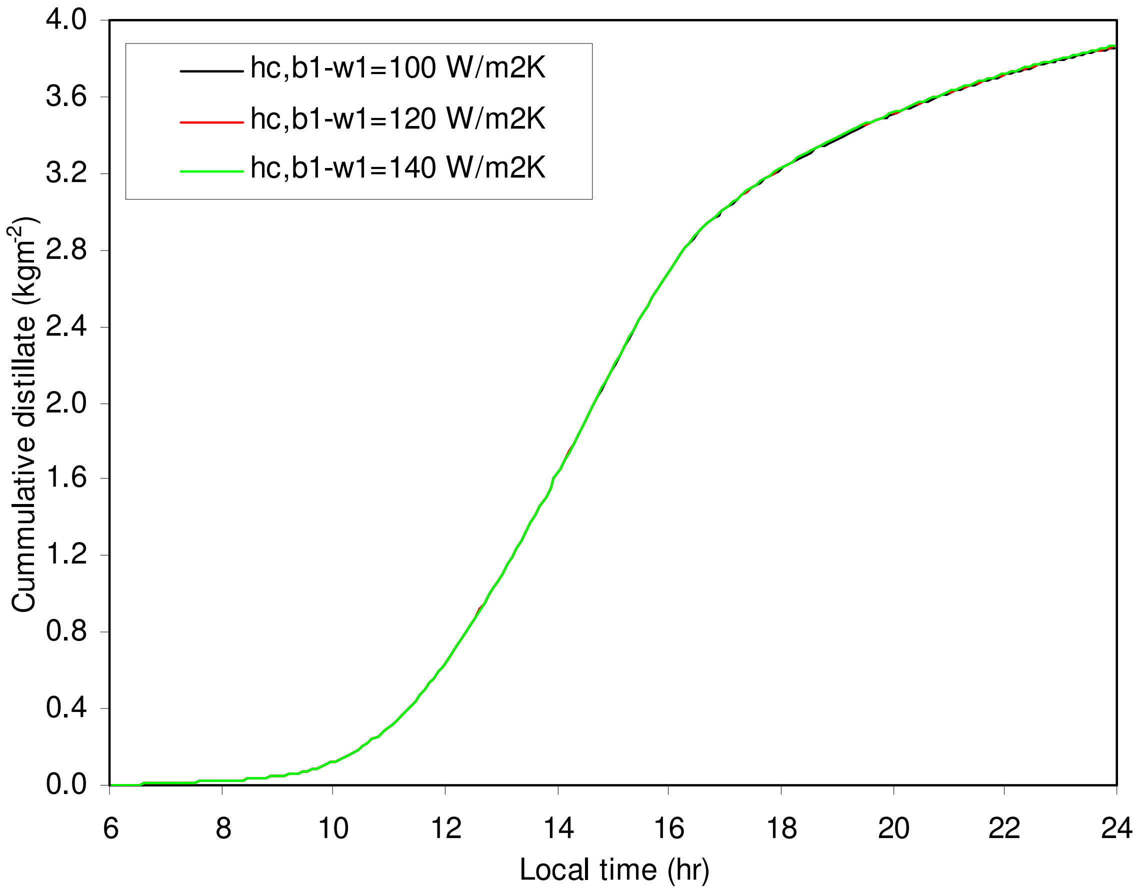

Fig.3.15: Effect of the coefficient of convective heat transfer from the evaporator basin liner (b1) to saline water (w1) on distillate yield (for m_{w1}=20 kg, m_{w2}=13 kg, m_{w3}=13 kg, R′=0.65, U_{bo}=1.203 $Wm^{-2}K^{-1}$ and α_{bl}=0.90).

The effect of the mass of water in the first (m_{wl}), second (m_{w2}) and third (m_{w3}) basins on the distillate productivity are presented in Fig.3.16. Productivity decreases by 0.763 kg m^{-2} when m_{wl} is increased from 10 to 30 kg, due to an increase in the thermal mass of water which results in low temperatures being attained by the water (for the same amount of solar radiation intercepted by the system).These results conform to well-known previous findings on the effect of m_{wl} on distillate productivity. Productivity decreases by 0.332 kg m^{-2} when m_{w2} is increased from 10 to 30 kg. Similarly, distillate productivity decreases by 0.026 kg m^{-2} when m_{w3} increased from 10 to 30 kg, which shows that the effect of m_{w3} on distillate productivity is not significant.

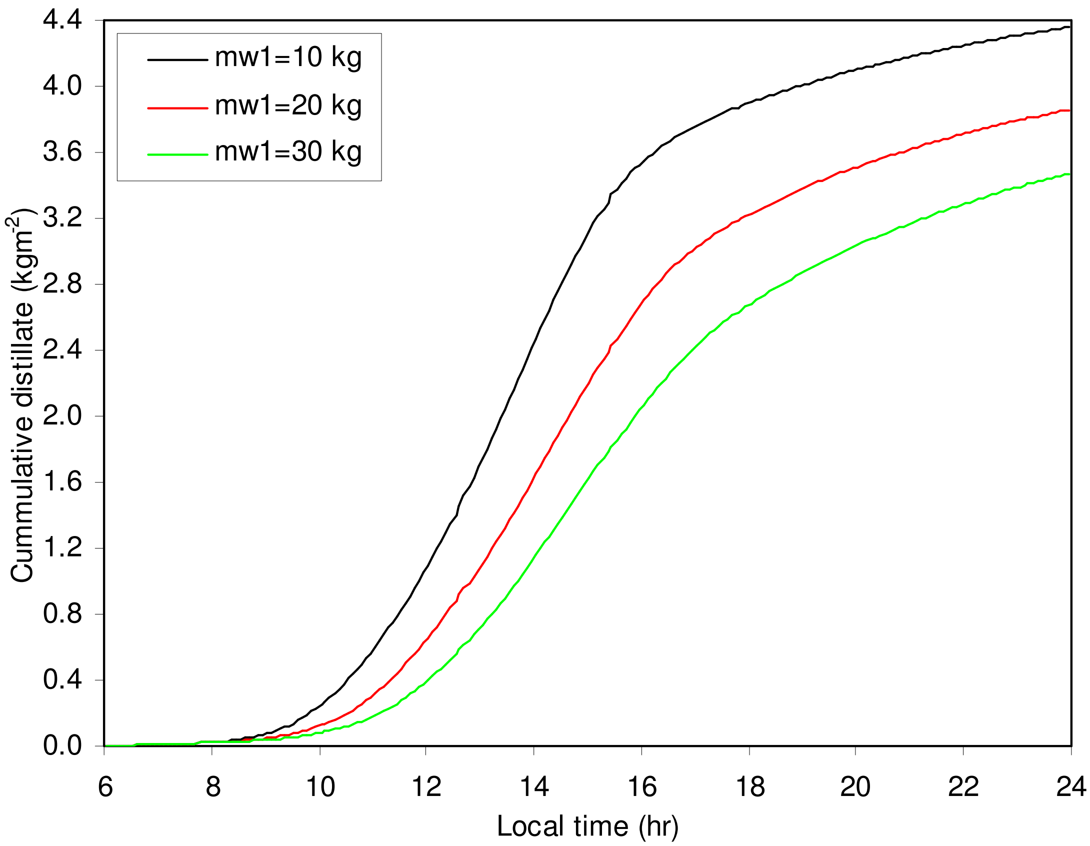

Fig.3.16 (a): Effect of the mass of water in basin 1 (m_{w1}) on distillate productivity. (for $h_{c,b1-w1}$=100 $Wm^{-2}K^{-1}$, m_{w2}=13 kg, m_{w3}=13 kg, R'=0.65, U_{bo}=1.203 $Wm^{-2}K^{-1}$ and α_{bl}=0.90).

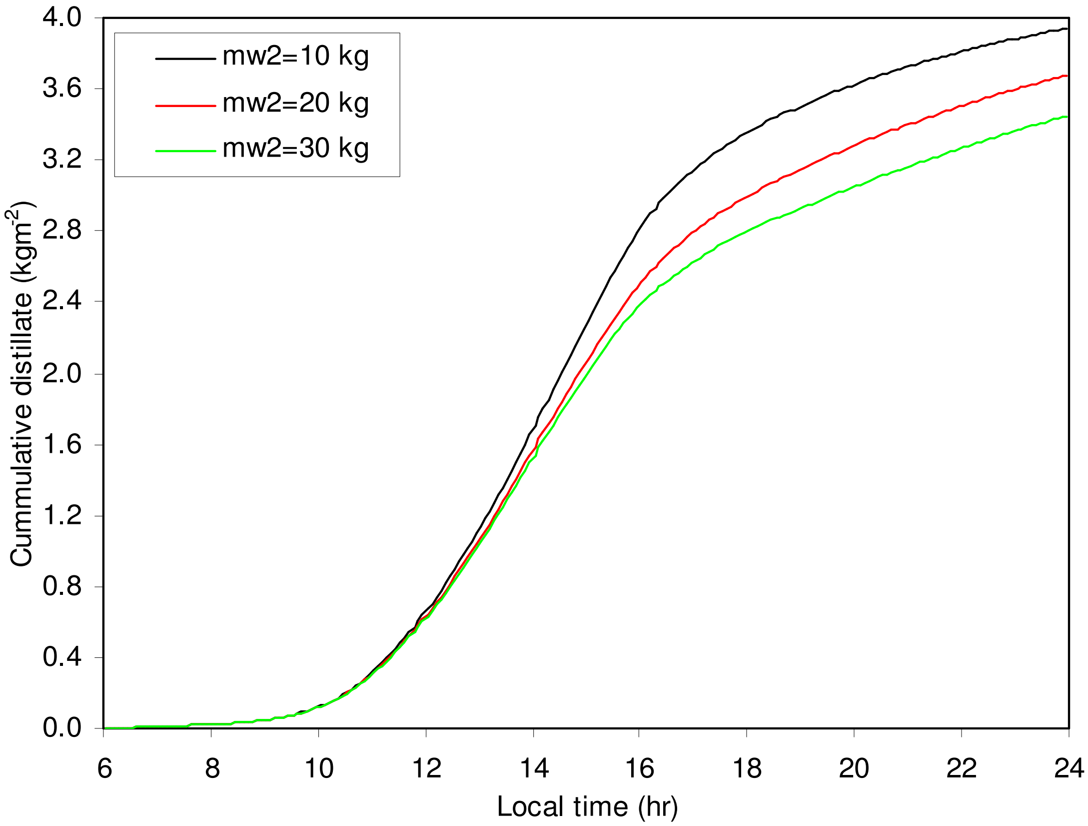

Fig.3.16 (b): Effect of the mass of water in basin 2 (m_{w2}) on distillate productivity (for $h_{c,b1-w1}$=100 $Wm^{-2}K^{-1}$, m_{w1}=20 kg, m_{w3}=13 kg, R′=0.65, U_{bo}=1.203 $Wm^{-2}K^{-1}$ and α_{bl}=0.90).

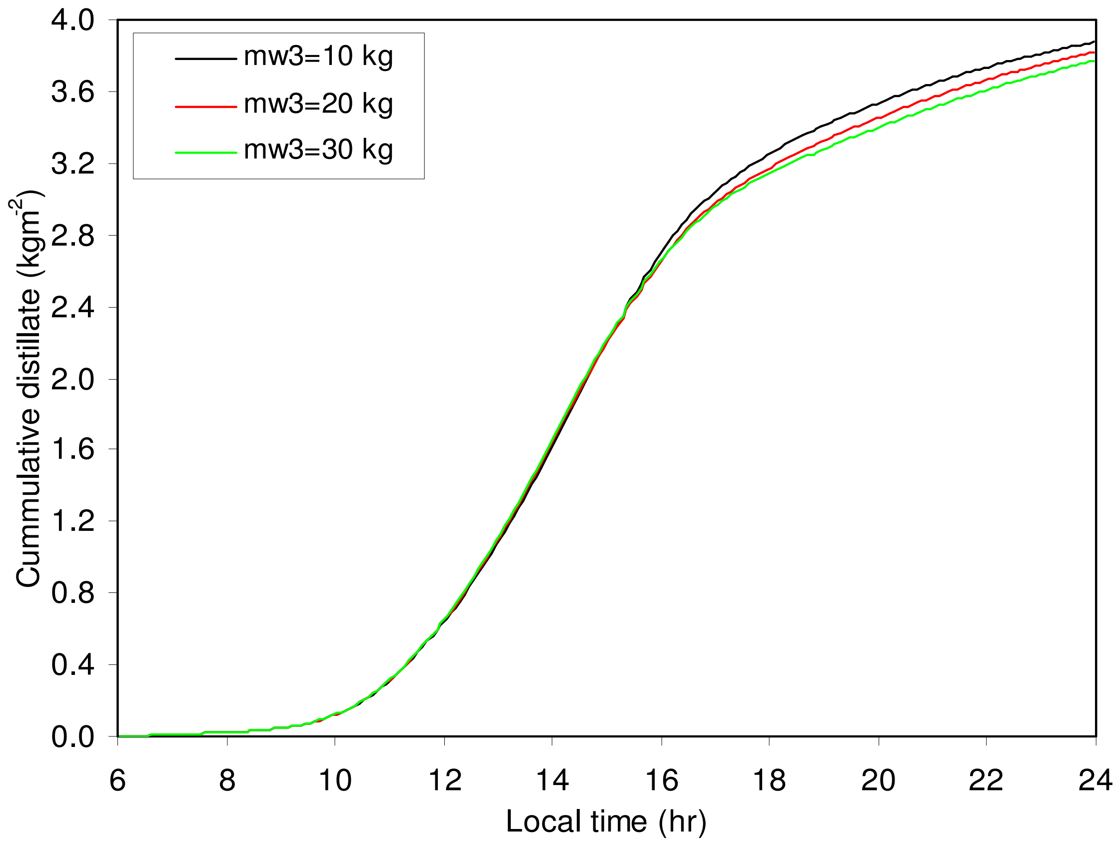

Fig.3.16 (c): Effect of the mass of water in basin 3 (m_{w3}) on distillate productivity (for $h_{c,b1-w1}$=100 $Wm^{-2}K^{-1}$, m_{w1}=20 kg, m_{w2}=13 kg, U_{bo}=1.203 $Wm^{-2}K^{-1}$, R'=0.65 and α_{bl}=0.90).

The effect of heat loss from the bottom of a still on distillate production is shown in Fig.3.17. It is observed that distillate production drastically decreases with increasing heat loss from the bottom part of the still. In particular, distillate production decreases by 1.713 kg m^{-2} when U_{bo} is increased from 1 to 9 $Wm^{-2}K^{-1}$. This trend of results is attributed to the fact that a small amount of energy is available to elevate the temperature of saline water when a large proportion of the input heat is lost to the environment through the bottom of the still. Cooper (1969, 1973) also found that distillate production significantly decreased with the coefficient of bottom heat loss.

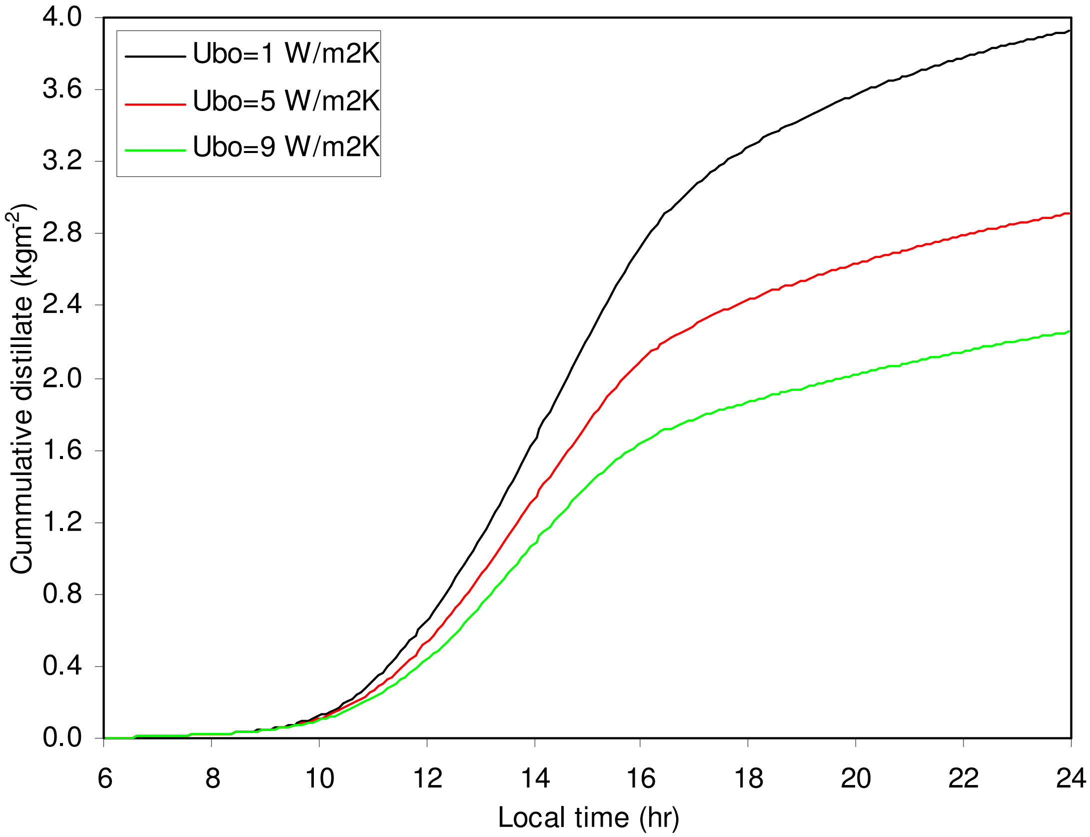

Fig.3.17: Effect of the bottom heat loss (U_{bo}) on distillate productivity (for $h_{c,b1-w1}$=100 $Wm^{-2}K^{-1}$, m_{w1}=20 kg, m_{w2}=13 kg, m_{w3}=13 kg, R′=0.65 and α_{bl}=0.90).

A summary of the sensitivity analysis is presented in Table 3.4. It is observed that the ASS is sensitive to the absorptance of basin liner 1 (α_{bl}), ratio of the evaporator to condenser chamber volumes (R′), mass of water in basins 1 (m_{w1}) and 2 (m_{w2}), and coefficient of heat loss from the bottom of the still. However, the mass of water in basin 3 (m_{w3}) marginally affects the performance of the still. Distillate production is insensitive to the variation in the coefficient of heat transfer from the evaporator basin liner to saline water. The proposed model was used to appraise the performance of prototype conventional and advanced solar stills. So, the design philosophy of a solar still is given in the next chapter.

Table 3.4: Summary of the results of the effects of various parameters on distillate productivity of the ASS.

Parameter	Effect
$h_{c,b1-w1}$ (W m^{-2} K^{-1})	Insensitive
m_{w1} (kg)	Sensitive
m_{w2} (kg)	Sensitive
m_{w3} (kg)	Marginally sensitive
R' (dimensionless)	Sensitive
U_{bo} (W m^{-2} K^{-1})	Sensitive
α_{bl} (dimensionless)	Sensitive

3.5 Summary

In this chapter, a mathematical model for simulating the performance of single slope solar stills has been presented. Simulation involves four tasks: a) drawing a physical model, b) formulating a mathematical model and solving the system of equations in the numerical model. These equations can be solved by using a special purpose or general purpose computer program. Following this approach, a new model for calculating the distribution of solar radiation inside a single slope solar still has been proposed. This model takes into account characteristics of solar radiation, and view factors of surfaces that exchange radiation. The model is used to calculate effective irradiance required in the energy balance equations for a conventional solar still (CSS) and an advanced solar still (ASS). These equations are then solved by using a special purpose computer program in MATLAB. The model is calibrated using empirical data from previous work, and its sensitivity is analysed. It is found that the CSS theoretically produces less distilled water than the ASS under the same meteorological conditions. In addition, there is good agreement between theoretical and empirical distillate yield. The productivity of the ASS is sensitive to the absorptance of the evaporator basin liner, ratio of the evaporator to condenser chamber volumes, mass of water in basins 1 (m_{w1}) and 2 (m_{w2}) and coefficient of heat loss from the bottom of the still. These numerical results were used to design and construct prototype conventional and advanced solar stills described in Chapter 4.

3.6 References

Abdallah, S., Badran, O. and Abu-Khader, M.M., 2008. Performance evaluation of a single slope solar still. *Desalination*, 219, pp.222-230.

Abu-Arabi, M., Zurigat, Y., Al-Hinai, H. and Al-Hiddabi, S., 2002. Modelling and performance analysis of a solar desalination unit with double-glass cover cooling. *Desalination*, 143, pp.173-182.

Abu-Qudais, M., Abu-Hijleh, B.A.K. and Othman, O.N., 1996. Experimental study of a solar still using external condenser. *Energy*, 21, pp.851-855.

Al-Hinai, H., Al-Nassri, M.S. and Jubran, B.A., 2002. Parametric investigation of a double-effect solar still in comparison with a single-effect solar still. *Desalination*, 150, pp.75-83.

Al-Kharabsheh, S. and Goswami, D.Y., 2003. Experimental study of an innovative solar water desalination system utilizing a passive vacuum technique. *Solar Energy*, 75, pp.395-401.

Andesron, E.E., 1983. *Fundamentals of solar energy conversion*. Reading: Addison-Wesley Publishing Company, pp.52-53, 193-195.

ASHRAE, 2001. *ASHRAE Handbook Fundamentals*. SI ed. Atlanta: American Society of Heating, Refrigerating and Air-Conditioning Engineers.

Banat, F., Jumah, R. and Garaibeh, M., 2002. Exploitation of solar energy collected by solar stills for desalination by membrane distillation. *Renewable Energy*, 25, pp.293-305.

Belessiotis, V., Voropoulos, E. and Delyannis, E., 1995. Experimental and theoretical method for determination of the daily output of a still: input-output method. *Desalination*, 100, pp.99-104.

Burden, R.L. and Faires, J.D., 1985. *Numerical Analysis*. 3rd ed. Boston: PWS Publishers.

Clarke, J.A. and Strachan, P.A., 1994. Simulation of conventional and renewable building energy systems. *Renewable Energy*, 5, pp.1178-1189.

Cooper, P.I., 1969. Digital simulation of transient solar still processes. *Solar Energy*, 12, pp.313-331.

Cooper, P.I., 1973. The maximum efficiency of single-effect solar stills. *Solar Energy*, 15, pp.205-217.

Cooper, P.I. and Read, W.R.W., 1974. Design philosophy and operating experience for Australian stills. *Solar Energy*, 16, pp.1-8.

Diabate´, L., Blanc, Ph. and Wald, L., 2004. Solar climate in Africa. *Solar Energy*, 76, pp.733–744.

Duffie, J.A. and Beckman, W.A., 2006. *Solar Engineering of Thermal Processes*. 3rd ed. New York: John Wiley & Sons Inc., pp.85-113, 855-856.

Dunkle, R.V., 1961. Solar water distillation: the roof type still and a multiple effect diffusion still. *International Development in Heat Transfer: International Heat Transfer Conference*. University of Colorado, 895-902 (part 5).

El-Bahi, A. and Inan, D., 1999a. Analysis of a parallel double glass solar still with separate condenser. *Renewable Energy*, 17, pp.509-521.

El-Bahi, A. and Inan, D., 1999b. A solar still with minimum inclination, coupled to an outside condenser. *Desalination*, 123, pp.79-83.

El-Nashar, A.M., 1990. Computer simulation of the performance of a solar desalination plant. *Solar Energy*, 44, pp.193-205.

El-Nashar, A.M., 1992. Optimizing the operating parameters of a solar desalination plant. *Solar Energy*, 48, pp.207-213.

Fath, H.E.S. and Elsherbiny, S.M., 1993. Effect of adding a passive condenser on solar still performance. *Energy Conversion and Management*, 34, pp.63-72.

Fath, H.E.S., 1996. High performance of a simple design, two effect solar distillation unit. *Desalination*, 107, pp.223-233.

Gandhidasan, P. and Abualhamayedl, H.I., 1994. A simple analysis of solar desalination of seawater. *Desalination*, 99, pp.137-147.

Garg, H.P. and Mann, H.S., 1976. Effect of climatic, operational and design parameters on the year round performance of single-sloped and double-sloped solar still under Indian arid zone conditions. *Solar Energy*, 18, pp.159-164.

Hoffbeck, J.P., Sarwar, M. and Rix,,E.J., 2001. Interfacing MATLAB with a parallel virtual processor for matrix algorithms. *Journal of Systems and Software*, 56, pp.77-80.

Houbak, N., 1995. Simulation of energy systems – guidelines and pitfalls. *Mathematics and computers in simulation*, 39, pp.559-564.

Howell, J.R., Bannerot, R.B. and Vliet, G.C., 1982. *Solar-thermal energy systems: Analysis and design*. New York: MacGraw-Hill Book Company, pp.124-154.

IAPWS, 1996. *The IAPWS Formulation 1995 for the thermodynamic properties of ordinary water substance for general and scientific use*. International Association for the Properties of Water and Steam.

Incropera, F.P., DeWitt, D.P., Bergman, T.L. and Lavine, A.S., 2007. *Fundamentals of heat and mass transfer*. 6th ed. New Jersey: John Wiley & Sons, pp.256-317, 560-595,724-776, 929-956.

Kalogirou, S., 1997. Survey of solar desalination systems and system selection. *Energy*, 22, pp.69-81.

Klein, S.A., 1975. Calculation of flat-plate collector loss coefficients. *Solar Energy*, 17, pp.79-80.

Klein, S.A. et al., 1975. A method of simulation of solar processes. *Solar Energy*, 17, pp.29-37.

Kumar, S. and Tiwari, G.N., 1996. Estimation of convective mass transfer in solar distillation systems. *Solar Energy*, 57, pp.459-464.

Lenel, U.R. and Mudd, P.R., 1984. A review of materials for solar heating systems for domestic hot water. *Solar Energy*, 32, pp.109-120.

Lienhard IV, J.H., and Lienhard V, J.H., 2006. *A heat transfer textbook*. 3rd ed. Cambridge Massachusetts: Phlogiston Press.

Loutzenhiser, P.G. etal., 2007. Empirical validation of models to compute solar irradiance on inclined surfaces for building energy simulation. *Solar Energy*, 81, pp.254-267.

Madhlopa, A., 2006. Solar radiation climate in Malawi. *Solar Energy*, 80, pp.1055-1057.

Madhlopa, A. and Ngwalo, G., 2007. Solar dryer with thermal storage and biomass-backup heater. *Solar Energy*, 81, pp.449-462

Madhlopa, A. and Johnstone, C., 2009. Model for computation of solar fraction in a single-slope solar still. *Solar Energy*, 83, pp.873-882 .

Malik, M.A.S. and Van Tran, V., 1973. A simplified mathematical model for predicting the nocturnal output of a solar still. *Solar Energy*, 14, pp.371-385.

Muneer, T., Hawas, M.M. and Sahili, K., 1984. Correlation between hourly diffuse and global radiation for New Delhi. *Energy Conversion and Management*, 24, pp.265-267.

Mowla, D. and Karimi, G., 1995. Mathematical modelling of solar stills in Iran. *Solar Energy*, 55, pp.389-393.

Muneer, T., 1997. *Solar radiation & daylight models for the energy efficient design of buildings*. Oxford: Reed Educational and Professional Publishing Ltd.

Nafey, A.S., Abdelkader, M., Abdelmotalip, A. and Mabrouk, A.A., 2000. Parameters affecting solar still productivity. *Energy Conversion and Management*, 41, pp.1797-1809.

Nafey, A.S., 2005. Simulation of solar heating systems – an overview. *Renewable and Sustainable Energy Reviews*, 9, pp.576-591.

Norton, B. and Probert, S.D., 1987. Diurnal performance of a thermosyphonic solar water heaters – an empirical prediction method. *Solar Energy*, 39, pp.257-265.

Porta, M.A., Chargoy, N. and Fernández, J.L., 1997. Extreme operating conditions in shallow solar stills. *Solar Energy*, 61, pp.279-286.

Radhwan, A.M., 2004. Transient performance of a stepped solar still with built-in latent heat thermal energy storage. *Desalination*, 171, pp.61-76.

Shaw, B.D., 1993. Asymptotic analysis of the lumped-capacitance approximation. *Heat and Mass Transfer*, 36, pp.999-1006.

Stone, R.J., 1993. Improved statistical procedure for the evaluation of solar radiation estimation models. *Solar Energy*, 51, pp.289-291.

Tan, Z., Su, G. and Su, J., 2009. Improved lumped models for combined convective and radiative cooling of a wall. *Applied Thermal Engineering*, 29, pp.2439-2443.

Tchinda, R., Kaptouom, E. and Njomo, D., 1999. Heat and mass transfer processes in a solar still with an indirect evaporator-condenser. *Energy Conversion and Management*, 41, pp.93-107.

Tiwari, G.N., Singh, H.N. and Tripathi, R., 2003. Present status of solar distillation. *Solar Energy*, 75, pp.367-73.

Tiwari, A.K. and Tiwari, G.N., 2007. Thermal modelling based on solar fraction and experimental study of the annual performance of a single slope passive solar still: The effect of water depths. *Desalination*, 207, pp.184-204.

Tleimat, B.W. and Howe, E.D., 1966. Nocturnal production of solar distillers. Solar *Energy* 10, pp.61-66.

Tripathi, R. and Tiwari, G.N., 2004. Performance evaluation of solar still by using the concept of solar fraction. *Desalination*, 169, pp.69-80.

Tripathi, R. and Tiwari, G.N., 2006. Thermal modelling of passive and active solar stills for different depths of water by using the concept of solar fraction. *Solar Energy*, 80, pp.956-967.

Vestlund, J., Rönnelid, M. and Dalenbäck, J., 2009. Thermal performance of gas-filled flat plate solar collectors. *Solar Energy*, 83, pp.896-904.

Voropoulos, K., Mathioulakis, E. and Belesssiotis, V., 2003. Experimental investigation of the behaviour of a solar still coupled with hot water storage tank. *Desalination*, 156, pp.315-322.

Zurigat, Y.H. and Abu-Arabi, M.K., 2002. Modelling and performance analysis of a Solar desalination unit with double-glass cover cooling. *Desalination*, 143, pp.173-182.

Zurigat, Y.H. and Abu-Arabi, M.K., 2004. Modelling and performance analysis of a regenerative solar desalination unit. *Applied Thermal Engineering* 24, pp.1061-1072.

Chapter 4

Experimental design

4.0 Introduction

Development of an engineering process or product involves designing and testing stages (Fig.4.1). A new process or product is often designed, tested, re-designed and re-tested until a satisfactory outcome is achieved (Grove and Davis, 1992). Thus, some kind of experimentation is required to assess the effect of a change in an independent variable (factor) on a dependent variable (outcome). A factor may be qualitative or quantitative, with the former type having no numerical difference between its levels. In contrast, a quantitative factor is measured on a suitable scale. The possible qualities or values taken by a factor are known as levels. Brown and Melamed (1993) reported that dependent variables ought to be always quantitative.

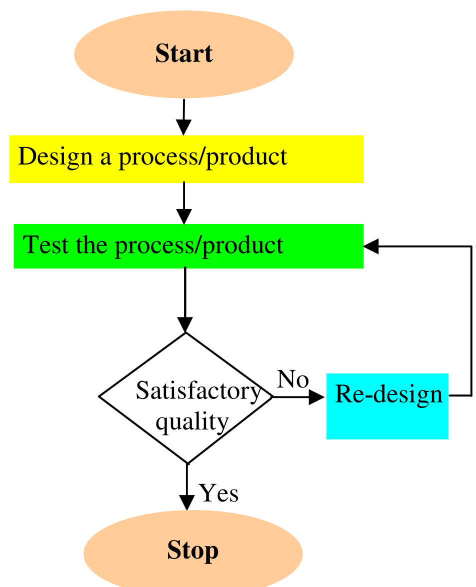

Fig.4.1: Flow chart of the development of an engineering process or product.

A hypothetical example of an experiment with three factors (A_{bl}, D and m_{w1}) and two levels for each factor is presented in Table 4.1. In this example, distillate output is a dependent variable. It should particularly be noted that the design factor has qualitative levels while the other factor levels have numerical differences. All factors have two levels but it is possible for factors to take different values of levels in an experiment (NIST/SEMATECH, 2005).

Table 4.1: Example of an experiment with three factors and two levels.

Factor	Type	Level	
		1	2
Area of still basin (A_{bl})	Quantitative	A=1.0 m^2	A=3.0 m^2
Solar still design (D)	Qualitative	CSS	ASS
Mass of saline water (m_{w1})	Quantitative	m_{w1}=10 kg	m_{w1}=40 kg

An experiment is a trial formulated to assess the effect of changing the level of one or more factors on the outcome. Such an assessment requires measurements for analysis, interpretation and decision-making. So, it is important to collect valid data. This can be achieved by using a suitable experimental design. An experimental design is a plan for carrying out experimental activities in order to collect data of good quality, and it is influenced by the objectives of the experiment, number of factors under investigation and economic factors (NIST/SEMATECH, 2005).

In this chapter, the purpose of an experimental design, and procedures for data acquisition and processing are described. A randomized block design was found suitable for this investigation, and it was used to take measurements for analysis and interpretation.

4.1 Experimental design

4.1.1 Purpose and classification of experimental designs

Once the need to conduct an experiment is established, the next step is to formulate a suitable experimental design which is aimed at collecting data of high quality. It should also be mentioned that the number of observations influences the statistical significance of data (Lachin, 1981; Rasch et al., 2007). So, the design of an experiment needs to incorporate test sequence, instrumentation and procedures for data collection. Standard instruments and procedures ensure collection of valid data which is commonly presented in columns as variables (NIST/SEMATECH, 2005). Then, the collected data is analyzed to understand the underlying influences, establish relationships amongst variables and statistically test some hypotheses.

Factor levels are combined to construct an experimental design, and each combination of the levels is a run (Grove and Davis, 1992). For instance, factor levels of Table 4.1 are combined to yield 8 runs presented in Table.4.2. All the 8 possible runs collectively constitute the experiment for studying the effects of changing factor levels on distillate output. It is observed that all the three factors are set at the normal level in the first configuration (run 1) of this experimental design. Only factor m_{w1} is changed in run 2. Various factors are changed from run 3 through run 8, forming a matrix of factor levels (with runs as rows and factors as columns). Each run is then assigned to a test unit by using random or non-random sampling. In random sampling, all the test units have equal chances of being chosen. Consequently, randomization is recommended if its implementation is practically feasible (Grove and Davis, 1992). On the other hand, test units do not have equal chances of being selected in non-random sampling. This approach creates bias, and its application is therefore limited to situations where a random approach is extremely difficult to use in practice.

Table 4.2: An experimental design constructed from Table 4.1.

Run	Factor		
	A_{bl}	D	m_{w1}
1	1	1	1
2	1	1	2
3	1	2	1
4	2	1	1
5	2	1	2
6	2	2	1
7	1	2	2
8	2	2	2

Experimental designs can be classified according to the objectives of the experiment (NIST/SEMATECH, 2005):

a) Comparative objective

   In this category of experimental designs, an experiment is conducted to compare one or more factors at different levels. The design is completely randomized or randomized with blocking.

b) Screening objective

   An experiment is conducted to choose major important effects from a group of many important ones in an objective experimental design. This class comprises factorial and Plackett-Burman experimental designs.

c) Surface objective

   An experiment is carried out to enable estimation of the interaction and quadratic effects, and to give an idea about the outcome surface being investigated. Central composite or Box-Behnken experimental designs are in this class of plans for experimentation.

4.1.2 Data processing

Techniques for data analysis fall into graphical and quantitative parts. Graphical techniques include scatter plots, probability plots, lag plots and box plots. They provide a quick way of getting insight into the data sets with regard to testing assumptions, selection of probability distribution, identification of relationships amongst variables, determination of the effect of a given factor and determination of outlying data points (NIST/SEMATECH, 2005).

Quantitative techniques give a value or set of values which can then be interpreted. These techniques include testing of hypotheses, analysis of variance, estimation of points and confidence intervals, and regression (Rasch et al., 2007). Qualitative and quantitative techniques may complement each other. For instance, a probability plot may yield information about the underlying distribution for use in hypothesis testing.

4.2 Purpose of present experimentation

The main objective of the present research was to develop a solar still with improved distillate output. To achieve this goal, it was found necessary to work with the model developed in Chapter 3 to design and construct a conventional solar still as a bench mark and a prototype of the advanced solar distillation system with improved output and then test them. This approach is consistent with the developmental cycle of an engineering process (Grove and Davis, 1992). It should also be mentioned that modelling is a vital tool for the development of an engineering product or process. Nevertheless, it is necessary to verify any new model before it is applied, and the verification process requires empirical input and output data. The empirical input data is used to determine theoretical output from a solar still, and the predicted yield is compared with the experimental output (Kumar and Tiwari, 1996; Tripathi and Tiwari, 2004).

The performance of a solar still is affected by design, operating and meteorological parameters (Garg and Mann, 1976; Nafey et al., 2000). It is therefore necessary to test a new solar still design under a given set of operating and environmental conditions in order to establish its performance under real conditions. Consequently, experimentation and a suitable experimental design were needed to collect empirical data for model verification and system evaluation in the present research.

4.3 Present experimental design

In theoretical analysis of solar stills, data on input variables (design, operating and climatic parameters) is used to predict the distillate output. It is shown in Chapter 2 that previous models for computing effective irradiance in a single-slope solar still have limited accuracy. So, a new model was proposed to overcome this limitation. For a given set of design, operating and meteorological factors, the level of predicated effective beam irradiance is influence by solar azimuth (γ_s) and altitude (ψ) angles (Tripathi and Tiwari, 2004; Madhlopa and Johnstone, 2009a). The effects of γ_s and ψ on beam irradiance intercepted by a vertical surface have been discussed in Chapter 2. It should be noted that ψ is always less than 90^o at locations outside the tropical region. On the other hand, the sun traverses the sky overhead (γ_s=0 and ψ=90^o at solar noon) during certain times of the year at tropical sites. Consequently, location was taken to be one of the factors. It should also be mentioned that the cost of implementation increases with the number of locations at which the experiment is executed. So, two locations (University of Strathclyde and Malawi Polytechnic) were used. These locations were chosen based on astronomical, meteorological and logistical factors. The University of Strathclyde is located outside the tropical region at a latitude of 55^o 52′ N and longitude of 4^o 15′ W with a temperate climate while the Malawi Polytechnic is a tropical site at a latitude of 15^o 48′ S and longitude of 35^o 02′ E with a tropical climate. Such a contrast between the test sites would provide experimental outcomes with possible universal application. It was also convenient for the researcher to execute the project at these locations because of an existing formal link between the two institutions. It should also be mentioned that similar meteorological conditions are required for comparison of the theoretical performance of solar stills with different designs (Al-Hinai et al., 2002; Zurigat and Abu-Arabi, 2004; Madhlopa and Johnstone, 2009b). This indicates that it was necessary to simultaneously test different solar still designs at any given location.

Another research gap identified in this study was in the design of solar stills. This investigation sought to compare the performance of different designs of solar stills. Again, it should be noted that the cost of the project increases with the number designs used in the investigations. So, the design factor was also limited to a conventional solar still (CSS) and the advanced solar still (ASS), with level 1= CSS and level 2= ASS. In addition, different designs of solar stills are experimentally compared under similar meteorological conditions for valid results (Garg and Mann, 1976; El-Swify and Metias, 2002).

The foregoing discussion shows that a randomized block design (RBD), with system design and location as primary and blocking factors respectively, would be suitable in this research. For a two-factor RBD, the number of runs (N′) was computed from the levels of each factor according to NIST/SEMATECH (2005):

$$N' = \dot{L}_1 \dot{L}_2 \tag{4.1}$$

From Eq.(4.1), 4 possible ways of running the experiment were found and this experimental design is presented in Table 4.3. It is observed that the first and third runs were planned to be done at the University of Strathclyde with the other two runs being carried out at the Malawi Polytechnic. Each run was assigned to an experimental unit depending on the level of the design appearing in the run. For instance, runs 1 and 2 would be assigned to the available units of the CSS while runs 3 and 4 required units of the ASS. This experimental design was used to design and construct prototype solar stills, and collect data on meteorological parameters and distillate production.

Table 4.3: Experimental design for the present investigation.

Run	Factor	
	System design	Location
1	1	1
2	1	2
3	2	1
4	2	2

4.4 Solar still design philosophy

The aim of successful still design is to maximize distillate yield for a given set of environmental and operating factors. This can be achieved by developing and applying a well-structured design methodology. Still design factors can broadly be classified into optical, heat transfer and heat loss characteristics (Cooper and Read, 1974). Optical characteristics are absorption, reflection and transmission of solar radiation when incident on the still. Moreover, solar radiation is the most influential environmental factor in solar energy systems. Once the radiation is absorbed by the still, it is converted to heat which is transferred from the absorber to other components of the still and the environment.

4.4.1 Optical characteristics

Solar radiation can be directly converted to thermal energy through the use of a solar collector, which consists of an absorber plate, preferably painted black for maximum absorption characteristics, with a parallel plate (or plates) and a transparent cover fixed above the absorber plate (Mohamad, 1997). Solar collectors are broadly classified as flat-plate and concentrating collectors (Duffie and Beckman, 2006). Flat-plate collectors are suitable for low temperature applications (from ambient to about 333 K) while concentrating collectors are appropriate for intermediate and high temperatures (Bansal et al., 1984). Depending on the type of fluid used for removing heat from the collector, flat-plate and concentrating collectors are further classified as air heating or liquid heating. A solar collector may be mounted on a tracker (tracking collector) or fixed plane (non-tracking collector). The former type of collectors follows the sun on daily (one-axis) or daily and seasonal (two-axis) basis to maintain a low zenith angle and thereby increase the transmission of solar radiation through the transparent cover and absorption by the absorber plate. In contrast, a non-tracking collector remains fixed in the same position as time changes, and so it needs to be mounted in a plane with optimal inclination and orientation to optimize solar collection.

Non-tracking solar collectors (including distillers) are generally inclined to the horizontal to augment solar collection. Garg and Mann (1976) reported that the optimum tilt angle (β) of the transparent cover on the top part of a conventional solar still is 10^{o} which just enables the distillate to flow downwards on the inner surface of the cover without dropping back into the basin. Nevertheless, β also affects the transmission of solar radiation through the cover (as reported in Chapter 2). So, $\beta > 10^{o}$ is sometimes used depending on the latitude (ϕ) of the site (Nafey et al., 2000). Normally, $\beta=\phi-10^{o}$ for summer season, $\beta=\phi$ for annual performance and $\beta=\phi+10^{o}$ for winter season (Samee et al., 2007). Fixed collectors often face the Equator to optimize solar collection ($\gamma_p=0$ for south-facing surfaces, $\gamma_p=180^{o}$ for north-facing surfaces). It should be mentioned that optimization is necessary for achieving the best possible yield of distilled water. Nevertheless, non-optimal values of design parameters have been used in some of the previous work, depending on the objective of the study. Porta et al. (1997) validated their model on thermal inertia in solar distillers by using a still with $\beta=4^{o}$. Tripathi and Tiwari (2004) used $\beta=8.8^{o}$ for a conventional still tested at a latitude of $28^{o}35'$ N, to validate their model on solar fraction. Later, Tripathi and Tiwari (2006) used an inclination angle of 10.2^{o} to verify the performance of the same model when applied to passive and active solar stills with single slopes at the same location.

Collection of solar energy is also affected by the aspect ratio (AR) of the still. El-Swify and Metias (2002) reported that solar radiation reflected from the walls of a conventional still is optimal when the length is twice the width ($AR= L_{b1}/B_{b1} \approx 2.0$). Nevertheless, non-optimal values of design parameters have been used in some of the previous work, depending on the objective of the study. Porta et al. (1997) validated their model on thermal inertia in solar distillers by using a still with AR=11.3. Tripathi and Tiwari (2004) used AR=1.0 for a conventional still tested at a latitude of $28^{o}35'$ N, to validate their model on solar fraction. Later, these authors used an AR =1.0 to verify the performance of the same model when applied to passive and active solar stills (Tripathi and Tiwari, 2006). Moreover, optical view factors were not taken into account in previous work. Thus, their models for the distribution of solar energy inside a solar still would have limited accuracy.

For given angle of inclination and aspect ratio, the amount of solar radiation directly and indirectly reaching the surface of saline water also depends on the height of the front wall of the still as shown in Section 3.1.1. The area of saline water directly receiving beam radiation increases with decreasing the height of the front wall for fixed length and width of the still (Eq.3.15). In addition, the surface of saline water in basin 1 views a larger proportion of the sky which results in an increase in the amount of diffuse radiation directly received by the water as the height of the front wall (Z_{fw}) decreases (Eq.3.21). It should be noted that a relatively small proportion of solar radiation is indirectly received by the saline water in basin 1 due to the effect of view factors (W_{bw-w1}=0.29 for CSS and W_{bw-w1}=0.30 for the ASS, W_{er-w1}=0.09 in this study) as reported in Chapter 3. So, the design of a single slope solar still aims at reducing Z_{fw} in order to enhance direct interception of solar radiation by the saline water. Ideally, Z_{fw} =0 would be optimal but consideration is also given to distillate drainage fittings between the top of the front wall and basin 1 (Fig.4.2). In Fig.4.2, the bend was circular to prevent it from trapping distillate. Therefore, $Z_{fw} > 0$ has been used by some of the previous researchers. Samee et al. (2007) studied a conventional single slope solar still with Z_{fw} =0.28 m. They found a still efficiency of 30.65 % which is satisfactory for this design of stills (Al-Kharabsheh and Goswami, 2003). Phadatare and Verma (2007) found efficiencies of up to 34 % for a plastic solar still with Z_{fw} =0.32 m. So, $Z_{fw} > 0$ was also used in this investigation. Solar radiation that is absorbed by a solar still is converted to thermal energy, and part of this energy is lost to ambient air through the bottom and sides of the still.

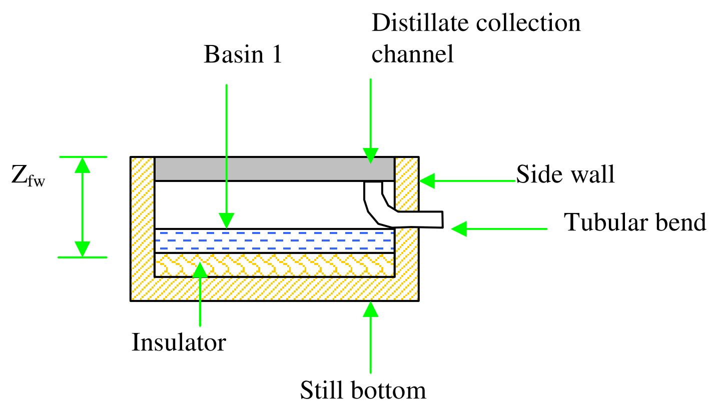

Fig.4.2: Gap between basin 1 and the top of the front wall.

4.4.2 Internal heat transfer

Heat generated by the basin liner of a solar still is transferred to the saline water in the basin by convection ($h_{c,b1-w1}$). Then, the hot saline water releases heat to the transparent cover and walls of the still through convection, evaporation and radiation. This elevates the temperature of the transparent cover, thereby reducing the temperature gradient between the cover and the water, and the rate of distillation. It should be noted that the rates of convection and evaporation are affected by the geometry of the still (Eqs.2.73 to 2.74). In addition, the coefficients of convective and evaporative heat transfer are influenced by the values of d and S (Eq.2.73). Nevertheless, Tsilingiris (2009) reported that a value of d=1/3 can be used in a wide range of operating temperatures for a practical solar still. This value of d was therefore used in the present investigation. In this case, the coefficients of convective and evaporative heat transfer were independent of the average height of the evaporator unit.

To maintain a relatively low temperature of the cover, part of the heat from hot saline water can be transferred into a separate condenser by diffusion and purging. This approach allows part of the water vapour to be condensed in a separate unit. Previous work showed that the contribution of vapour diffusion to distillate production is insignificant (Fath and Elsherbiny, 1993). Thus, most of the heat channelled into a separate condenser is through purging. This mode of heat transfer depends on the pressure difference inside the hot chamber (evaporator) and the cool chamber (condenser) because the pressure of a given mass of gas increases with decreasing its volume at a specified temperature (ASHRAE, 2001). Decreasing the volume of the evaporator relative to that of a condenser unit would therefore augment the pressure difference between the two chambers and rate of purging. Again, this indicates that the geometry of a solar still with separate condenser would affect the rate of heat purging.

4.4.3 Heat loss to the environment

Heat is lost to the environment through the top, bottom and sides of the system. Heat loss through the top is desirable because it helps to keep the transparent cover temperature low, thereby increasing the rate of condensation and distillate production (Eq.2.79). Top heat loss occurs through convection and radiation. Convective heat loss from the top is influenced by the speed of wind over the transparent cover (Eq.2.75) while radiative heat loss from the top to the sky depends on the temperature and emittance of the transparent cover, and temperature of the sky (Eq.2.76).

On the other hand, heat loss through the bottom and side walls reduces useful thermal energy for the distillation process, and the productivity of the still. The problem of heat loss from the bottom of a solar still is worse because of the higher temperature gradient between the basin liner and the ambient air temperature outside the still. This leads to a reduction in the distillate production. To overcome this problem, Cooper (1969) proposed insulation of the bottom part of a solar still. Later, Cooper (1973) recommended the use of low cost insulation materials in order to minimize the cost of distilled water. He observed that the distillate output increased by 15 % when the bottom part of a solar still was insulated by polystyrene of thickness of 0.0254 m. Garg and Mann (1976) used a sawdust insulation layer of 0.025 m thick. It was found that distillate production increased by 10 %. One advantage of using sawdust is its low cost. Similarly, heat loss from the walls of a solar still can be reduced by using a side insulation layer (Khalifa and Hamood, 2009a). For a given insulation material, the rate of heat loss to the environment decreases with increasing the thickness of the insulation layer (Eq.2.78). So, the type and thickness of insulation need to be considered in solar still design.

4.4.4 Prototype solar stills

Optical, heat transfer and heat loss characteristics were used to design a single slope conventional solar still (CSS) as a bench mark and a prototype advanced single slope solar still (ASS) with separate condenser. The main components of the CSS were glass cover, basin 1 with saline water, polystyrene bottom insulation layer and plywood box (Fig.4.3 a). So, the evaporator and condenser were integrated in one unit. In contrast, the ASS comprised separate evaporator and condenser chambers (Fig.4.3b). The main components of the evaporator chamber were similar to those of the CSS for valid comparison of the thermal performance of the two distillation systems. Saline water in basin 1 of the ASS constituted the first effect. The condenser chamber housed basin 2 with saline water (second effect) and basin 3 with saline water (third effect) with a metallic condensing cover over the third effect and an opaque insulation shield over the condensing cover.

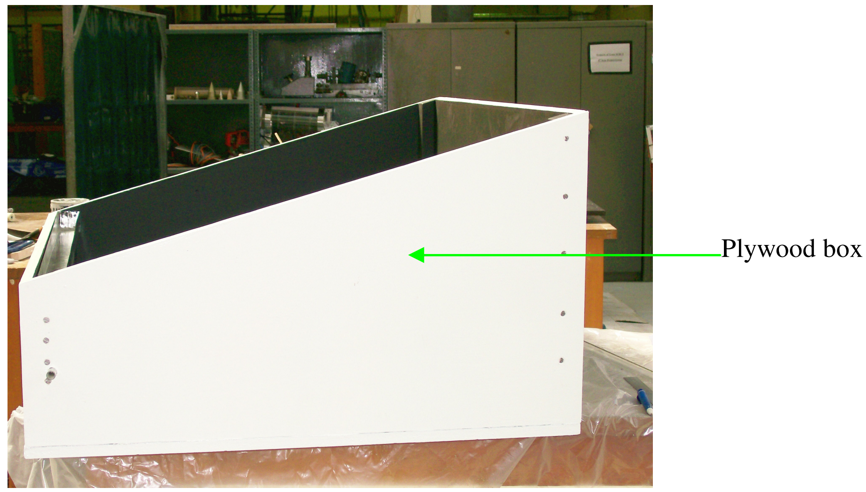

Fig.4.3 (a) Perspective view of a conventional solar still.

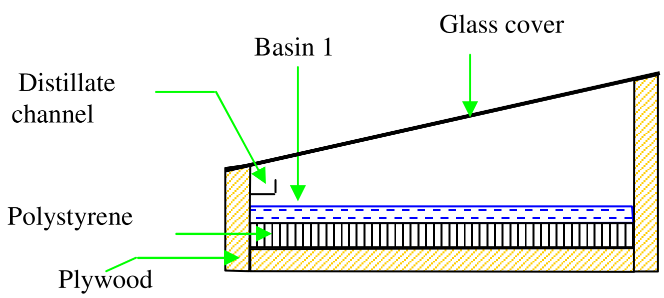

Fig.4.3 (b): Cross-section of a conventional solar still, showing components of the system.

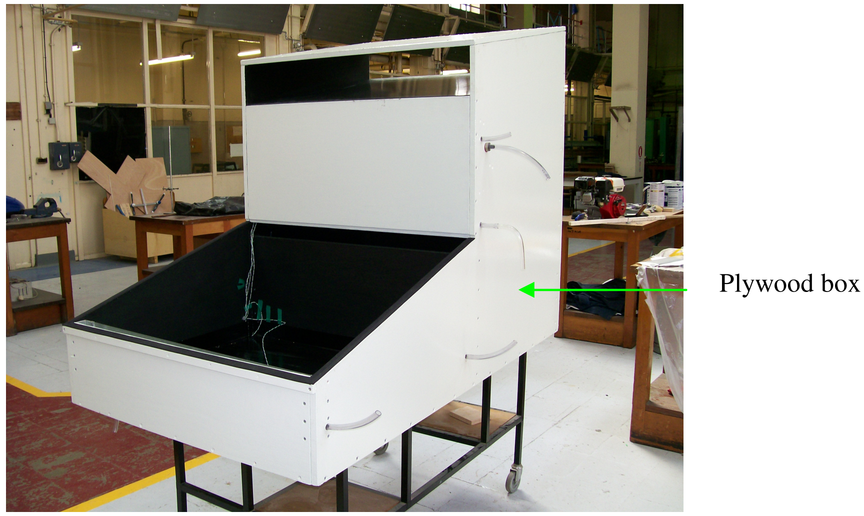

Fig.4.3 (c) Perspective view of an advanced solar still.

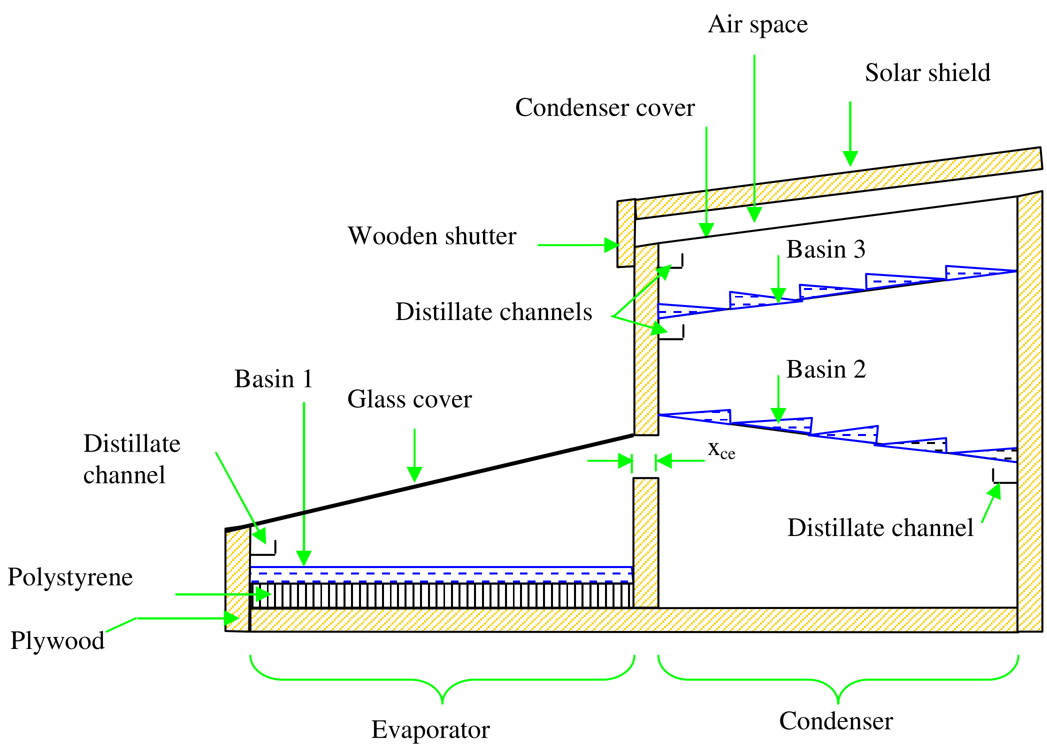

Fig.4.3 (d): Cross-section of an advanced solar still, showing components of the system.

a) Solar optics

The evaporator chamber was covered with glass on the top part to enable solar radiation reach saline water in basin 1. This glass cover was inclined at $\beta=16^o$ for optimal annual performance at the Malawi Polytechnic in Malawi although the two solar stills were also tested at the University of Strathclyde in the United Kingdom. The basis of this approach was that there is greater potential for application of solar distillation systems in Malawi than in the United Kingdom because the former country is located within the tropical region where solar radiation is abundant while the United Kingdom is located in the high-latitude belt with a limited number of sunshine hours. Moreover, Malawi is a developing country with 72 % and 96 % of the population in rural and urban areas respectively having access to clean water while 100 % of the population in the United Kingdom has access to water that meets specifications of the World Health Organization (WHO, 2008). In addition, the transmittance and reflectance of the glass cover were considered in sizing the distillation systems as shown in the proposed mathematical model in Chapter 3.

When the sun is in front of a solar still, the front wall casts a shadow on the surface of saline water in basin 1 which reduces the amount of solar radiation received by the water. So, it is necessary to minimize the height of the front wall as shown in Section 4.3.1. In this investigation, the channel and tubular bend for draining out distilled water could be fitted between basin 1 and the top edge of the front wall when $Z_{fw}=0.195$ m.

The proportion of solar radiation intercepted by saline water is also influenced by AR. El-Swify and Metias (2002) reported that AR≈2.0 gives optimal solar collection in a conventional solar still. However, other researchers have designed basin type solar stills with AR≠2 depending on the focus of the study (Porta et al., 1997; Tripathi and Tiwari, 2004; Tripathi and Tiwari, 2006). The objectives of this research were a) to model the performance of conventional and advanced solar stills, b) to design, construct and test prototype solar stills, and c) to verify the accuracy of the proposed model for predicting the performance of the solar stills. View factors were taken into consideration and it was found that a value of AR≈1.1 was optimal for $A_{b1}=0.72$ m^2. Therefore, a rectangular evaporator basin (L_{b1}=0.9 m and B_{b1}=0.8 m) was used in the present investigation. The various dimensions of the CSS and ASS are presented in Fig.4.4.

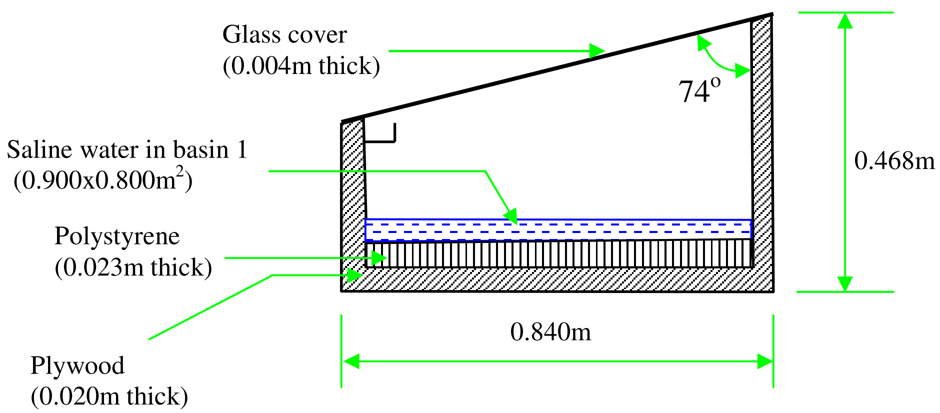

(a)

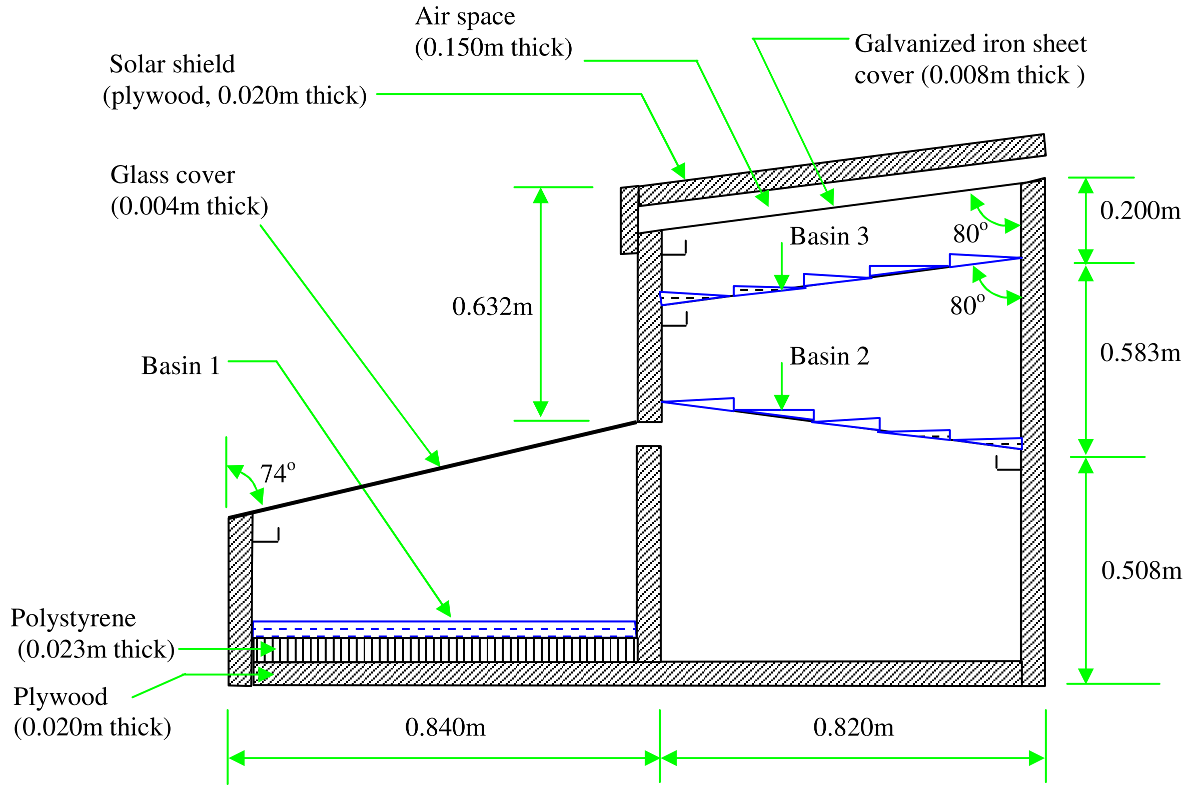

(b)

Fig.4.4: Dimensions of a) conventional and b) advanced solar stills.

The walls of the evaporator unit and external reflector reflected part of the incoming solar radiation onto the surface of saline water in basin 1 of the ASS. These surfaces exchange radiation with the water and other surfaces. This exchange of radiation is influenced by optical view factors. However, previous work on solar stills with internal and external reflectors did not incorporate view factors in their models for computation of solar distribution (Tripathi and Tiwari, 2004, 2006; Tanaka and Nakatake, 2006, 2007; .Tiwari and Tiwari, 2007). So, their mathematical models would have limited accuracy in predicting the performance of this variety of distillation systems. In this investigation, optical view factors of surfaces that exchange radiation are taken into account in the design of solar stills with single slope (Madhlopa and Johnstone, 2009a). These view factors were computed from the dimensions of the stills as shown in Section 3.1. It should be noted from Table 3.1 that W_{bw-sk}=0.23 for both the CSS and ASS. Similarly, the values of W_{bw-w1} for both stills are comparable (W_{bw-w1}=0.29 for the CSS and W_{bw-w1}=0.30 for the ASS). Nevertheless, W_{w1-sk} =0.53 for the CSS is higher than W_{w1-sk} =0.39 for the ASS. This indicates that the saline water surface in the CSS 'sees' a higher proportion of the sky than the water surface in the ASS. The geometry of the evaporator chamber is essentially the same for both stills but the inclusion of an external reflector increases the obstruction of the sky from the saline water in the evaporator basin of the ASS, which would account for the observed levels of view factors. It is seen that W_{er-wl} =0.09 is significantly lower than W_{bw-w1}=0.30, due the location of the external reflector relative to the surface of saline water. This reflector is vertically farther away from the water surface than the back wall.

b) Internal heat and mass transfer characteristics

Saline water in basin 1 is heated by solar radiation absorbed by basin liner 1 and the water itself. Heat is then transferred from the hot saline water to the glass cover and walls of the still through convection, evaporation and radiation. This results in the elevation of the temperature of the glass and a reduction in distillate production in a conventional solar still. To overcome this problem, a separate condenser was incorporated. So, part of the heat transferred by convection and evaporation from the hot water was diverted into this condenser, thereby keeping the glass cover relatively cool. The pattern of water vapour flow is shown in Fig.4.5.

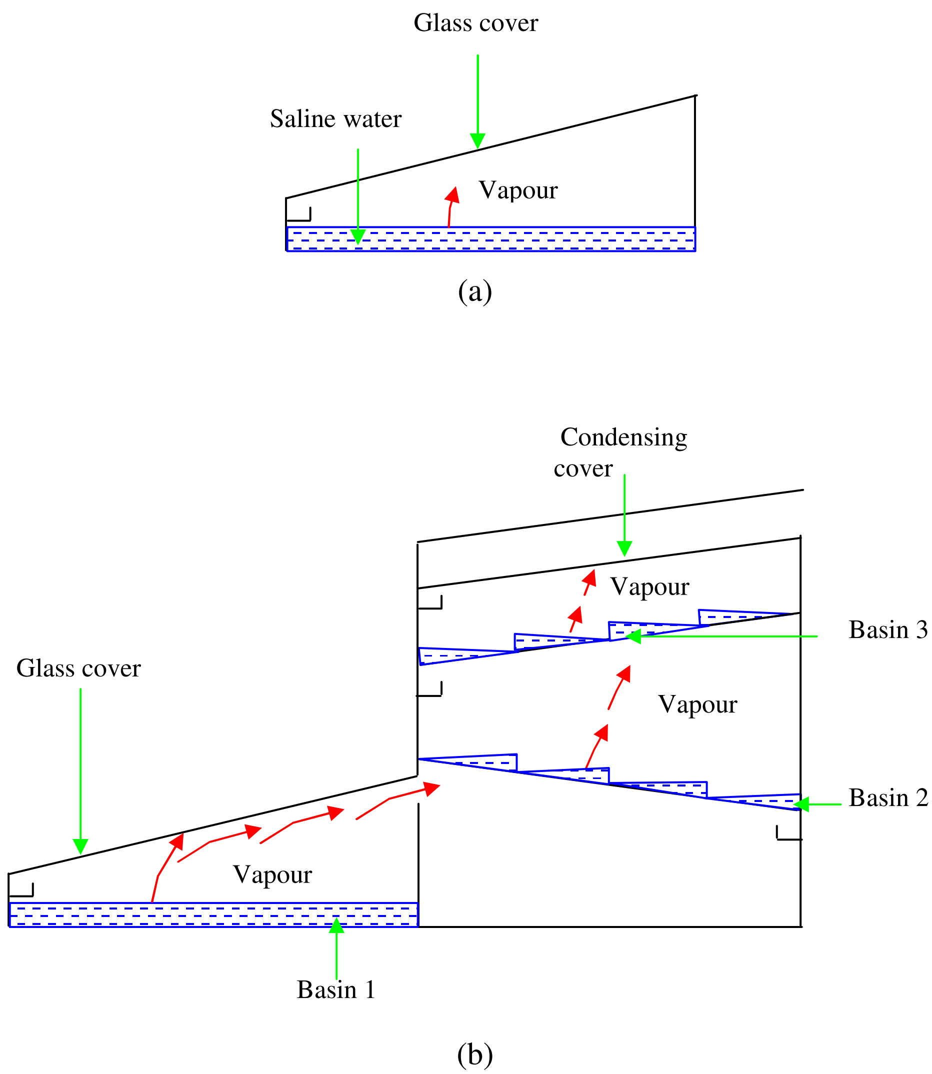

Fig.4.5: Flow patterns of water vapour in a) conventional and b) advanced solar stills.

Basins 2 and 3 were included in the condenser unit to recover heat and increase the efficiency of the distillation system. Basically, water vapour from basin 1 rose up and condensed on the inner side of the glass while part of the vapour flowed into the condensing chamber by purging and diffusion where it would condense on the outer surface of basin liner 2, thereby recovering part of the heat from the first effect. Similarly, water vapour from the second effect condensed on the outer surface of basin liner 3 to recover heat from the second effect. A condensing cover was fixed directly above basin 3, with an inclined air channel (with a single open end) over the cover for cooling, and the condensing cover was shielded from solar radiation by an opaque insulation cover which formed part of the air channel. Three effects were used for optimal performance (Mahdi, 1992). Distillate was collected through drainage channels on the bottom lower parts of the glass cover, basin liner 2, basin liner 3 and condensing cover.

c) Heat loss

Distillate production increases with decreasing heat loss (Cooper, 1969; Sahoo et al., 2008). Based on recommendations reported by Cooper (1973), it was necessary to consider the type and thickness of insulation layer in order to reduce heat loss from the bottom and side walls. For a given type of material, distillate production increases to an optimum level with increasing the thickness of the insulation layer (Dhiman, 1990; Khalifa and Hamood, 2009b). This indicates that heat loss decreases with increasing the thickness of the insulation layer. Cooper (1973) found a significant improvement when polystyrene (thickness = 0.0254 m) was used on the bottom part of a basin type solar still.

In the present system design, polystyrene (thickness = 0.023 m) was used as an insulator on the bottom because this material is relatively cheap (Cooper, 1973). It was also assumed that the box housing the basins of saline water was made of plywood (thickness =0.020 m), which also has both structural and insulation properties and it is readily-available in many developing countries where solar stills can be exploited to increase the proportion of people with access to clean water.

4.5 Solar still construction

4.5.1 Materials

a) Still glazing

A transparent cover is fitted on the top part of the evaporator unit to allow solar radiation to reach saline water in basin 1 placed under the cover. One or more transparent covers can be used with an air gap between them to reduce heat losses from the top of the evaporator. For instance, El-Bahi and Inan (1999a) fitted two glass covers on the top part of the evaporator chamber of a solar still with separate condenser. However, Bansal et al. (1984) reported that the selection of the number of covers has to be based on the economic performance aimed at minimizing the life cycle cost of the thermal energy collected by heating systems. Moreover, multiple glazing reduces top heat loss significantly which leads to high temperatures of the glazing and a decrease in the rate of evaporation-condensation. Thus, single glazing is commonly used for solar distillation systems (Tleimat and Howe, 1969; Phadatare and Verma, 2007; Dev and Tiwari, 2009).

The most influential property of a transparent material needed in solar technology is transmittance (Eqs.3.54 to 3.55). For instance, a single layer of Teflon can transmit as much as 97 % of solar radiation at normal incidence (Duffie, 1962). Similarly, low-iron (clear) glass has transmission values of 88- 92% at normal incidence (Duffie, 1962; Greenwald and McHugh, 1985). So, plastics and glass are commonly used as cover materials in solar systems. Advantages of plastics include low cost, flexibility and absence of joints like those found in glass covers (Tleimat and Howe, 1969). However, most of these plastic materials have a relatively high rate of degradation (Das and Chakraverty, 1991; Köhl et al., 2005). On the other hand, glass has long life (if it is properly fitted) and transmits a small proportion of long wave radiation (Duffie, 1962; Brow and Schmitt, 2009). Moreover, solar stills with glass covers perform better than those with plastic covers (Tleimat and Howe, 1969; Qiblawey and Banat, 2008). The disadvantages of glass are its fragility and relatively high cost compared to plastics. Nevertheless, its cost can be offset by its long life and better performance in solar distillation systems. In view of this, a float glass cover (0.004 m thick) was fitted on the top part of the evaporator basin in this investigation.

b) Basin liner

Solar radiation that passes through the transparent cover is absorbed by saline water and the basin liner of a solar still. So, the basin liner acts as an absorber of solar radiation and it is important for the liner to have a relatively high absorptance for solar radiation (Duffie, 1962). Increasing the absorptance of the liner increases the proportion of solar radiation that is converted to thermal energy (long-wave radiation) which is transferred (through convection) to the water layer on the top part of the liner (Eq.3.55). In turn, this augments the distillate yield from the distillation system as observed in the simulation results in Chapter 3.

In practical applications, basin liners can be made of plastic or metal-sheet (Cooper and Ready, 1974; Mowla and Karimi, 1995). Some plastics are relatively cheap while others are expensive (Köhl et al., 2005). For instance, a butyl rubber sheet costs 2 times as much as a heavy duty polythene sheet of the same volume but Cooper and Ready (1974) recommended the former material because of its relatively longer life than polythene. Nevertheless, plastics have limited durability. On the other hand, metal sheets last longer if properly protected against chemical attack from the environment. A metallic liner is often painted black to increase its absorptance. In this case, the paint is a coating while the metal sheet is a substrate. In view of these considerations, a metallic liner was used in the present work.

Common metal sheets applied in solar collection are copper, aluminium and steel (Martin and Goswami, 2005). The important property of a metal for application in solar engineering is thermal conductivity. Copper and aluminium have relatively high thermal conductivities ($k=200\ Wm^{-1}K^{-1}$ for aluminium and $k=390\ Wm^{-1}K^{-1}$ for copper) while the thermal conductivity of steel is relatively low ($k=48\ Wm^{-1}K^{-1}$). Nevertheless, copper and aluminium are more expensive (more than two times the cost of galvanized steel). With these considerations, all basin liners 1, 2 and 3 were made of galvanized steel but only basin 1 was painted black to increase its solar absorptance.

c) Insulation

Heat loss from the bottom and sides of a solar still is undesirable because it reduces distillate yield. Consequently, it is necessary to minimise this loss by insulating the relevant surfaces. This enables most of the absorbed solar radiation to contribute to the evaporation of saline water and thereby augment the distillate yield.

The most important property of an insulator is the coefficient of heat conduction (k). Materials with low values of k are suitable for use as insulators due to their relatively high resistance to flow of heat. Common insulation materials exploited in solar engineering are shown in Table 4.4 (Simond, 1965; Lenel and Mudd, 1984; Incropera et al., 2007). It should be noted that plastic foam insulation materials have low values of k and density, with wood-based insulation materials being most inferior. So, plastic foam materials provided a potential candidate insulation material in this work. Polyurethane foam has the lowest k-value but polystyrene and urea formaldehyde foam are relatively cheap (<40 % the cost of a unit volume of polyurethane foam). Nevertheless, urea formaldehyde foam has an open-cell structure with low mechanical resistance, and therefore less favoured in thermal applications (Simond, 1965). In contrast, polystyrene has a low k-value with a closed-cell structure which enables it to maintain its shape, and therefore thermal properties, during operation. In view of these considerations, it was used to insulate the bottom parts of the two solar stills.

Table 4.4: The density (φ) and coefficient of thermal conductivity (k) of common insulation materials.

Insulation material	T (K)	φ ($kg\ m^{-3}$)	K ($W\ m^{-1}\ K^{-1}$)
Ebonite, expanded	283	64	0.0303
Phenolic foam	297	32	0.033
Pine fibreboard	297	256	0.0519
Polystyrene, expanded	283	16	0.0346
Polyurethane foam	297	32	0.023
Urea formaldehyde foam	297	10	0.032
Wood, shredded/cemented	300	350	0.0870

d) Still structure

Basins of saline water and the bottom insulation layer were all housed in a box, and the top part of the evaporator unit was covered by a transparent cover. So, a strong box was required to support these components. In addition, it was advantageous to make the box from a material with a relatively low k-value to avoid adding another insulation layer on the sides of the still.

Consideration was therefore given to structural materials that could also act as insulators on the still sides. In this vein, common structural materials are presented in Table 4.5 (Incropera et al., 2007). It should be noted that steel provides a strong structure but its density and thermal conductivity are relatively high. So, it would yield a heavy solar still that also requires another insulation layer on the side walls. On the other hand, plywood has relatively low values of both k and φ. In addition, the cost per unit volume of this material is about 9 % that of steel. Therefore, plywood was chosen as a structural material for the solar still box.

Table 4.5: Structural materials and their density (φ) and thermal conductivity (k).

Structural material	T (K)	φ (kg m^{-3})	K (W m^{-1} K^{-1})
Plywood	300	545	0.120
Hardboard, siding	300	640	0.094
Hardboard, high density	300	1010	0.150
Wood, hard (oak)	300	720	0.160
Wood, soft (pine)	300	510	0.120
Particle board, low density	300	590	0.078
Particle board, high density	300	1000	0.170
Steel	-	7900	48

4.5.2 Fabrication

Based on the design considerations described in the preceding section, prototype conventional and advanced solar stills were constructed in the Department of Mechanical Engineering Workshops, University of Strathclyde, United Kingdom. The evaporator chambers for both systems had a single slope with identical evaporator basins for valid comparison of the two distillation systems. Readily-available materials were employed to construct the stills for ease of exploitation of these distillation systems in developing countries. Particular attention was given to optical, heat transfer and heat loss characteristics of solar stills.

a) Optical characteristics

Distillate production increases with the amount of solar radiation that is intercepted by a solar still. So, a float glass cover (0.004 m thick) was fitted (using galvanized steel angle brackets) on the top part of the evaporator chamber, tilted at 16 ^{o}, to optimise collection of solar radiation at the Malawi Polytechnic (15 ^{o} 48′ S, 35 ^{o} 02′ E). The glass cover was sandwiched between foam tapes to absorb shocks. In addition, silicon sealant was filled between gaps to make the still air-tight. Float glass has a transmittance of 0.78 and excellent durability (Martin and Goswami, 2005). It is therefore a suitable material for solar still glazing. At the optimal angle of inclination, the height of the front wall of both the CSS and ASS was set at Z_{fw}=0.195 m to reduce the effect of shading on basin 1.

The amount of solar energy collected by a solar still is also influenced by the aspect ratio (AR) of the distillation system. In this investigation, AR=1.1 was found optimal for A_{b1}=0.72 m^2, which falls within the range reported in previous work (Porta et al., 1997; El-Swify and Metias, 2002; Tripathi and Tiwari, 2004, 2006). Consequently, basin 1 (0.90 m x 0.80 m) was constructed from galvanized steel (0.0008 m thickness). In addition, basin liner 1 was painted black (Crown Hammerite metal paint) on the inner part to increase its solar absorptance. The inner part of the box that housed the basins was also painted black (Crown vinyl emulsion paint) to increase its solar absorptance and therefore avert condensation of vapour on the still walls (Fig.4.6).

On the other hand, a thin coat of Crown light green pastel paint was applied on the outer surface of the box and the external reflector to enhance reflection and protect the plywood against weathering.

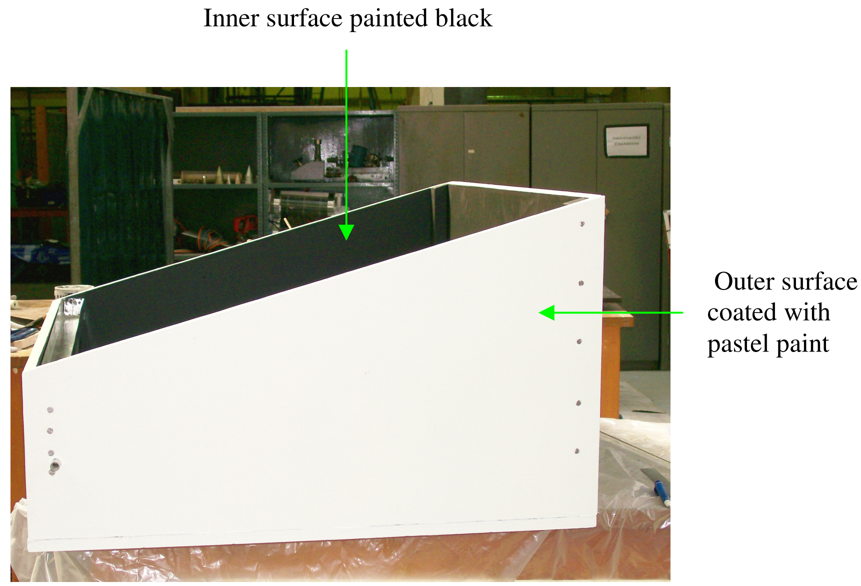

Fig.4.6 (a): A conventional solar still under construction in the workshop at the University of Strathclyde.

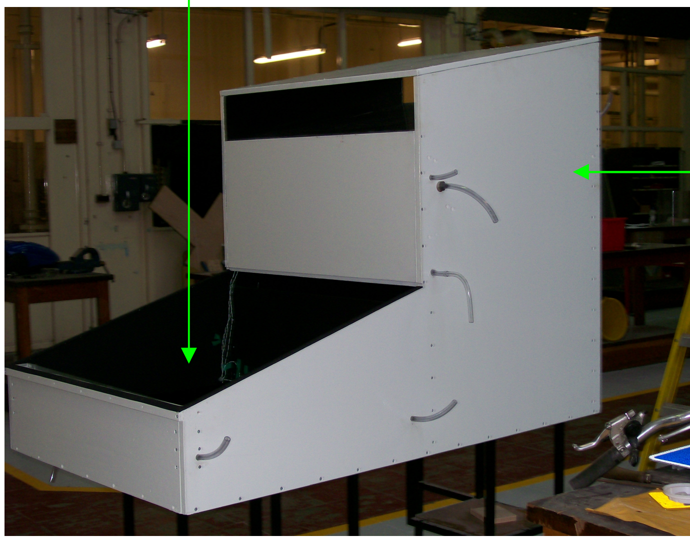

Fig.4.6 (b): An advanced solar still under construction in the workshop at the University of Strathclyde.

b) Characteristics of internal heat transfer

Basin 1 was placed horizontally inside the evaporator unit with a glass cover on the top part to allow incoming solar radiation reach saline water (first effect) inside this basin. For the CSS, this heat would flow upwards from the hot water by convection, evaporation and radiation to the glass cover and still walls. For the ASS, there is also upward flow of heat from the hot saline water in basin 1. In view of this, basin 2 was fitted at a higher level within the condenser chamber than basin 1 in the evaporator chamber to take advantage of the upward flow of heat by natural convection. Thus, part of the heat from basin 1 was transferred to the bottom part of basin 2 thereby heating the saline water (second effect) in basin 2. The volume of the evaporator was constructed smaller than that of the space under basin 2 in the condenser chamber to enhance vapour purging from the evaporator into the condenser. Similarly, heat from the second effect was transferred by convection, evaporation and radiation. Convective and evaporative heat flows were again upward. So, basin 3 was fitted directly above the second effect to recover heat from this effect, and a galvanized steel cover was fitted on the top part of the third effect to enable water vapour from the third effect condense on the inner surface of this cover. In addition, basins 2 and 3 were inclined at 10^o to enable distillate flow downward into the collection channel, and stepped up to minimize the mass of water in them. The liners of these two basins were also made from the same metal sheet as that for basin 1 but they were not painted to reduce resistance to heat conduction. In addition, the condensing cover was inclined at 10^o to the horizontal to allow distillate flow downward into the collection channel. A solar shield (made of plywood) was fixed above the condensing cover to keep the cover relatively cool. A rectangular channel (made of galvanized steel) was installed inside the wooden box, on the lower edge of each condensing surface to collect distilled water. It should be noted that part of the heat generated inside the still is lost to the environment through the bottom and side walls. The heat flow pattern in prototype conventional and advanced solar stills is presented in Fig.4.7. There is no heat recovery in the CSS, and all the heat that reaches the glass cover is therefore ultimately lost to the environment. In contrast, part of the heat from the hot water surface (h_{pu}) is channelled into the condenser of the ASS to augment its efficiency.

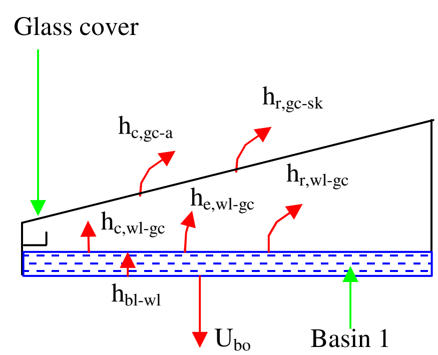

Fig.4.7(a): Heat flow pattern in a conventional solar still.

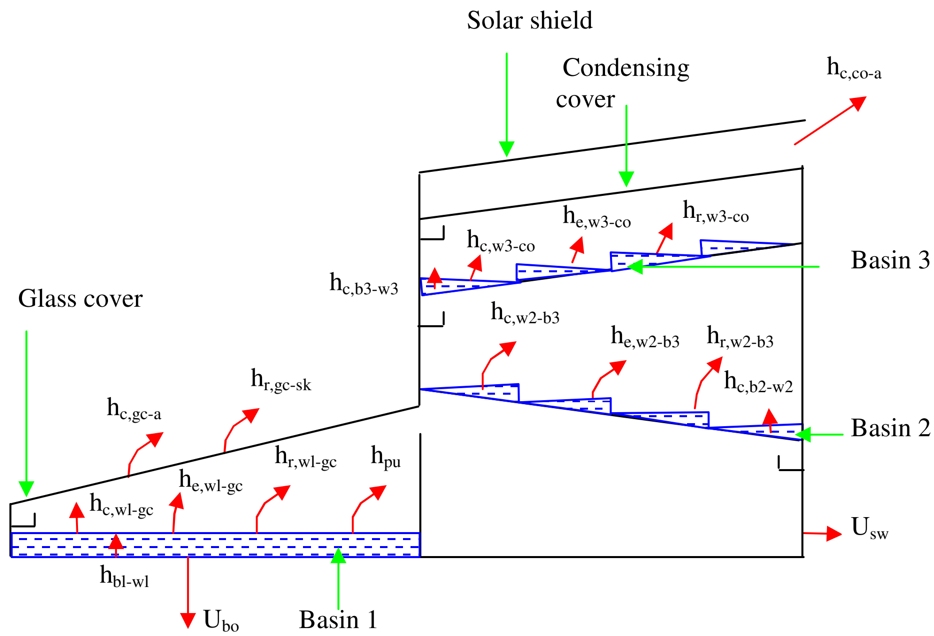

Fig.4.7(b): Heat flow pattern in an advanced solar still.

c) Characteristics of heat loss

Conduction of heat through the bottom and side walls of a solar still reduces the amount of thermal energy that evaporates saline water. Consequently, solar still construction aims at reducing this loss by insulating the relevant surfaces. This increases useful heat for distillate production.

To curtail heat loss from the conventional and advanced solar stills, a sheet of polystyrene (0.023 m thick) was sandwiched between basin liner 1 and the wooden base (0.020 m thick) of the still box, forming two layers of insulation (Fig.4.8). Cooper (1973) observed that the distillate output increased by 15 % when the bottom part of a solar still was insulated by polystyrene of thickness of 0.0254 m. It was therefore expected that the total thickness of insulation used in the present investigation would produce an increase greater than 15 %.

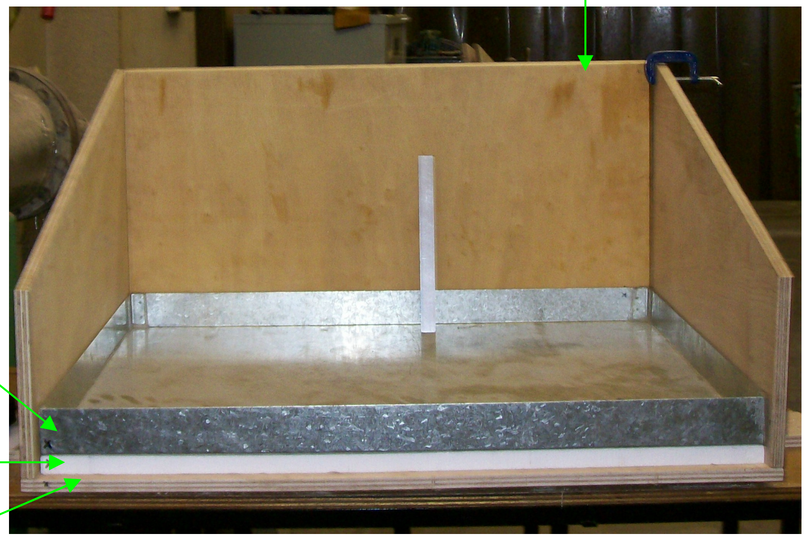

Perspective view of a CSS under construction showing basin liner 1, and polystyrene and plywood insulation layers.

4.6 Data acquisition

Model verification and empirical evaluation of the performance of solar stills requires a high quality of data on meteorological conditions and distillate output for a given set of design and operating conditions. This can be achieved by using standard methods which give guidelines on instrumentation and procedures for data collection.

Significant advances have been made in the development of standard methods for testing solar thermal systems of various types and designs. For instance, standard methods for testing flat plate solar collectors are well-documented (ISO, 1994; ASHRAE, 2003; BSI, 2006; CEN, 2006). Nevertheless, there is lack of a standard method for performance evaluation of solar stills. In view of this, data for evaluation of solar stills is collected by using guidelines from standard methods and practices for other solar thermal energy systems. A similar approach to data acquisition was adopted in this investigation.

4.6.1 Test sequence

The mass of distilled water produced is used in the computation of the still efficiency. Nevertheless, the values of efficiency computed over periods lower than 24 hours are often invalid (Yates and Woto, 1988 cited in Smyth et al., 2005). So, hourly production was measured on days with favourable weather conditions while the daily yield was monitored on all test days for model verification and evaluation of the empirical performance of the conventional and advanced solar stills.

Different test sequences for solar stills have been reported in literature. Kumar and Tiwari (1996) conducted experiments for 30 days to validate the performance of a model for estimating convective mass transfer in solar stills. They found good agreement between empirical and simulated results. Banat et al. (2002) evaluated the outdoor performance of a solar still with a membrane module over a period of 12 days. Results showed that the temperature of the brine significantly influenced the distillate flux of the still and membrane module. To validate the performance of a model for calculating the distribution of solar radiation in a single slope solar still, Tripathi and Tiwari (2004) used data collected on one day (27th March 2002). They observed that solar fraction was very influential in the performance of the still at low values of the altitude of the sun. More recently, Abdallah et al. (2008) used a test sequence of 3 days to evaluate the performance of a single slope solar still with a modified design. It was found that using a step-wise basin and sun-tracking system was most effective in improving the distillate production. ASHRAE/ANSI standard 93-2003 recommended 16 test data points for complete characterization of the thermal performance of a flat plate collector under steady-state conditions (ASHRAE, 2003). The 16 data points are adequate for statistical analysis and characterization of the collector. So, it was planned that at least 16 daily data points should be collected at each test site in the present investigation.

To collect data, the conventional and advanced solar stills were tested outdoors at the University of Strathclyde (55^o 52′ N, 4^o 15′ W) and the Malawi Polytechnic (15^o 48′ S, 35^o 02′ E), (Fig.4.9). It should be noted that the time taken to collect the minimum required data points under outdoor conditions would depend on the prevailing weather conditions. At the University of Strathclyde, 22 daily data points were collected from

6th September to 5th November 2007 while 18 data points were captured over the period from 25th September to 23rd October 2008 at the Malawi Polytechnic. Missing data on some test days was due to unfavourable weather conditions. Moreover, a pre-data period is required to enable the solar energy systems 'settle' down after mounting them outdoors (BSI, 2006).

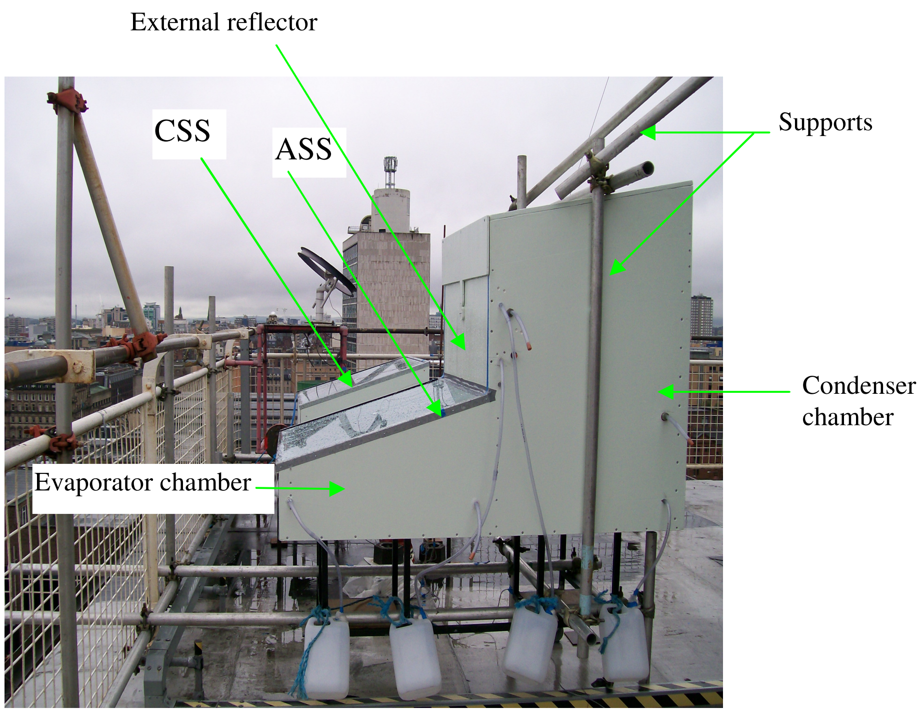

Fig.4.9(a): Perspective view of the advanced solar still (ASS), mounted on roof top along side a conventional solar still (CSS) at the University of Strathclyde.

Fig.4.9(b): Perspective view of the advanced solar still (ASS), mounted on roof top along side a conventional solar still (CSS) at the Malawi Polytechnic.

4.6.2 Instruments

In this investigation, data of high quality was required for model verification and empirical evaluation of conventional and advanced solar stills. It was therefore necessary to use accurate instruments at both the University of Strathclyde and Malawi Polytechnic test sites. Standard calibrated instruments were employed to capture data on the intensity of solar radiation, temperature, surface wind speed, mass, electrical conductivity (EC), total dissolved solids (TDS) and pH of water. Solar irradiance, ambient air temperature and surface wind speed were input variables to the model for predicting the mass of distillate yield (output variable). The level of distillate output was also useful in the empirical evaluation of still performance. In addition, EC, TDS and pH were used as indicators of water quality before and after solar distillation.

a) Solar radiation

Solar radiation is the most influential environmental factor in solar systems. Its values are required in the modelling, design and testing of solar stills. So, it was necessary to use accurate radiometers for measuring irradiance. BSI (2006) specified the use of pyranometers in class 1 (or better class) to measure solar radiation when testing a solar thermal system and its components. It should also be mentioned that secondary class pyranometers are the most accurate radiometers (Kipp & Zonen, 2006). In view of this, Kipp & Zonen CM 6B (class 1) and CM 11 (secondary class) pyranometers were used to measure irradiance in this investigation. Characteristics of these radiometers are presented in Table 4.6.

Table 4.6: Characteristics of Kipp & Zonen CM 6 and CM 11 pyranometers.

Characteristic	CM 6	CM 11
Sensitivity (x10^{-6} V/(Wm^{-2}))	13.35	4.61
Spectral range (x10^{-6} m)	310-2800	310-2800
Response time (s)	18	6
Directional error (Wm^{-2})	20	10
Maximum irradiance (Wm^{-2})	2000	4000
Tilt error (%)	<1	<0.2
Uncertainty in daily total (%)	<5	<2

Global and diffuse irradiance on a horizontal surface was measured by using CM 11 pyranometers at the University of Strathclyde. These pyranometers were part of the instrumentation for a meteorological station located within the Department of Mechanical Engineering at the University of Strathclyde. So, another pair of radiometers had to be found for solar still experimentation at the Malawi Polytechnic. CM 11 and CM 6B pyranometers were used to measure global and diffuse irradiance respectively at this site. For diffuse irradiance, a Kipp & Zonen shadow ring (model CM 121B) was fitted over the pyranometer and the recorded data was corrected for the shadow ring (Kipp & Zonen, 2004). Irradiance in the plane of the glass cover and at various selected points inside the solar still was not measured due to the limitation of radiometers.

Moreover, the area (A_{di}) of saline water that directly receives beam radiation is dynamic which would lead to a significant variation amongst the values of irradiance recorded at different locations within the distiller during certain times of the day (Madhlopa and Johnstone, 2009a).

b) Temperature

Once solar radiation is absorbed, it results in increases of component temperatures except for cases where the heat is used for latent changes. The temperature of a body can be measured by using a thermometer which may operate on the principles of resistance, thermal expansion of a liquid-in-glass, thermoelectric effect and radiation (Nicholas and White, 1994). Resistance thermometers have a very high resolution (up $1x10^{-3}$ K) and wide range of operation (14 to 1233 K) but they require an external voltage or current signal, which results in errors pertaining to resistance-measuring sensors. Liquid-in-glass thermometers operate on the principle of liquid thermal expansion and they can be operated in the range of 83 to 873 K with a resolution of up to $1x10^{-3}$ K. They find application in many fields but they are limited to taking a few measurements because the readings are taken manually. Thermocouple thermometers operate on the principle of thermoelectric effect and they are the most-widely used temperature sensors. In addition, they can be connected to most data loggers (Delta-T Devices, 2000). Errors in thermocouples may arise from thermal, inhomogeinity, isothermal, reference junction, interference, wire resistance, and linearization. The principle of operation of radiation thermometers is that the electromagnetic radiation from an incandescent object is a function of its temperature. The intensity of radiation from a given surface increases with the temperature of the body (Incropera et al., 2007). So, these thermometers can be used remotely without touching the surface of the test object. Nevertheless, they are often less accurate than contact thermometers (Nicholas and White, 1994).

All thermometers have associated errors but standard methods for evaluating thermal solar systems recommended the measurement of ambient air to an uncertainty of 0.5 K (ISO, 1994; Mathioulakis et al., 1999; BSI, 2006). In view of the discussion in the preceding paragraph, a thermocouple that meets these specifications was sought. Common types of thermocouples are given in Table 4.7 (Delta-T Devices, 2000). The application range of these thermocouples includes temperatures (about 273 to 373 K) encountered in solar distillation. It is however observed that the T-type thermocouple exhibits the smallest magnitude of error. Therefore, T-type thermocouples were found to be appropriate for sensing the temperatures of solar still components in this study. A linearization curve of this type of thermocouples, based on the manufacturer's data, is shown in Fig.4.10.

Table 47: Specifications of J, K and T type thermocouples.

Characteristic	J type	K type	T type
Operational range (K)	153-473	153-473	153-473
Accuracy (K)	±1.5	±1.5	±0.5

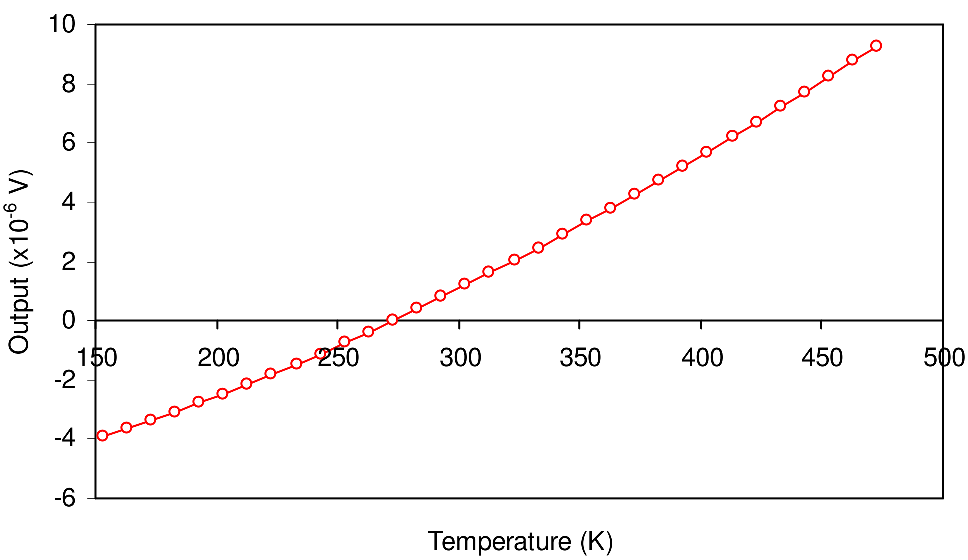

Fig.4.10: Linearization curve for the T-type thermocouple.

Initially, temperatures were measured component by component because of the initial constraint of available channels on the data logger. Five T-type thermocouples were inserted into saline water in basin 1 (one thermocouple in the middle, and one in each corner of the basin).The temperature of the glass cover was also measured using five thermocouples in similar locations as for the saline water in basin 1. For water in basins 2 and 3, temperature was measured by twelve thermocouples in each basin (uniformly distributed) while the condenser cover temperature was determined by using nine thermocouples. The choice of locations for thermocouples was aimed at incorporating edge effects (Fig.4.11). Moreover, all layers of saline water were heated from the bottom which would lead to mixing and insignificant temperature gradients within each layer. As shown in Chapter 3, Biot numbers for the glass cover and basin liners were within the acceptable limit for the application of a lumped capacitance method. This indicates that there were negligible temperature gradients in these components. An average value of temperature measurements taken all over the component would therefore be reasonable.

It should be mentioned that solar radiation could reach thermocouples located in the evaporator chamber and on the outer surface of the glass cover. Consequently, these thermocouples were guarded against solar radiation (ASTM, 2006). Each thermocouple in basin 1 was inserted into an open ended un-reinforced PVC flexible tube (internal diameter =0.012 m, wall thickness=0.0015 m and length =0.025 m). The tube was supported against a transparent glass rod (diameter =0.0127 m, length=0.025) that was glued (using araldite) to the basin liner. White PVC tape was wrapped around the tube to reduce solar absorption by the tube. The junction of the thermocouple was well secured and completely surrounded by water, and it was suspended half way between the bottom and top parts of the saline water layer (Fig.4.12a). The junctions of thermocouples for measuring glass temperature were also shielded against solar rays by using the same type of tape.

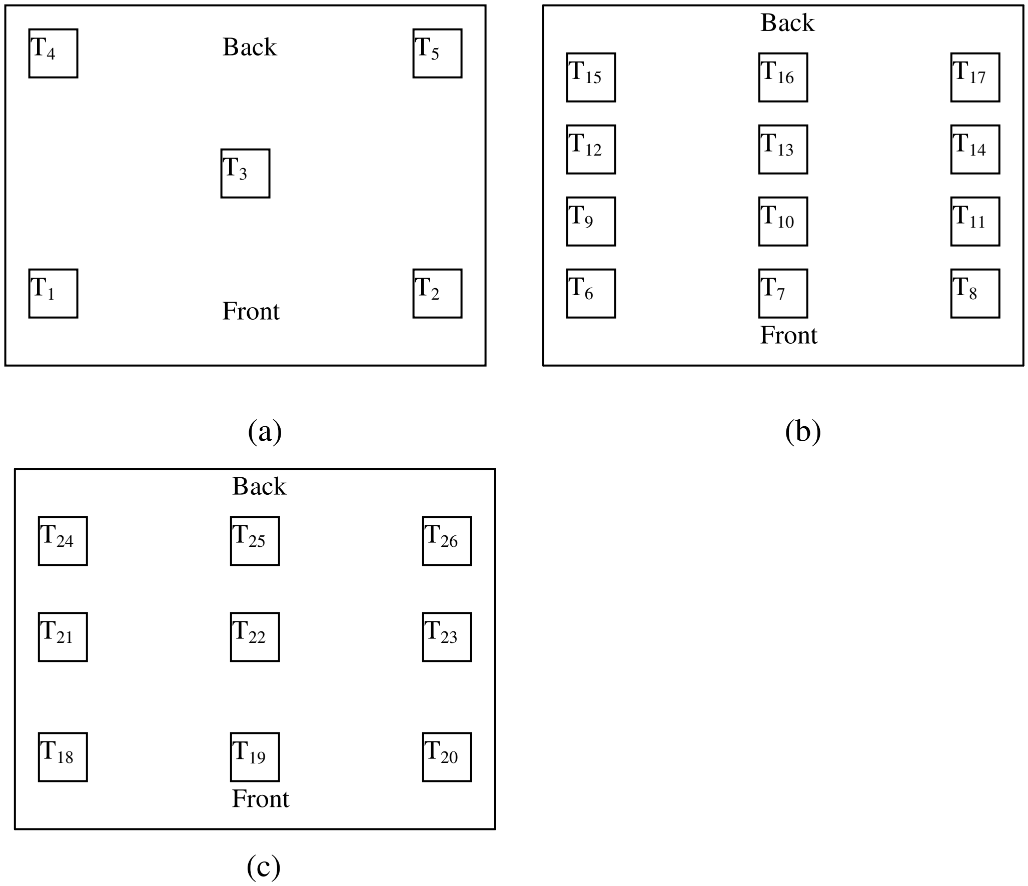

Fig.4.11: Plan view of the location of thermocouples in a) basin 1 and glass cover, b) basins 2 and 3, and c) condenser cover.

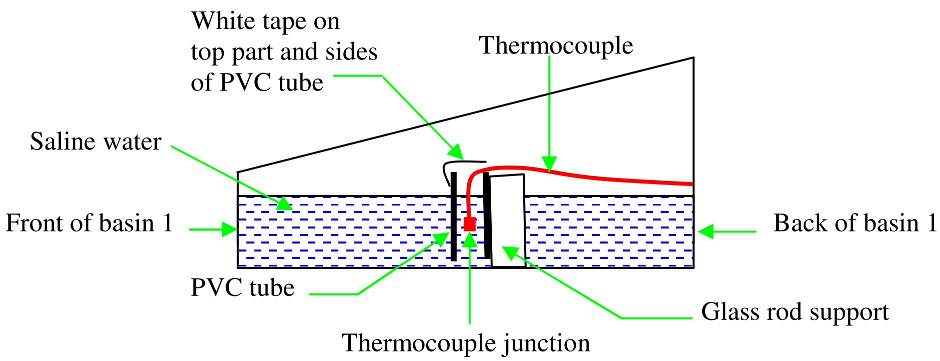

Fig.4.12(a): Setup of a thermocouple for measuring the temperature of saline water in basin 1.

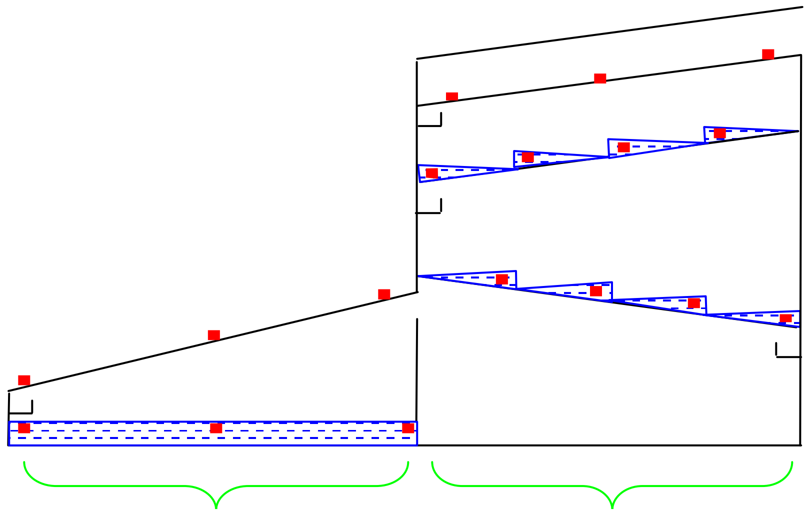

Fig.4.12(b): Location of thermocouples in an advanced solar still (▪). For the conventional solar still, thermocouples were located in similar positions to those in the evaporator chamber of the advanced still.

c) Surface wind speed

Wind speed influences the rate of heat loss from a solar still, and this variable can be measured by using a radar or an anemometer (Laghrouche et al., 2005). A radar is suitable for measuring wind profiles while an anemometer is used for ground-based measurements. Surface wind speed was required for model verification in this investigation, and, so, an anemometer was suitable for acquisition of wind data. In addition, the recommended start velocity of an anemometer is 0.5 ms^{-1} with uncertainties of 0.25 and 0.5 ms^{-1} when testing glazed and unglazed solar collectors respectively (BSI, 2006). Solar stills are glazed on the top part, and high wind speeds (V_{wd}>25 ms^{-1}) were less likely to be encountered at both at the University of Strathclyde and Malawi Polytechnic (Sinden, 2007; Wisse and Stigter, 2007). So, a Vector Instruments cup anemometer (model A100L2) and a Delta-T Devices cup anemometer (model AN4) were found to conform to these standard requirements for capturing accurate surface wind data. Characteristics of these instruments are presented in Table 4.8. It should be mentioned that the Vector Instruments anemometer (model A100L2) was part of the instrumentation for a meteorological station located within the Department of

Mechanical Engineering at the University of Strathclyde. This anemometer would yield results within the stipulated tolerance of 0.5 ms^{-1} for wind speeds of up to 50 ms^{-1} while the Delta-T Devices anemometer (model AN 4) operated within the recommended uncertainty for wind speeds of up to 10 ms^{-1}. So, the former anemometer was used at the University of Strathclyde where wind speeds exceeding 10 ms^{-1} were possible (Saluja and Douglas, 1996; Sinden, 2007), with the latter anemometer being suitable for application at the Malawi Polytechnic with speeds that were likely to be low (V_{wd}<4 ms^{-1}), (Madhlopa et al., 2006; Wisse and Stigter, 2007).

Table 4.8: Characteristics of Delta-T Devices anemometer (model AN4) and Vector Instruments cup anemometer (model A100L2). Accuracy is specified for different values of wind speed (V_{wd}).

Characteristic	A100L2	AN4
Threshold (ms^{-1})	0.15	0.5
Operational range (ms^{-1})	0-75	0-40
Maximum wind speed (ms^{-1})	77	60
Accuracy (V_{wd}<10.27ms^{-1})	±0.10ms^{-1}	-
(10.27ms^{-1}≤V_{wd} ≤56.51ms^{-1})	±1% of reading	-
(V_{wd} >56.51ms^{-1})	±2% of reading	-
0.5ms^{-1}≤V_{wd} ≤10ms^{-1}	-	±0.5ms^{-1}
10ms^{-1}<V_{wd} ≤40ms^{-1}	-	±5%

e) Data recording

A data recorder was required to enable capturing of meteorological data at short intervals during day and night. BSI (2006) specified that a data acquisition instrument should have an error equal to or less than 0.5% of the full scale reading, and an input impedance exceeding 1000 fold the impedance of the sensors. If 1000 times the impedance of the sensors is less than $10x10^6$ Ω then the impedance of the recorder should exceed $10x10^6$ Ω. Consequently, pyranometers, thermocouples and anemometers were all connected to a Delta-T Devices Ltd data logger (model DL2e) which meets these specifications. This data recorder has analogue cards LAC1 and ACD1, and a 4-wire card LFW1 and its characteristics are given in Table 4.9. A program was written in the logger software to enable sampling and logging at specified intervals. BSI (2007) recommended a maximum sampling interval of 30 s, and the sampled values should be logged at an interval of 300 s for characterization of a solar water heater. In this investigation, sampling and logging were therefore set at 10 s and 300 s respectively (Fig.4.13).

Table 4.9: Characteristics of a Delta-T Devices Ltd data logger (model DL2e). The resolution is for different ranges of DC voltage readings through LAC1, ACD1 or LFW 1 cards, with the full scale error expressed at different values of the logger temperature (T_L).

Characteristic	Value
Input impedance	100 $x10^6$ Ω
Resolution, first range ±4$x10^{-3}$ V	1$x10^{-6}$V
second range ±32$x10^{-3}$ V	8$x10^{-6}$V
Third range ±262$x10^{-3}$ V	64$x10^{-6}$V
Fourth range ±2.097 V	5$x10^{-4}$V
Full scale error	±0.02 % for 253K≤ T_L ≤333K

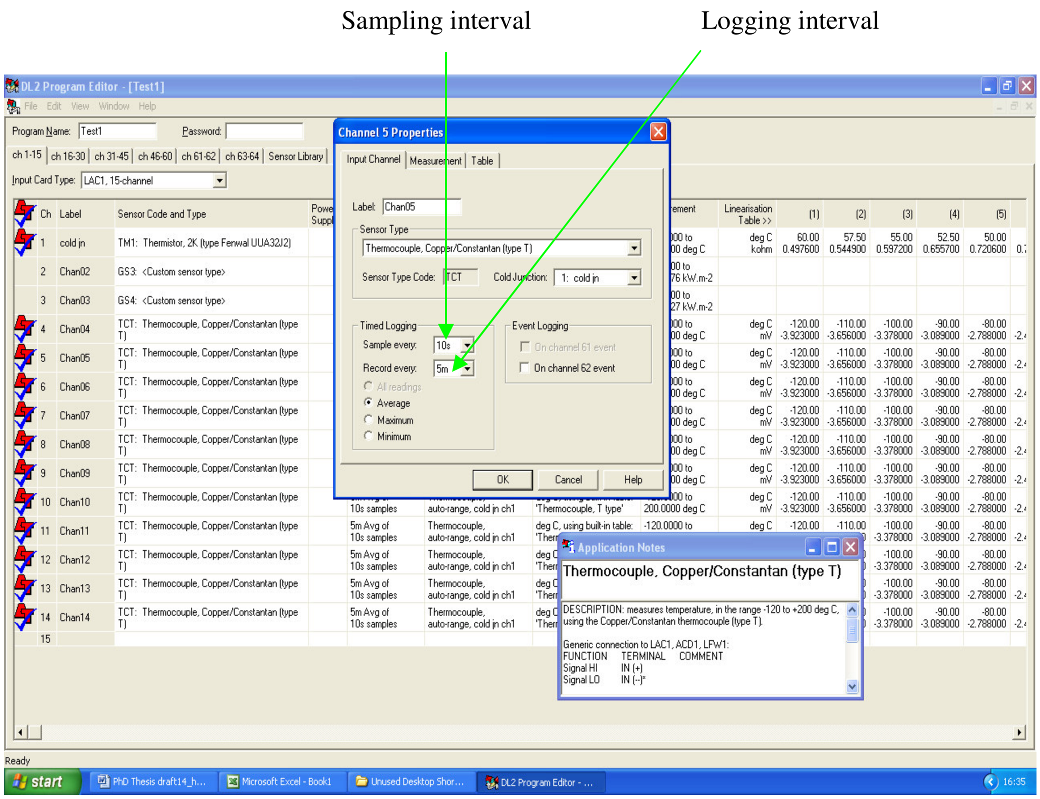

Fig.4.13: Dialog box for a typical logging program in a DL2 program editor.

f) Distilled water

The objective of solar distillation is to produce clean water, and its quantity can be measured by using volumetric apparatus or balance. Some researchers reported the volumes of distilled water (Kumar and Tiwari, 1996; Porta et al., 1997; El-Bahi, 1999a and Abdallah et al., 2008) while others used the mass of distillate (Cooper, 1973; Fath and Elsherbiny, 1993; Banat et al., 2002; Voropoulos et al., 2003). The drawback with using volume is that the density of water varies with temperature. When pure water at 273.15 K and standard atmospheric pressure is heated, its density increases from about 999.84 kg m^{-3} to a maximum value of 999.97 kg m^{-3} at 277.13 K, and thereafter the density decreases with increasing temperature (Crawly et al., 2006). So, the same volume of water may have different masses and this would introduce errors in attempts to compare distillate production at different water temperatures. Moreover, the mass of water is required in the heat balance equations. Consequently, it was determined by using a weighing balance in this work.

A balance can be electronic or mechanical (Birello, 1989). An electronic balance generates an electrical output (such as current or voltage) that is proportional to the mass of the object being weighed. On the other hand, a mechanical balance gives a mechanical output such as displacement that depends on the mass of the object being weighed. Balances fall into analytical, commercial, industrial and other types, and they have a variety of characteristics suitable for different tasks. For example, an analytical balance is manufactured to provide measurements with a high level of precision and accuracy and is appropriate for scientific application. So, an analytical balance was required to collect accurate data for model verification and evaluation of the performance of conventional and advanced solar stills.

In this study, simulated results showed that the ASS could produce up to 4.101 kg m^{-2} with a root mean square error of 15 %. Based on this, it was estimated that distillate production could slightly exceed 5.000 kg m^{-2}. A balance with a capacity of 5 to 6 kg would therefore be appropriate. In addition, simulation results were reported to an accuracy of 0.001 kg m^{-2}. Thus, a weighing balance with a resolution of 0.001 kg m^{-2} or higher would be satisfactory. Analytical balances conforming to these specifications were therefore used to capture the required data on distillate yield. The yield was measured by using digital top-loading balances (Jadever Scale Ltd balance model JB-6000 at the University of Strathclyde and Ohaus balance model B500A at the Malawi Polytechnic). Daily production was measured for model verification because the values of still efficiency computed over periods lower than 24 hours are often invalid (Yates and Woto, 1988; as cited by Smyth et al., 2005). Specifications of the two balances are presented in Table 4.10.

Table 4.10: The capacity and resolution of Jadever Scale Ltd (model JB-6000) and Ohaus (model B500A) balances.

Characteristic	B5000A	JB-6000
Capacity (kg)	5.000	6.000
Resolution (kg)	0.0001	0.001

In addition, the quality of distilled water was monitored. Previous work has already shown that solar distillation is effective in removing micro-organisms and non-volatile chemical constituents as long as there is no cross contamination (Hanson et al., 2004). Samee et al. (2007) used electrical conductivity (EC), total dissolved solids (TDS) and pH as indicators of the quality of solar distilled water. Similar indicators of water quality were determined in this study.

Instruments for measuring EC can be equipped with a) a flow- or dip-type cell that has two or more electrodes, or b) electrodes of the induction variety. In this study, both EC and TDS were measured by using a Jenway EC/TDS meter (model 470) equipped with a dip-type cell. The operational range and resolution of this meter conform to standard requirements (BSI, 1999a). The pH of water can be determined by using colorimetric and potentiometric techniques (King and Kester, 1989; Yao et al., 2007). Colorimetric techniques employ indicators that change colours at different pH levels and have limited accuracy (BSI, 1999b). Recently, Yao et al. (2007) also reported that the presence of impurities within chemical reagents used as indicator dyes limits the accuracy of colorimetric methods. On the other hand, potentiometric techniques operate on the principle of measuring the voltage that is developed by an electrochemical cell which comprises the solution sample, a glass electrode and a reference electrode. Potentiometric sensors cover a wide range of pH with a relatively low magnitude of error (<0.05), (BSI (1999b). It should also be mentioned that BSI (1999b) recommended the use of a pH meter with a resolution of 0.01 or better. So, the pH of water in this investigation was determined by using an Orion Research digital pH meter (model 601A). This sensor has a wide range of pH and a resolution that conforms to the specification of BSI (1999b). Characteristics of the CE/TDS and pH meters are given in Table 4.11. The quality of water was not monitored at the University of Strathclyde because clean water was used in the still basins and tests were initially aimed at assessing the thermal performance of the stills before they were shipped to Malawi for further data collection.

Table 4.11: Specifications of Jenway EC/TDS meter (model 470) and Orion pH meter (model 601A).

Characteristic	EC meter	TDS meter	pH meter
Operational range	0-1.999 S/m	0-1.999 kg/litre	0-13.99
Resolution	$1x10^{-8}$-$1x10^{-3}$ S/m	$1x10^{-8}$-$1x10^{-3}$ kg/litre	0.01
Accuracy	±0.5 %	±0.5 %	±0.02

4.7 Data processing

The data collected by employing different instruments was stored in an Excel computer program on a Dell Inspiron laptop (model 6000). In the data matrix, each variable was in a separate column with values running along the rows (Fig.4.14). Label, channel number, sensor type and units were indicated in the database. On each test day, 4,320 meteorological data points were logged. Thus, 95,040 data points were captured over a test period of 22 days at the University of Strathclyde, and 77,760 data points were generated over a test period of 18 days at the Malawi polytechnic. In addition, distillate production data was collected. It should be noted that irradiance and temperature were sensed in kWm^{-2} and ^{o}C respectively. These units were converted to appropriate SI units for these quantities. The data base was relatively large and it therefore required checking for quality before analysis. The data logger flagged outliers by a red mark as shown in Fig.4.15. For instance, a record of -0.0001 Wm^{-2} at 24:00 hr would be flagged and so it was corrected to 0 Wm^{-2} to ensure accurate data points were analysed for valid interpretation.

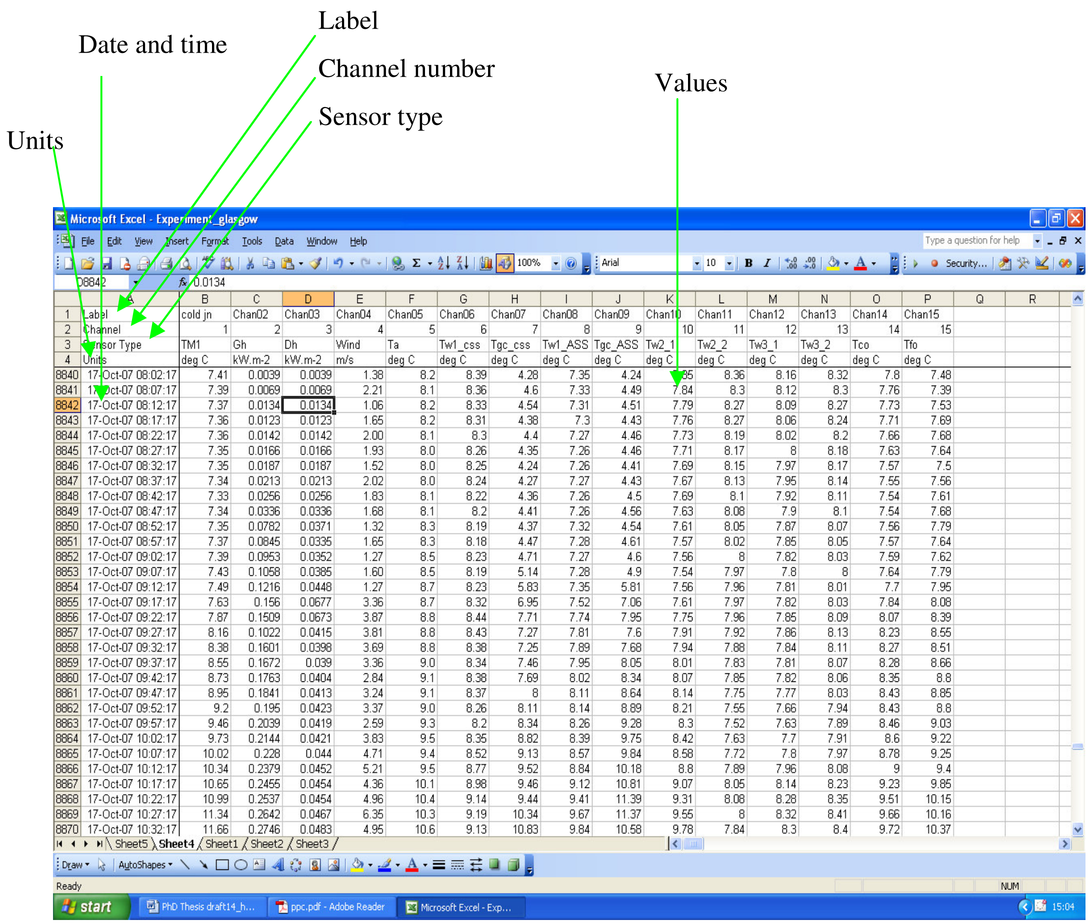

	A	B	C	D	E	F	G	H	I	J	K	L	M	N	O	P
1	Label	cold jn	Chan02	Chan03	Chan04	Chan05	Chan06	Chan07	Chan08	Chan09	Chan10	Chan11	Chan12	Chan13	Chan14	Chan15
2	Channel	1	2	3	4	5	6	7	8	9	10	11	12	13	14	15
3	Sensor Type	TM1	Gh	Dh	Wind	Ta	Tw1_css	Tgc_css	Tw1_ASS	Tgc_ASS	Tw2_1	Tw2_2	Tw3_1	Tw3_2	Tco	Tfo
4	Units	deg C	kW.m-2	kW.m-2	m/s	deg C	deg C	deg C	deg C	deg C	deg C	deg C	deg C	deg C	deg C	deg C
8840	17-Oct-07 08:02:17	7.41	0.0039	0.0039	1.38	8.2	8.39	4.28	7.35	4.24	[illegible]	8.36	8.16	8.32	7.8	7.48
8841	17-Oct-07 08:07:17	7.39	0.0069	0.0069	2.21	8.1	8.36	4.6	7.33	4.49	7.84	8.3	8.12	8.3	7.76	7.39
8842	17-Oct-07 08:12:17	7.37	0.0134	0.0134	1.06	8.2	8.33	4.54	7.31	4.51	7.79	8.27	8.09	8.27	7.73	7.53
8843	17-Oct-07 08:17:17	7.36	0.0123	0.0123	1.65	8.2	8.31	4.38	7.3	4.43	7.76	8.27	8.06	8.24	7.71	7.69
8844	17-Oct-07 08:22:17	7.36	0.0142	0.0142	2.00	8.1	8.3	4.4	7.27	4.46	7.73	8.19	8.02	8.2	7.66	7.68
8845	17-Oct-07 08:27:17	7.35	0.0166	0.0166	1.93	8.0	8.26	4.35	7.26	4.46	7.71	8.17	8	8.18	7.63	7.64
8846	17-Oct-07 08:32:17	7.35	0.0187	0.0187	1.52	8.0	8.25	4.24	7.26	4.41	7.69	8.15	7.97	8.17	7.57	7.5
8847	17-Oct-07 08:37:17	7.34	0.0213	0.0213	2.02	8.0	8.24	4.27	7.27	4.43	7.67	8.13	7.95	8.14	7.55	7.56
8848	17-Oct-07 08:42:17	7.33	0.0256	0.0256	1.83	8.1	8.22	4.36	7.26	4.5	7.69	8.1	7.92	8.11	7.54	7.61
8849	17-Oct-07 08:47:17	7.34	0.0336	0.0336	1.68	8.1	8.2	4.41	7.26	4.56	7.63	8.08	7.9	8.1	7.54	7.68
8850	17-Oct-07 08:52:17	7.35	0.0782	0.0371	1.32	8.3	8.19	4.37	7.32	4.54	7.61	8.05	7.87	8.07	7.56	7.79
8851	17-Oct-07 08:57:17	7.37	0.0845	0.0335	1.65	8.3	8.18	4.47	7.28	4.61	7.57	8.02	7.85	8.05	7.57	7.64
8852	17-Oct-07 09:02:17	7.39	0.0953	0.0352	1.27	8.5	8.23	4.71	7.27	4.6	7.56	8	7.82	8.03	7.59	7.62
8853	17-Oct-07 09:07:17	7.43	0.1058	0.0385	1.60	8.5	8.19	5.14	7.28	4.9	7.54	7.97	7.8	8	7.64	7.79
8854	17-Oct-07 09:12:17	7.49	0.1216	0.0448	1.27	8.7	8.23	5.83	7.35	5.81	7.56	7.96	7.81	8.01	7.7	7.95
8855	17-Oct-07 09:17:17	7.63	0.156	0.0677	3.36	8.7	8.32	6.95	7.52	7.06	7.61	7.97	7.82	8.03	7.84	8.08
8856	17-Oct-07 09:22:17	7.87	0.1509	0.0673	3.87	8.8	8.44	7.71	7.74	7.95	7.75	7.96	7.85	8.09	8.07	8.39
8857	17-Oct-07 09:27:17	8.16	0.1022	0.0415	3.81	8.8	8.43	7.27	7.81	7.6	7.91	7.92	7.86	8.13	8.23	8.55
8858	17-Oct-07 09:32:17	8.38	0.1601	0.0398	3.69	8.8	8.38	7.25	7.89	7.68	7.94	7.88	7.84	8.11	8.27	8.51
8859	17-Oct-07 09:37:17	8.55	0.1672	0.039	3.36	9.0	8.34	7.46	7.95	8.05	8.01	7.83	7.81	8.07	8.28	8.66
8860	17-Oct-07 09:42:17	8.73	0.1763	0.0404	2.84	9.1	8.38	7.69	8.02	8.34	8.07	7.85	7.82	8.06	8.35	8.8
8861	17-Oct-07 09:47:17	8.95	0.1841	0.0413	3.24	9.1	8.37	8	8.11	8.64	8.14	7.75	7.77	8.03	8.43	8.85
8862	17-Oct-07 09:52:17	9.2	0.195	0.0423	3.37	9.0	8.26	8.11	8.14	8.89	8.21	7.55	7.66	7.94	8.43	8.8
8863	17-Oct-07 09:57:17	9.46	0.2039	0.0419	2.59	9.3	8.2	8.34	8.26	9.28	8.3	7.52	7.63	7.89	8.46	9.03
8864	17-Oct-07 10:02:17	9.73	0.2144	0.0421	3.83	9.5	8.35	8.82	8.39	9.75	8.42	7.63	7.7	7.91	8.6	9.22
8865	17-Oct-07 10:07:17	10.02	0.228	0.044	4.71	9.4	8.52	9.13	8.57	9.84	8.58	7.72	7.8	7.97	8.78	9.25
8866	17-Oct-07 10:12:17	10.34	0.2379	0.0452	5.21	9.5	8.77	9.52	8.84	10.18	8.8	7.89	7.96	8.08	9	9.4
8867	17-Oct-07 10:17:17	10.65	0.2455	0.0454	4.36	10.1	8.98	9.46	9.12	10.81	9.07	8.05	8.14	8.23	9.23	9.85
8868	17-Oct-07 10:22:17	10.99	0.2537	0.0454	4.96	10.4	9.14	9.44	9.41	11.39	9.31	8.08	8.28	8.35	9.51	10.15
8869	17-Oct-07 10:27:17	11.34	0.2642	0.0467	6.35	10.3	9.19	10.34	9.67	11.37	9.55	8	8.32	8.41	9.66	10.16
8870	17-Oct-07 10:32:17	11.66	0.2746	0.0483	4.95	10.6	9.13	10.83	9.84	10.58	9.78	7.84	8.3	8.4	9.72	10.37

Fig.4.14: Part of meteorological data captured on 17th October 2007 at the University of Strathclyde, Glasgow.

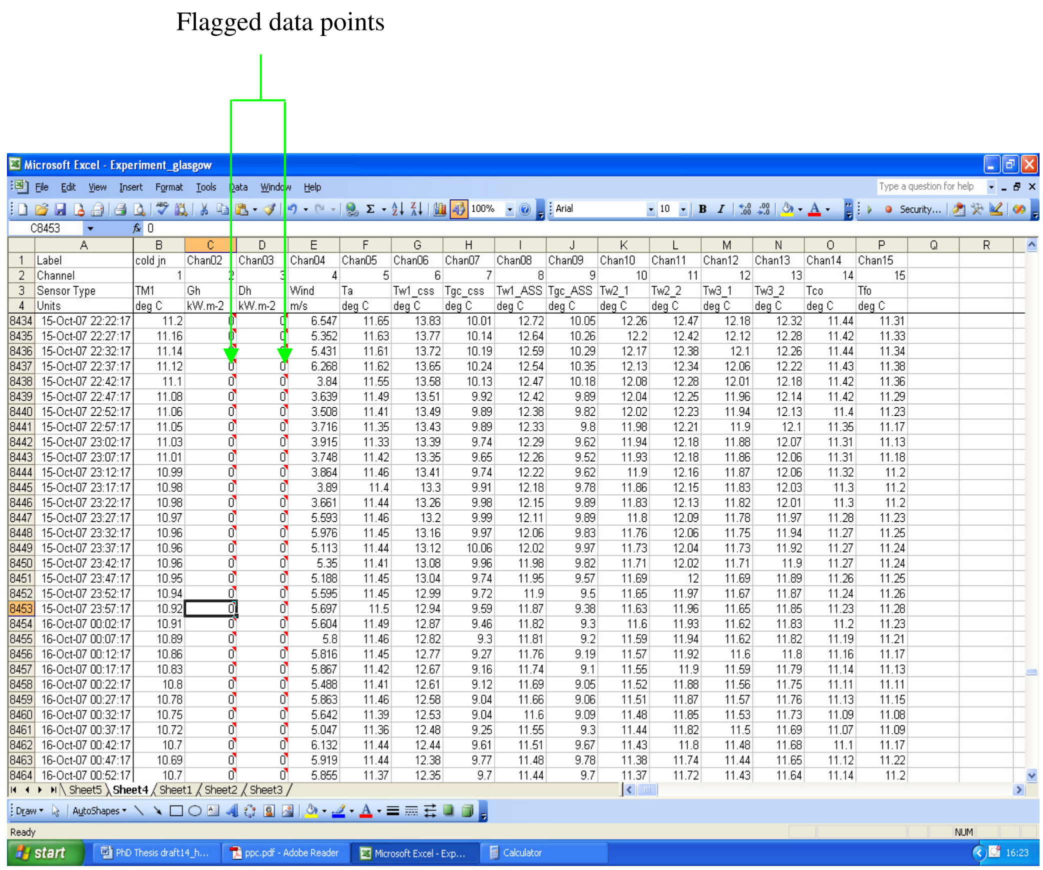

Fig.4.15: Flagged readings of global and diffuse irradiance data on 15-16th October 2007 at the University of Strathclyde, Glasgow.

For water in the evaporator basin and glass cover, the average temperature of each component was linearly correlated with the temperature of the central part of the component (T_3). For water in basins 2 and 3, the average temperature of each component was correlated with T_7 and T_{16} while the average temperature of the condenser cover (T_{co}) was correlated with T_{22}.

$$T_{gc},T_{wl}=a_o+a_1T_3 \qquad (4.2)$$

$$T_{w2},T_{w3} = b_o+b_1T_7+b_2T_{16} \qquad (4.3)$$

$$T_{co}=c_o+c_1T_{22} \qquad (4.4)$$

where a_o, a_1, b_o, b_1, b_2, c_o and c_1 are coefficients.

In subsequent measurements of temperature, only values of T_3, T_7, T_{16} and T_{22} were simultaneously captured for performance comparison of the two solar stills.

In any given logging time interval, the solar azimuth and altitude angles at the midpoint of the time interval were computed from the geometry of the still, latitude and longitude of the site. The astronomical duration between sunrise and sunset was shortened by 2400 s to avert errors in the computation of effective irradiance at low solar altitude (Cooper, 1969).

The beam solar irradiance (G_{bh}) on a horizontal surface was calculated from measured values of G_{gh} and G_{dh}.

$$G_{bh}=G_{gh}-G_{dh} \tag{4.5}$$

In addition, the efficiency of desalination (η_{ds}) was calculated as the ratio of the change in the concentration of TDS to that in raw water (Hanson et al., 2004).

Empirical meteorological data was used to predict distillate yields from the two varieties of solar stills. Then, computed and experimental distillate outputs were statistically compared by using the *t*-statistic at a significance level of 0.1 % (Stone, 1993). Critical values of the *t*-statistic were obtained from statistical tables (Cambridge University Press, 1980). In addition, the difference between the mean of experimental distillate yield from the CSS and ASS was evaluated by using the *t*-test. It should be mentioned that the application of this statistic assumes that the data is random and from a population with normal distribution (Brown and Melamed, 1993). If these assumptions do not hold, then the statistical test is invalid. So, it is necessary to establish these assumptions. In this investigation, assumptions about randomness and distribution type were verified by using lag and normal probability distribution plots respectively (NIST/SEMATECH, 2005). The lag and probability plots were drawn by using Microsoft Excel (version 2003) and SPSS (version 17.0) programs respectively. In addition, skewness and kurtosis were determined by using descriptive statistics in SPSS (version 17.0) to assist in selecting an appropriate distribution (Stuart and Ord, 1987; Joanes and Gill, 1998; Ianetz et al., 2000).

4.8 Summary

Experimentation is vital in the development of an engineering process or product. It aims at assessing the effect of a factor change on an observation. So, there is need to design it properly to ensure valid data is acquired. In this regard, different experimental designs are available but the choice of a particular design depends on the objectives of the investigation, number of factors under investigation and economic constraints. Experimental designs can be classified into comparative, screening and surface objectives. In this study, a randomized block design was used to carry out the required experiments, with design and location as primary and blocking factors respectively. Both factors were set at two levels, which gave 4 possible runs of the experiment. Two designs of solar stills were identified for testing under similar meteorological conditions at each site.

Basically, still design considerations fall into optical, heat transfer and loss characteristics. Optical characteristics comprise absorptance, transmittance and reflection of solar radiation. In this regard, the tilt angle of the transparent cover affects the optical efficiency of a solar still. Further, the inner part of the evaporator basin is often painted black (or covered with any other black thin film) to increase the absorptance of solar radiation by the still base. Once radiation is absorbed by the basin liner and saline water, it is transferred to different components of the system and ultimately lost to the environment. Heat loss through the bottom part of the still significantly reduces the performance of a solar still. So, insulation of the bottom and sides of the still helps to increase distillate productivity. Using these design considerations, prototype solar distillation systems were designed and constructed using materials and skills that are readily-available in developing countries. These solar stills were tested outdoors to establish their empirical performance and to verify the performance of the proposed model for calculating the distribution of solar radiation inside a single slope solar still. Instrumentation for system testing has been described in this chapter. Appropriate statistics were used to determine the validity of results. Finally, the implementation of the proposed experimental design is presented in the next chapter.

4.9 References

Abdallah, S., Badran, O. and Abu-Khader, M.M., 2008. Performance evaluation of a modified design of a single slope solar still. *Desalination*, 219, pp.222-230.

Al-Hinai, H., Al-Nassri, M.S. and Jubran, B.A., 2002. Parametric investigation of a double-effect solar still in comparison with a single-effect solar still. *Desalination*, 150, pp.75-83.

Al-Kharabsheh, S. and Goswami, D.Y., 2003. Experimental study of an innovative solar water desalination system utilizing a passive vacuum technique. *Solar Energy*, 75, pp.395-401.

ASHRAE, 2001. *ASHRAE Handbook Fundamentals*. SI ed. Atlanta: American Society of Heating, Refrigerating and Air-Conditioning Engineers.

ASHRAE, 2003. *ASHRAE/ANSI standard 93-2003: Methods of testing to determine the thermal performance of solar collectors*. Atlanta: American Society of Heating, Refrigerating and Air-conditioning Engineers.

ASTM, 2006. *General methods and instrumentation: Temperature measurement*. vol. 14.03. Conshohocken: American Society for Testing and Materials.

Banat, F., Jumah, R. and Garaibeh, M., 2002. Exploitation of solar stills for desalination by membrane distillation. *Renewable Energy*, 25, pp.293-305.

Bansal, N.K.; Chandra, R. and Malik, M.A.S., 1984. Solar air heater. In: M.S Sodha, S.S. Mathur and M.A.S. Malik, eds. 1984. *Reviews of Renewable Energy Resources*. vol.2. New Dehli: Wiley Eastern Ltd, pp.327-431.

Birello, G. et al., 1989. Advances in density measurements by means of an automatic hydrostatic weighing system of 100 g capacity. *Measurement*, 7, pp.157-162.

Brow, R.K. and Schmitt, L.M., 2009. A survey of energy and environmental applications of glass. *European Ceramic Society*, 29, pp.1193-1201.

Brown, S.R. and Melamed, L.E., 1993. *Experimental design and analysis*. In: M.S. Lewis-Beck, ed. 1993. Experimental design & methods, vol.3. London: SAGE Publications Ltd, , pp.75-159.

BSI, 1999a. *BS EN 27888:1993*:*Water quality – method for the determination of electrical conductivity*.London: British Standards Institution.

BSI, 1999b. *BS 6068 – 2.50:1995*:*Water quality – part 2: Physical, chemical and biochemical methods – Section 2.50 Determination of pH*. London: British Standards Institution.

BSI, 2006. *BS EN 12975 – 2:2006: Thermal solar systems and components – solar collectors – part 2: Test methods*. London: British Standards Institution.

BSI, 2007. *BS ISO 9459-5:2007: Solar heating – solar water heating systems – Part 5: System performance characterization by means of whole-system tests and computer simulation*. London: British Standards Institution.

Cambridge University Press, 1980. *Advanced tables*. 3rd ed. Cambridge: Cambridge University..

Cawley, M.F., McGlynn, D. and Mooney, P.A., 2006. Measurement of the temperature of density maximum of water solutions by using a convective flow technique. *Heat and Mass Transfer*, 49, pp.1763-1772.

CEN, 2006. *European Standard EN 12975-2: Thermal solar systems and components – Solar collectors – Part 2: Test methods*. Brussels: European Committee for Standardization.

Cooper, P.I., 1969. The absorption of radiation in solar stills. *Solar Energy*, 12, pp.333-346.

Cooper, P.I., 1973. The maximum efficiency of single-effect solar stills. *Solar Energy*, 15, pp.205-217.

Cooper, P.I. and Read, W.R.W., 1974. Design philosophy and operating experience for Australian stills. *Solar Energy*, 16, pp.1-8.

Das, S.K. and Chakraverty, A., 1991. Performance of a solar collector with different glazing materials and their degradation under the condition prevailing in a solar collector. *Energy Conversion and Management*, 31, pp.233-242.

Delta-T Devices, 2000. *User manual for DL2e data logger*. Cambridge : Delta-T Devices Ltd.,

Dev, R. and Tiwari, G.N., 2009. Characteristic equation of a passive solar still. *Desalination*, 245, pp.246-265.

Dhiman, N.K., 1990. Evaluation of optimum thickness of bottom insulation for a conventional solar still. *Desalination*, 78, pp.201-208.

Duffie, J.A., 1962. New materials in solar energy utilization. *Solar Energy*, 6, pp.114-118.

Duffie, J.A. and Beckman, W.A., 2006. *Solar Engineering of Thermal Processes*. 3rd ed. New York:Wiley Interscience, 238-239

El-Bahi, A. and Inan, D., 1999a. Analysis of a parallel double glass solar still with separate condenser. *Renewable Energy*, 17, pp.509-521.

El-Bahi, A. and Inan, D., 1999b. A solar still with minimum inclination, coupled to an outside condenser. *Desalination*, 123, pp.79-83.

El-Swify, M.E. and Metias, M.Z., 2002. Performance of double exposure still. *Renewable Energy*, 26, pp.531-547.

Fath, H.E.S. and Elsherbiny, S.M., 1993. Effect of adding a passive condenser on solar still performance. *Energy Conversion and Management*, 34, pp.63-72.

Garg, H.P. and Mann, H.S., 1976. Effect of climatic, operational and design parameters on the year round performance of single-sloped and double-sloped solar still under Indian arid zone conditions. *Solar Energy*, 18, pp.159-164.

Greenwald, M.L. and McHugh, T.K., 1985. *Practical Solar Energy Technology*. New Jersey: Prentice-Hall, Inc., pp.18-40.

Grove, D.M. and Davis, T.P., 1992. *Engineering, quality and experimental design*. Essex: Longman Scientific & Technical, pp.1-73.

Hanson, A. et al., 2004. Distillate water quality of a single-basin solar still: laboratory and field studies. *Solar Energy*, 76, pp.635-645.

Ianetz, A. et al., 2000. A method for characterization and inter-comparison of sites with regard to solar energy utilization by statistical analysis of their solar radiation data as performed for three sites in the Israel Negev Region. *Solar Energy*, 69, pp.283-293.

Incropera, F.P., DeWitt, D.P., Bergman, T.L. and Lavine, A.S., 2007. *Fundamentals of heat and mass transfer*. 6th ed. New Jersey: John Wiley & Sons, 724-770, 929-956.

ISO, 1994. *Standard 9806-1: Test methods for solar collectors-part 1. Thermal performance of glazed liquid heating collectors including pressure drop*. Geneva: International Organization for Standardization.

Joanes, D.N. and Gill, C.A., 1998. Comparing measures of sample skewness and kurtosis. *Journal of the Royal Statistical Society: The Statistician*, 47, pp.183-189.

Khalifa, A.J.N. and Hamood, A.M., 2009a. On the verification of the effect of water depth on the performance of basin type solar stills. *Solar Energy*, 83, pp.1312-1321.

Khalifa, A.J.N. and Hamood, A.M., 2009b. Effect of insulation thickness on the productivity of basin type solar stills: An experimental verification under local climate. *Energy Conversion and Management*, 50, pp.2457-2461.

King, D.W. and Kester, D.R., 1989. Determination of sea water from 1.5 to 8.5 using colorimetric indicators. *Marine Chemistry*, 26, pp.5-20.

Kipp & Zonen, 2004. *Instruction manual: CM 121 shadow ring*. Delft: Kipp & Zonen.

Kipp & Zonen, 2006. *Instruction manual: CMP series 11/CMA series pyranometers / albedometer*. Delft: Kipp & Zonen.

Köhl, M. et al., 2005. Durability of polymeric materials. *Solar Energy*, 79, pp.618-623.

Kumar, S. and Tiwari, G.N., 1996. Estimation of convective mass transfer in solar distillation systems. *Solar Energy*, 57, pp.459-464.

Lachin, J.M., 1981. Introduction to sample size determination and power analysis for clinical trials. *Controlled Clinical Trials*, 2, pp.93-113.

Laghrouche, M. et al., 2005. A miniature silicon hot sensor anemometer for automatic wind measurements. *Renewable Energy*, 30, pp.1881-1896.

Lenel, U.R. and Mudd, P.R., 1984. A review of materials for solar heating systems for domestic hot water. *Solar Energy*, 32, pp.109-120.

Madhlopa, A., Mgawi, R. and Taulo, J., 2006. Experimental study of temperature stratification in an integrated collector-storage solar water heater with two horizontal tanks. *Solar Energy*, 80, pp.989-1002.

Madhlopa, A. and Johnstone, C., 2009a. Model for computation of solar fraction in a single-slope solar still. *Solar Energy*, 83, pp.873-882.

Madhlopa, A. and Johnstone, C., 2009b. Numerical study of a passive solar still with separate condenser. *Renewable Energy*, 34, pp.1668-1677.

Mahdi, N.A., 1992. Performance prediction of a multi-basin solar still. *Energy*, 17, pp.87-93.

Martin, C.L. and Goswami, D.Y., 2005. *Solar energy pocket reference*. Freiburg: International Solar Energy Society.

Mathioulakis, E., Voropoulos, K. and Belessiotis, V., 1999. Assessment of uncertainty in solar collector modelling and testing. *Solar Energy*, 66, pp.337-347.

Mohamad, A.A., 1997. High efficiency solar air heater. *Solar Energy*, 60, pp.71-76.

Mowla, D. and Karimi, G., 1995. Mathematical modelling of solar stills in Iran. *Solar Energy*, 55, pp.389-393.

Nafey, A.S., Abdelkader, M., Abdelmotalip, A. and Mabrouk, A.A., 2000. Parameters affecting solar still productivity. *Energy Conversion and Management*, 41, pp.1797-1809.

Nicholas, J.V. and White, D.R., 1994. Traceable temperatures: An introduction to temperature measurement and calibration. New York: John Wiley & Sons, pp.154-326.

NIST/SEMATECH, 2005. *E-Handbook of statistical methods*, http://www.nist.gov/div898/handbook/, 9/11/2005.

Phadatare, M.K. and Verma, S.K., 2007. Influence of water depth on internal heat and mass transfer in a plastic solar still. *Desalination*, 217, pp.267-275.

Porta, M.A., Chargoy, N. and Fernández, J.L., 1997. Extreme operating conditions in shallow solar stills. *Solar Energy*, 61, pp.279-286.

Qiblawey, H.M. and Banat, M., 2008. Solar thermal desalination technologies. *Desalination*, 220, pp.633-644.

Rasch, D., Teuscher, F. and Guiard, V., 2007. How robust are tests for two independent samples? *Statistical Planning and Inference*, 137, pp.2706-2720.

Sahoo, B.B. et al., 2008. Performance assessment of a solar still using blackned surface and thermocol insulation. *Renewable Energy*, 33, pp.1703-1708.

Saluja, G.S. and Douglas, N.G., 1996. Verification of wind resource study in a Scottish region. *Renewable Energy*, 9, pp.798-801.

Samee, M.A., Mirza, U.K., Majeed, T. and Ahmad, N., 2007. Design and performance of a simple solar still. *Renewable and Sustainable Energy Reviews*, 11, pp.543-549.

Simond, B., 1965. Rigid foam markets in Europe. *Cellular Plastics*, 1, pp.229-233.

Sinden, G., 2007. Characteristics of the UK wind resources: Long-term patterns and relationship to electricity demand. *Energy Policy*, 35, pp.112-127.

Smyth, M., Norton, B. and Byres, W., 2005. Measured effect of reflector augmentation of simple basin type solar stills. *Ambient Energy*, 26, pp.59-70.

Stone, R.J., 1993. Improved statistical procedure for the evaluation of solar radiation estimation models. *Solar Energy*, 51, pp.289-291.

Stuart, A. and Ord, J.K., 1987. *Kendall's advanced theory of statistics*: *Distribution Theory*. vol. 1. London: Charles Griffin & Company Ltd., pp.106-108, 210-220.

Tanaka, H. and Nakatake, Y., 2006. Theoretical analysis of a basin type solar still with internal and external reflectors. *Desalination*, 197, pp.205-216.

Tanaka, H. and Nakatake, Y., 2007. Effect of inclination of external flat plate reflector of basin type still in winter. *Solar Energy*, 81, pp.1035-1042.

Tiwari, A.K. and Tiwari, G.N., 2007. Thermal modelling based on solar fraction and experimental study of the annual performance of a single slope passive solar still: The effect of water depths. *Desalination*, 207, pp.184-204.

Tleimat, B.W. and Howe, E.D., 1969. Comparison of plastic and glass condensing covers for solar stills. *Solar Energy*, 12, pp.293-304.

Tripathi, R. and Tiwari, G.N., 2004. Performance evaluation of solar still by using the concept of solar fraction. *Desalination*, 169, pp.69-80.

Tripathi, R. and Tiwari, G.N., 2006. Thermal modelling of passive and active solar stills for different depths of water by using the concept of solar fraction. *Solar Energy*, 80, pp.956-967.

Tsilingiris, P.T., 2009. Analysis of the heat and mass transfer processes in solar stills. *Solar Energy*, 83, pp.420-431.

Voropoulos, K., Mathioulakis, E. and Belesssiotis, V., 2003. Experimental investigation of the behaviour of a solar still coupled with hot water storage tank. *Desalination*, 156, pp.315-322.

Yates, R. and Woto, T., 1988. *Small scale desalination for areas of Botswana*. Ottawa: International Development Centre..

Yao, W., Liu, X. and Byrne, R.H., 2007. Impurities in indicators used for spectrometric pH measurements: Assessment and remedies. *Marine Chemistry*, 107, pp.167-172.

WHO, 2008. *World Health Statistics 2008*. Geneva: World Health Organization.

Wisse, J.A. and Stigter, K., 2007. Wind engineering in Africa. *Wind Engineering and Industrial Aerodynamics*, 95, pp.908-927.

Zurigat, Y.H. and Abu-Arabi, M.K., 2004. Modelling and performance analysis of a regenerative solar desalination unit. *Applied Thermal Engineering*, 24, pp.1061-1072.

Chapter 5

Experimentation

5.0 Introduction

Testing of an engineering process or product is vital to establish its performance under real conditions as shown in the previous chapter. In this vein, it is necessary to know how a solar system collects and dissipates energy. This includes the transmission-absorption of solar radiation and transfer of heat from the system to the environment. Test methods are required to evaluate the performance of a solar system to obtain accurate results and provide a reliable common basis for comparing system performance.

The design of this experiment and instruments for data acquisition and processing were discussed in Chapter 4. In this chapter, instrumentation and procedures used during the present experimentation are presented and discussed.

5.1 Test methods

The development of different designs of solar collectors prompted the need to devise standard methods for testing various solar systems (Duffie and Beckman, 2006). These methods stipulate the design, environmental conditions, operational and instrumentation requirements for specified tests. However, it has been pointed in Section 4.6 that standard methods for evaluating solar stills are lacking. Most of the measurements for the determination of still efficiency are taken by using guidelines from relevant standard methods and practices for other solar thermal systems. These guidelines are acceptable and so they yield valid results. For instance, BSI (2006) recommended the use of pyranometers in class 1 (or better class) to measure solar radiation when testing a solar thermal system and its components. This specification is aimed at capturing a high quality of solar radiation data for performance evaluation of a solar thermal system. Thus, exploitation of the stipulated category of radiometers should nonetheless yield accurate data for testing a solar still.

Yates and Woto (1988), as cited in Smyth et al. (2005), reported that the values of still efficiency (η_{st}) computed over periods lower than 24 hours are usually invalid because the distillation continues after sun set. In view of this, the still efficiency (total latent heat of vaporization as a percentage of the daily solar energy intercepted by the still aperture) was computed on daily basis (Cooper, 1973; El-Bahi and Inan, 1999):

$$\eta_{st} = \frac{100 A_{w1} L' Y_{dd}}{A_{gc} H_{gc}} \tag{5.1}$$

where Y_{dd} is the daily distillate yield and L' is the specific latent heat of water computed at the daily mean temperature of saline water.

5.2 Solar still mounting

Solar radiation is the most influential environmental factor in the performance of a solar technology (Nafey et al., 2000). In addition, the position of the sun affects the amount of solar energy intercepted by a given surface (as reported in Chapter 2). So, the location and orientation of a solar energy system affect its performance. A solar energy system may be obstructed from the sun during most of the day when tall structures are nearby. In view of these considerations, BSI (2007a) recommended that a non-tracking solar collector should face the equator and be clear of structures that may cause shading. This location and orientation aims at optimizing solar collection.

In this study, the conventional and advanced solar stills were mounted at the University of Strathclyde located in the northern hemisphere (55^{o} 52′ N, 4^{o} 15′ W) and Malawi Polytechnic in the southern hemisphere (15^{o} 48′ S, 35^{o} 02′ E). To reduce the effect of shading, the two solar stills were mounted outdoors adjacent to each other on steel frames on top of a horizontal roof 35 m and 6 m above the ground at the former and latter test sites respectively. In addition, the distillation systems faced south at the

University of Strathclyde with a reversed orientation at the Malawi Polytechnic in accordance with standard guidelines for testing solar collectors (ASHRAE, 2003; BSI, 2007a). This orientation was aimed at allowing the sun to be in front of the systems during most of the day and optimizing the transmission of solar radiation through the glass covers. The solar stills were secured against high wind speeds using supports (Figs.5.1(a) and (b)). It should be mentioned that t_{dy} = 1 hr during the test period at the University of Strathclyde, and t_{dy}=0 throughout the year at the Malawi Polytechnic.

Un-reinforced PVC flexible tubes (internal diameter =0.012 m, wall thickness=0.0015 m) were fitted to the stills to drain distilled water from the distillate collection channels into distillate collection bottles. Theses tubes were tightly-fitted on both ends to avert leakage of water vapour and distilled water. One plastic bottle (of capacity 5 litres) was fitted to the CSS while 4 bottles of the same capacity were fitted to the ASS because the latter solar distillation system had 4 distillate channels (2 x channels for the first effect, 1 x channel for the second effect and 1 x channel for the third effect). The distillate collection bottles were tied to the steel frames, on which the stills were installed, to ensure they did not topple over and spill the collected distilled water.

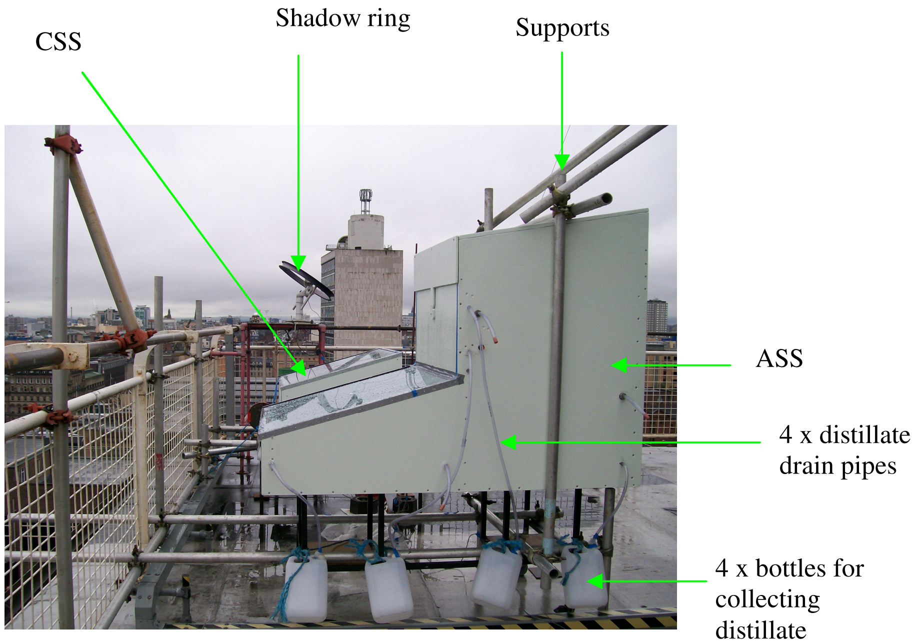

(a)

(b)

Fig.5.1: Conventional and advanced solar stills mounted at a) the University of Strathclyde and b) the Malawi Polytechnic.

5.3 Instrumentation and procedures

5.3.1 Irradiance

Solar radiation drives the heat and mass transfer processes in a solar still. So, it is necessary to measure this environmental factor with a high degree of accuracy. To achieve this, pyranometers of high grade were used to measure irradiance at both the University of Strathclyde and Malawi Polytechnic. BSI (2007a) recommended that the pyranometer should be installed in the same plane as that of the solar collector. Nevertheless, global solar radiation is commonly measured on a horizontal surface (Thekaekara, 1976), and it can be used to compute diffuse radiation (as reported in Chapter 2). Consequently, the model proposed in this study requires irradiance on a horizontal surface for ease of application in different parts of the world. To verify the performance of this model, it was therefore necessary to measure irradiance on a horizontal surface.

Global and diffuse irradiance on a horizontal surface was measured by using Kipp & Zonen CM11 pyranometers within 3 m of the solar stills at the University of Strathclyde. These radiometers are part of the instrumentation for a meteorological station within the Department of Mechanical Engineering at the University of Strathclyde. The pyranometers were connected to the data recorder used in this investigation during the experimental period to synchronize all the data points for ease of analysis. For diffuse radiation, a Kipp & Zonen shadow ring (model CM 121B) was fitted over the pyranometer and the recorded data was corrected for the shadow ring (Kipp & Zonen, 2004). Figs.5.2 (a) and (b) show the location of solar stills and irradiance instrumentation respectively, at the University of Strathclyde.

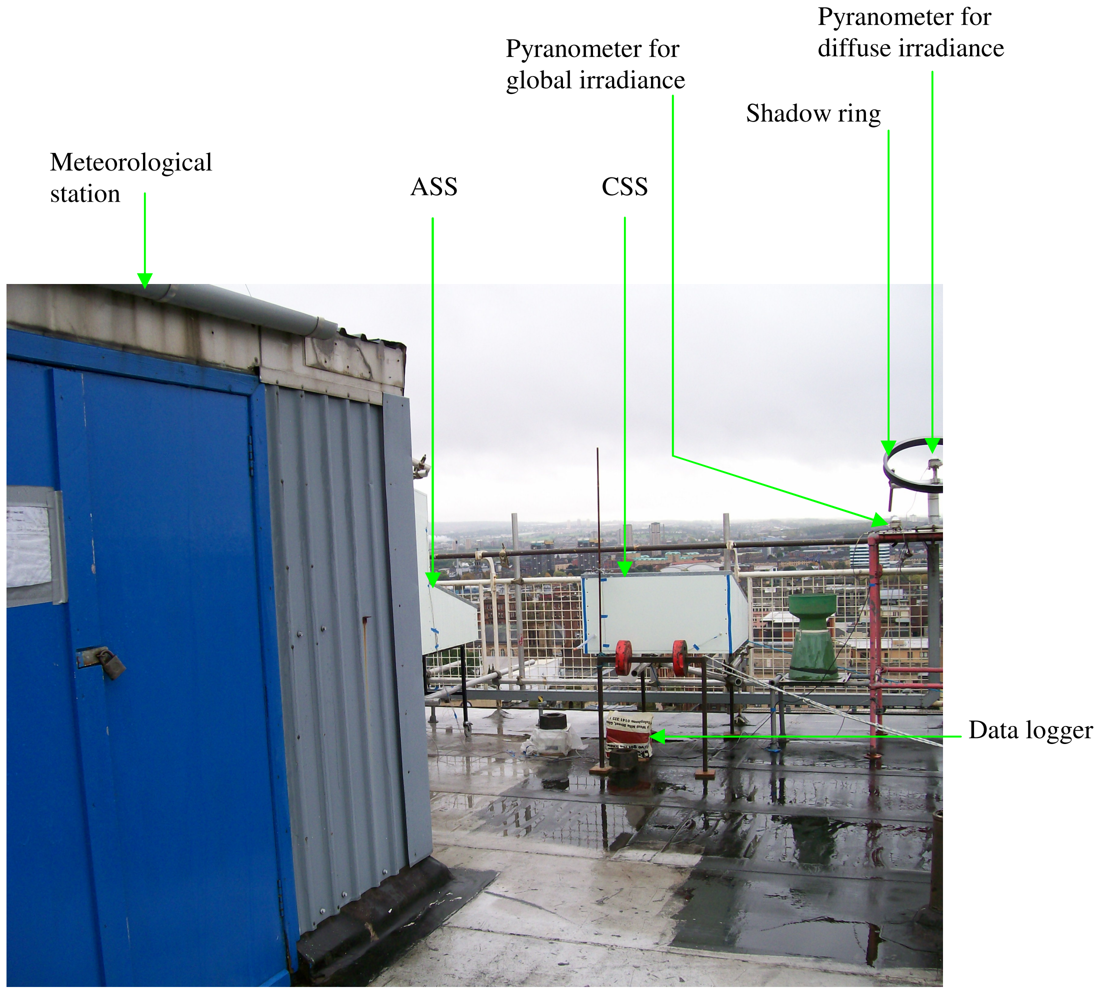

Fig.5.2 (a): Location of solar stills and instruments at the University of Strathclyde.

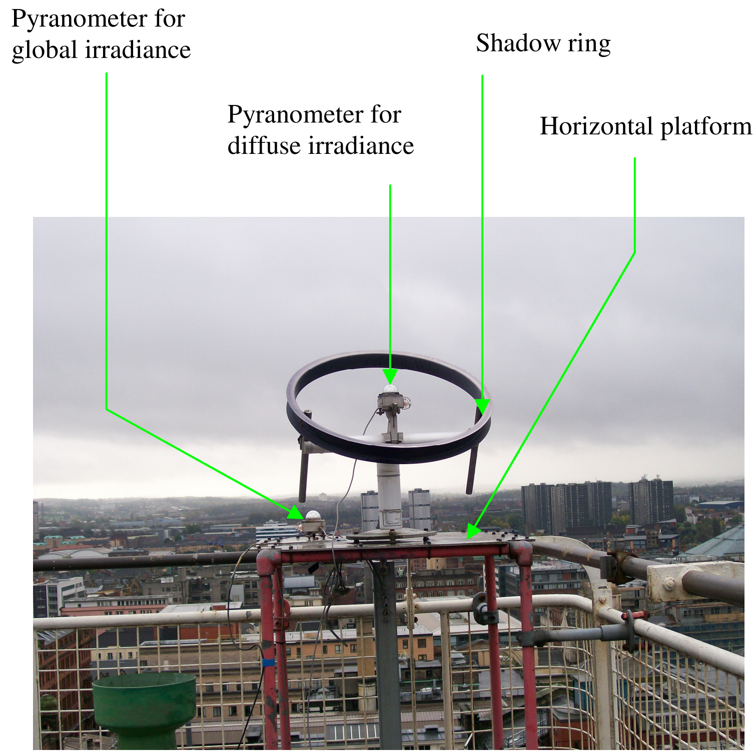

Fig.5.2 (b): Full view of the irradiance instrumentation at the University of Strathclyde.

At the Malawi Polytechnic, global irradiance on a horizontal surface was measured by using a Kipp & Zonen CM11 pyranometer while diffuse irradiance was sensed by a Kipp & Zonen CM 6B pyranometer within 3 m of the distillation systems. For diffuse radiation, a Kipp & Zonen shadow ring (model CM 121B) was again fixed over the pyranometer and adjusted after every 2 days, and the recorded data was corrected for the shadow ring (Kipp & Zonen, 2004). The location of solar stills and irradiance instrumentation at the Malawi Polytechnic are shown in Figs.5.3 (a) and (b).

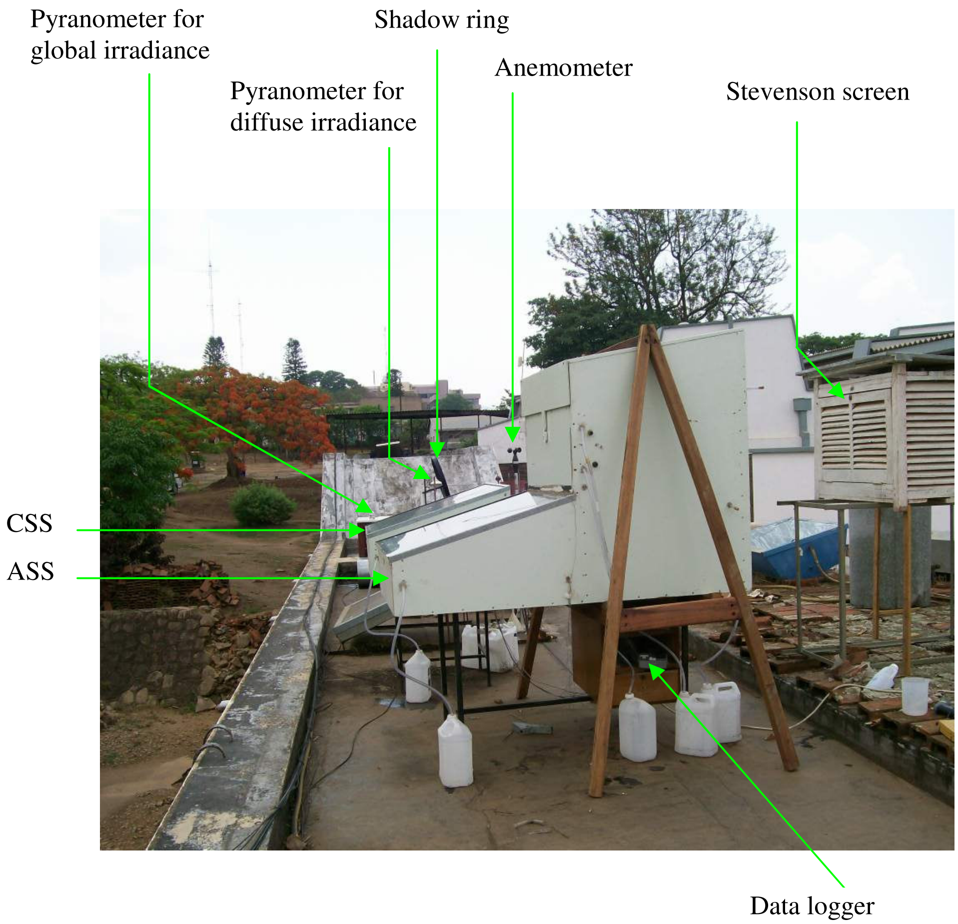

Fig.5.3 (a): Location of solar stills and instruments at the Malawi Polytechnic.

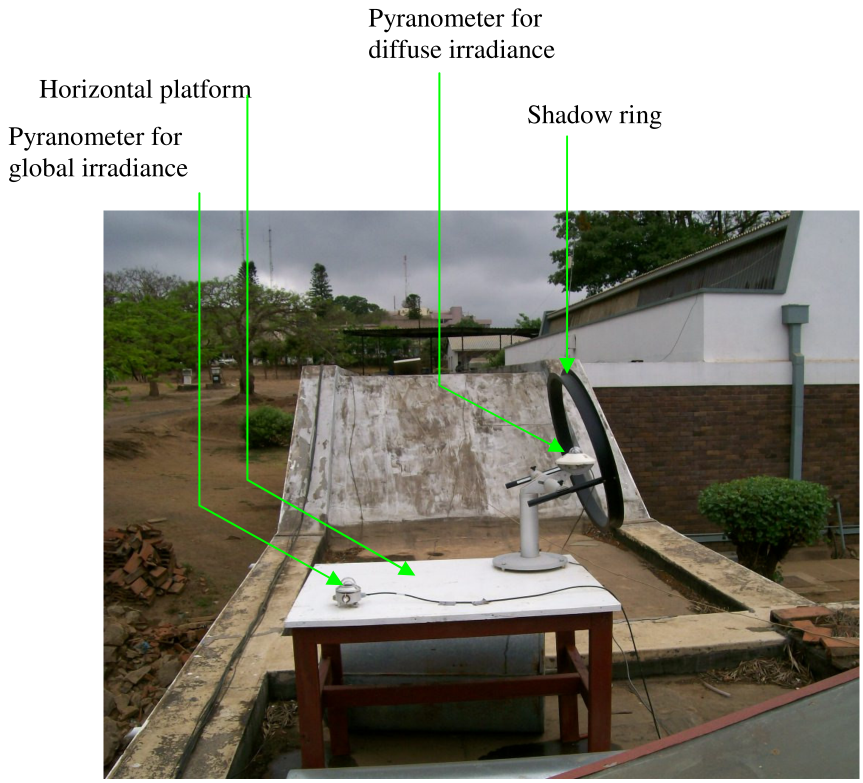

Fig.5.3 (b): Full view of the irradiance instrumentation at the Malawi Polytechnic.

5.3.2 Temperature

The temperature of ambient air and components of the solar stills were measured by using T-type thermocouple as reported in Chapter 4. BSI (2007a) recommended that the sensor for ambient air should be shaded from solar radiation, located within 10 m from the test system and at least 1 m above the ground to avert the effect of heat from the ground. At the University of Strathclyde, the sensor for the temperature of ambient air was mounted in an open ended un-reinforced PVC flexible tube (internal diameter =0.012 m, wall thickness=0.0015 m and length =0.025 m) to allow free air circulation, and white PVC tape was wrapped around the tube to shield it against solar radiation. The tube was mounted horizontally on the under side of a wooden table located within a radius of 2 m from the solar stills and about 1 m above the plane of a horizontal roof where the two solar stills were installed (Fig.5.4). At the Malawi Polytechnic, the sensor for ambient air temperature was housed in a Stevenson screen located within a radius of

3m from the distillation systems (Fig.5.1). Again, the sensor was about 1 m above the plane of the roof of the building. The locations of thermocouples for measuring the temperatures of the other components of the solar stills have been described in Chapter 4, and they were the same at both test sites.

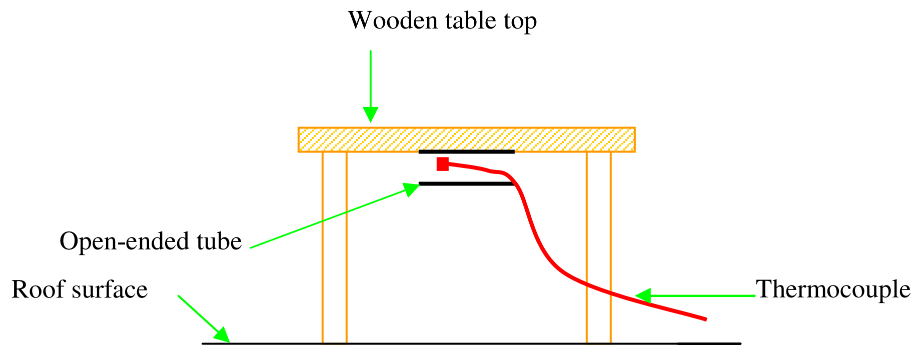

Fig.5.4: Installation of a thermocouple for measuring ambient air temperature at the University of Strathclyde.

5.3.3 Wind speed

Observations of surface wind speed are made by employing anemometers at different meteorological stations in different parts of the world. The WMO (2003) recommended that wind instruments should be installed on a level open ground at 10 m above the ground. However, heights of lower or greater than 10 m have also been used by other observers, depending on the application of the data (Saluja and Douglas, 1996; Wisse and Stigter, 2007). Surface wind data is also required in solar collector testing because of the influence of wind speed on the coefficient of heat transfer from the collector to the surrounding air.

Oliphant (1980) used a height of 0.10 m above the plane of two flat plate solar collectors to measure air speed over the collectors. BSI (2007a) recommended that an anemometer should be located within 1 m from the collector and at a height nearly equal to the height of the collector centre. Nevertheless, the difference between meteorological wind speed and the speed of air over a collector depends on the location of the collector under test (BSI, 2006). Thus, if a collector is tested in a location with negligible obstruction from tall structures such as mountains and buildings then the air speed over the collector would be comparable to the meteorological wind speed recorded within the vicinity of the collector. Moreover, the influence of wind direction on heat losses from a solar collector is not well understood (BSI, 2006). So, an anemometer for the meteorological station in the Department of Mechanical Engineering was used at the University of Strathclyde. This anemometer was on the roof of the weather station within 6 m of the solar stills and at about 8 m above the glass covers. In addition, the anemometer and the stills were located on the roof of a building 35 m high from the local ground to reduce obstruction from tall structures. Consequently, the wind speed sensor would give values that were close to those of air speed over the collector. At the Malawi Polytechnic, an anemometer and solar stills were again located on the roof of a building about 6 m above the local ground. The anemometer was installed 0.10 m above the plane of the glass covers and within 1 m from the solar distillation systems in conformity with the procedures reported by Oliphant (1980) and BSI (2006).

5.3.4 Data recording

Pyranometers, thermocouples and anemometers were all connected to a Delta-T Devices data logger (model DL2e) at both test sites. At the University of Strathclyde, the logger was covered on top and placed on a wooden plate under the CSS to shield it from adverse weather, and it was powered by a 12 V lead acid battery. The same data recorder was employed at the Malawi Polytechnic where it was placed in a wooden tray under the ASS, again, to protect it from adverse weather. At this test site, the logger was powered through a 12 V adapter connected to a mains supply extended onto the roof where the two solar stills were installed. The layout for instrumentation for automatic data acquisition at both test sites is shown in Fig.5.5.

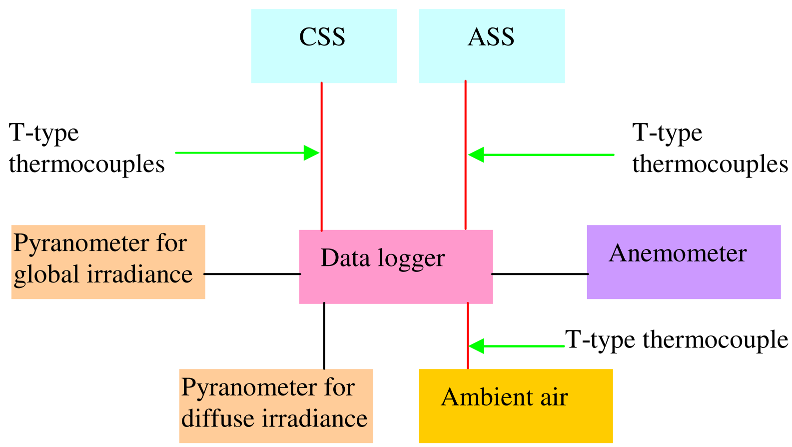

Fig.5.5: Layout of instrumentation for automatic data acquisition.

A program for logging was written using the DL2 software on a laptop (Dell Inspiron 6000) before data recording commenced. In this program, the appropriate card in the logger and the properties of a given sensor were specified and a channel was allocated to each sensor (Fig.5.6). Then, the program was sent from the laptop to the logger before logging was initiated to start (Fig.5.7). When all the instruments were ready, the logging process was commenced and checked to ensure that every sensor was working well. The recorded data was imported from the logger into Microsoft Windows 2003 Excel software on the laptop once a week (Figs.5.8 to 5.9).

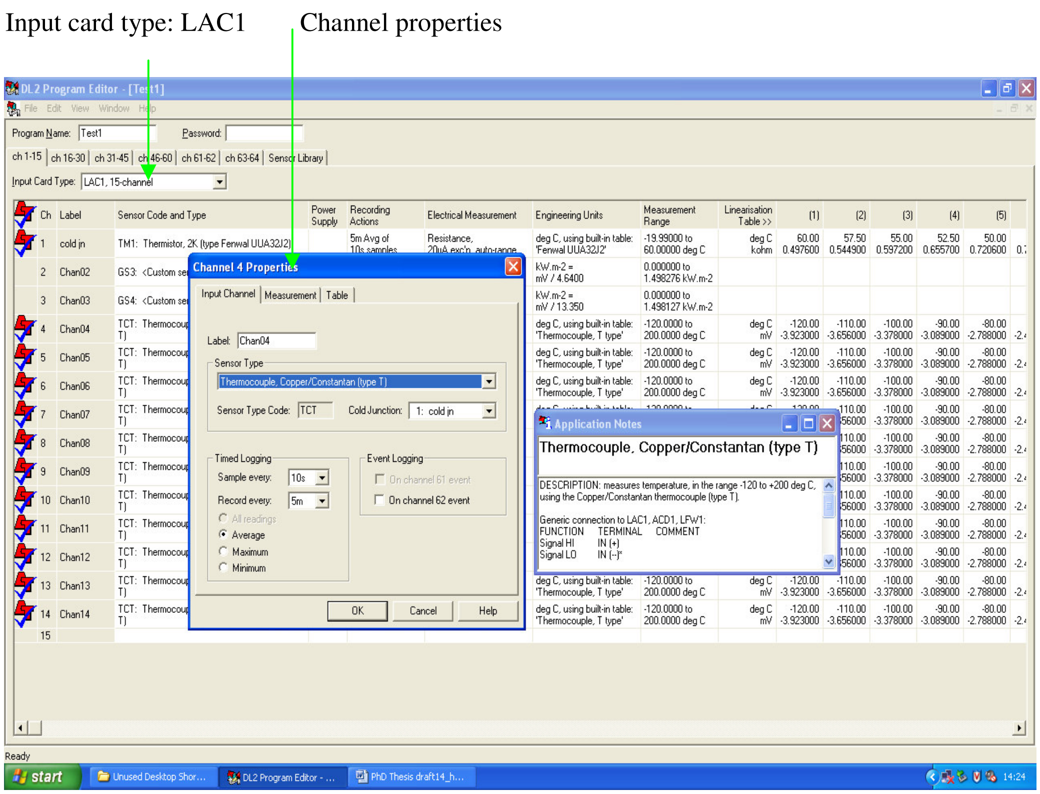

Fig.5.6: Specifying properties of sensors in DL2 program editor: A T-type thermocouple was allocated to channel 4.

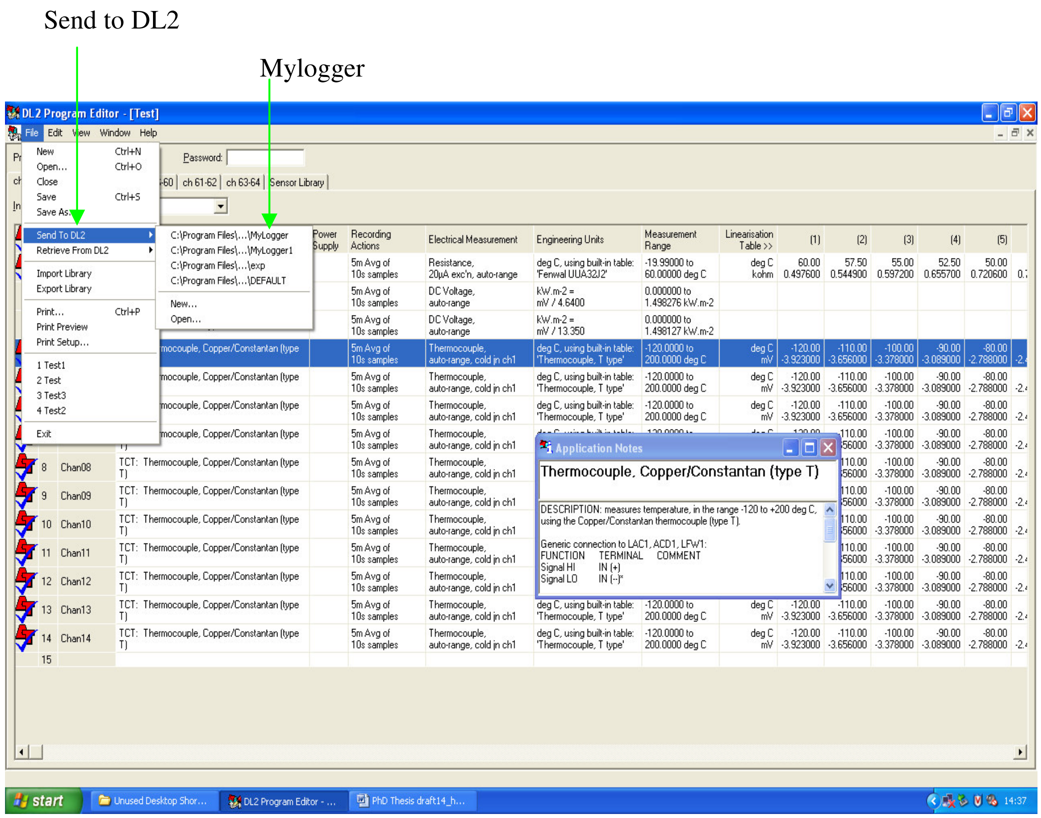

Fig.5.7: Sending a program for logging from the laptop to the logger: Select ‘Send To DL2’ under ‘file’ then click on ‘Mylogger’.

Data import dialog box within an Excel window

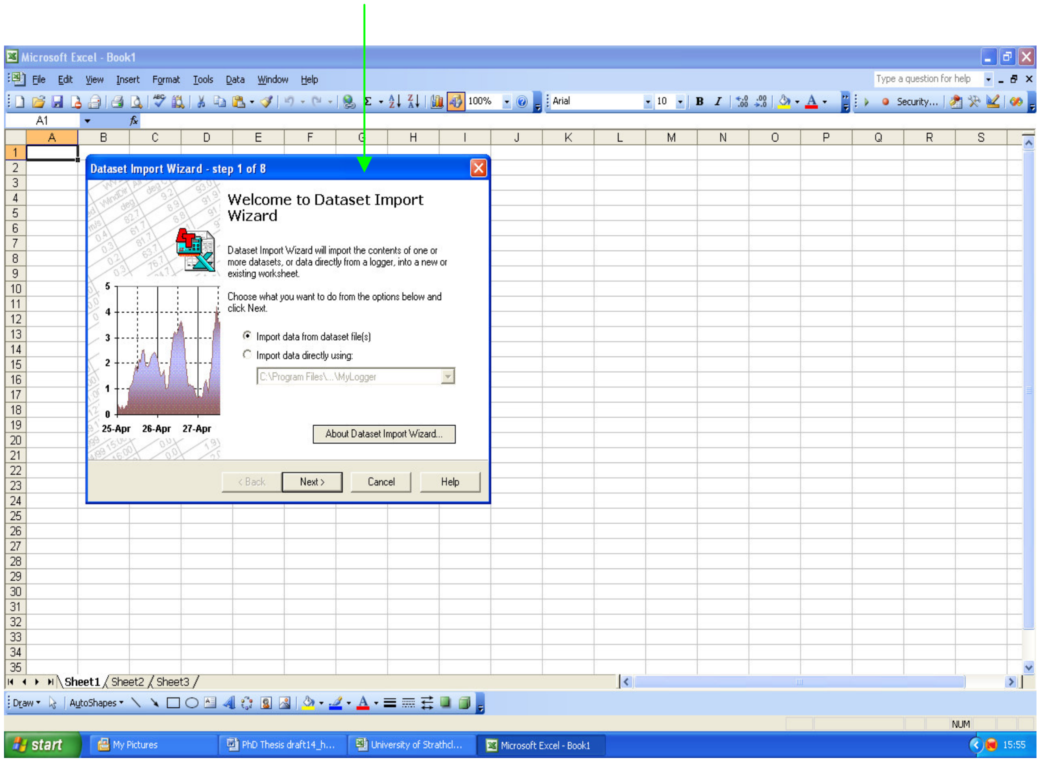

Fig.5.8: Importing recorded data from the logger into Microsoft Windows Excel software.

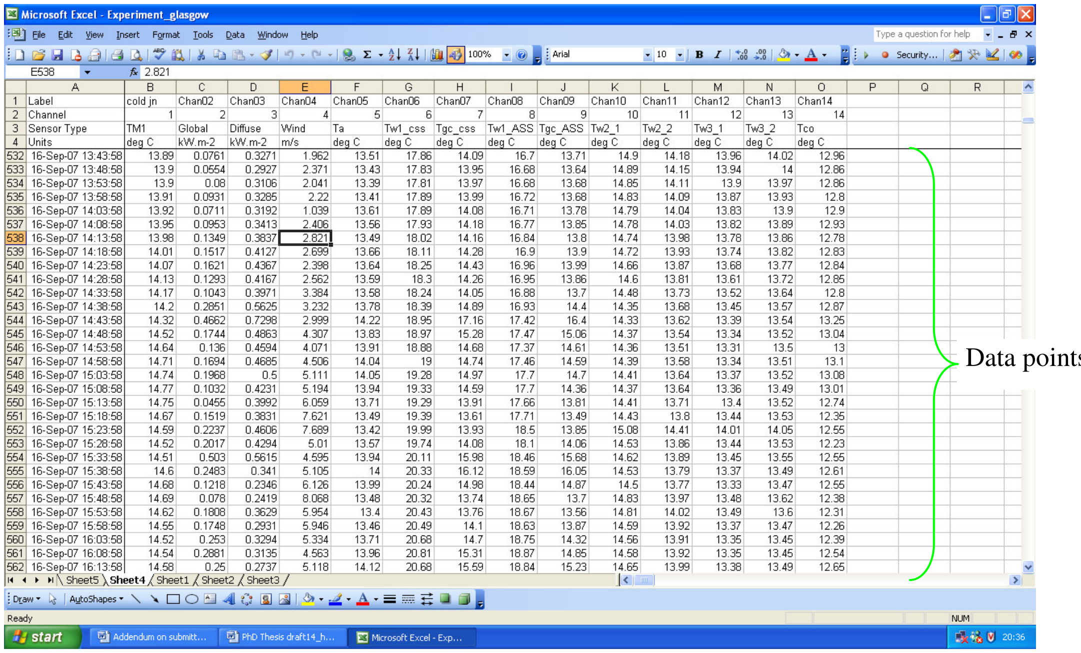

	A	B	C	D	E	F	G	H	I	J	K	L	M	N	O
1	Label	cold jn	Chan02	Chan03	Chan04	Chan05	Chan06	Chan07	Chan08	Chan09	Chan10	Chan11	Chan12	Chan13	Chan14
2	Channel	1	2	3	4	5	6	7	8	9	10	11	12	13	14
3	Sensor Type	TM1	Global	Diffuse	Wind	Ta	Tw1_css	Tgc_css	Tw1_ASS	Tgc_ASS	Tw2_1	Tw2_2	Tw3_1	Tw3_2	Tco
4	Units	deg C	kW.m-2	kW.m-2	m/s	deg C	deg C	deg C	deg C	deg C	deg C	deg C	deg C	deg C	deg C
532	16-Sep-07 13:43:58	13.89	0.0761	0.3271	1.962	13.51	17.86	14.09	16.7	13.71	14.9	14.18	13.96	14.02	12.96
533	16-Sep-07 13:48:58	13.9	0.0554	0.2927	2.371	13.43	17.83	13.95	16.68	13.64	14.89	14.15	13.94	14	12.86
534	16-Sep-07 13:53:58	13.9	0.08	0.3106	2.041	13.39	17.81	13.97	16.68	13.68	14.85	14.11	13.9	13.97	12.86
535	16-Sep-07 13:58:58	13.91	0.0931	0.3285	2.22	13.41	17.89	13.99	16.72	13.68	14.83	14.09	13.87	13.93	12.8
536	16-Sep-07 14:03:58	13.92	0.0711	0.3192	1.039	13.61	17.89	14.08	16.71	13.78	14.79	14.04	13.83	13.9	12.9
537	16-Sep-07 14:08:58	13.95	0.0953	0.3413	2.406	13.56	17.93	14.18	16.77	13.85	14.78	14.03	13.82	13.89	12.93
538	16-Sep-07 14:13:58	13.98	0.1349	0.3837	2.821	13.49	18.02	14.16	16.84	13.8	14.74	13.98	13.78	13.86	12.78
539	16-Sep-07 14:18:58	14.01	0.1517	0.4127	2.699	13.66	18.11	14.28	16.9	13.9	14.72	13.93	13.74	13.82	12.83
540	16-Sep-07 14:23:58	14.07	0.1621	0.4367	2.398	13.64	18.25	14.43	16.96	13.99	14.66	13.87	13.68	13.77	12.84
541	16-Sep-07 14:28:58	14.13	0.1293	0.4167	2.562	13.59	18.3	14.26	16.95	13.86	14.6	13.81	13.61	13.72	12.85
542	16-Sep-07 14:33:58	14.17	0.1043	0.3971	3.384	13.58	18.24	14.05	16.88	13.7	14.48	13.73	13.52	13.64	12.8
543	16-Sep-07 14:38:58	14.2	0.2851	0.5625	3.232	13.78	18.39	14.89	16.93	14.4	14.35	13.68	13.45	13.57	12.87
544	16-Sep-07 14:43:58	14.32	0.4662	0.7298	2.999	14.22	18.95	17.16	17.42	16.4	14.33	13.62	13.39	13.54	13.25
545	16-Sep-07 14:48:58	14.52	0.1744	0.4863	4.307	13.83	18.97	15.28	17.47	15.06	14.37	13.54	13.34	13.52	13.04
546	16-Sep-07 14:53:58	14.64	0.136	0.4594	4.071	13.91	18.88	14.68	17.37	14.61	14.36	13.51	13.31	13.5	13
547	16-Sep-07 14:58:58	14.71	0.1694	0.4685	4.506	14.04	19	14.74	17.46	14.59	14.39	13.58	13.34	13.51	13.1
548	16-Sep-07 15:03:58	14.74	0.1968	0.5	5.111	14.05	19.28	14.97	17.7	14.7	14.41	13.64	13.37	13.52	13.08
549	16-Sep-07 15:08:58	14.77	0.1032	0.4231	5.194	13.94	19.33	14.59	17.7	14.36	14.37	13.64	13.36	13.49	13.01
550	16-Sep-07 15:13:58	14.75	0.0455	0.3992	6.059	13.71	19.29	13.91	17.66	13.81	14.41	13.71	13.4	13.52	12.74
551	16-Sep-07 15:18:58	14.67	0.1519	0.3831	7.621	13.49	19.39	13.61	17.71	13.49	14.43	13.8	13.44	13.53	12.35
552	16-Sep-07 15:23:58	14.59	0.2237	0.4606	7.689	13.42	19.99	13.93	18.5	13.85	15.08	14.41	14.01	14.05	12.55
553	16-Sep-07 15:28:58	14.52	0.2017	0.4294	5.01	13.57	19.74	14.08	18.1	14.06	14.53	13.86	13.44	13.53	12.23
554	16-Sep-07 15:33:58	14.51	0.503	0.5615	4.595	13.94	20.11	15.98	18.46	15.68	14.62	13.89	13.45	13.55	12.55
555	16-Sep-07 15:38:58	14.6	0.2483	0.341	5.105	14	20.33	16.12	18.59	16.05	14.53	13.79	13.37	13.49	12.61
556	16-Sep-07 15:43:58	14.68	0.1218	0.2346	6.126	13.99	20.24	14.98	18.44	14.87	14.5	13.77	13.33	13.47	12.55
557	16-Sep-07 15:48:58	14.69	0.078	0.2419	8.068	13.48	20.32	13.74	18.65	13.7	14.83	13.97	13.48	13.62	12.38
558	16-Sep-07 15:53:58	14.62	0.1808	0.3629	5.954	13.4	20.43	13.76	18.67	13.56	14.81	14.02	13.49	13.6	12.31
559	16-Sep-07 15:58:58	14.55	0.1748	0.2931	5.946	13.46	20.49	14.1	18.63	13.87	14.59	13.92	13.37	13.47	12.26
560	16-Sep-07 16:03:58	14.52	0.253	0.3294	5.334	13.71	20.68	14.7	18.75	14.32	14.56	13.91	13.35	13.45	12.39
561	16-Sep-07 16:08:58	14.54	0.2881	0.3135	4.563	13.96	20.81	15.31	18.87	14.85	14.58	13.92	13.35	13.45	12.54
562	16-Sep-07 16:13:58	14.58	0.25	0.2737	5.118	14.12	20.68	15.59	18.84	15.23	14.65	13.99	13.38	13.49	12.65

(a)

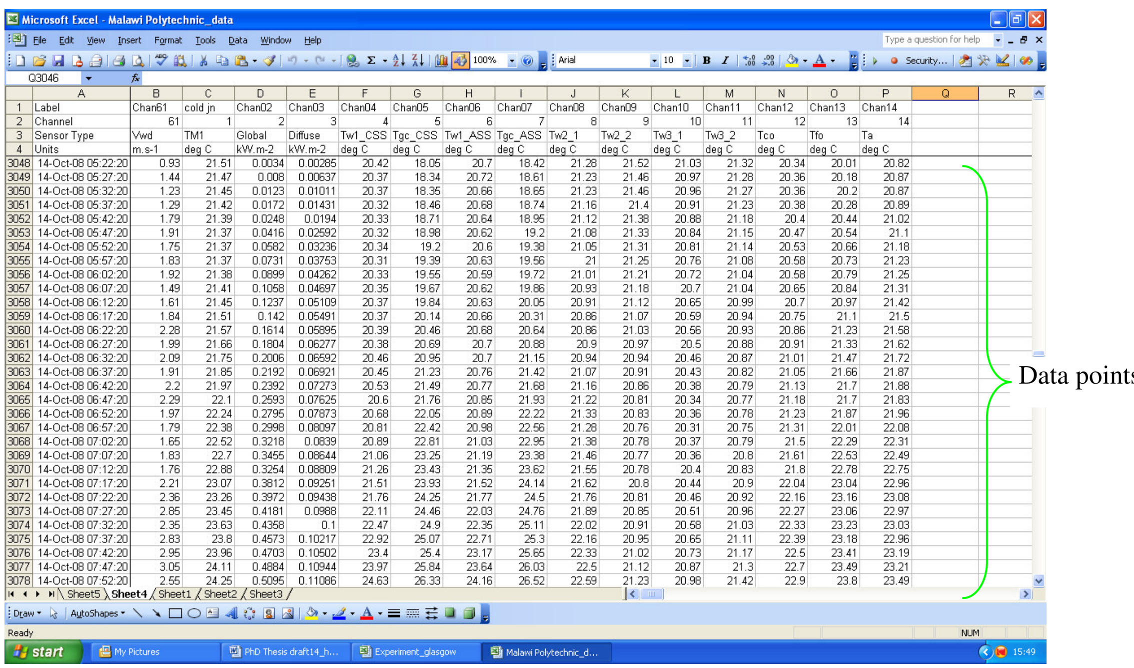

	A	B	C	D	E	F	G	H	I	J	K	L	M	N	O	P
1	Label	Chan61	cold jn	Chan02	Chan03	Chan04	Chan05	Chan06	Chan07	Chan08	Chan09	Chan10	Chan11	Chan12	Chan13	Chan14
2	Channel	61	1	2	3	4	5	6	7	8	9	10	11	12	13	14
3	Sensor Type	Vwd	TM1	Global	Diffuse	Tw1_CSS	Tgc_CSS	Tw1_ASS	Tgc_ASS	Tw2_1	Tw2_2	Tw3_1	Tw3_2	Tco	Tfo	Ta
4	Units	m.s-1	deg C	kW.m-2	kW.m-2	deg C	deg C	deg C	deg C	deg C	deg C	deg C	deg C	deg C	deg C	deg C
3048	14-Oct-08 05:22:20	0.93	21.51	0.0034	0.00285	20.42	18.05	20.7	18.42	21.28	21.52	21.03	21.32	20.34	20.01	20.82
3049	14-Oct-08 05:27:20	1.44	21.47	0.008	0.00637	20.37	18.34	20.72	18.61	21.23	21.46	20.97	21.28	20.36	20.18	20.87
3050	14-Oct-08 05:32:20	1.23	21.45	0.0123	0.01011	20.37	18.35	20.66	18.65	21.23	21.46	20.96	21.27	20.36	20.2	20.87
3051	14-Oct-08 05:37:20	1.29	21.42	0.0172	0.01431	20.32	18.46	20.68	18.74	21.16	21.4	20.91	21.23	20.38	20.28	20.89
3052	14-Oct-08 05:42:20	1.79	21.39	0.0248	0.0194	20.33	18.71	20.64	18.95	21.12	21.38	20.88	21.18	20.4	20.44	21.02
3053	14-Oct-08 05:47:20	1.91	21.37	0.0416	0.02592	20.32	18.98	20.62	19.2	21.08	21.33	20.84	21.15	20.47	20.54	21.1
3054	14-Oct-08 05:52:20	1.75	21.37	0.0582	0.03236	20.34	19.2	20.6	19.38	21.05	21.31	20.81	21.14	20.53	20.66	21.18
3055	14-Oct-08 05:57:20	1.83	21.37	0.0731	0.03753	20.31	19.39	20.63	19.56	21	21.25	20.76	21.08	20.58	20.73	21.23
3056	14-Oct-08 06:02:20	1.92	21.38	0.0899	0.04262	20.33	19.55	20.59	19.72	21.01	21.21	20.72	21.04	20.58	20.79	21.25
3057	14-Oct-08 06:07:20	1.49	21.41	0.1058	0.04697	20.35	19.67	20.62	19.86	20.93	21.18	20.7	21.04	20.65	20.84	21.31
3058	14-Oct-08 06:12:20	1.61	21.45	0.1237	0.05109	20.37	19.84	20.63	20.05	20.91	21.12	20.65	20.99	20.7	20.97	21.42
3059	14-Oct-08 06:17:20	1.84	21.51	0.142	0.05491	20.37	20.14	20.66	20.31	20.86	21.07	20.59	20.94	20.75	21.1	21.5
3060	14-Oct-08 06:22:20	2.28	21.57	0.1614	0.05895	20.39	20.46	20.68	20.64	20.86	21.03	20.56	20.93	20.86	21.23	21.58
3061	14-Oct-08 06:27:20	1.99	21.66	0.1804	0.06277	20.38	20.69	20.7	20.88	20.9	20.97	20.5	20.88	20.91	21.33	21.62
3062	14-Oct-08 06:32:20	2.09	21.75	0.2006	0.06592	20.46	20.95	20.7	21.15	20.94	20.94	20.46	20.87	21.01	21.47	21.72
3063	14-Oct-08 06:37:20	1.91	21.85	0.2192	0.06921	20.45	21.23	20.76	21.42	21.07	20.91	20.43	20.82	21.05	21.66	21.87
3064	14-Oct-08 06:42:20	2.2	21.97	0.2392	0.07273	20.53	21.49	20.77	21.68	21.16	20.86	20.38	20.79	21.13	21.7	21.88
3065	14-Oct-08 06:47:20	2.29	22.1	0.2593	0.07625	20.6	21.76	20.85	21.93	21.22	20.81	20.34	20.77	21.18	21.7	21.83
3066	14-Oct-08 06:52:20	1.97	22.24	0.2795	0.07873	20.68	22.05	20.89	22.22	21.33	20.83	20.36	20.78	21.23	21.87	21.96
3067	14-Oct-08 06:57:20	1.79	22.38	0.2998	0.08097	20.81	22.42	20.98	22.56	21.28	20.76	20.31	20.75	21.31	22.01	22.08
3068	14-Oct-08 07:02:20	1.65	22.52	0.3218	0.0839	20.89	22.81	21.03	22.95	21.38	20.78	20.37	20.79	21.5	22.29	22.31
3069	14-Oct-08 07:07:20	1.83	22.7	0.3455	0.08644	21.06	23.25	21.19	23.38	21.46	20.77	20.36	20.8	21.61	22.53	22.49
3070	14-Oct-08 07:12:20	1.76	22.88	0.3254	0.08809	21.26	23.43	21.35	23.62	21.55	20.78	20.4	20.83	21.8	22.78	22.75
3071	14-Oct-08 07:17:20	2.21	23.07	0.3812	0.09251	21.51	23.93	21.52	24.14	21.62	20.8	20.44	20.9	22.04	23.04	22.96
3072	14-Oct-08 07:22:20	2.36	23.26	0.3972	0.09438	21.76	24.25	21.77	24.5	21.76	20.81	20.46	20.92	22.16	23.16	23.08
3073	14-Oct-08 07:27:20	2.85	23.45	0.4181	0.0988	22.11	24.46	22.03	24.76	21.89	20.85	20.51	20.96	22.27	23.06	22.97
3074	14-Oct-08 07:32:20	2.35	23.63	0.4358	0.1	22.47	24.9	22.35	25.11	22.02	20.91	20.58	21.03	22.33	23.23	23.03
3075	14-Oct-08 07:37:20	2.83	23.8	0.4573	0.10217	22.92	25.07	22.71	25.3	22.16	20.95	20.65	21.11	22.39	23.18	22.96
3076	14-Oct-08 07:42:20	2.95	23.96	0.4703	0.10502	23.4	25.4	23.17	25.65	22.33	21.02	20.73	21.17	22.5	23.41	23.19
3077	14-Oct-08 07:47:20	3.05	24.11	0.4884	0.10944	23.97	25.84	23.64	26.03	22.5	21.12	20.87	21.3	22.7	23.49	23.21
3078	14-Oct-08 07:52:20	2.55	24.25	0.5095	0.11086	24.63	26.33	24.16	26.52	22.59	21.23	20.98	21.42	22.9	23.8	23.49

(b)

Fig.5.9: Typical data captured a) on 16th September 2007 at the University of Strathclyde and b) on 14th October 2008 at the Malawi Polytechnic.

5.3.5 Mass of saline and distilled water

The mass of water was weighed by using digital top-loading balances (Jadever Scale Ltd balance model JB-6000 at the University of Strathclyde and Ohaus balance model B500A at the Malawi Polytechnic). For saline water, 20 kg of water was initially weighed to establish the level of this mass of cold water in basin 1. This level was marked by a white PVC tape and used on the rest of test days to top up the level of water in the morning using an inlet PVC tube. The level of water was topped up in the morning to maintain the mass of water and reduce the effect of cooling, according to the assumptions of the energy balance equations. In addition, saline water over flowed when approximately 13 kg was loaded into basin 2 or 3. So, these basins were also topped up in the morning using an inlet PVC tube until the water overflowed.

Data on the daily distillate mass was required for calculation of the still efficiency (Yates and Woto, 1988 cited in Smyth et al., 2005). Therefore, hourly production was measured on days with favourable weather conditions while the daily yield was monitored on all test days. To determine the mass of distilled water, a given distillate drain pipe was withdrawn from the corresponding bottle for distillate collection and folded to form a U-tube in order to avoid losing some of the distilled water as the distillation process continued from the still. Then, distilled water collected in any given period of time was transferred from the distillate collecting bottle into an empty pre-weighed 0.5-litre plastic beaker (or 5-litre plastic bottle if the distillate yield exceeded 0.5 litre). The distillate drain pipe was fitted back into the distillate collecting bottle, and the beaker (or bottle) with distilled water was then weighed on a balance to obtain the mass of distilled water. After each weighing, the empty container was placed on the balance that was then tared to prevent mass crossover from the preceding distillate yield. Samples of distilled water were analysed to establish the quality of the distillate.

5.3.6 Water quality

The quality of water was not monitored at the University of Strathclyde because tap water was used and tests were initially aimed at assessing the thermal performance of the stills before they were shipped to the Malawi Polytechnic. At the latter site, tap water was again employed for assessing the thermal performance of the stills. To establish the quality of solar-distilled water, batches of saline water from a local borehole were collected in dry pre-cleaned 25-litre plastic bottles according to (BSI, 2007b). These bottles were sealed as recommended by BSI (1999a,b; 2007b), and a laboratory water sample of 1.0 litre was taken from each batch and analyzed for electrical conductivity (EC), total dissolved solids (TDS) and pH as indicators of water quality (Samee et al., 2007).

The EC and TDS were concurrently measured by using a Jenway CE/TDS meter (model 470). The meter was prepared according to the manufacturer's instructions and guidelines given by BSI (1999a). For saline water, duplicate water samples from each batch were measured for CE and TDS at 298 K. It should be mentioned that the temperature of water ranged from 301 to 306 K when laboratory samples were taken from a given batch. So, the samples (in sealed plastic bottles) were cooled in a KIC refrigerator (model 010ETF33) and then readings of CE and TDS were taken when the temperature of water was 298 K. An average value was then calculated for each batch. Similarly, the pH of duplicate samples of saline water was measured by using an Orion Research digital pH meter (model 601A) at 298 K (BSI, 1999b), and an average value was computed for a given batch. All these measurements on the quality of a particular batch of water were done on the same day when the batch was distilled. For distilled water, duplicate water samples were again taken from each batch and measured for CE, TDS and pH at 298 K using similar procedures applied to the saline water, and experimental results are reported in Chapter 7.

5.4 Summary

Standard methods of testing some solar thermal systems such as liquid and air heaters are available. However, there is lack of standard methods for evaluating the performance of solar stills. In view of this, solar stills are evaluated using standard methods and procedures developed for other solar thermal systems. A similar approach was adopted to collect empirical data in the present investigation. Standard sensors and guidelines were employed to capture accurate data for model verification and evaluation of the empirical performance of conventional and advanced solar stills. Results obtained from this experimental process are given and discussed in Chapters 6 and 7.

5.5 References

ASHRAE, 2003. *ASHRAE/ANSI standard 93-2003: Methods of testing to determine the thermal performance of solar collectors*. Atlanta: American Society of Heating, Refrigerating and Air-conditioning Engineers.

BSI, 1999a. *BS EN 27888:1993: Water quality – method for the determination of electrical conductivity.* London: British Standards Institution.

BSI, 1999b. *BS 6068 – 2.50:1995: Water quality – part 2: Physical, chemical and biochemical methods – Section 2.50 Determination of pH*. London: British Standards Institution.

BSI, 2006. *BS EN 12975 – 2:2006: Thermal solar systems and components – solar collectors – part 2: Test methods*. London: British Standards Institution.

BSI, 2007a. *BS ISO 9459-5:2007: Solar heating – solar water heating systems – Part 5: System performance characterization by means of whole-system tests and computer simulation*. London: British Standards Institution.

BSI, 2007b. *BS EN 15216:2007: Characterization of waste – determination of total dissolved solids in water and eluates.* London: British Standards Institution.

Cooper, P.I., 1973. The maximum efficiency of single-effect solar stills. *Solar Energy*, 15, pp.205-217.

Duffie, J.A. and Beckman, W.A., 2006. *Solar Engineering of Thermal Processes*. 3rd ed. New York: John Wiley & Sons Inc., 290-309.

El-Bahi, A. and Inan, D., 1999. Analysis of a parallel double glass solar still with separate condenser. *Renewable Energy*, 17, pp.509-521.

Kipp & Zonen, 2004. *Instruction Manual: CM 121 shadow ring*. Delft: Kipp & Zonen.

Nafey, A.S., Abdelkader, M., Abdelmotalip, A. and Mabrouk, A.A., 2000. Parameters affecting solar still productivity. *Energy Conversion and Management*, 41, pp.1797-1809.

Oliphant, M.V., 1980. Measurement of wind speed distributions across a solar collector. *Solar Energy*, 24, pp.403-405.

Saluja, G.S. and Douglas, N.G., 1996. Verification of wind resource study in a Scottish region. *Renewable Energy*, 9, pp.798-801.

Samee, M.A., Mirza, U.K., Majeed, T. and Ahmad, N., 2007. Design and performance of a simple solar still. *Renewable and Sustainable Energy Reviews*, 11, pp.543-549.

Smyth, M., Norton, B. and Byres, W., 2005. Measured effect of reflector augmentation of simple basin type solar stills. *Ambient Energy*, 26, pp.59-70.

Thekaekara, M.P., 1976. Solar radiation measurement: Techniques and instrumentation. *Solar Energy*, 18, pp.309-325.

Tiwari, G.N., Singh, H.N. and Tripathi, R., 2003. Present status of solar distillation. *Solar Energy*, 75, pp.367-373.

Wisse, J.A. and Stigter, K., 2007. Wind engineering in Africa. *Wind Engineering and Industrial Aerodynamics*, 95, pp.908-927.

WMO, 2003. *Manual on the global observation system*. vol.1, 2003 ed. Geneva: World Meteorological Organization.

Yates, R. and Woto, T., 1988. *Small scale desalination for areas of Botswana*. Ottawa: International Development Centre.

Chapter 6

Results for model verification

6.0 Introduction

The aim of this investigation was to develop a solar still with improved distillate output. To achieve this, the first objective was to formulate a suitable computational tool to appraise different configurations of solar stills. Thus, conventional and advanced stills were simulated under the same weather conditions. Simulation results showed that an advanced solar still yielded 28 % more distilled water per unit area of basin 1 than a conventional distillation system under the same prevailing meteorological conditions. The model was calibrated using data reported by Tripathi and Tiwari (2004). There was close agreement between simulated and experimental distillate yield. In view of this, a sensitivity analysis was performed to study the effect of design and operation parameters on distillate output. Based on this theoretical analysis, prototype stills were designed, constructed and tested at the University of Strathclyde and Malawi Polytechnic as reported in Chapters 4 and 5. Empirical data was collected on the prevailing meteorological conditions and distillate yield during the test. This data base was used to verify the performance of the proposed model and empirical thermal performance of the test stills.

The performance of solar stills is influenced by design, operating and environmental factors. So, these factors have to be taken into account in system modelling. Fundamental concepts that govern the solar distillation process have been described in Chapter 2, and design and operating conditions have been presented in Chapter 3. Chapters 4 and 5 focus on experimental procedures used to acquire valid data for model verification. In this chapter, empirical data on meteorological conditions and distillate yield for model verification are reported. For a given set of design and operating conditions, the performance of the two solar stills was predicted from the levels of irradiance, ambient air temperature and wind speed. Previous and present models for computation of solar distribution in a single slope solar still are inter-compared, and theoretical and experimental results are presented and discussed in this chapter.

6.1. Meteorological conditions

Figs.6.1 (a) and (b) show the variation of weather conditions on typical dates of 17th October 2007 at the University of Strathclyde and 14th October 2008 at the Malawi Polytechnic. These days were chosen to demonstrate the extent of variation in the magnitudes of irradiation, ambient air temperature and surface wind speed on a given day. For the weather at the University of Strathclyde, it is observed that beam irradiance was higher than diffuse irradiance during the most part of the day. Irradiance was intermittent especially around solar noon but the observed levels are satisfactory for a site at high altitude in the northern hemisphere during the month of October. The daily insolation was 2.0 to 12.1×10^6 J m^{-2}, with some overcast days during the test period at this location. At the Malawi Polytechnic, it is also seen that beam irradiance was higher than diffuse irradiance during the most part of the day. Irradiance was significantly intermittent after solar noon due to partly-cloudy weather conditions on this day but the observed levels were still satisfactory for solar distillation. The daily insolation was 14.2 to 25×10^6 J m^{-2} during the corresponding test period. It should be mentioned that solar radiation is the most influential environmental parameter in distillate productivity (Nafey et al., 2000). So, distillate production would be higher at the latter test site.

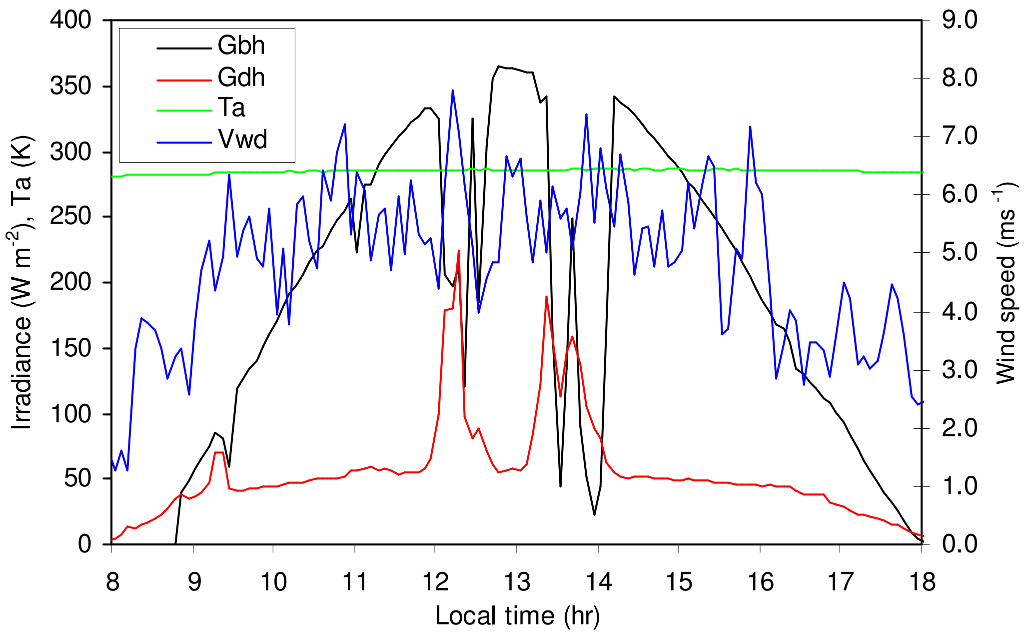

(a)

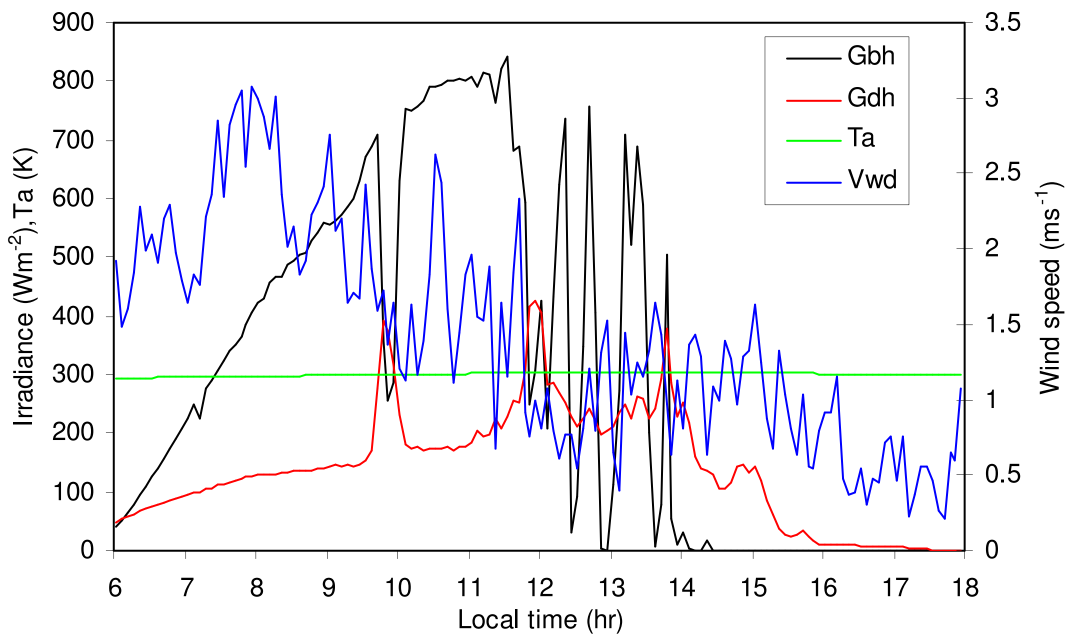

(b)

Fig.6.1: Variation of beam (G_{bh}) and diffuse (G_{dh}) irradiance on a horizontal surface, ambient air temperature (T_a) and wind speed (V_{wd}) with local time on a) 17th October 2007 at the University of Strathclyde and b) 14th October 2008 at the Malawi Polytechnic.

At the University of Strathclyde, it is seen that ambient air temperature was relatively low, varying between 279 and 288 K during the test period. On daily basis, the range of average air temperature was 280 to 287 K at this site. In contrast, ambient air temperature was relatively high at the Malawi Polytechnic, varying between 294 and 305 K. The average daily air temperatures were within 291 to 299 K at this site. Distillate production tends to increase with ambient air temperature (Cooper, 1969; Nafey et al., 2000). Thus, distillate yield would be lower at the University of Strathclyde than Malawi Polytechnic.

At the University of Strathclyde, wind speed (V_{wd}) varied between 0.2 to 7.8 ms^{-1}, and it exceeded 4.0 ms^{-1} from 9:00hrs to 16:00hrs. On other test days, values of $V_{wd} > 10$ ms^{-1} were recorded during certain times. The average daily wind speeds were 0.8 to 6.8 ms^{-1}. At the Malawi Polytechnic, V_{wd} varied between 0.21 to 3.07 ms^{-1}, and it did not exceed 3.10 ms^{-1} throughout the day. On all test days, values of $V_{wd} < 4$ ms^{-1} were recorded. The average daily wind speeds were 0.5 to 1.7 ms^{-1}. These observations are consistent with previous work (Saluja and Douglas, 1996; Wisse and Stigter, 2007; Sinden, 2007). El-Sebaii (2004) found that still productivity decreased with increasing V_{wd} until a typical value was reached, for water masses (m_{wl}) less than 45 kgm^{-2}. Distillate production would be adversely affected by the levels of wind speed because m_{wl}=28 kgm^{-2} in the present study. Average meteorological conditions are presented in Table 6.1. It is seen that the average values of weather variables were less favourable for distillate production at the University of Strathclyde than the Malawi Polytechnic.

Table 6.1: Average daily horizontal global insolation, ambient air temperature and wind speed over the test periods at the University of Strathclyde and Malawi Polytechnic.

Site	Number of days	Insolation ($x10^6$ J m^{-2})	Air temperature (K)	Wind speed (m s^{-1})
University of Strathclyde	22	6.733	284	3.10
Malawi Polytechnic	18	19.889	297	0.93

6.2 Distribution of solar radiation inside a solar still

Solar energy intercepted by a solar still drives the heat and mass processes in the still. Therefore, it is necessary to know its distribution inside the evaporator chamber of the still. In this section, the distribution of solar radiation inside the CSS and ASS is computed using the new model which takes into account the fundamental characteristics of solar radiation and optical view factors of surfaces that exchange radiation.

6.2.1 Directly and indirectly received solar radiation

Solar energy reaches the surface of saline water in the evaporator chamber directly and indirectly (from the walls and external reflector of a solar still). This energy comprises beam and diffuse components in varying proportions. Fig.6.2 shows profiles of beam (G_b) and diffuse (G_d) irradiance directly and indirectly arriving at the still base on a typical date at the University of Strathclyde. The curves for $G_{b,css}$ and $G_{b,Ass}$ coincided with each other. Consequently, one line was plotted for both data sets. This observation shows that there is no significant difference in the beam irradiance ($G_{b,di}$) directly intercepted by saline water in basin 1 of the CSS and ASS throughout the day, attributed to the geometry of the evaporator chambers. These chambers had the same geometry for both stills for meaningful performance comparison of the two distillation systems. Consequently, saline water in the evaporator chambers would directly receive the same amount of beam radiation. In contrast, saline water in the CSS directly received more diffuse solar radiation ($G_{d,di}$) than that in basin 1 of the ASS, due to the influence of view factors. The surface of saline water in the CSS views a higher proportion of the sky ($W_{w1\text{-}sk}$=0.53) than that ($W_{w1\text{-}sk}$=0.39) viewed by saline water in the ASS. A lower proportion of the sky is viewed by the water surface in the ASS probably because of the external condenser unit which protrudes above the evaporator chamber. This unit increases the proportion of sky obstruction. These results indicate that the CSS directly captured more global solar radiation ($G_{g,di}$) than the ASS.

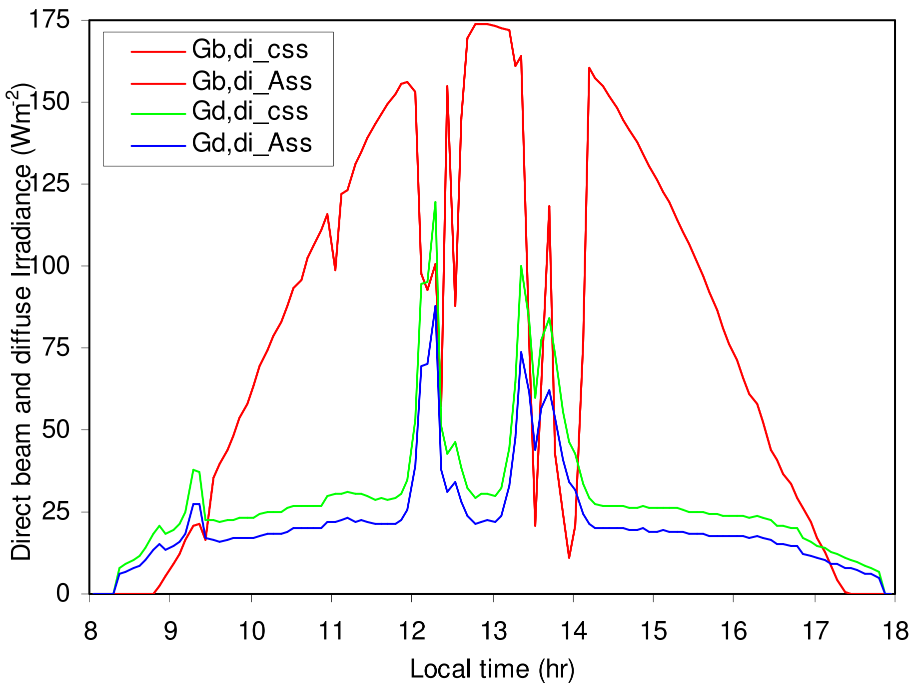

(a)

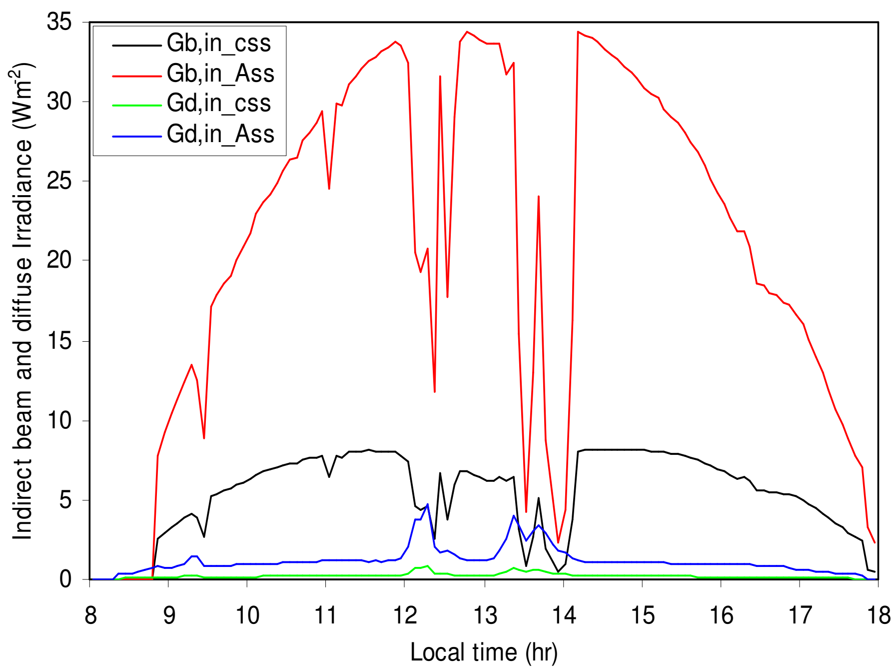

(b)

Fig.6.2: Variation of computed values of beam (G_b) and diffuse (G_d) irradiance a) directly and b) indirectlyintercepted by the still bases of the CSS and ASS on 17th October 2007 at the University of Strathclyde.

Indirectly, the CSS intercepted significantly less beam solar energy ($G_{b,in}$) than the ASS probably due to the external reflector in the ASS. This reflector was not obstructed from beam radiation. So, it received a relatively higher proportion of the beam radiation. The CSS also indirectly intercepted a lower level of diffuse irradiance ($G_{d,in}$), ascribed to the influence of view factors. Walls have a lower value ($W_{ew-sk}= W_{ww-sk}=0.14$) of view factors relative to the sky than that ($W_{er-sk}= 0.50$) of the external reflector. It is inferred that the CSS indirectly captured less global irradiance ($G_{g,in}$) than the ASS.

Fig.6.3 shows the variation of beam and diffuse irradiance directly and indirectly intercepted by the still base on a typical date at the Malawi Polytechnic. It is observed that saline water in the CSS directly captured a slightly higher proportion of beam radiation than the ASS before 08:00 hr, with no difference thereafter. This is attributed to the effect of shading by the condenser of the ASS when the sun is behind the solar stills. At this site the sun is in front of the solar stills when $|\gamma_s| > 90^o$, (inequality signs in Eq.(3.4) are reversed for a north-facing surface). It was found that $|\gamma_s| > 90^o$ from 08:00 to 16:00 hr. So, the sun was behind the stills before 08:00 hr and after 16:00 hr. This difference between G_{b,di_css} and G_{b,di_Ass} is not noticeable in the afternoon because it was cloudy with $G_{bh}=0$ from about 14:30 hr to sunset. Tanaka and Nakatake (2006) also reported obstruction of the sun's rays by the back wall and external reflector of a basin type solar still in the morning and evening during certain months of the year. Saline water in the CSS directly received more diffuse solar radiation than that in basin 1 of the ASS. These results indicate that the CSS directly received a higher level of solar radiation than the ASS at both the University of Strathclyde and Malawi Polytechnic.

Indirectly, the CSS intercepted less beam solar energy than the ASS during the most part of a typical date at the Malawi Polytechnic, for the same reasons applicable to the observations made at the University of Strathclyde. Saline water in the CSS also indirectly received a lower level of diffuse radiation than the ASS, ascribed to the influence of view factors. This indicates that the CSS indirectly captured less solar radiation than the ASS. It should be noted that the total irradiance inside a solar still depends on the solar energy received by both direct and indirect optical paths.

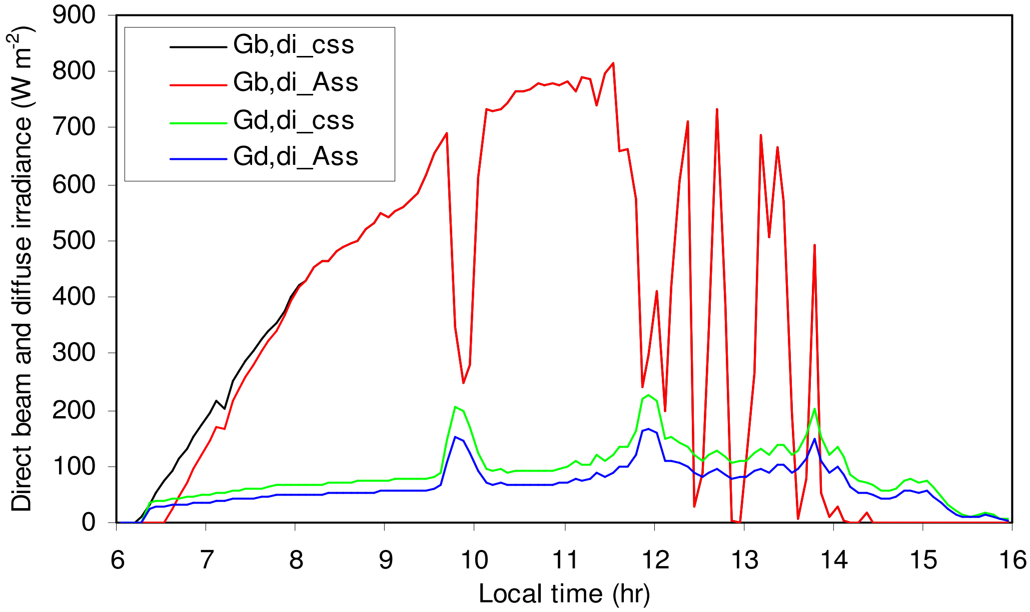

(a)

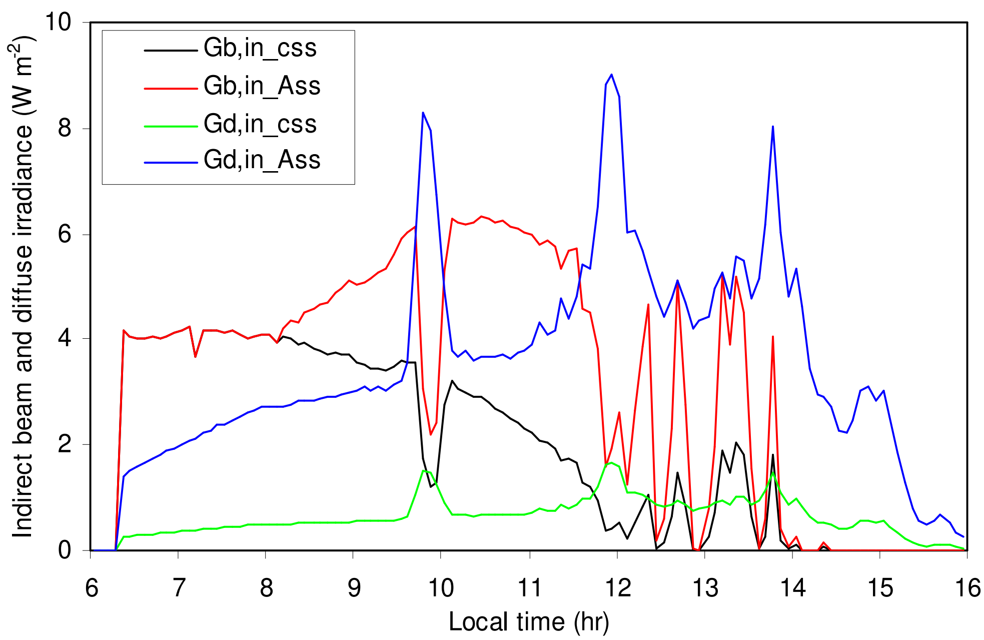

(b)

Fig.6.3: Variation of computed values of beam (G_b) and diffuse (G_d) irradiance a) directly and b) indirectly intercepted by the still bases of the CSS and ASS on 14th October 2008 at the Malawi Polytechnic.

Fig. 6.4 shows the variation of global solar radiation directly and indirectly intercepted by saline water in the evaporator chambers of the CSS and ASS at the University of Strathclyde. It is observed that the CSS directly intercepted more solar energy than the ASS, commensurate with the levels of beam and diffuse solar radiation directly intercepted by each still.

Indirectly, the CSS intercepted a lower level of global solar energy than the ASS during most of the day at the University of Strathclyde, commensurate with the levels of indirectly captured beam and diffuse radiation. This shows that saline water in the evaporator basin of the CSS indirectly captured less global radiation than the ASS.

Fig. 6.5 shows the variation of directly and indirectly received global solar radiation inside the CSS and ASS on a typical day at the Malawi Polytechnic. It is again observed that the CSS directly intercepted more global radiation than the ASS, commensurate with the levels of beam and diffuse solar radiation directly intercepted by an individual still.

Indirectly, the CSS intercepted a smaller amount of global solar energy than the ASS during most of the day at the Malawi Polytechnic, commensurate with the levels of indirectly captured beam and diffuse radiation. Global irradiance was integrated to obtain the daily insolation that was directly ($H_{g,di}$) and indirectly ($H_{g,in}$) captured at each site.

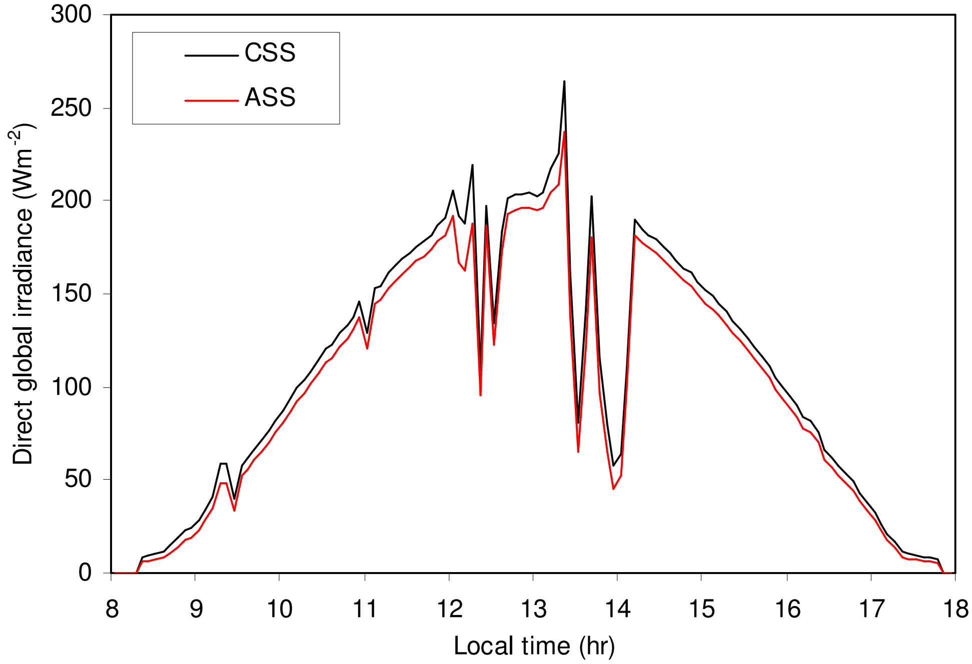

(a)

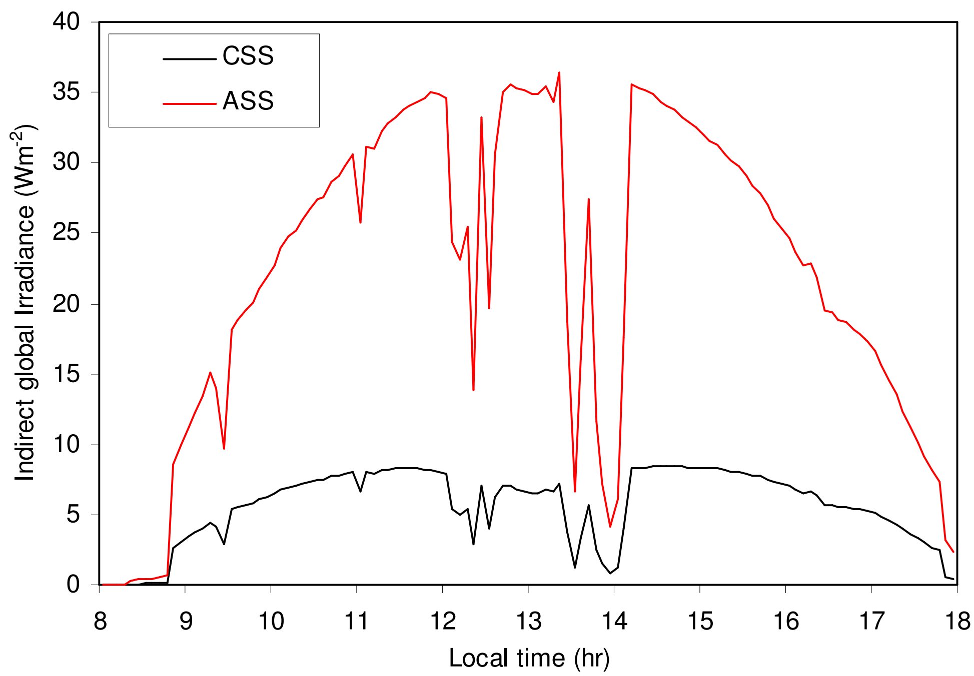

(b)

Fig.6.4: Variation of computed values of solar power a) directly and b) indirectly reaching the surface of saline water in basin 1 the CSS and ASS on 17th October 2007 at the University of Strathclyde.

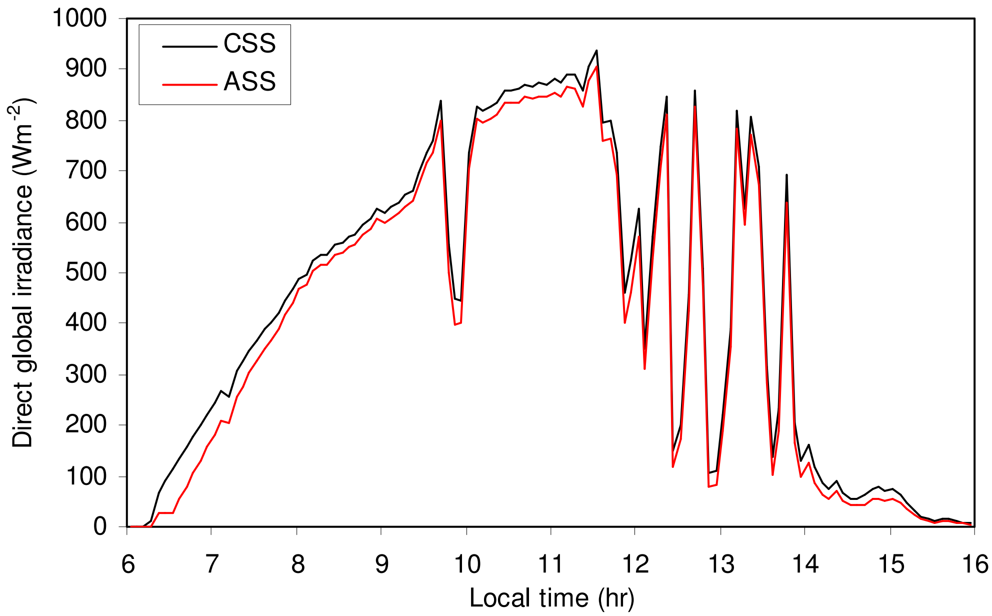

(a)

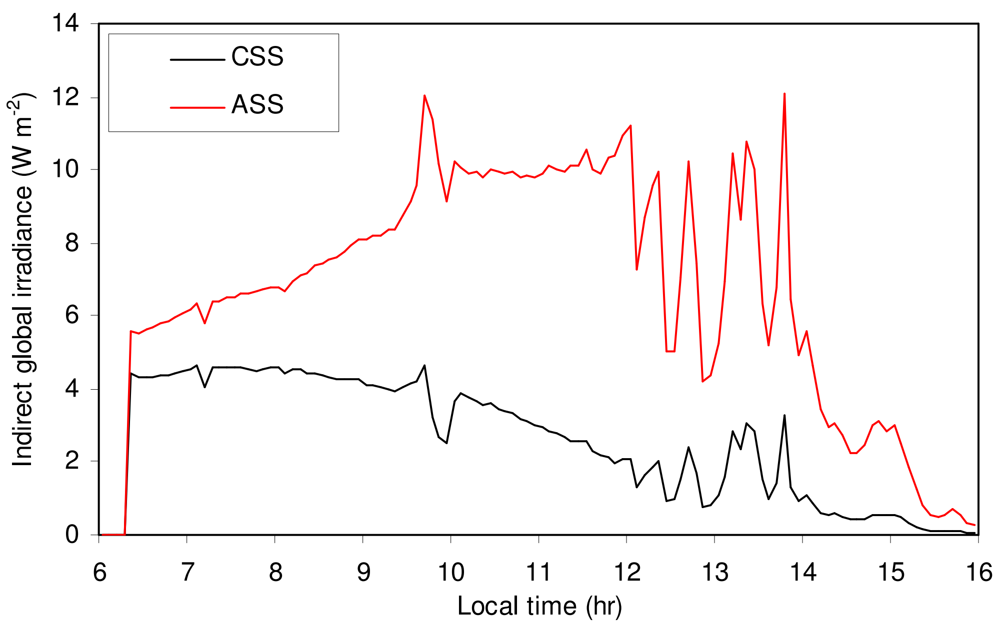

(b)

Fig.6.5: Variation of computed values of global radiation a) directly and b) indirectly reaching the surface of saline water in basin 1 of the CSS and ASS on 14th October 2008 at the Malawi Polytechnic.

On daily basis, the variation of $H_{g,di}$ and $H_{g,in}$ with test day at the University of Strathclyde are shown in Fig.6.6. It is observed that saline water in the CSS directly received more solar energy than that in the ASS on all test days, as expected. On the average, saline water in the evaporator basins of the CSS and ASS directly received 98 and 89 % respectively of the total intercepted energy ($H_{g,ef}$).

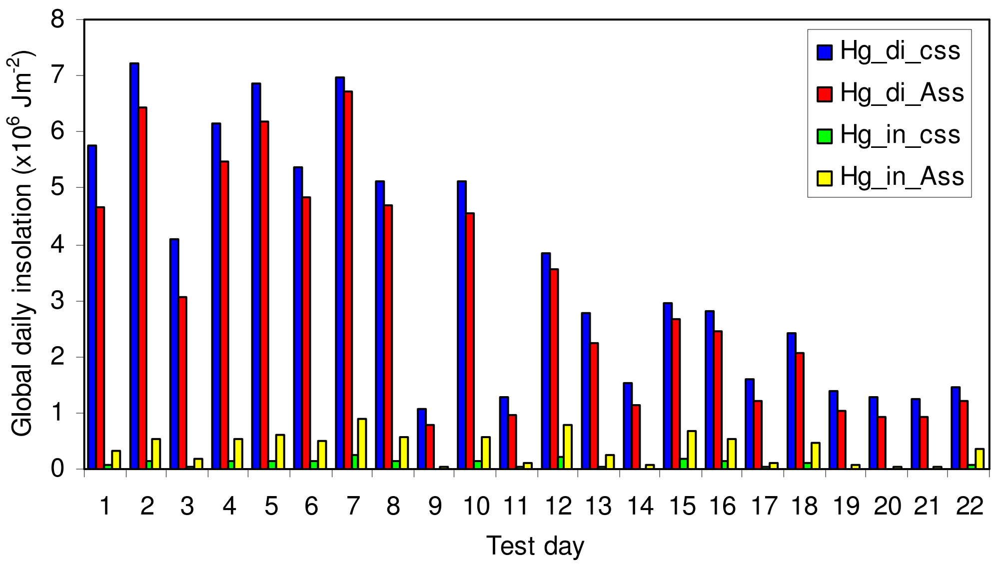

Fig. 6.6: Computed values of daily global solar radiation directly ($H_{g,di}$) and indirectly ($H_{g,in}$) intercepted by saline water in basin1 of the CSS and ASS at the University of Strathclyde.

Indirectly, the CSS captured less global radiation than the ASS on all test days. This is expected because the ASS has an external reflector which augments solar energy reaching the surface of saline water (Tiwari et al, 2003). On the average, the walls of the CSS contributed 2 % of $H_{g,ef}$ while the contributions from the walls and external reflector of the ASS were respectively 2 % and 9 %. It should be noted that the fraction of solar contribution from walls is the same for both stills, consistent with the geometry of the evaporator chambers of the two solar stills (when the sun is in front of the systems during most of the day). The external reflector of the ASS contributed a higher proportion of solar energy to the water than the walls. This reflector receives a high proportion of both beam and diffuse radiation when the sun is in front of the systems because it is not blocked from the sun's rays by other components of the system, with a relatively high view factor of the sky ($W_{er\text{-}sk}$=0.50). Nevertheless, beam radiation is unable to reach the back wall and external reflector when the sun is behind the systems.

Fig. 6.7 shows the variation of $H_{g,di}$ and $H_{g,in}$ with test day at the Malawi Polytechnic. It is again seen that saline water in the CSS directly received more solar energy than that in the ASS on all test days for similar reasons applicable to the observations made at the University of Strathclyde. On the average, the CSS and ASS directly captured 99 and 98 % respectively of $H_{g,ef}$. It is inferred that the CSS directly captured a higher level of solar energy than the ASS (H_{g,di_css}>H_{g,di_Ass}) at both test locations.

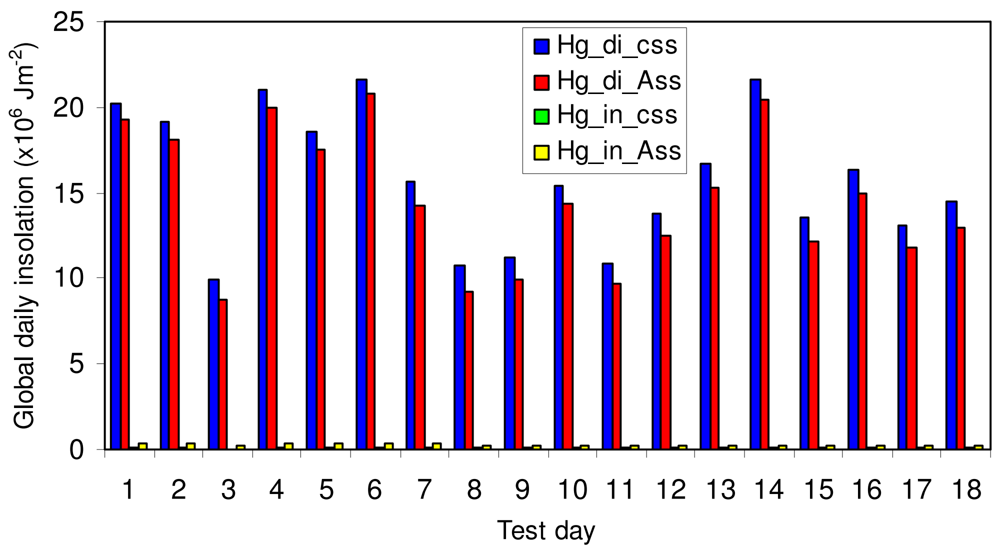

Fig 6.7: Computed values of daily global solar radiation directly ($H_{g,di}$) and indirectly ($H_{g,in}$) intercepted by saline water in basin 1of the CSS and ASS at the Malawi Polytechnic.

Indirectly, the CSS contributed a smaller amount of solar energy than the ASS on all test days. This observation is again ascribed to the influence of the external reflector in the ASS. On the average, the CSS and ASS indirectly contributed 1 and 2 % respectively of the total solar energy that reached the surface of water. The average daily contributions of solar energy reflected from the walls (1 %) and external reflector (1 %)

of the PSS were the same. This indicates that the effect of the external reflector was less significant (1 %) at the Malawi Polytechnic than (9 %) at the University of Strathclyde, probably due to astronomical influence. During the test period, solar altitudes were relatively low ($\psi \approx 18$ to 36^o at solar noon) at the University of Strathclyde compared to those ($\psi \approx 79$ to 85^o at solar noon) at the Malawi Polytechnic. So, the walls and external reflector received a higher proportion of beam radiation at the University of Strathclyde than at the latter location. It is inferred that that the CSS indirectly received less solar energy than the ASS ($H_{g,in\text{-}css} < H_{g,in\text{-}Ass}$) at both test locations. Solar energy received directly and indirectly was used to compute effective irradiance inside the stills.

6.2.2 Effective irradiance

Fig.6.8 shows the variation of effective global irradiance ($G_{g,ef}$) inside the CSS and ASS, and observed irradiance (G_{gh}) on a typical date at the University of Strathclyde. These results show that effective irradiance is lower in the CSS than the ASS probably because of the additional solar energy reflected from the external reflector onto the surface of saline water in the evaporator basin, consistent with findings from previous work (Anderson, 1983; Tanaka and Nakatake, 2007). It is also seen that effective irradiance is less than the observed irradiance on a horizontal surface for both stills, which indicates that the use of horizontal global solar radiation (G_{gh}) in the energy balance equations would lead to erroneous estimation of distillate production.

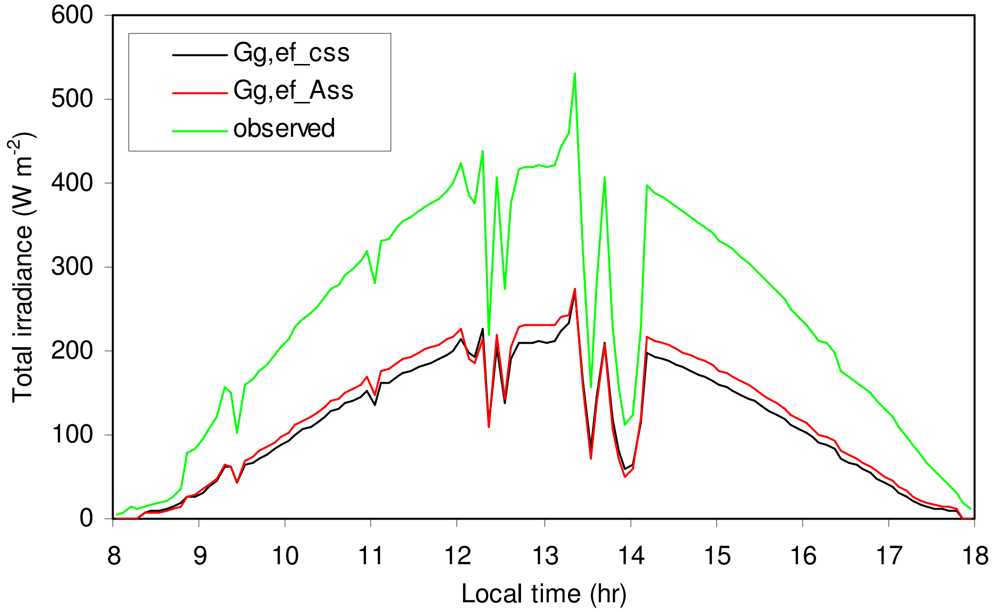

Fig.6.8: Variation of computed values of the total effective ($G_{g,ef}$) irradiance inside the CSS and ASS, and observed values of irradiance(G_{gh}) on 17th October 2007 at the University of Strathclyde.

Fig.6.9 shows the variation of effective global irradiance ($G_{g,ef}$) inside the CSS and ASS, and observed irradiance (G_{gh}) on a typical date at the Malawi Polytechnic. It is seen that effective irradiance is higher in the CSS than the ASS probably due to the influence of solar altitude as discussed in Section 6.2.1. In addition, effective irradiance is less than the observed irradiance on a horizontal surface for both stills, similar to results obtained at the University of Strathclyde.

On daily basis, the values of global effective radiation ($H_{g,fe}$) at the University of Strathclyde are shown in Table 6.2. It is observed that saline water in the CSS effectively received more solar radiation than that in the ASS ($H_{g,ef\text{-}css}$- $H_{g,ef\text{-}Ass}$ >0) on most days, except on days when the diffuse ratio (H_{dh}/H_{gh}) was relatively low. It should be noted that the ASS intercepted more solar energy than the CSS when ($H_{g,ef\text{-}css}$ <$H_{g,ef\text{-}Ass}$). In terms of solar energy received directly and indirectly, this condition can be expressed as:

$$H_{g,di\text{-}css} - H_{g,di\text{-}Ass} < H_{g,in\text{-}Ass} - H_{g,in\text{-}css} \tag{6.1}$$

where $H_{g,in} = H_{b,in}+H_{d,in}$ and $H_{g,di}=H_{b,di}+H_{d,di}$.

Nevertheless, saline water in basin 1 of the CSS views a higher proportion of the sky than that in the ASS. So, it directly receives more diffuse radiation than saline water in basin 1 of the ASS, and the difference on the left hand side of inequality (6.1) increases with the level of diffuse radiation.

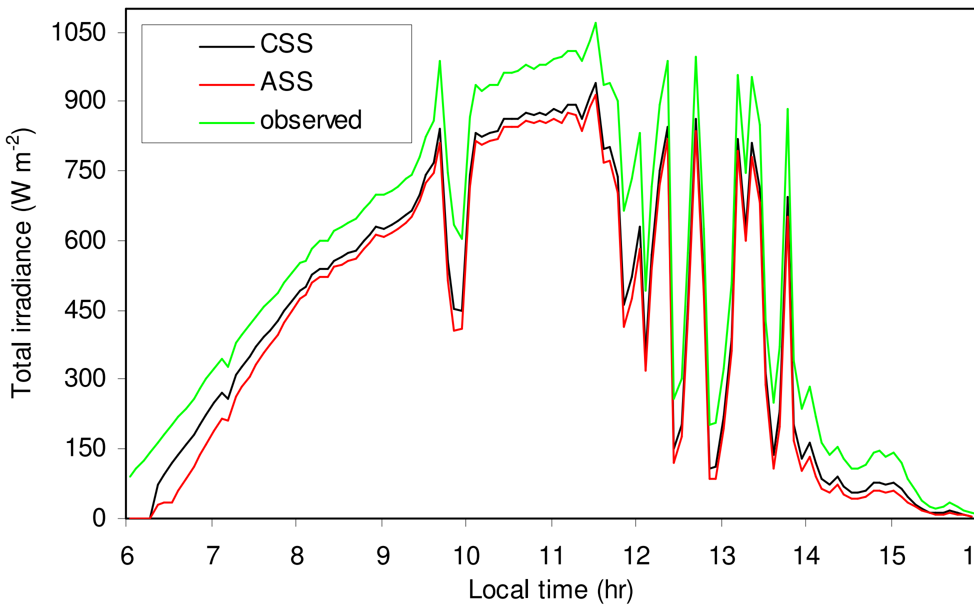

Fig.6.9: Variation of computed values of total effective irradiance in the CSS and ASS, and observed values of irradiance at the MalawiPolytechnic on 14th October 2008.

Indirectly, saline water in the evaporator basin of the CSS captured less beam radiation ($H_{b,in}$) and diffuse ($H_{d,in}$) radiation than that in the ASS. It should also be noted that $H_{b,in}$ increases with decreasing solar altitude (Eq.2.20). At the site under discussion, solar altitudes were relatively low ($\psi \approx 18\text{-}36^{o}$ at solar noon) during the test period which was conducive for indirect capturing of beam radiation. In addition, the daily diffuse fraction was relatively high on most days which favoured direct solar capturing by the CSS. So, the difference on the right hand side of inequality (6.1) was relatively high while the difference on the left hand was low on clear days. On days with high diffuse fraction, there was an opposite effect on solar interception. This accounts for the observed trend of the optical performance of the systems at the University of Strathclyde. On the average, the CSS and ASS effectively captured 54 and 51 % of the daily insolation on a horizontal plane respectively, and the CSS collected 5 % more solar energy than the ASS.

Table 6.2: Daily effective global solar radiation ($H_{g,ef}$) intercepted by saline water in basin 1 of the CSS and ASS at the University of Strathclyde.

Test day	H_{gh} ($x10^6Jm^{-2}$)	H_{dh}/H_{gh}	$H_{g,ef}$ ($x10^6Jm^{-2}$)		$H_{g,ef\text{-}css}$- $H_{g,ef\text{-}Ass}$ ($x10^6Jm^{-2}$)
			CSS	ASS	
1	10.242	0.77	5.831	4.971	0.861
2	11.903	0.46	7.345	6.989	0.356
3	7.669	0.95	4.105	3.247	0.858
4	10.652	0.46	6.280	6.012	0.268
5	11.717	0.40	7.003	6.824	0.179
6	9.282	0.41	5.479	5.323	0.156
7	12.097	0.13	7.188	7.638	-0.450*
8	9.182	0.35	5.270	5.241	0.029
9	2.016	1.00	1.076	0.829	0.247
10	9.393	0.43	5.242	5.095	0.147
11	2.520	0.85	1.289	1.065	0.224
12	8.591	0.23	4.037	4.345	-0.309*
13	5.450	0.68	2.813	2.493	0.320
14	2.936	0.95	1.541	1.216	0.324
15	7.211	0.29	3.105	3.334	-0.229*
16	6.595	0.37	2.931	3.018	-0.087*
17	3.162	0.93	1.635	1.299	0.336
18	5.912	0.45	2.536	2.534	0.001
19	2.751	0.97	1.417	1.105	0.312
20	2.448	1.00	1.278	0.985	0.293
21	2.421	1.00	1.265	0.974	0.291
22	3.981	0.47	1.552	1.561	-0.010*
Mean	6.733	0.62	3.646	3.459	0.187

*Optical performance of the ASS was higher than that of the CSS.

On daily basis, the values of effective global radiation ($H_{g,fe}$) at the Malawi Polytechnic are shown in Table 6.3. At this site, saline water in basin 1 of the CSS effectively received a larger amount of solar energy than that in the ASS on all test days. The CSS directly intercepted more solar energy than the ASS ($H_{g,di\text{-}css}$>$H_{g,di\text{-}Ass}$), similar to the results found at the University of Strathclyde. So, the observed trend in $H_{g,ef}$ is again possibly due to the levels of solar energy received indirectly. On the average, the CSS and ASS effectively intercepted 80 and 75 % of the daily insolation respectively, and the CSS collected 7 % more solar energy than the ASS.

Table 6.3: Daily effective global solar radiation ($H_{g,ef}$) intercepted by saline water in basin 1 of the CSS and ASS at the Malawi Polytechnic.

Test day	H_{gh} ($x10^6 Jm^{-2}$)	H_{dh}/H_{gh}	$H_{g,ef}$ ($x10^6 Jm^{-2}$)		$H_{g,ef\text{-}css}$- $H_{g,ef\text{-}Ass}$ ($x10^6 Jm^{-2}$)
			CSS	ASS	
1	23.948	0.25	20.315	19.632	0.683
2	23.171	0.30	19.230	18.423	0.806
3	14.199	0.59	10.001	9.015	0.985
4	24.927	0.26	21.146	20.350	0.796
5	22.322	0.29	18.648	17.818	0.830
6	25.013	0.21	21.768	21.051	0.717
7	20.895	0.49	15.758	14.525	1.232
8	16.148	0.68	10.799	9.494	1.306
9	15.719	0.56	11.298	10.129	1.169
10	18.975	0.32	15.569	14.637	0.932
11	14.726	0.49	10.970	9.960	1.010
12	17.924	0.44	13.889	12.751	1.139
13	21.370	0.40	16.854	15.583	1.272
14	24.979	0.22	21.737	20.715	1.022
15	17.871	0.44	13.698	12.426	1.271
16	20.353	0.34	16.486	15.240	1.247
17	16.643	0.39	13.123	11.994	1.129
18	18.822	0.42	14.595	13.246	1.349
Mean	19.889	0.40	15.882	14.833	1.050

Indirectly, the ASS captured more beam radiation ($H_{b,in}$) and diffuse ($H_{d,in}$) radiation than the CSS at the Malawi Polytechnic. Nevertheless, solar altitudes were relatively high ($\psi \approx 79$ to 85^o at solar noon) during the test period at this site which suppressed indirect capturing of beam radiation. Consequently, both solar stills indirectly intercepted relatively small amounts of solar energy in spite of the high levels of irradiance measured outside the stills. This might have resulted in relatively low values of the difference on the right hand side of inequality (6.1), and suppression of the effect of diffuse levels on the left hand side of this inequality. Thus, the CSS captured more solar energy than the ASS on all days at the Malawi Polytechnic. Tripathi and Tiwari (2004) found that solar contribution from a wall was significant at low solar altitude. So, findings at both the University of Strathclyde and Malawi Polytechnic are consistent with previous work.

6.3 Model performance

6.3.1 Effective irradiance

Figs.6.10 (a) and (b) show the levels of effective irradiance estimated by the previous and new models from the irradiance data that was captured on a horizontal plane at the University of Strathclyde. For the CSS, it is observed that both previous models yield slightly higher effective irradiance than the present model at low solar altitude (in the morning and afternoon). At relatively high solar altitudes, the model suggested by Tripathi and Tiwari (2004) still yields the largest estimates of effective irradiance. The disagreement amongst these models is possibly due to variations in the assumptions about the optical properties of solar radiation. In the model proposed by Tripathi and Tiwari (2004), all incoming solar radiation is treated as beam radiation and a given wall is assumed to view 100 % of the saline water surface when calculating radiation exchange between the two surfaces. In the model proposed by Tanaka and Nakatake (2006), global radiation is split into beam and diffuse radiation but view factors and the proportion of diffuse radiation intercepted by a given wall are not taken into consideration. They assumed that the saline water surface views 100 % of the sky and a reflecting surface (a wall or an external reflector) also views 100 % of the saline water surface. Nevertheless, it is known that global radiation comprises beam and diffuse components that have different characteristics, and that optical view factors also influence radiation exchange between two surfaces (Duffie and Beckman, 2006; Incropera et al., 2007). Moreover, the walls reflect part of the intercepted diffuse radiation onto the surface of saline water. In the previous investigations, a wall reflected ρ_{wa} of the available solar energy onto the surface of water while it effectively reflect ($\rho_{wa}W_{wa\text{-}wl}$) of the intercepted solar energy in the new model. For instance, ρ_{bw} =0.05 and $W_{bw\text{-}wl}$= 0.29 in the present investigation. In this case, the back wall reflects 5 % of the intercepted solar radiation in the previous model but it effectively reflects 1.45 % in the new model. This indicates that previous models would overestimate radiation exchange between the two surfaces. It should also be noted that the water surface and walls view part of the sky as shown in Table 3.1. A given surface can view 100 % of the sky if it is horizontal and not obstructed. In a practical basin-type solar still, the water surface is horizontal but it is shaded by the walls of the still. Moreover, these walls are vertical and shade each other. So, each surface of saline water and walls directly receives less than 100 % of the diffuse irradiance measured on a horizontal surface. It is also seen that the effective irradiance is lower than the observed levels during the most part of the day, probably due to attenuation of solar radiation before it actually reaches the surface of saline water.

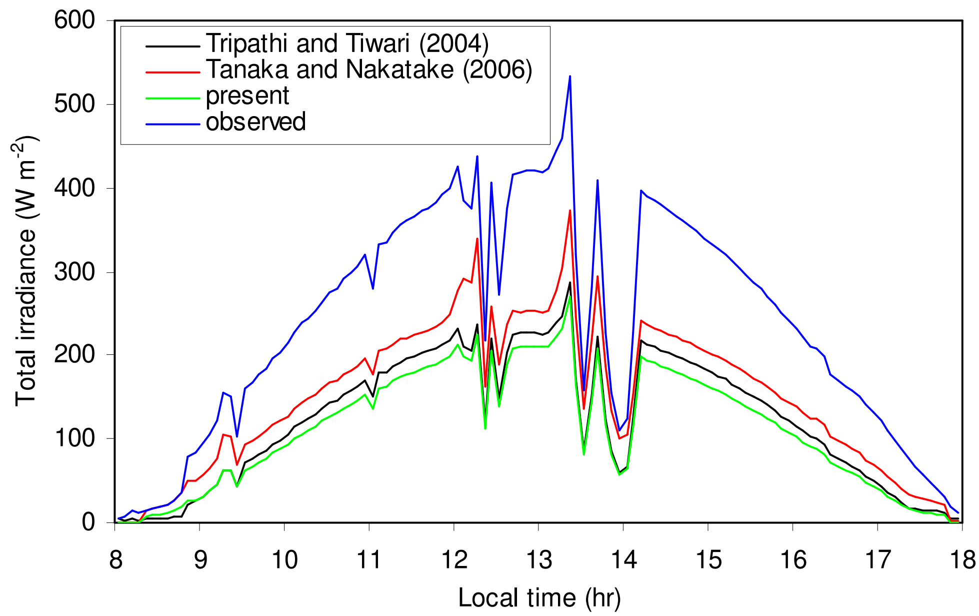

(a)

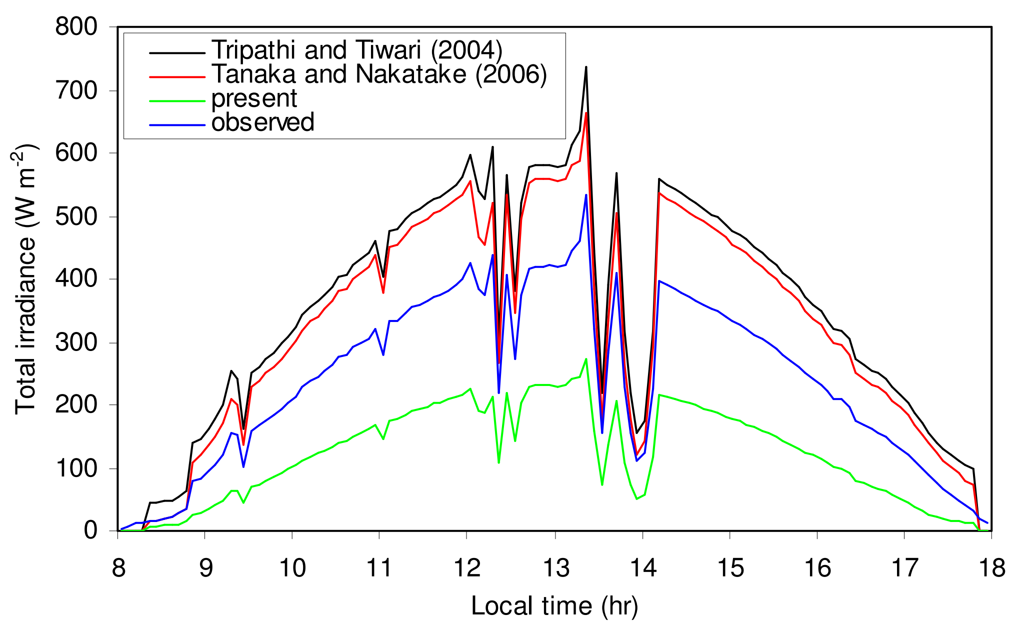

(b)

Fig.6.10: Variation of the total observed irradiance on a horizontal surface and computed effective irradiance in a) conventional solar still (CSS) and b) an advanced solar still (ASS) at the University of Strathclyde on 17th October 2007.

For the ASS, it is seen that both previous models yield distinctly higher effective irradiance than the present model during most of the day, for reasons similar to those of the CSS given in the preceding paragraph. It should however be noted that the external reflector reflects ρ_{er} of the available solar energy onto the surface of water in the previous models while the reflector effectively reflects ($\rho_{er}W_{er-wl}$) of the intercepted solar energy in the new model. In the present design, ρ_{er} =0.50 and W_{er-wl}=0.09. Therefore, the external reflector reflects 50 % of the intercepted global solar radiation onto the surface of saline water in the previous models. In contrast, the reflector effectively reflects 4.5 % in the new model, which shows that the previous models would overestimate radiation exchange between the reflector and water surface. In addition, the water surface and external reflector view 0.39 and 0.50 of the sky respectively. So, the water surface and reflector directly receive 39 and 50 % of the diffuse radiation measured on a horizontal surface respectively. It should be noted that the water surface views a lager fraction (W_{wl-sk}=0.53) of the sky in the CSS than in the ASS (W_{wl-sk}=0.39) due to obstruction by the condenser unit which protrudes above the level of the back wall. These observations indicate that view factors are significant in the computation of radiation distribution in a solar still. Again, it is seen that the effective irradiance is lower than the observed levels during most of the day, similar to the CSS.

Fig.6.11 shows the levels of effective irradiance estimated by the previous and present models from irradiance data captured on a horizontal plane at the Malawi Polytechnic. For the CSS, it is observed that both previous models yield higher values of effective irradiance than those obtained by using the present model during most of the day. This outcome is ascribed to differences in the assumptions about the characteristics of solar radiation as discussed in the first paragraph of this section.

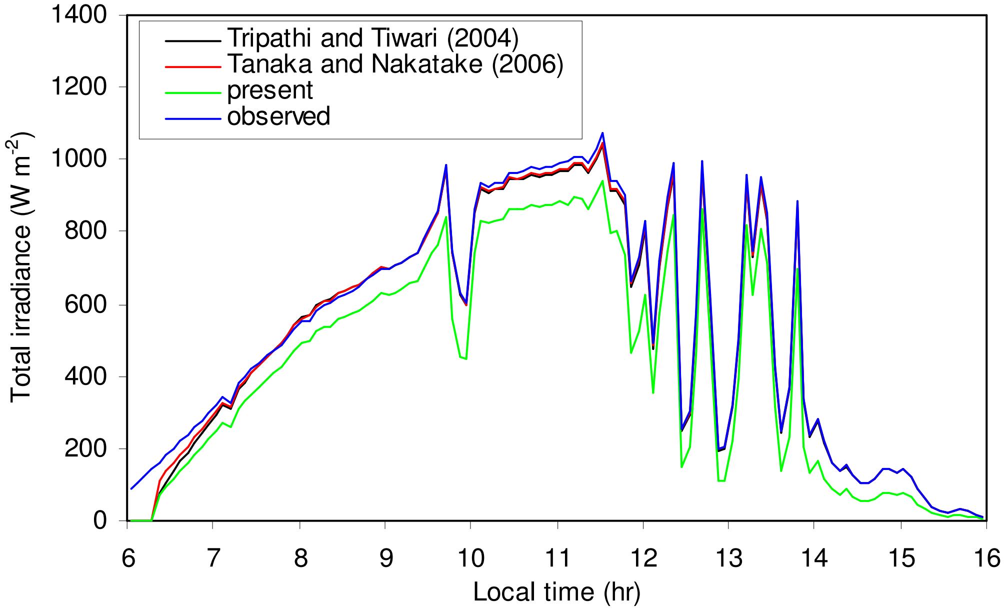

(a)

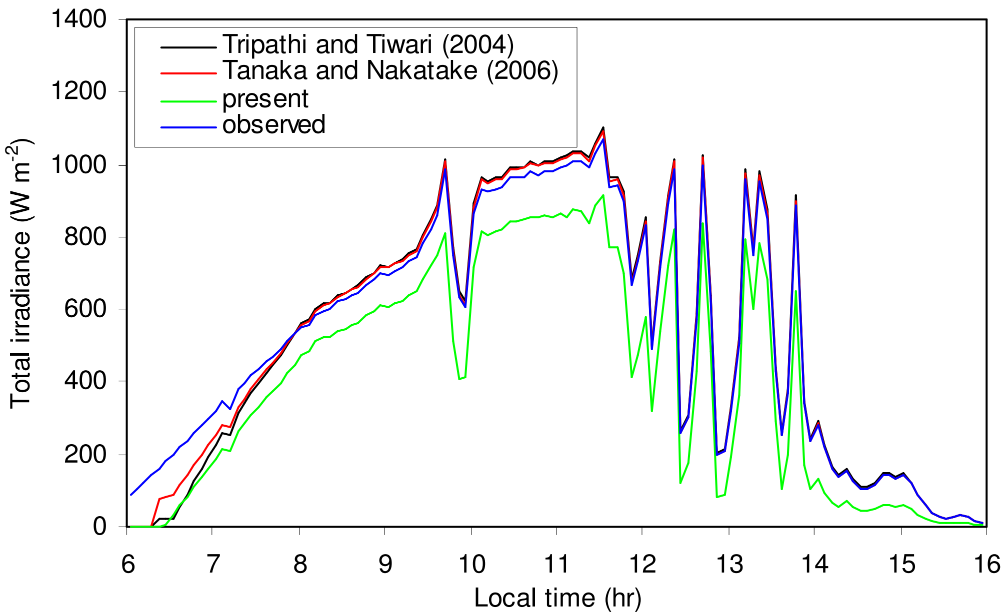

(b)

Fig.6.11: Variation of the total observed and effective irradiance in the a) conventional solar still (CSS) and advanced solar still (ASS) at Malawi Polytechnic on 14th October 2008.

For the ASS, it is again observed that both previous models yield higher effective irradiance than the present model during most of the day. The difference between effective and observed irradiance is higher at the University of Strathclyde than that at the Malawi Polytechnic, probably due to the lower solar altitudes at the former site. A higher proportion of incoming radiation is indirectly intercepted by the surface of saline water, with a small amount of the radiation directly reaching the water at low solar altitudes. This shows that the use of global irradiance on a horizontal surface (G_{gh}) in the energy balance equations would lead to inaccurate estimation of the solar load on saline water, especially at low solar altitudes.

Models proposed by Tripathi and Tiwari (2004), Tanaka and Nakatake (2006) and in this study were used to estimate the effective daily solar energy ($H_{g,ef}$) intercepted by saline water in basin 1 of the CSS and ASS at the University of Strathclyde and Malawi Polytechnic.

On daily basis, the values of global effective radiation ($H_{g,fe}$) estimated by the different models at the University of Strathclyde are shown in Figs. 6.12 and 6.13. It is observed that the previous models overestimated the solar energy that was effectively received by saline water in the CSS and ASS on all test days. On the average, the proportions of $H_{g,fe}$/ H_{gh} given by the Tripathi and Tiwari (2004), Tanaka and Nakatake (2006) and present models were respectively 60, 80 and 54 % for the CSS, and 138, 117 and 51 % for the ASS. The reasons for these observations are similar to those discussed in the first and second paragraphs of this section.

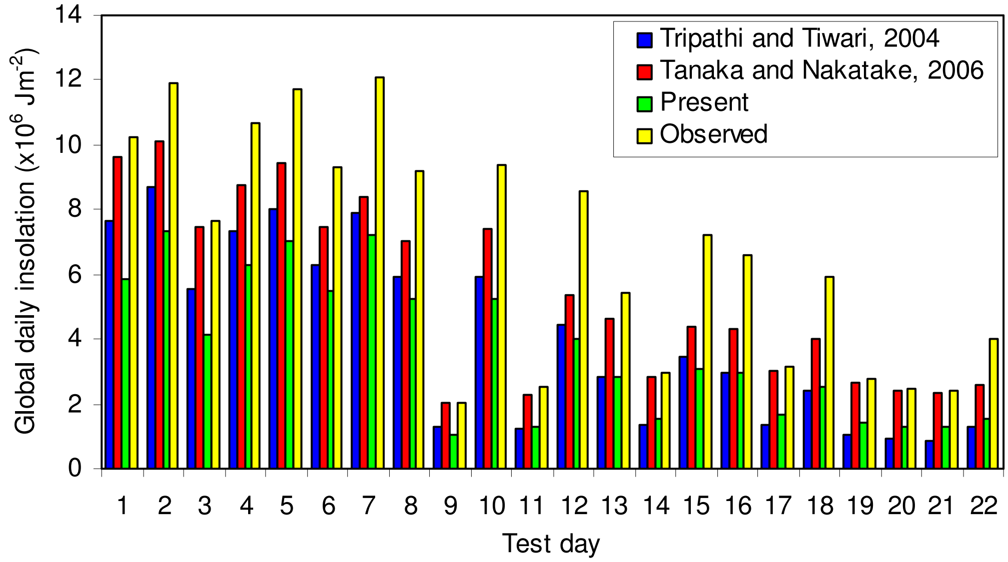

Fig. 6.12: Values of the daily effective global solar radiation ($H_{g,ef}$) estimated by different models inside the CSS, and observed values of the daily insolation on a horizontal surface at the University of Strathclyde.

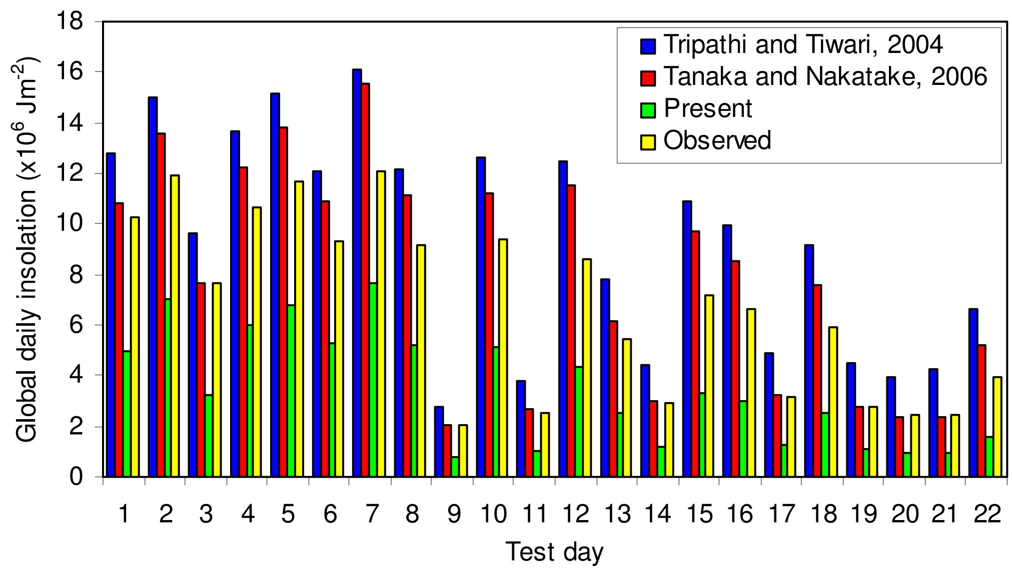

Fig.6.13: Values of the daily effective global solar radiation ($H_{g,ef}$) estimated by different models inside the ASS, and observed values of the daily insolation on a horizontal surface at the University of Strathclyde.

On daily basis, the values of global effective radiation ($H_{g,fe}$) estimated by the different models at the Malawi Polytechnic are shown in Figs. 6.14 and 6.15. It is again seen that the previous models overestimated the solar energy that was effectively received by saline water in the CSS and ASS on all test days. On the average, the proportions of $H_{g,fe}/ H_{gh}$ given by the Tripathi and Tiwari (2004), Tanaka and Nakatake (2006) and present models were respectively 97, 98 and 80 % for the CSS, and 99, 99 and 75 % for the ASS. The reasons for these observations are similar to those discussed from the first through the fourth paragraphs of this section.

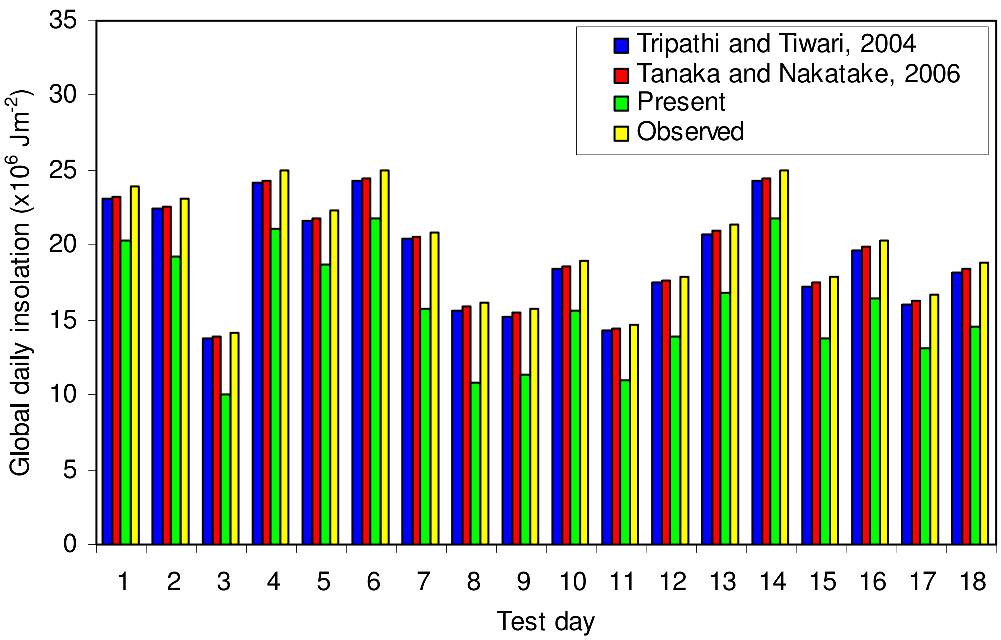

Fig. 6.14: Values of the daily effective global solar radiation ($H_{g,ef}$) estimated by different models inside the CSS, and observed values of the daily insolation on a horizontal surface at the Malawi Polytechnic.

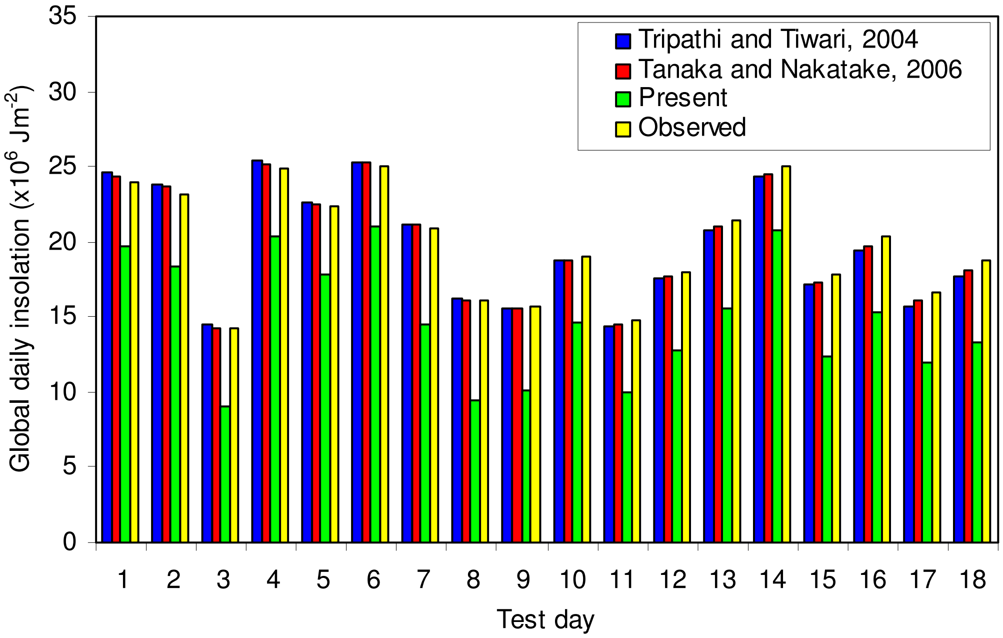

Fig. 6.15: Values of the daily effective global solar radiation ($H_{g,ef}$) estimated by different models inside the ASS, and observed values of the daily insolation on a horizontal surface at the Malawi Polytechnic.

6.3.2 Temperature of water

The variation of simulated and experimental temperatures of saline water in basin 1 of the CSS and ASS at the University of Strathclyde is presented in Fig.6.16. For the CSS, there is close agreement between simulated and experimental values from morning to about 14:00 hr. However, both previous models yield higher estimates than the new model after 14:00 hr, commensurate with the levels of effective irradiance. The previous models overestimate the levels of effective irradiance, which leads to overestimation of the energy that drives the heat and mass transfer processes in the solar stills.

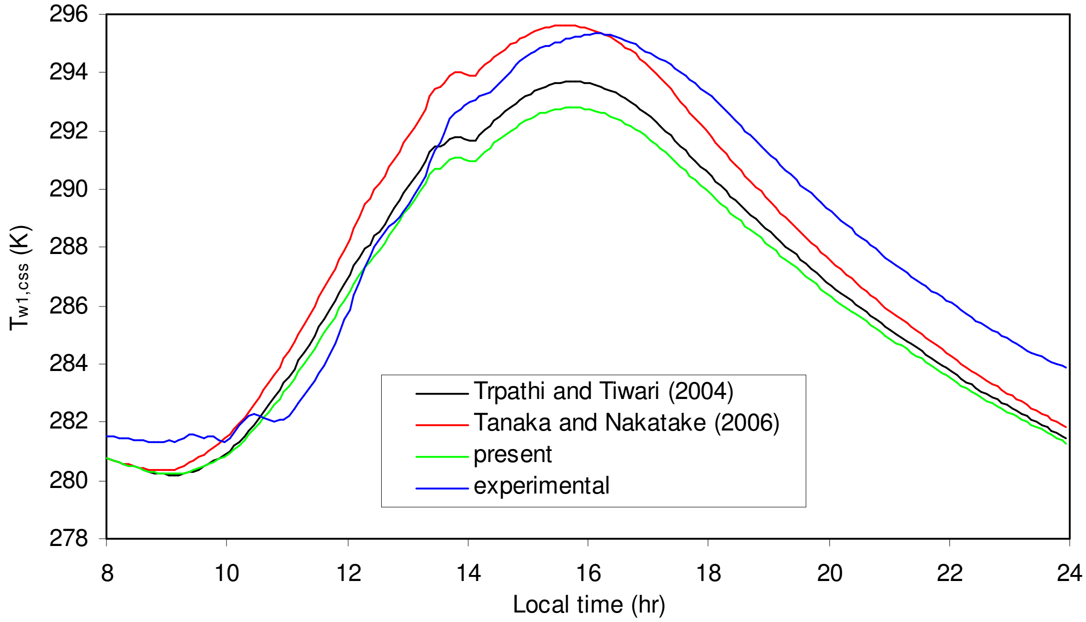

(a)

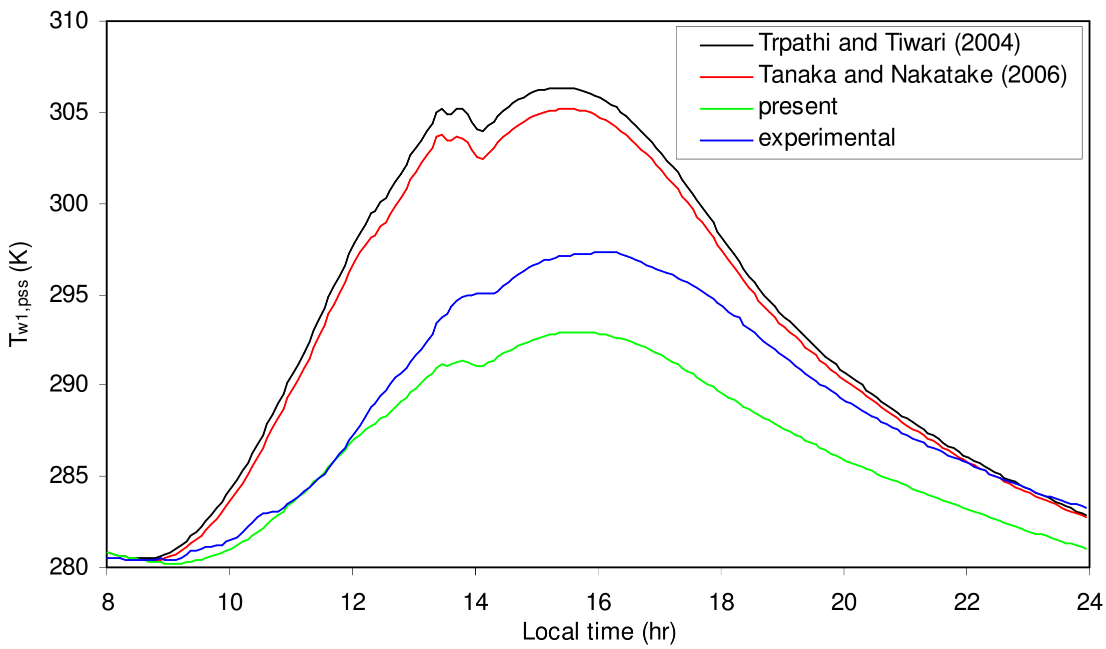

(b)

Fig.6.16: Variation of simulated and experimental temperature of saline water in the Basin 1 of a) CSS and b) ASS on 17th October 2007 at the University of Strathclyde.

For the ASS, the previous models again overestimate the temperature of saline water in the evaporator basin. In contrast, the present model yields estimates that are closer to experimental data. This observation is consistent with the corresponding levels of effective irradiance predicted by the individual models for calculating the distribution of solar radiation inside a basin type solar still.

Fig 6.17 shows the profiles of simulated and experimental temperatures of saline water in the evaporator basins of the CSS and ASS at the Malawi Polytechnic. For the CSS, there is close agreement between simulated and experimental values for all the three models in the morning and afternoon. However, both previous models yield significantly higher estimates of the temperature of saline water than the new model, ascribed to the levels of effective irradiance.

For the ASS, it is also observed that the previous models overestimate the temperature of water in basin 1. The present model yields estimates that are closer to experimental values. This observation is again consistent with the corresponding levels of effective irradiance predicted by the individual models. The estimated temperatures were used to predict distillate output.

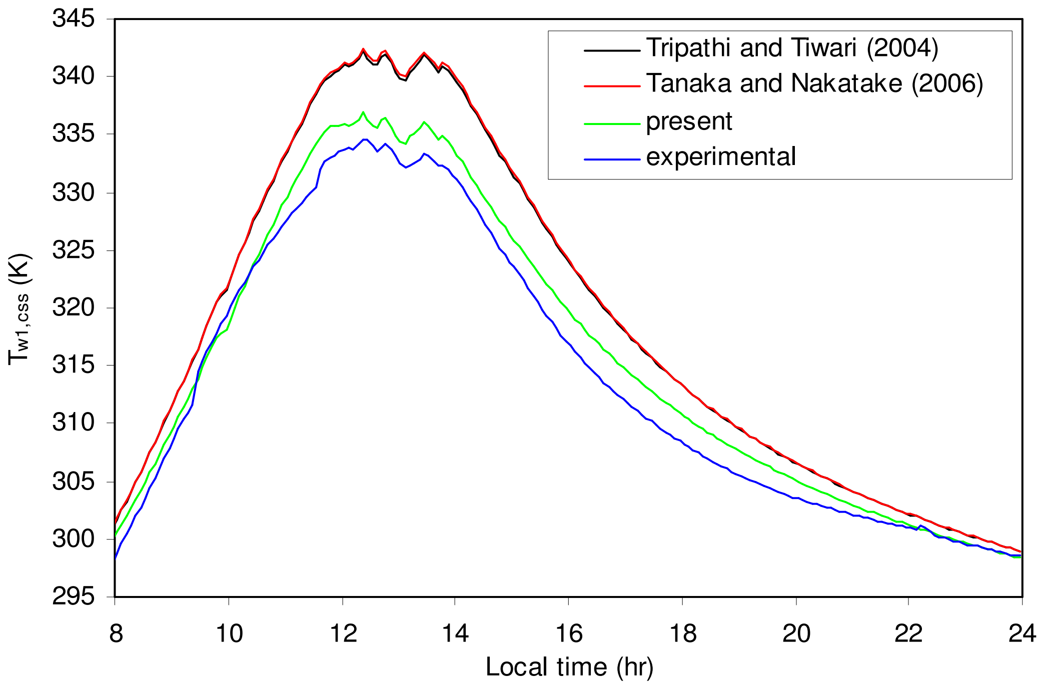

(a)

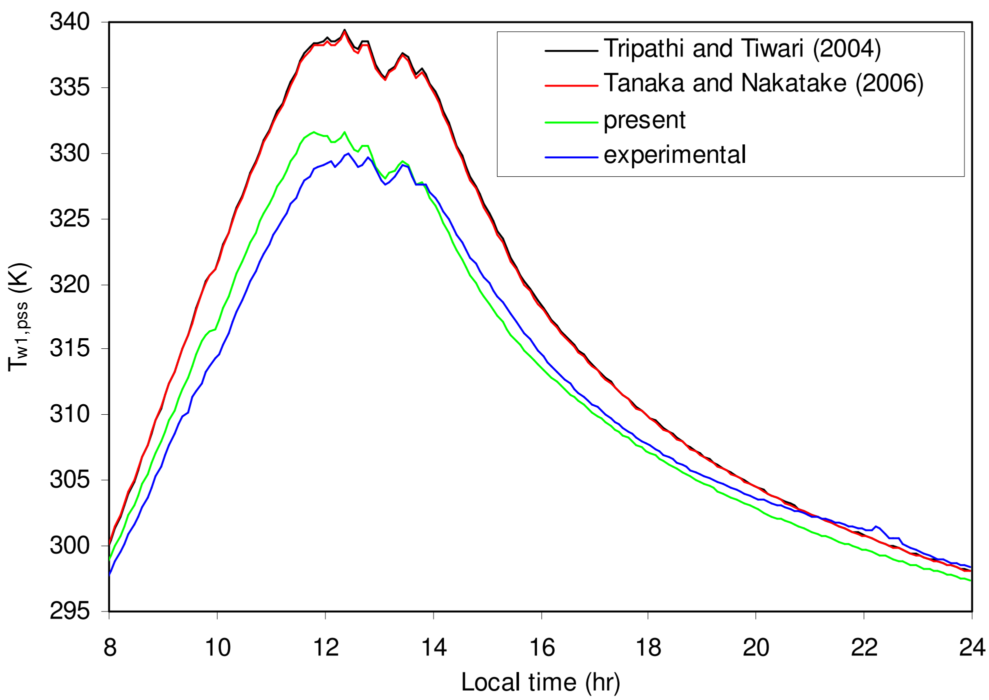

(b)

Fig.6.17: Variation of simulated and experimental temperature of saline water in basin 1 of a) CSS and b) ASS on 14th October 2008 at the Malawi Polytechnic.

6.3.3 Distillate yield

Fig.6.18 shows the variation of simulated and experimental cumulative distillate production at the University of Strathclyde. For the CSS, it is observed that the previous models give higher estimates than the present model, in agreement with effective irradiance. Estimates from the present model are closer to the experimental data. It should also be mentioned that all the three models slightly overestimate the distillate yield probably due to vapour and distillate leakage from a practical solar still and measurement errors.

For the ASS, the previous models also give significantly higher estimates than the present model. Estimates from the present model are again closer to the experimental values. It should be noted that these observations conform to the computed levels of effective irradiance.

The performance of the three models at the Malawi Polytechnic is presented in Fig.6.19. For the CSS, it is again observed that the previous models give higher estimates than the present model, with estimates from the present model being closer to the experimental data. These observations are commensurate with the levels of effective irradiance computed by using these models.

For the ASS, it is seen that the previous models give higher estimates than the present model. Estimates from the present model are again closer to the experimental data. It should also be noted that the hourly production rates were relatively low for both solar stills when the level of insolation was low, which would make it difficult to measure the distillate yield with higher accuracy. So, the daily distillate outputs were found to be more reliable in model verification (Yates and Woto, 1988 as cited by Smyth et al., 2005).

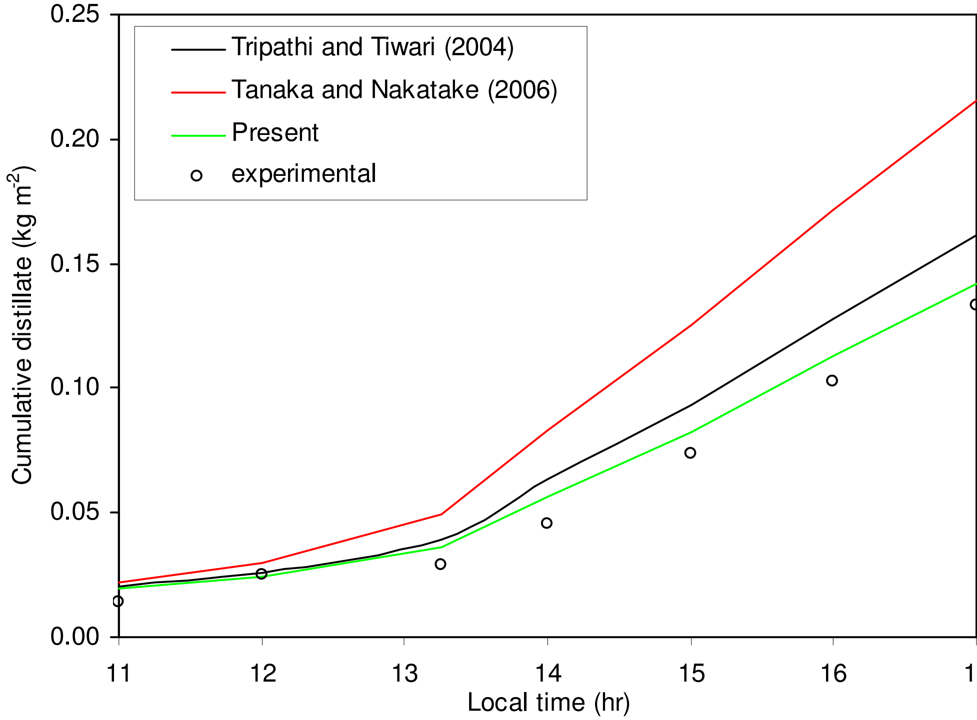

(a)

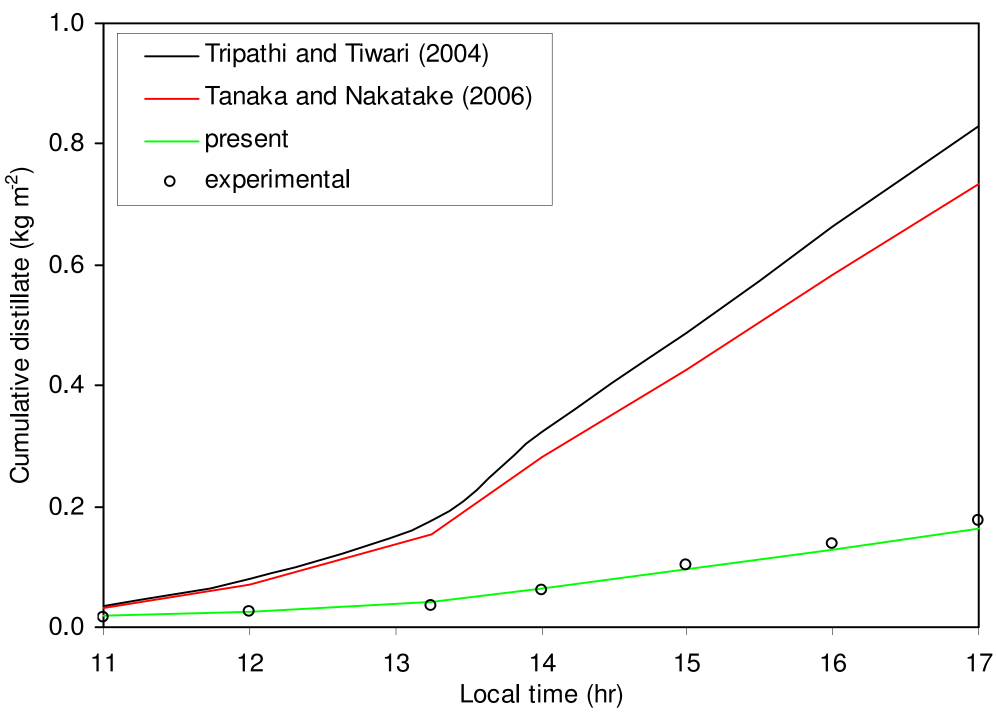

(b)

Fig.6.18: Variation of simulated and experimental distillate output for a) CSS and b) ASS on 17th October 2007 at the University of Strathclyde.

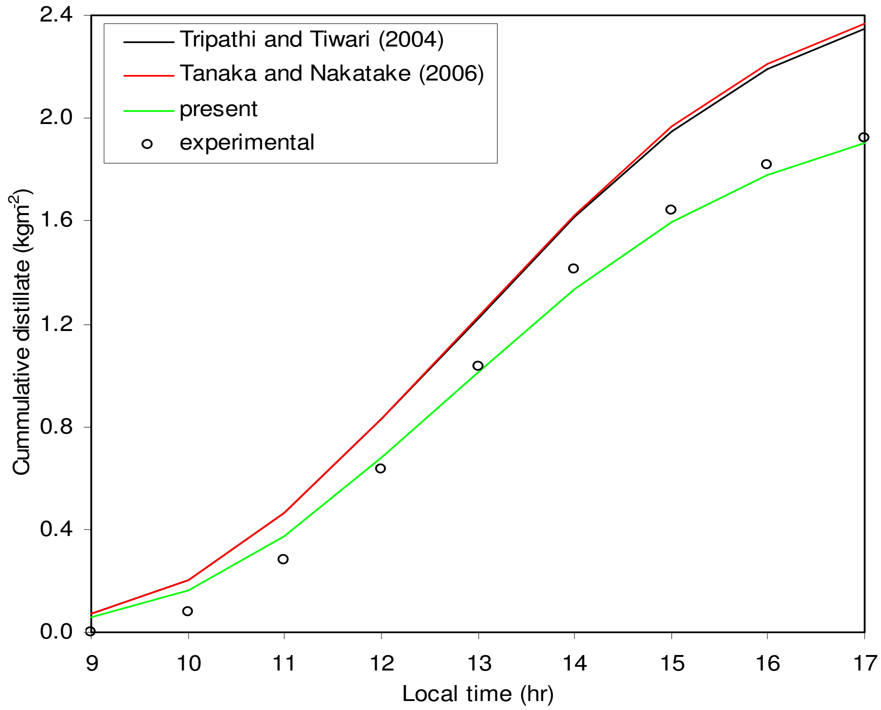

(a)

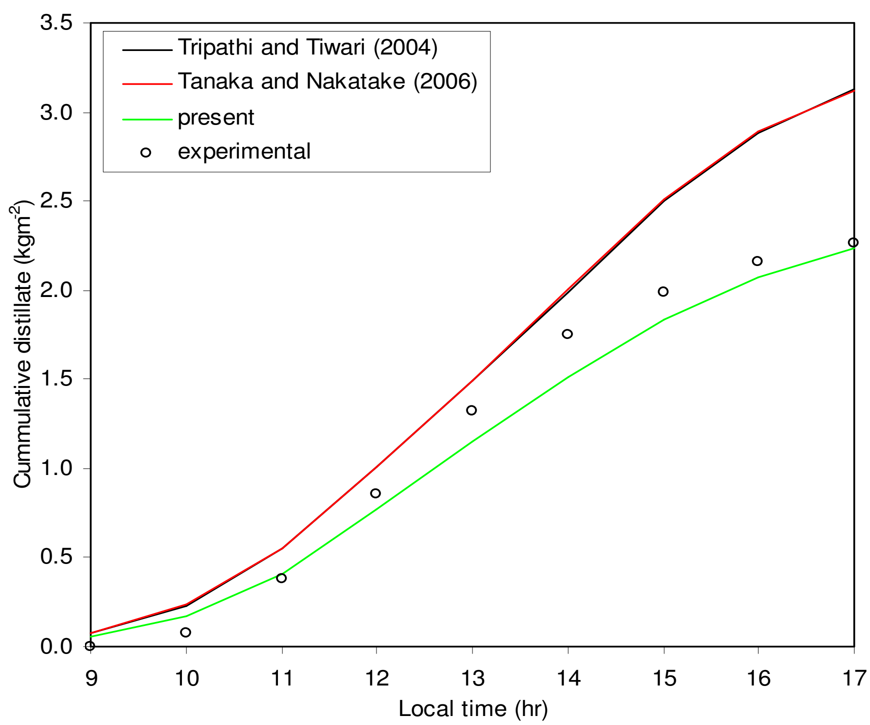

(b)

Fig.6.19: Variation of simulated and experimental distillate output for a) CSS and b) ASS on 14th October 2008 at the Malawi Polytechnic.

Table 6.4 shows results of statistical analysis for the daily distillate output from the CSS and ASS tested at the University of Strathclyde. For the CSS, it is observed that previous models exhibit higher *t*-values than the present model. In addition, the *t*-values for the Tripathi and Tiwari (2004) and present models are less than the corresponding critical value, which shows that these two models gave estimates of distillate yield that are not significantly different from the empirical values. Estimates given by the Tanaka and Nakatake (2006) model were significantly different from experimental data.

Table 6.4: *t*-values of the various models for the test data captured at the University of Strathclyde.

System	*t*-value for model			Critical *t*-value
	Tripathi and Tiwari (2004)	Tanaka and Nakatake (2006)	Present	
CSS	2.42	7.14	1.93	3.82
ASS	2.85	2.42	0.12	12.9

For the ASS, it is again seen that the previous models exhibit higher *t*-values than present model. The *t*-values for all the three models are less than the critical value, which indicates that the estimated and experimental values of distillate output are not significantly different for all the models.

Table 6.5 shows results of statistical analysis for the data captured at the Malawi Polytechnic. For the CSS, it is observed that the previous models exhibit higher *t*-values than the present model. In addition, the *t*-values for the previous models are higher than the critical value while that of the present model is lower than the critical value. This indicates that the previous models gave estimates of distillate output that are significantly different from the corresponding experimental values. In contrast, distillate estimates from the present model are not significantly different from experimental distillate yield.

Table 6.5: *t*-values of the various models for the test data captured at the Malawi Polytechnic.

System	*t*-value for model			Critical *t*-value
	Tripathi and Tiwari (2004)	Tanaka and Nakatake (2006)	Present	
CSS	15.72	16.20	1.56	3.97
ASS	18.57	17.94	3.46	3.97

For the ASS, it is again seen that the previous models exhibit higher *t*-values than the present model. Moreover, the *t*-values of the previous models exceed the critical level. On the other hand, the *t*-value for the new model is less than the cut-off point. Stone (1993) reported that a model with a smaller value of the *t*-statistic performs better than the one with a higher value. In addition, estimates from a model with a *t*-value that is below the critical level are not significantly different from experimental data. These observations indicate that the performance of the new model is most satisfactory at both test sites.

6.4 Summary

In this chapter, prevailing meteorological conditions and results for verification of models that compute the distribution of solar energy in single slope conventional and advanced solar stills have been presented. Astronomical and meteorological conditions were diverse at the University of Strathclyde and Malawi Polytechnic. Empirical data for irradiance, ambient air temperature and wind speed were employed to predict distillate output from the CSS and ASS. Theoretically, saline water in the evaporator basins of the CSS and ASS intercepted most of the global solar radiation directly at both sites. The CSS directly received more solar energy than the ASS, regardless of weather and locality. Theoretical and experimental results have been compared. It is inferred that the performance of the new model is most satisfactory at both test sites.

6.5 References

Anderson, E.E., 1983. *Fundamentals of solar energy conversion*. Addison-Wesley Publishing Company, pp.410-412.

Cooper, P.I., 1969. Digital simulation of transient solar still processes. *Solar Energy*, 12, pp.313-331.

Duffie, J.A. and Beckman, W.A., 2006. *Solar Engineering of Thermal Processes*. 3rd ed. New York: John Wiley & Sons Inc., pp.85-115

El-Sebaii AA (2004). Effect of wind speed on active and passive solar stills. *Energy Conversion and Management*, 45, pp.1187-1204.

Incropera, F.P., DeWitt, D.P., Bergman, T.L. and Lavine, A.S., 2007. *Fundamentals of heat and mass transfer*. 6th ed. New Jersey: John Wiley & Sons, 724-770.

Nafey, A.S., Abdelkader, M., Abdelmotalip, A. and Mabrouk, A.A., 2000. Parameters affecting solar still productivity. *Energy Conversion and Management*, 41, pp.1797-1809.

Saluja, G.S. and Douglas, N.G., 1996. Verification of wind resource study in a Scottish region. *Renewable Energy*, 9, pp.798-801.

Samee, M.A., Mirza, U.K., Majeed, T. and Ahmad, N., 2007. Design and performance of a simple solar still. *Renewable and Sustainable Energy Reviews*, 11, pp.543-549.

Sinden, G., 2007. Characteristics of the UK wind resources: Long-term patterns and relationship to electricity demand. *Energy Policy*, 35, pp.112-127.

Smyth, M., Norton, B. and Byres, W., 2005. Measured effect of reflector augmentation of simple basin type solar stills. *Ambient Energy*, 26, pp.59-70.

Stone, R.J.,1993. Improved statistical procedure for the evaluation of solar radiation estimation models. *Solar Energy*, 51, pp.289-291.

Tanaka, H. and Nakatake, Y., 2006. Theoretical analysis of a basin type solar still with internal and external reflectors. *Desalination*, 197, pp.205-216.

Tanaka, H. and Nakatake, Y., 2007. Effect of inclination of external flat plate reflector of basin type still in winter. *Solar Energy*, 81, pp.1035-1042.

Tiwari, G.N., Singh, H.N. and Tripathi, R., 2003. Present status of solar distillation. *Solar Energy*, 75, pp.367-373.

Tripathi, R. and Tiwari, G.N., 2004. Performance evaluation of solar still by using the concept of solar fraction. *Desalination*, 169, pp.69-80.

Wisse, J.A. and Stigter, K., 2007. Wind engineering in Africa. *Wind Engineering and Industrial Aerodynamics*, 95, pp.908-927.

Yates, R. and Woto, T., 1988. *Small scale desalination for areas of Botswana*. Ottawa: International Development Centre.

Chapter 7

Results and discussion

7.0 Introduction

Knowledge about the theoretical and empirical performance of an engineering system is vital for the development and application of the system. The theoretical performance of a conventional solar still (CSS) and advanced solar still (ASS) was examined in Chapter 3 by using a new model that calculates the distribution of solar radiation in a single slope solar still. It was found that the ASS was more efficient in producing distilled water than the CSS when operated under the same meteorological conditions. These results were employed to design and construct prototype stills which were tested at the University of Strathclyde and Malawi Polytechnic to generate an empirical data base. This data was then used to validate the proposed model as reported in Chapter 6. In this chapter, the empirical performance of the CSS and ASS under the prevailing meteorological conditions is presented. The chapter focuses on the temperatures of system components, quantity and quality of distilled water, efficiency of the solar stills and statistical validity of the empirical results. It is found that the ASS produced more distilled water per unit area of basin 1 than the CSS. Other results are discussed in detail.

7.1 Temperature of system components

Solar radiation is converted to heat when it is incident on the various components of solar stills, resulting in temperature rise of the components. In particular the difference between the temperature of saline water and a condensing cover drives the distillation process. The rate of evaporation-condensation increases with this temperature difference. Further, heat loss also increases with the temperature gradient between the system and ambient environment. Consequently, it is necessary to know temperature levels attained by the components of a given solar still.

Measured values of the temperatures of the glass cover (T_{gc}), water (T_{wl}, T_{w2} and T_{w3}) and condenser cover (T_{co}) were used to determine the coefficients of Eqs. (4.2 to 4.4) reported in Table 7.1. It is seen that the coefficient of determination (r^2) is greater than 0.99 for all the correlations which shows that these correlations are satisfactory, with more than 99 % of the errors being explained by each model used in predicting the average temperature of a given component. With this level of confidence, the correlations were used to calculate the temperatures of the various components of the solar stills.

Table 7.1: Coefficients of Eqs.(4.2 to 4.4) for calculating average temperatures of components.

Temperature (K)	Coefficient							r^2
	a_o	a_1	b_o	B_1	B_2	c_o	C_1	
T_{gc}	50.291	0.830	-	-	-	-	-	0.997
T_{wl}	7.856	0.972	-	-	-	-	-	1.000
T_{w2}, T_{w3}	-	-	2.059	0.483	0.510	-	-	1.000
T_{co}	-	-	-	-	-	5.110	0.983	0.993

Fig.7.1 shows the variation of the observed temperature of ambient air (T_a), glass cover (T_{gc}), saline water (T_{w1}, T_{w2} and T_{w3}) on a typical date at the University of Strathclyde. It is observed that the values of T_{gc} for the CSS ($T_{gc,css}$) are lower than those of the ASS ($T_{gc,Ass}$) from about 11: 00 hr to 17:00 hr, with maximum values of $T_{gc,css}$=292 K and $T_{gc,Ass}$= 294 K. In addition, the temperature of water in basin 1 for the CSS ($T_{w1,css}$) is lower than that of the ASS ($T_{w1,Ass}$), with maximum values of $T_{wl,css}$=295 K and $T_{wl,Ass}$=297 K. It should be mentioned that part of the heat from the evaporator basin flows into the condenser chamber by purging and diffusion, which would tend to lower the glazing temperature of the ASS (Fath and Elsherbiny, 1993; El-Bahi and Inan, 1999a; Madhlopa and Jonstone, 2009). Moreover, the CSS has less thermal mass than the ASS which would result in higher values of the $T_{gc,css}$ and $T_{w1,css}$ than those of $T_{gc,Ass}$ and $T_{w1,Ass}$ respectively. So, the observed trend is ascribed to the lower amount of solar

energy intercepted by saline water in basin 1 of the CSS compared to that of the ASS on this particular date (test day 12 in Table 6.4). It was found that the maximum values of ($T_{wl,css}$-$T_{gc,css}$) and ($T_{wl,Ass}$-$T_{gc,Ass}$) were respectively 7 and 9 K around 18:00 hr for the CSS and ASS. This shows that the CSS would produce less distilled water than the ASS on the typical date.

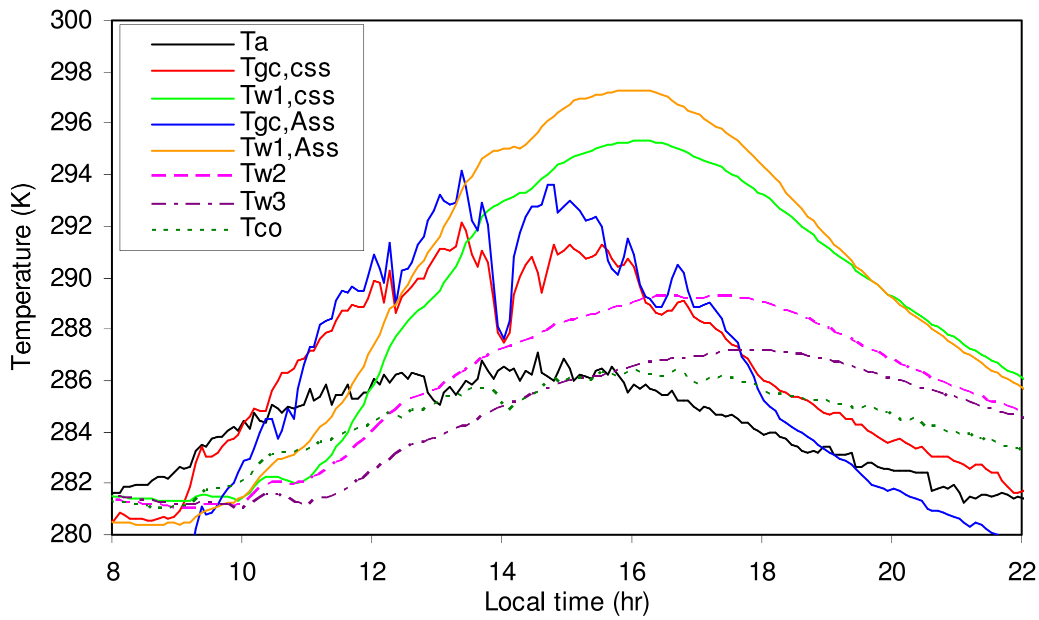

Fig.7.1**:** Variation of the temperature of ambient air (T_a), glass cover (T_{gc}), water temperature (T_{wl}, T_{w2} and T_{w3}) and condenser cover (T_{co}) for the CSS and ASS on 17th October 2007 at the University of Strathclyde.

It is also seen that the temperature of water (maximum value of T_{w2}=289 K) in basin 2 (second effect) is below that of basin 1 of the advanced solar still from 13:30 hr until midnight, with a maximum observed difference of about 9 K. Thus, vapour could condense under basin liner 2 during this period. In addition, the temperature of water in basin 3 (maximum value of T_{w3}=287 K) was lower than that of water (T_{w2}) in basin 2 from 9:00 hr to about 23:00 hr, with a maximum observed difference (T_{w2}-T_{w3}) of 2 K which was relatively low for significant production of distilled water by the second effect.

It should also be mentioned that the temperature of the condenser (T_{co}) was lower than that of the third effect from 15:30 hr until after 24:00 hr, with a maximum observed difference (T_{w3}-T_{co}) of 2 K, which is again relatively low for significant distillate production from the third effect (maximum value of T_{co}=286 K). Further, the temperature of the condenser cover was lower than that of ambient air from morning to about 16:00 hr. A reversal of the trend (T_a>T_{co}) is observed after 16:00 hr, attributed to convective, evaporative and radiative heat transfer from the third effect which proceeds even after sun set due to the effect of thermal storage. The absolute value of (T_{co}-T_a) did not exceed 2 K, which indicates that the solar shield was effective in blocking off solar radiation from reaching the condenser cover.

Fig.7.2 shows profiles of observed temperatures on a typical date at the Malawi Polytechnic. It is seen that the values of T_{gc} for the CSS ($T_{gc,css}$) are higher than those of the ASS ($T_{gc,pss}$) from about 9:30 hr to 17:20 hr, with maximum values of $T_{gc,css}$=322 K and $T_{gc,Ass}$=318 K. In addition, the temperature of water in basin 1 for the CSS (maximum value of $T_{w1,css}$=335 K) is higher than that of the ASS (maximum value of T_{w1-Ass}=330 K), commensurate with the computed effective irradiance. The CSS intercepted more solar energy compared to the ASS on all test days at this site. It was found that the maximum values of ($T_{wl,css}$-$T_{gc,css}$) and ($T_{wl,Ass}$-$T_{gc,Ass}$) were respectively 17 and 16 K around 14:30 hr for the CSS and ASS respectively.

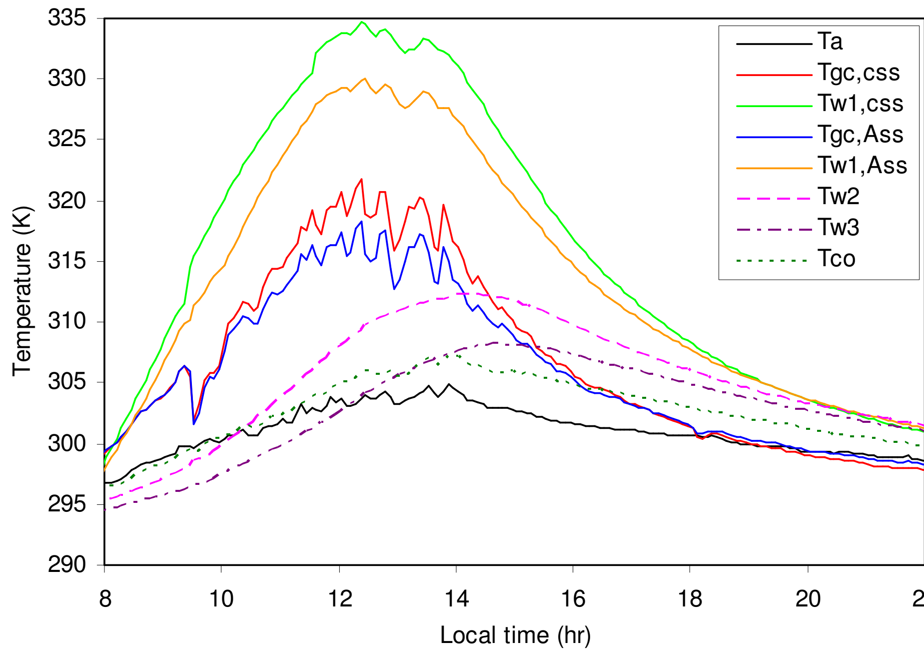

Fig.7.2: Variation of the temperature of ambient air (T_a), glass cover (T_{gc}), water temperature (T_{wl}, T_{w2} andT_{w3}) and condenser cover (T_{co}) for the CSS and ASS on 14th October 2008 at the Malawi Polytechnic.

It is also seen that the temperature of water (maximum value of T_{w2}=312 K) in basin 2 (second effect) is below that of water in basin 1 of the ASS from morning until 21:00 hr, with a maximum observed difference of about 22 K. This shows that water vapour from the first effect could condense under basin liner 2 during this period. In addition, the temperature of water in basin 3 (maximum value of T_{w3}=308 K) was lower than that of water in basin 2 during most of the day, with a maximum observed difference (T_{w2}-T_{w3}) of 6 K which indicates the potential for distillate production to proceed from the second effect. It should also be mentioned that the temperature of the condenser cover (maximum value of T_{co}=307 K) was lower than that of the third effect from about 3:30 until after midnight, with a maximum observed difference (T_{w2}-T_{co}) of 3 K, which is relatively low for significant distillate production from the third effect. Further, the temperature of the condenser cover was lower than that of ambient air from morning to about 10:00 hr. A reversal of the trend is observed after this time probably due to the convective, evaporative and radiative heat transfer from the third effect.

Nevertheless, the absolute value of (T_{co}-T_a) did not exceed 3 K. A similar trend was observed on other test days. El-Bahi and Inan (1999b) found a maximum value of T_{co} = 433 K when T_a=309 K for an unshielded separate condenser. These findings indicate that the proposed solar shield was effective in obstructing the rays of the sun from reaching the condenser cover under both temperate and tropical weather conditions, and justify the assumption that $T_{co} \approx T_a$ in the energy balance equations in the present investigation. System components attained higher values of corresponding temperatures at the Malawi Polytechnic than at the University of Strathclyde, commensurate with the prevailing meteorological conditions at the two test sites.

7.2 Distillate output

7.2.1 Yield of distilled water

The main objective of this investigation was to develop a solar still with higher distillate yield per unit area of basin 1. It was perceived that the ASS could produce clean water from saline water in basin 1 (first effect), basin 2 (second effect) and basin 3 (third effect). Fig.7.3 shows the variation of cumulative distillate productivity of the CSS and ASS on a typical date at the University of Strathclyde, with the productivity of the ASS being a total of contributions from all the three effects. It is seen that the amount of distilled water is low for both stills in the morning. This is expected because production starts when air inside the still is saturated with water vapour. From about 11:00 hr, the productivity of the CSS was lower than that of the ASS. On the typical date, the CSS and ASS produced 0.319 and 0.426 kg m^{-2} of distilled water, respectively. On other days, the daily productivity of the CSS ranged from 0.132 to 0.496 kg m^{-2} while the ASS yielded 0.168 to 0.528 kg m^{-2} under the same weather conditions (maximum uncertainty of daily distillate productivity =0.002 kg m^{-2}). Improvement in the daily production of distilled water ranged from 6 to 34 % over the productivity of the CSS, depending on the prevailing weather conditions. On the average, it was found that the first, second and third effects of the ASS contributed 87, 12 and 1 % of the total distilled water respectively. This shows that the third effect acted as a heat sink to promote distillate production from the second effect.

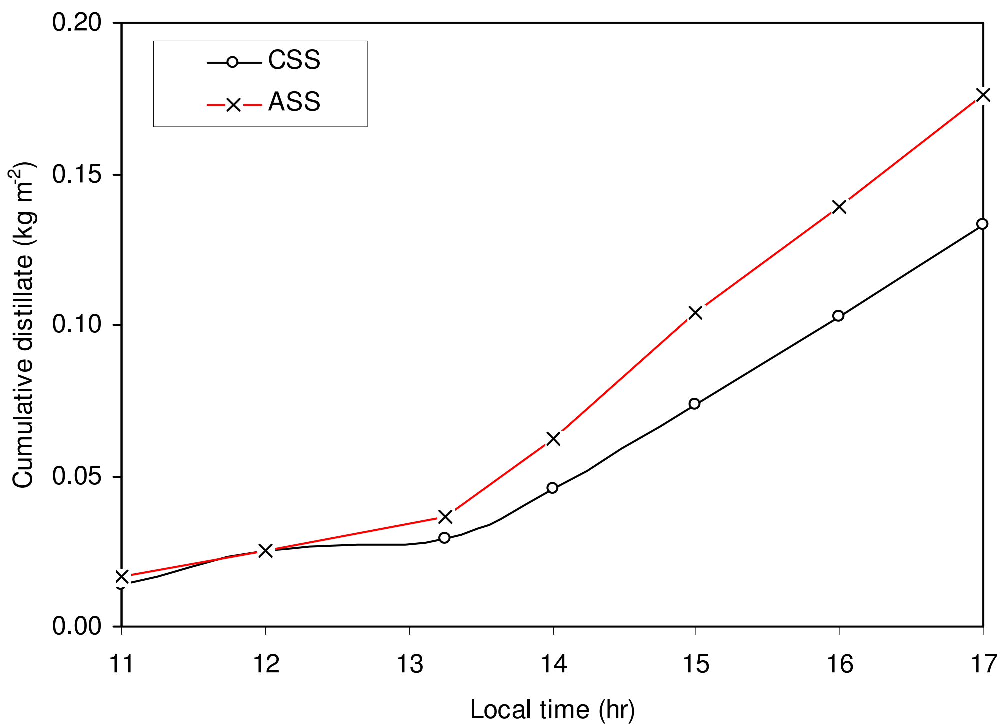

Fig.7.3: Variation of cumulative distillate production for the conventional solar still (CSS) and present solar still (ASS) on 17 October 2007 at the University of Strathclyde.

The observed levels of production are attributed to the optical and heat transfer characteristics of the distillation systems. Saline water in basin 1 of the CSS was less efficient in capturing solar energy than that in the ASS on this particular test day. Consequently, less energy was available to drive the heat and mass transfer processes in the CSS. In addition, there is heat recovery in the ASS which also contributes to an increase in distillate production. It is also noted that the distillate contribution from the third effect was negligible, commensurate with the low temperature gradient between the third effect and the condenser cover (T_{w3}-T_{co}).

Cumulative distillate yield on a typical date at the Malawi Polytechnic is presented in Fig.7.4. It is observed that distillate production is insignificant before 10:00 hr, for the same explanation applicable to the yield at the University of Strathclyde. After 10:00 hr, the rate of productivity for the CSS was lower than that for the ASS. On daily basis, the ASS produced 2.632 kg m^{-2}, an improvement of 14 % over the productivity of the CSS. On other days, the CSS produced 1.311 to 3.347 kg m^{-2} while the yield from the ASS was 1.488 to 4.599 kg m^{-2}. Improvement in the daily production of distilled water ranged from 9 to 22 % over the productivity of the CSS, depending on the prevailing weather conditions. On the average, it was found that the first, second and third effects of the ASS contributed 88, 11 and 1 % of distilled water respectively. These percentages compare very well with findings at the University of Strathclyde. It should be noted that the daily productivity of the solar stills was significantly higher at the Malawi Polytechnic than that at the other location probably due to the influence of astronomical and meteorological factors (discussed in Chapters 4 and 6). Under favourable weather conditions, the daily productivity of a CSS is about 3 to 4 kg m^{-2}, (Al-Kharabsheh and Goswami, 2003). El-Bahi and Inan (1999b) reported a daily distillate productivity of 4 kg m^{-2} for a double-glass solar still with separate condenser and reflector. So, findings from this investigation are comparable with previous results.

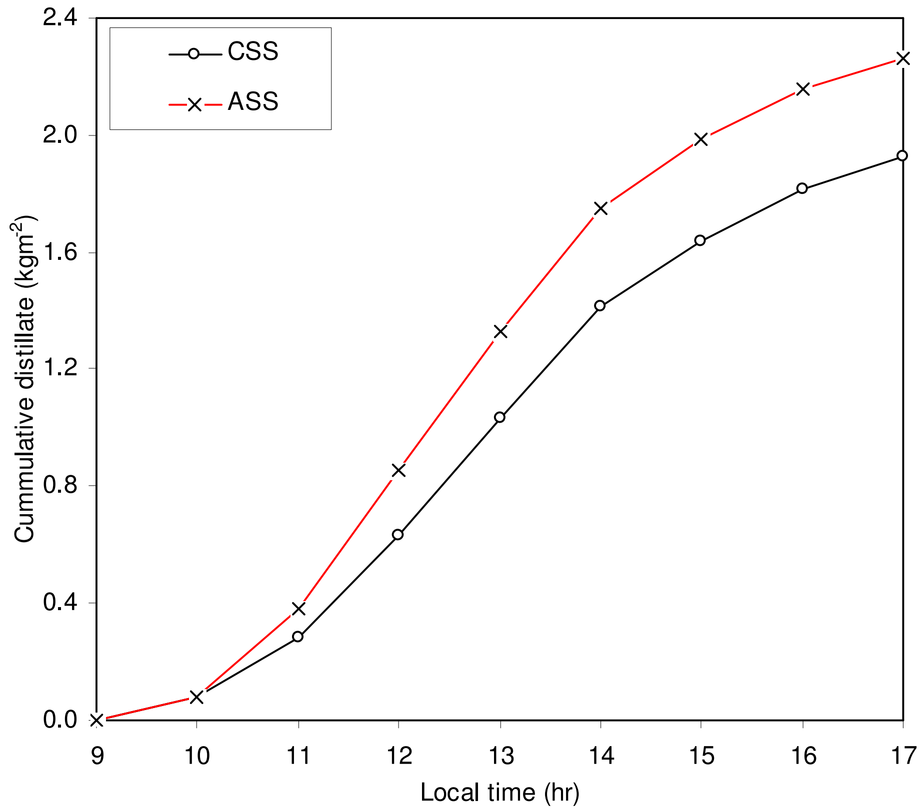

Fig.7.4: Variation of cumulative distillate production for the conventional solar still (CSS) and advanced solar still (ASS) on 14th October 2008 at the Malawi Polytechnic.

Table 7.2 shows mean daily distillate outputs according to experimental runs determined in Chapter 4. It is seen that run 1 (CSS) has a lower mean daily yield than run 3 (ASS) for tests conducted at location 1 (University of Strathclyde). Similarly, run 2 (CSS) has a lower mean daily yield than run 4 (ASS) for tests carried out at the Malawi Polytechnic.

Table 7.2: Summary of mean daily distillate yield ($\hat{Y}$) according to experimental run.

Run	Factor		$\hat{Y}$
	Design	Location	(kgm^{-2})
1	1	1	0.280
2	1	2	2.247
3	2	1	0.327
4	2	2	2.667

7.2.2 Distribution of daily distillate yield

The main objective of this investigation was to develop a solar still that can augment distillate production. To achieve this aim, a conventional solar still (CSS) and advanced solar still (ASS) were modelled, designed, constructed and tested. A randomised block experimental design was formulated to compare the distillate yield (Y) of the two stills. So, a matched pair of data points for the CSS and ASS was generated on a given test day. This approach was taken because the systems were tested under the same meteorological conditions on any given test day, and the weather varied from one day to another. Consequently, a paired *t*-test was suitable for statistical comparison of the means of the daily distillate yield from the CSS and ASS (Brown and Melamed, 1993). This statistical test requires randomness and normal distribution of the empirical data. The randomness of the daily distillate data was verified by using lag plots while the distribution type was determined by using probability plots, skewness and kurtosis.

Fig.7.5 shows lag plots for the daily distillate yield for the CSS and ASS. For each plot, it is observed that the yield (Y_i) on the i^{th} test day changes randomly with the yield (Y_{i-1}) on the previous test day, with points that are below and above the mean daily distillate yield. There are no distinct trends in the distribution of points on the Cartesian plane, which indicate that each set of the daily distillate data is random (NIST/SEMATECH, 2005).

Probability plots for the daily distillate yield for the CSS and ASS are presented in Fig.7.6. It is seen that the points in the normal probability plot for each still follow a linear trend with a high degree of correlation between expected and observed probabilities (r^2=0.97 for the CSS, and r^2=0.98 for the ASS). NIST/SEMATECH (2005) reported that if the normal probability plot is linear then the distribution of the data is normal. In addition, the values of skewness and kurtosis for the daily distillate data, shown in Table 7.3, fell within the acceptable limits for a normal distribution (Ianetz et al., 2000). So, each set of the daily distillate data was random and distributed almost normally, and the use of the *t*-test was valid.

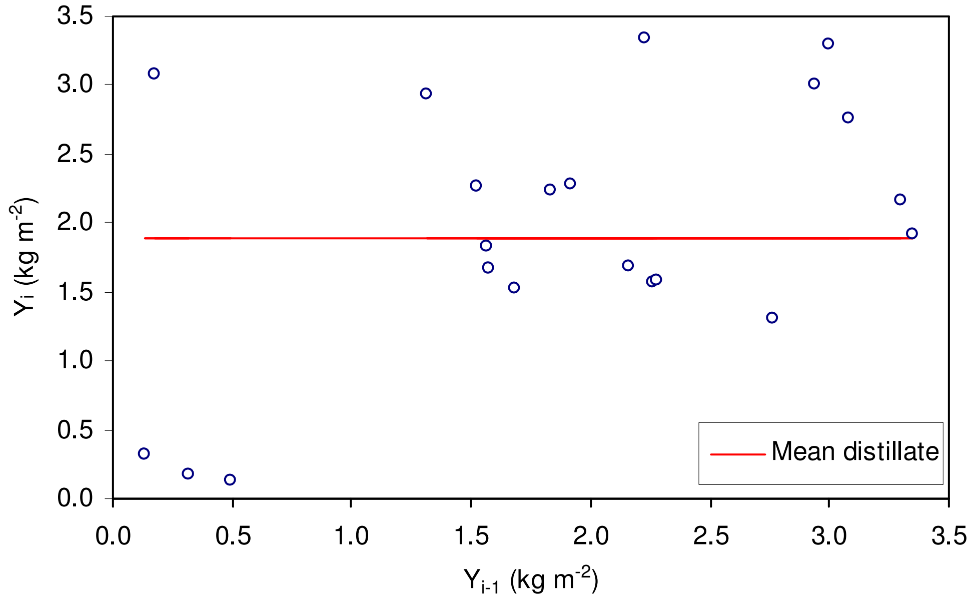

(a)

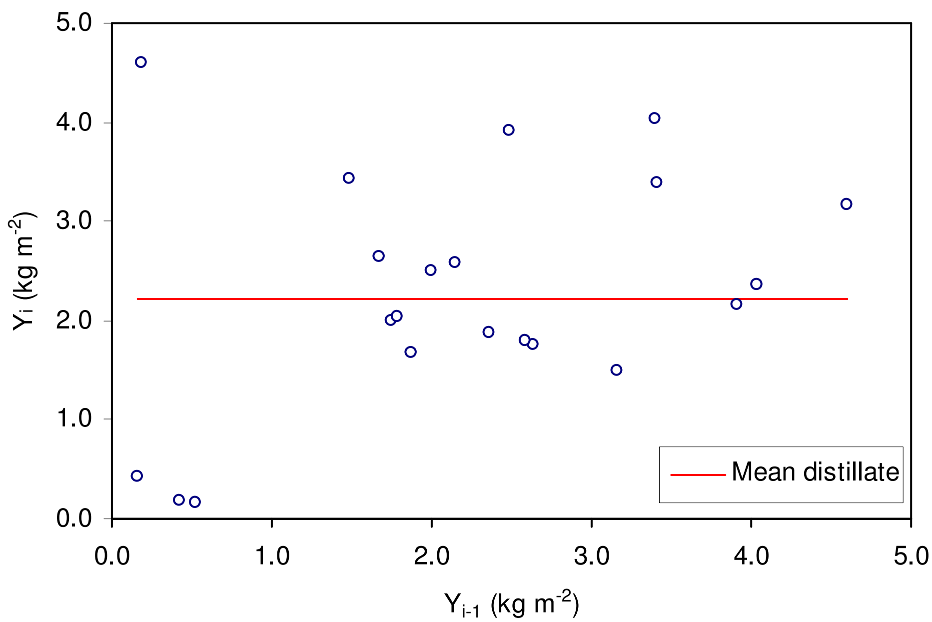

(b)

Fig.7.5: Lag plots for daily distillate yield from the a) CSS and b) ASS.

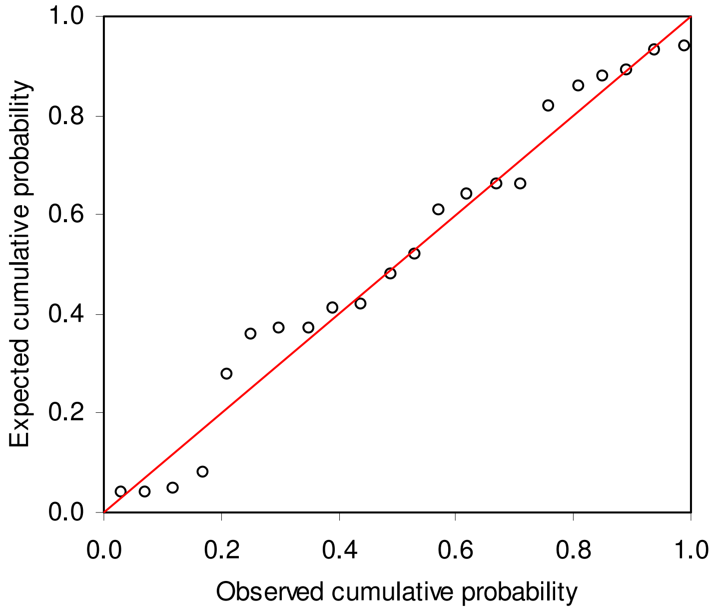

(a)

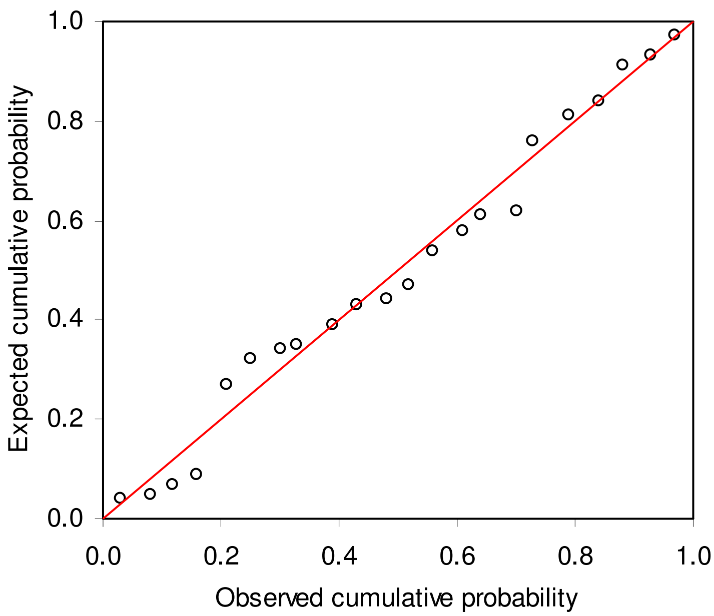

(b)

Fig.7.6: Probability plots for distillate yield from a) CSS and b) ASS.

Table 7.3: Skewness and kurtosis of daily distillate data for the CSS and ASS.

Data	Skewness	Kurtosis
CSS	-0.356	-0.630
ASS	0.026	-0.445
Normal	-0.4 to 0.4	-0.8 to 0.8

After confirmation that the daily distillate data was random and distributed normally, a paired *t*-test was applied to the data. Results of this test show that the means of the daily distillate yield from the CSS and ASS were significantly different (p-value=0.000). It should be noted that the CSS consistently produced less distilled water than the ASS on all test days although the former solar still captured more solar energy than the later. This observation is probably due to the heat transfer characteristics of the two still designs. Saline water in the evaporator chamber absorbs solar radiation that heats the water to produce vapour. Part of the absorbed solar energy is lost to the environment through the bottom and sides of the still. For the CSS, part of the heat from hot water is transferred to the glass cover through convection, evaporation and radiation. All the heat absorbed by the glass cover is ultimately dissipated to the environment through convection and radiation, without heat recovery. For the ASS, heat from hot water in basin 1 is transferred onto the inner surface of the glass cover (through convection, evaporation and radiation) and onto the underside of basin liner 2 in the condenser chamber (through purging and diffusion). So, a proportion the heat from hot water drives the second effect. In turn, heat from the second effect drives the third effect. This flow pattern of heat leads to the recovery of a proportion of the heat from hot water in the evaporator chamber and augmentation of the distillate yield from the ASS. Thus, the CSS optically performed better than the ASS but the heat transfer characteristics of the ASS were more satisfactory. It appears therefore that the ASS produced a higher quantity of distilled water than the CSS due to the pattern of heat flow from saline water in the evaporator basin, through the various system components, to the environment.

7.3 Still efficiency

The daily still efficiency (η_{st}) of the CSS and ASS were calculated using the data captured at the University of Strathclyde and Malawi Polytechnic. At the University of Strathclyde, the values of η_{st} were 6 to 11 % and 7 to 14 % for the CSS and ASS respectively. The relatively low efficiency values are attributed to astronomical and meteorological influences. Solar altitude angles were relatively low even around solar noon at this test site. Thus, the surface of saline water in basin 1 was significantly shaded during most of the day (Eq.3.15). Meteorological conditions were not very favourable for distillate production at the University of Strathclyde (as reported in Section 6.1). On the average, the CSS and ASS usefully converted 8 and 10 % of the intercepted solar energy, which shows that the ASS performed better than the CSS (maximum uncertainty=0.2 %).

At the Malawi Polytechnic, the values of η_{st} were 22 to 32 % and 25 to 39 % for the CSS and ASS respectively. It is observed that η_{st} was relatively high at this test site probably due to astronomical and meteorological influences. Solar altitude angles were relatively high (low angles of incidence) at solar noon. Thus, transmission of solar radiation through the glass cover was relatively high (Eq.2.28) and the surface of saline water in basin 1 was not shaded during most of the day (Eq.3.15). Meteorological conditions were favourable for distillate production at this test site (Section 6.1). On the average, the CSS and ASS converted 26 and 30 % of the intercepted solar energy respectively, which again shows that the ASS performed better than the CSS (maximum uncertainty=1 %). A summary of the average daily still efficiency results are presented in Table 7.4. For a conventional solar still, Cooper (1973) observed that the maximum efficiency would be 50 % under favourable weather conditions while El-Bassuoni and Tayebu (1994) reported efficiency values of 24 to 26 %. Smyth et al. (2005) reported typical-day values of η_{st}=28.5 % for a conventional single-slope solar still, η_{st}=20.6 % for a single-slope solar still with an asymmetric compound parabolic concentrator (CPC), and η_{st}=10 % for a single-slope solar still with a CPC and extra vessel (filled with water) that acted as a heat sink on the top part of the evaporator unit of a single-slope solar still. Samee et al. (2007) found a daily efficiency of 30.65 % for single slope solar still. For a solar still with separate condenser, El-Bahi and Inan (1999b) found daily efficiencies of about 22 to 50 % depending on the prevailing weather. So, the present results are consistent with previous findings.

Table 7.4: Average daily still efficiency (η_{st}) of the CSS and ASS.

Test site	η_{st} (%)	
	CSS	ASS
Strathclyde	8	10
Malawi Polytechnic	27	31

7.4 Water quality

Table 7.5 shows the electrical conductivity (EC), total dissolved solids (TDS) and pH of 4 batches of water from a borehole at Phalombe in Malawi. Batches 1(a) and 1(b) were distilled on the same day. Similarly, batches 2(a) and 2(b) were distilled on the same day. It is observed that the EC of distilled water is lower than that of raw water, which indicates that there are less dissolved substances in the distilled water, in close conformity with findings of Samee et al. (2007). The concentration of TDS in distilled water is also lower than that of raw water, commensurate with the levels of conductivity. The WHO (2006) reported that the palatability of water is acceptable when the level of TDS is less than 600 x 10^{-6} kg/litre. Consequently, the concentration of TDS in raw water falls outside the recommended limits. On the other hand, the levels of TDS in solar-distilled water meet acceptable limits. Again, the pH of distillate is lower than that of raw water, probably due to the effect of solar desalination Nevertheless, the pH of both raw and distilled water are within the range (6.5 to 8.5) recommended by the WHO (2006). Moreover, pH does not directly affect consumers but it is an important operational factor (WHO, 2006).

Table 7.5: Variation of EC, TDS and pH of raw and distilled water samples, and efficiency of distillation (η_{ds}).

.

Batch	System	EC (Sm^{-1})		TDS ($x10^{-6}$ kg/litre)		pH		η_{ds} (%)
		Raw	Distilled	Raw	Distilled	Raw	Distilled	
1(a)	CSS	0.241	0.005	1446	29	8.12	6.30	98
1(b)	ASS	0.242	0.004	1452	27	8.21	6.56	98
2(a)	CSS	0.243	0.010	1458	60	7.89	6.29	96
2(b)	ASS	0.244	0.010	1464	59	8.12	6.87	96

It is observed that the efficiency of TDS removal is in the range 96-98 %, and both the CSS and ASS exhibited comparable values of η_{ds}. These results agree with findings of Hanson et al. (2004) on the quality of water from a single-basin solar still, indicating that the extent of distillation was satisfactory.

7.5 Summary

Experimental results from the testing of solar stills under temperate and tropical conditions have been presented in this chapter. The advanced solar still produced more distilled water than the conventional type under the same meteorological conditions. Distillate output from both stills was higher at the Malawi Polytechnic than at the University of Strathclyde due to variations in astronomical and meteorogical factors. Solar distillation significantly improved the quality of water.

7.6 References

Al-Kharabsheh, S. and Goswami, D.Y., 2003. Experimental study of an innovative solar water desalination system utilizing a passive vacuum technique. *Solar Energy*, 75, pp.395-401.

Brown, S.R. and Melamed, L.E., 1993. Experimental design and analysis. In: M.S. Lewis-Beck, ed. 1993. *Experimental design & methods*. vol.3. London: SAGE Publications Ltd, pp.75-159

Cooper, P.I., 1973. The maximum efficiency of single-effect solar stills. *Solar Energy*, 15, pp.205-217.

El-Bahi, A. and Inan, D., 1999a. A solar still with minimum inclination, coupled to an outside condenser. *Desalination*, 123, pp.79-83.

El-Bahi, A. and Inan, D., 1999b. Analysis of a parallel double glass solar still with separate condenser. *Renewable Energy*, 17, pp.509-521.

El-Bassuoni, A.A. and Tayeb, A.M., 1994. Factors influencing the performance of basin-type solar desalination units. *Energy Conversion and Management*, 35, pp.693-698.

Fath, H.E.S. and Elsherbiny, S.M., 1993. Effect of adding a passive condenser on solar still performance. *Energy Conversion and Management*, 34, pp.63-72.

Hanson, A.et al., 2004. Distillate water quality of a single-basin solar still: laboratory and field studies. *Solar Energy*, 76, pp.635-645.

Ianetz, A. et al., 2000. A method for characterization and inter-comparison of sites with regard to solar energy utilization by statistical analysis of their solar radiation data as performed for three sites in the Israel Negev Region. *Solar Energy*, 69, pp.283-293.

Madhlopa, A. and Jonstone, C., 2009. Numerical study of a passive solar still with separate condenser. *Renewable Energy*, 34, pp.1668-1677.

NIST/SEMATECH, 2005. *E-Handbook of statistical methods*. http://www.nist.gov/div898/handbook/, 9/11/2005.

Samee, M.A., Mirza, U.K., Majeed, T. and Ahmad, N., 2007. Design and performance of a simple solar still. *Renewable and Sustainable Energy Reviews*, 11, pp.543-549.

Smyth, M., Norton, B. and Byres, W., 2005. Measured effect of reflector augmentation of simple basin type solar stills. *Ambient Energy*, 26, pp.59-70.

WHO, 2006. *Guidelines for drinking-water quality: First addendum to third edition*. vol. 1. Geneva: World Health Organization, pp.210-220, 426b.

Chapter 8

Conclusions and recommendations

8.0 Introduction

The need to increase access to clean water cannot be overemphasized as shown in Chapter 1. So, the present investigation sought to make a contribution toward the global efforts in addressing the shortage of clean water supply in many parts of the world. In this context, the aim of the present investigation was to develop an advanced solar still that would assist in increasing the availability of clean water in remote and isolated areas. To achieve this goal, the following specific objectives of the research were therefore set out: a) to model the performance of conventional and advanced solar stills, b) to design, construct and test prototype solar stills, and c) to verify the accuracy of the proposed model for predicting the performance of the solar stills.

Consequently, the first step was to formulate a suitable numerical tool for solar still development. It was found that the previous models for estimating the amount of solar energy that drives the heat and mass transfer processes inside a single slope solar still did not take into consideration some of the solar radiation characteristics. This deficiency in solar still modelling has been described in Chapter 2. In view of this, a new model that calculates the distribution of solar radiation in single slope solar stills has been proposed. In this model, solar radiation reaching a given surface is split into beam and diffuse components and the optical view factors of surfaces are taken into account. The proposed model computes solar radiation that is received directly and indirectly by saline water in the evaporator basin to determine the effective irradiance on the water surface. This model was used to theoretically compare the performance of a conventional solar still (CSS) and an advanced solar still (ASS) with one slope, under the same meteorological conditions. Details of the theoretical analysis are reported in Chapter 3, and modelled results were employed to design and construct prototype conventional and advanced solar stills.

A single slope conventional solar still was developed as a bench mark. It comprised basin 1 which was placed in a plywood box and a glass cover that was fixed on the top part of the box to allow incoming solar radiation reach saline water in basin 1. The ASS comprised an evaporator and a condenser, with one basin in the evaporator chamber (basin 1) and two stacked basins (2 and 3) in the condenser unit. Basins 1, 2 and 3 constituted the first, second and third effects respectively. The second effect recovered heat from the first one, and the third effect recovered heat from the second effect to augment the efficiency of the distillation system. A glass cover was fitted on the top part of the evaporator chamber to allow incoming solar radiation reach saline water in basin 1. In addition, the external front surface of the condenser acted as a reflector, and solar radiation was shielded from reaching the top part of the condenser. It should be mentioned that the geometry of the CSS was the same as that of the evaporator unit of the ASS for meaningful comparison of the two systems.

A randomised block experimental design was formulated to compare the performance of models and still designs at two locations (the University of Strathclyde and Malawi Polytechnic) as reported in Chapter 4. Implementation of this experimental design has been described in Chapter 5, and detailed results for model verification and empirical assessment of the two solar stills are given in Chapters 6 and 7 respectively. In this chapter, conclusions drawn from the research findings and recommendations for future work are presented.

8.1 Conclusions

A new model that calculates the distribution of solar radiation in basin type solar stills with a single slope has been developed. This model was applied in the design, appraisal and fabrication of conventional and advanced prototype solar stills which were then tested outdoors at the University of Strathclyde and Malawi Polytechnic to generate empirical data for model verification and performance evaluation of the two solar distillation systems. Results show that the new model performs better than previous models for calculating the distribution of solar radiation in a single slope solar still. In addition, the ASS yields more distilled water than the CSS. Consequently, the aim and all the three specific objectives set out in this investigation have been achieved. Based on the theoretical and experimental observations, the following conclusions are drawn:

8.1.1 Solar still modelling

Heat and mass transfer processes in the CSS and ASS were modelled, with irradiance as one of the input variables. The new model was used to compute solar energy received by the surface of saline water in basin 1, which yielded the level of effective irradiance inside a solar still. Theoretical results obtained by using this model showed that saline water in the evaporator basins of the CSS and ASS directly received 98 and 89 % of the daily mean insolation respectively at the University of Strathclyde. A similar trend was observed at the Malawi Polytechnic with the CSS and ASS directly intercepting 99 and 98 % of the daily insolation. It is inferred that the two solar stills captured most of the solar energy directly at both test sites. In addition, the CSS directly received more solar energy than the ASS, regardless of weather and locality because of the influence of view factors. Indirectly, saline water in basin 1 of the CSS received less solar energy than that in basin 1 of the ASS. On the average, the CSS and ASS effectively captured 54 and 51 % of the daily horizontal insolation respectively at the University of Strathclyde. Again, the CSS and ASS effectively intercepted 80 and 75 % of the horizontal insolation measured outside the stills at the Malawi Polytechnic. For both systems, effective irradiance was lower than the irradiance measured on a horizontal surface outside the still. These findings indicate that the direct use of measured irradiance in the energy balance equations would lead to overestimation of the distillate productivity.

Models proposed by Tripathi and Tiwari (2004) and Tanaka and Nakatake (2006) were applied to estimate the effective irradiance inside the stills. For the University of Strathclyde, the average daily effective radiation levels estimated by the former model were 60 and 138 % of the daily horizontal insolation for the CSS and ASS respectively, while the latter model yielded corresponding values of 80 and 117 % for the CSS and ASS respectively. For the Malawi Polytechnic, the average daily effective radiation levels estimated by the Tripathi and Tiwari (2004) model were 97 and 99 % of the daily horizontal insolation for the CSS and ASS respectively, while the Tanaka and Nakatake (2006) model yielded corresponding values of 98 and 99 % for the CSS and ASS respectively. It seems therefore that the two previous models overestimated effective solar radiation, with the discrepancy being higher at low solar altitude and for the ASS which had an external reflector. Effective irradiance was then used in the energy balance equations to numerically determine distillate output from the two solar stills.

Under the same meteorological conditions, the new model was employed to estimate distillate output and appraise the thermal performance of the CSS and ASS. It was found that the distillate yield from the ASS was 28 % higher than that of the CSS, and the extra water produced by the PSS would therefore pay for the additional cost of the condenser unit. Purging and diffusion contributed 99 and 1 % of the water vapour that condensed on the underside of basin 2. Thus, purging is the most significant mode of vapour transfer from the evaporator into the condenser chamber of the ASS. It is found that the productivity of the ASS is sensitive to the absorptance of basin liner 1, ratio of the volume of the evaporator to that of the condenser unit, mass of water in basins 1 and 2, and the coefficient of heat loss from the bottom of the still. The mass of water in basin 3 marginally influenced distillate production, while the coefficient of convective heat transfer from basin liner 1 to saline water in basin 1 does not affect distillate yield. Theoretical results were verified by using empirical data.

The new model was calibrated using data collected from another investigation (Tripathi and Tiwari, 2004). In addition, experiments were performed at the University of Strathclyde and Malawi Polytechnic to acquire empirical data for model verification. The two test locations have diverse astronomical and climatic conditions. Results for model calibration show that the new model has higher accuracy (root mean square error, RMSE=15 %) than that (RMSE=32.13 %) reported by Tripathi and Tiwari (2004) for the same data. It is also found that the values of the *t*-statistic for the models proposed by Tripathi and Tiwari (2004) and Tanaka and Nakatake (2006) were higher than the corresponding *t*-values for the new model. Moreover, distillate estimates provided by the new model were not significantly different from the experimental data at both test locations with such diverse conditions at 0.1 % of significance level. It appears therefore that the new model has higher accuracy and it can be applied universally.

8.1.2 Empirical performance

Following the experimental design described in Chapter 4, the CSS and ASS were tested outdoors. It was observed that the temperature of the condenser cover (T_{co}) remained comparable to that of ambient air (T_a) even under tropical weather conditions. This shows that the solar shield fitted on the top part of the condenser was effective in keeping the condenser relatively cool, a suitable condition for condensation of water vapour and augmentation of distillate production. The ASS practically yielded more distilled water than the CSS at both test locations (an improvement of 6 to 34 % at the University of Strathclyde and 9 to 22 % at the Malawi Polytechnic). The first, second and third effects contributed 87, 12 and 1 % respectively of the total distilled water from the ASS at the University of Strathclyde. Similarly, the first, second and third effects contributed 88, 11 and 1 % respectively of the total distilled water at the Malawi Polytechnic. It is therefore inferred that the third effect just acted as a thermal sink to improve distillate production from the second effect. For each solar still, it was found that the daily distillate yield data was random and normally distributed. Thus, the application of the *t*-test to compare the means of the two data sets was valid. This test showed that the means of distillate yield from the CSS and PSS were significantly different, and it was used to calculate the daily thermal efficiency of the solar stills. On most test days, the CSS captured more solar energy than the ASS. So, it appears that the ASS produced more distilled water at both test sites due to the inclusion of a separate condenser with heat recovery.

8.2 Recommendations

8.2.1 Solar still design

Results have shown that the new solar still gives a higher distillate output than a conventional type because of the integrated heat recovery unit. Nevertheless, there is need for further improvements. It was not possible to re-design and re-test this solar still because of time limitation in the present investigation. In particular, there is need to consider the following aspects of the design:

a) At present, the condenser unit protrudes above the evaporator chamber to accommodate basins 2 and 3, and to promote natural convection of heat from hot saline water in basin 1 into the condenser chamber. The protrusion of the condenser unit reduces the view factor of saline water in basin 1 relative to the sky ($W_{w1\text{-}sk}$), resulting in a lower optical efficiency. So, there is need to re-design the condenser unit in order to increase $W_{w1\text{-}sk}$ while maintaining an optimal geometry for heat transfer, by purging and diffusion, from hot saline water in the evaporator basin into the condenser chamber.

b) An insignificant amount of distilled water was collected from the third effect. This indicates that water in basin 3 acted as a heat sink to enhance distillate production from the second effect. So, there is need to investigate the effect of using warm water from the third effect to top up basin 1 in the evaporation chamber on distillate productivity. In this case, the third effect would preheat the water feed into the first effect. A thin water layer should be maintained in basin 1 to reduce the thermal capacitance of the first effect, and therefore, increase the rate of evaporation from this effect.

8.2.2 Economic analysis

Economic analysis is important for establishing the viability of an energy system. So, the method reported by Govin and Tiwari (1984) was used to estimate the cost of producing a unit mass of distilled water in the present work. Values of the still cost per unit area of the evaporator basin 1, initial cost of salvageable items, life span of the still, interest rate and maintenance cost (as a percentage of the annual cost) are required in this method. The data used in the present economic analysis is presented Table 8.1. It was found that the cost of producing distilled water (£0.08/kg) by using the CSS was 13 % higher than that for the ASS. It appears therefore that the extra water produced by the ASS can pay for the additional cost of the condenser.

Table 8.1: Data for calculating the cost of distilled water production by using the CSS and ASS.

Variable	Value	
	CSS	ASS
Cost of still (£/m^2)	521.73	689.58
Initial cost of salvageable items (£)	107.74	160.31
Life span (year)	10	10
Annual interest rate (%)	3	3
Maintenance cost (%)	5	5

However, it has been shown in Section 8.2.1 that the design of the ASS can be improved, in tandem with the developmental cycle of an engineering product. This design modification may affect the cost and performance of the still. Once a satisfactory design is achieved, there will be need to perform an economic analysis of the distillation system.

8.3 References

Govind and Tiwari, G.N., 1984. Economic analysis of some energy systems. Energy *Conversion and Management*, 24, pp.131-135.

Tanaka, H. and Nakatake, Y., 2006. Theoretical analysis of a basin type solar still with internal and external reflectors. *Desalination*, 197, pp.205-216.

Tripathi, R. and Tiwari, G.N., 2004. Performance evaluation of solar still by using the concept of solar fraction. *Desalination*, 169, pp.69-80.

Appendix A

Algorithm for solving system of heat balance equations in MATLAB

A1. Notes on the algorithm

This program (name of m-file: thesis) solves a system of discretized energy balance equations for modelling a conventional solar still (CSS) and advanced solar still (ASS). It computes the temperatures of system components (T_gc_css, T_w1_css, T_gc_Ass, T_w1_Ass, T_w2, and T_w3) and distillate outputs (Y_css, Y_Ass). Other variables can also be computed at any given time (t) of the day. Computations are performed over the period 06:00 hr on a given day to 06:00 hr the following day.

Symbols used in this algorithm are similar to those given in the nomenclature except for the ones that are not available in MATLAB or would create ambiguity. In such cases, descriptions of the relevant symbols are used. Lines that start with '%' are non-executable. The order of program execution is controlled by a number of statements to obtain a convergent solution (Etter, 1993). Only the major control statements are described here. The 'while~ …end' loop controls the number of iterations before the solution converges. In this loop, old temperatures are used to compute new temperatures. Then the old temperatures are updated to enable computation of new temperatures in the current iteration. The process is repeated until the absolute difference between the new and old temperatures is less than or equal to a set tolerance (TOL). The 'while~ …end' loop also nests all the temperature dependent variables (fluid properties, coefficients of heat transfer and saturation pressure to enable estimation of updated values of these variables. This loop is nested within the control statement 'for j=1:ts:300…end' which controls the order of execution from one time step to the next in a given logging interval (300 s). Solar angles and effective irradiance were assumed constant in each logging interval. So, the values for these variables are calculated outside the 'while~… end' control loop. All these statements are nested within the 'for i=1:288…end' statement which controls the order of execution from one logging interval to another. Using the length of each logging interval, a total of 288 logging intervals were obtained per day. Program execution ends when all the daily time steps are covered.

Meteorological databases for test sites were stored as a separate m-files. These file names were ‘met_data_1’ for Strathclyde and ‘met_data_2’ for Malawi Polytechnic. The site, test day, data file and model for calculating effective irradiance must be specified in order to compute the required outputs. Effective irradiance at any given time (t) is computed based on: 1) Tripathi and Tiwari (2004), 2) Tanaka and Nakatake (2006) and 3) present models. For instance, the following statement should be typed at the prompt in the command window of MATLAB to determine distillate outputs on test day number 12 at the University of Strathclyde using the present model (Fig.A1):

```
site=1;day=12;met_data_1;model=3;thesis
```

This statement should then be entered to run the program ‘thesis’. It is also possible to specify a range of test days (say, days 1 to 22) by using the loop ‘for day=1:22; …end’ in the command window of MATLAB. In this case, the statement should be typed as:

```
site=1;for day=1:22;met_data_1;model=3;thesis;end
```

Again, the statement should be entered to start computation of the daily distillate outputs for test days 1 through 22. It should be noted that there were 18 test days at the Malawi Polytechnic.

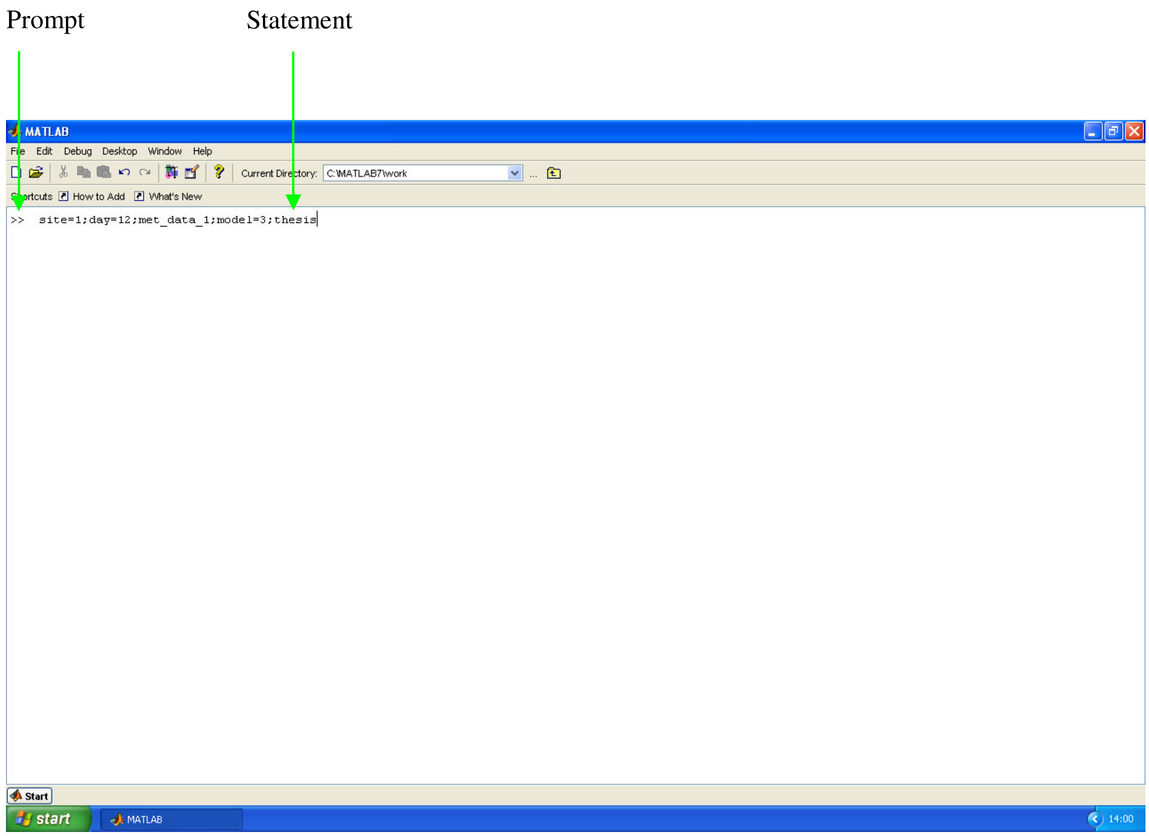

Fig.A1: Command window in MATLAB.

The output data is in column matrices for each variable. These matrices have the same number of rows. Thus, they can be combined to form any other required output data structures. One or more columns can be displayed simultaneously. For instance, time and temperature columns can be combined to form a single matrix, say M. Similarly, the output data for distillate yield can be displayed by using a yield matrix. When this program is run, the columns of t, Y_css and Y_pss are displayed. Any other outputs can be displayed by amending the output matrix as desirable.

A2. Algorithm

```
% This program iteratively solves a system of discretized equations for modelling a
% CSS and ASS. A tolerance temperature difference of TOL=0.5 K is used to end the
% iteration.
%
% Initialize design, operating and physical properties
A_b1=0.72; A_b2=0.73; A_b3=0.73;A_bw_css=0.383; A_bw_Ass=0.376;
A_er=0.569;A_ec=0.045; A_ew=0.248;  A_gc=0.750;A_s1_css=1.091;
A_s1_Ass=2.114;
A_s2=1.313; A_s3=0.680; A_ww=0.248; A_w1=0.72; A_w2=0.730; A_w3=0.730;
B_b1=0.8; h_c_b1_w1=100; K=26.34; L_b1=0.9; m_b1=5; m_b2=6; m_b3=6;
m_gc=10;
m_w1=20; m_w2=13; m_w3=13;n_a=1;n_gc=1.526;ratio_ec=0.65;S_b2=0.2135;
S_b3=0.2135;S_w1_gc=0.310;S_w2_b3=0.3185;S_w3_co=0.200; U_bo=1.203;
U_sw=0.5;W_bw_sk_css=0.23; W_bw_sk_Ass=0.23;W_bw_w1_css=0.30;
W_bw_w1_Ass=0.30; W_ew_sk_css=0.18; W_ew_sk_Ass=0.14; W_ew_w1=0.33;
W_ww_sk_css=0.18;W_ww_sk_Ass=0.14;W_ww_w1=0.33; W_er_sk=0.50;
W_er_w1=0.09; W_w1_sk_css=0.53;W_w1_sk_Ass=0.39; x_b1=0.0008;x_ps=0.020;
x_pw=0.023; x_ec=0.02; x_gc=0.004; Z_bw_css=0.425; Z_bw_Ass=0.418; Z_er=0.632;
Z_fc=1.057; Z_fw=0.195; Z_w1_gc=0.310;Z_w2_b3=0.3185;Z_w3_co=0.2;
beta_co=pi*10/180;beta_b2=pi*10/180; beta_b3=pi*10/180; beta_gc=pi*16/180;
beta_bw=pi/2; beta_ew=pi/2;beta_sa=pi/2; beta_ww=pi/2;C_p_b1=477; C_p_b2=477;
C_p_b3=477; C_p_gc=750; C_p_w1=4190; C_p_w2=4190; C_p_w3=4190; k_b1=47.6;
k_gc=1.05; k_ps=0.0346; k_pw=0.1200; M_v=18.02; M_a=28.97; n_gc=1.526;
Rv=461.52; alpha_b1=0.9; alpha_w1=0.05; epsilon_b1=0.80; epsilon_b2=0.80;
epsilon_b3=0.80; epsilon_co=0.80; epsilon_gc=0.88; epsilon_w=0.96; R_a=287;
rho_gc=0.12; rho_wa=0.05; rho_er=0.50; rho_gr=0.2; rho_w1=0.02; sigma=5.67*10^(-
8); g=9.807; Gsc=1367; epsilon_w1_gc=1/(1/epsilon_w+1/epsilon_gc-1);
epsilon_w2_b3=1/(1/epsilon_w+1/epsilon_b3-1);
epsilon_w3_co=1/(1/epsilon_w+1/epsilon_co-1);
```

```
% Initialize temperatures of components and fluids. These are guessed values, and
% To_i is a matrix of initial temperature (°C) on each test day.
Ta=To_i(:,day)+273.15;T_gc_css_old=Ta;T_w1_css_old=Ta;T_b1_css_old=Ta;
T_gc_Ass_old=Ta;T_b1_Ass_old=Ta;T_w1_Ass_old=Ta;T_b2_old=Ta;T_b2_old=Ta;
T_w2_old=Ta+0.01;T_b3_old=Ta;T_w3_old=Ta+0.01;TOL=0.5;
%
% Initialize daily insolation on a horizontal plane
H_gh_o=0;
%
% Initialize the rate of evaporation (RE) and distillate yield (Y)
RE_w1_css_old=0;RE_w1_Ass_old=0;RE_w2_old=0; RE_w3_old=0;
Y_df_old=0; Y_css_old=0;Y_Ass_old_1=0;Y_Ass_old_2=0;Y_Ass_old_3=0;
%
% time step (ts)
ts=20;
%
for i=1:288
% i is the number of logging intervals. Each logging interval was 300 s. So, there were
% 288 logging intervals on each test day.
%
% Compute solar angles: azimuth (gamma_s), incidence (theta), altitude (psi) and hour
% (omega) angles from longitude and latitude (phi) at any given time (t).
% Calculate the areas of saline water receiving beam radiation directly (A_b_di)
% and projected (A_pj) areas, and solar absorption factors (F) using solar
% angles and the dimensions of the stills.
%
% Determine effective irradiance in each solar still
if abs(omega)<omega_ss-pi*5/180
G_g_ef_css_1=G*(A_b_di_css+rho_wa*(A_bw_pj_css+A_ew_pj+A_ww_pj))/A_w1;
```

```
G_g_ef_css_2=Gb*(A_b_di_css+rho_w1*(A_bw_pj_css+A_ew_pj…
        +A_ww_pj))/A_w1+Gd;
G_g_ef_css_3=Gb*(A_b_di_css+rho_wa*(W_bw_w1_css*A_bw_pj_css…
        +W_ew_w1*A_ew_pj+W_ww_w1*A_ww_pj))/A_w1+Gd…
        *(A_w1*W_w1_sk_css+rho_wa*(W_bw_w1_css*W_bw_sk_css*A_bw_css…
        +W_ew_w1*W_ew_sk_css*A_ew+W_ww_w1*W_ww_sk_css*A_ww))/A_w1;
G_g_ef_Ass_1=G*(A_b_di_Ass+rho_wa*(A_bw_pj_Ass+A_ew_pj+A_ww_pj)…
        +rho_er*A_er_pj)/A_w1;
G_g_ef_Ass_2=Gb*(A_b_di_Ass+rho_wa*(A_bw_pj_Ass+A_ew_pj+A_ww_pj)…
        +rho_er*A_er_pj)/A_w1+Gd;
G_g_ef_Ass_3=Gb*(A_b_di_Ass+rho_wa*(W_bw_w1_Ass*A_bw_pj_Ass…
        +W_ew_w1*A_ew_pj+W_ww_w1*A_ww_pj)+rho_er*W_er_w1*A_er_pj)…
        /A_w1+Gd*(A_w1*W_w1_sk_Ass+rho_wa*(W_bw_w1_Ass
        *W_bw_sk_Ass*A_bw_Ass+W_ew_w1*W_ew_sk_Ass*A_ew+W_ww_w1
        *W_ww_sk_Ass*A_ww)+rho_er*W_er_w1*W_er_sk*A_er)/A_w1;
else G_g_ef_css_1=0; G_g_ef_css_2=0;G_g_ef_css_3=0; G_g_ef_Ass_1=0;
G_g_ef_Ass_2=0;G_g_ef_Ass_3=0; end
%
% Calculate solar absorption factors (F)
%
for j=1:ts:300
% j is the number of time steps in a logging interval (300 s)
solution=0;
% Iteration starts
while  ~solution
% Compute temperature-dependent thermophysical properties: coefficient of
% conductivity (k), specific latent heat of vaporization (LH), thermal diffusivity (TD),
% coefficient of thermal expansivity (TE), density (FD) and dynamic viscosity (DV) of
% fluids, and saturation pressure P at initial temperatures
% Calculate coefficients of heat transfer, then use them to determine each
```

```
% coefficient of the discretized equations and Biot numbers (Bi)
%
% Compute new temperatures (Tnew)
T_gc_css_new=a_10+a_11*T_gc_css_old+a_12*T_w1_css_old;
T_b1_css_new=a_20+a_21*T_b1_css_old+a_22*T_w1_css_old;
T_w1_css_new=a_30+a_31*T_w1_css_old+a_32*T_gc_css_new…
        +a_33*T_b1_css_new;
T_gc_Ass_new=b_10+b_11*T_gc_Ass_old+b_12*T_w1_Ass_old;
T_b1_Ass_new=b_20+b_21*T_b1_Ass_old+b_22*T_w1_Ass_old;
T_w1_Ass_new=b_30+b_31*T_w1_Ass_old+b_32*T_gc_Ass_new…
        +b_33*T_b1_Ass_new;
T_b2_new=b_40+b_41*T_b2_old+b_42*T_gc_Ass_new+b_43*T_w1_Ass_new…
        +b_44*T_w2_old;
T_w2_new=b_50+b_51*T_w2_old+b_52*T_b2_new+b_53*T_b3_old;
T_b3_new=b_60+b_61*T_b3_old+b_62*T_w2_new+b_63*T_w3_old;
T_w3_new=b_70+b_71*T_w3_old+b_72*T_b3_new;
%
% Extract matrices for old and new temperatures
temp_old=[T_gc_css_old,T_b1_css_old,T_w1_css_old,T_gc_Ass_old,…
        T_b1_Ass_old,T_w1_Ass_old,T_b2_old,T_w2_old,T_b3_old,T_w3_old];
temp_new=[T_gc_css_new,T_b1_css_new,T_w1_css_new,T_gc_Ass_new,…
        T_b1_Ass_new,T_w1_Ass_new,T_b2_new,T_w2_new,T_b3_new,T_w3_new];
temp_diff=abs(temp_new-temp_old);
%
% Update temperatures for the next iteration
T_gc_css_old=T_gc_css_new; T_b1_css_old=T_b1_css_new;
T_w1_css_old=T_w1_css_new; T_gc_Ass_old=T_gc_Ass_new;
T_b1_Ass_old=T_b1_Ass_new; T_w1_Ass_old=T_w1_Ass_new;
T_b2_old=T_b2_new; T_w2_old=T_w2_new; T_b3_old=T_b3_new;
T_w3_old=T_w3_new;
```

```
%
if all (temp_diff)<=TOL
  solution=1;
end
end
% this is the end of the iteration control loop
%
% Calculate daily insolation on horizontal (H_gh) and tilted (H_gp) planes
H_gh=H_gh_o+ts*G_gh;
H_gh_o=H_gh;
%
% Compute new distillate outputs and update old ones
Y_css_new=Y_css_old+ts*h_e_w1_gc_css*[T_w1_css_new…
        -T_gc_css_new]/LH_w1_css;
if Ts>Tcco;
   Y_df_new=0.256*10^[-4]*ts*[A_ec/x_ec]*[dsc-dcco];
else Y_df_new=0; end
Y_Ass_new_1=Y_Ass_old_1+ts*h_e_w1_gc_Ass*[T_w1_Ass_new…
        -T_gc_Ass_new]/LH_w1_Ass+ts*h_e_w1_b2*[T_w1_Ass_new…
        -T_gc_Ass_new]/LH_w1_Ass+yield_df_new;
Y_Ass_new_2=yield_Ass_old_2+ts*A_w2*h_e_w2_b3*[T_w2_new…
        -T_b3_new]/(A_w1*LH_w2);
Y_Ass_new_3=Y_Ass_old_3+ts*A_w3*h_e_w3_co*(T_w3_new…
        -T_co)/(A_w1*LH_w3);
Y_Ass_new=Y_Ass_new_1+Y_Ass_new_2+Y_Ass_new_3;
Y_matrix=[t;Y_css_new;Y_Ass_new_1;Y_Ass_new_2;Y_Ass_new_3;Y_Ass_new];
Y_css_old=Y_css_new; Y_df_old=Y_df_new;
Y_Ass_old_1=Y_Ass_new_1;Y_Ass_old_2=Y_Ass_new_2;
Y_Ass_old_3=Y_Ass_new_3;
Yd=[Y_css_new;Y_Ass_new_1;Y_Ass_new_2;Y_Ass_new_3;…
```

```
    Y_Ass_new];
% Calculate new rates of water evaporation and update old ones
RE_w1_css_new=h_e_w1_gc_css*[T_w1_css_new-T_gc_css_new]/LH_w1_css;
RE_w1_Ass_new=h_e_w1_gc_Ass*[T_w1_Ass_new-T_gc_Ass_new]/LH_w1_Ass…
        +h_e_w1_b2*[T_w1_Ass_new-T_gc_Ass_new]/LH_w1_Ass+yield_df_new/ts;
RE_w2_new=A_w2*h_e_w2_b3*[T_w2_new-T_b3_new]/(A_w1*LH_w2);
RE_w3_new=A_w3*h_e_w3_co*(T_w3_new-Ta)/(A_w1*LH_w3);
RE_w1_css_old=RE_w1_css_new; RE_w1_Ass_old=RE_w1_Ass_new;
RE_w2_old=RE_w2_new; RE_w3_old=RE_w3_new;
end
%
T(:,i)=temps; Y(:,i)=Yd;
end
%
% Temperature outputs
temp_matrix=T.'; t=temp_matrix(:,1); T_a=temp_matrix(:,2);
T_gc_css=temp_matrix(:,3); T_w1_css=temp_matrix(:,4);
T_gc_Ass=temp_matrix(:,5); T_w1_Ass=temp_matrix(:,6);
T_w2_Ass=temp_matrix(:,7); T_w3_Ass=temp_matrix(:,8);
%
% Distillate outputs
Y_matrix=Y.'; Y_css=Y_matrix(:,1); Y_Ass_1=Y_matrix(:,2);
Y_Ass_2=Y_matrix(:,3); Y_Ass_3=Y_matrix(:,4); Y_pss=Y_matrix(:,5);
%
M=[t,Y_css, Y_Ass];
disp(M)
% End of computation
```

A3. References

Etter, D.M., 1993. *Engineering problem solving with MATLAB*. Englewood Cliffs: Prentice Hall.

Tanaka, H. and Nakatake, Y., 2006. Theoretical analysis of a basin type solar still with internal and external reflectors. *Desalination*, 197, pp.205-216.

Tripathi, R. and Tiwari, G.N., 2004. Performance evaluation of solar still by using the concept of solar fraction. *Desalination*, 169, pp.69-80.

Appendix B

Equations for calculating temperature-dependent fluid properties

B1. Air properties

Properties of moist air at a temperature (T) inside a solar still were computed according to Tsilingiris (2007). The correlations reported by this author do not cover temperatures below 283 K but the observed temperatures in the present investigation were below this boundary during certain times of the day, especially at the University of Strathclyde. So, properties of dry air were used in the range 273.15 to 283.15 K. This was done by linear interpolation using thermophysical data of dry air reported by Incropera et al. (2007). In addition, saturation pressure was determined by using the correlation reported by ASHRAE (2001).

$$\begin{aligned} C_{p,a} &= 1000(1.088022802-0.01057758092(T-273.15)+4.76911055910^{-4}(T-273.15)^2 -7.898561559\text{x}10^{-6}(T-273.15)^3+5.122303796\text{x}10^{-8}(T-273.15)^4), \\ &\quad \text{for } T\geq 283.15 \\ &= 1006+0.02(T-250), \text{ for } T<283.15 \end{aligned} \tag{B1}$$

$$\begin{aligned} \varphi_a &= 1.299995662-6.043625845\text{x}10^{-3}(T-273.15)+4.697926602\text{x}10^{-5}(T-273.15)^2 \\ &\quad -5.760867827\text{x}10^{-7}(T-273.15)^3, \text{ for } T\geq 283.15 \\ &= 1.3947-0.004666(T-250), \text{ for } T<283.15 \end{aligned} \tag{B2}$$

$$\begin{aligned} k_a &= 0.02416826077+5.526004579\text{x}10^{-5}(T-273.15)+4.631207189\text{x}10^{-7}(T-273.15)^2 \\ &\quad -9.489325324\text{x}10^{-9}(T-273.15)^3, \text{ for } T\geq 283.15 \\ &= 0.0223+8\text{x}10^{-6}(T-250), \text{ for } T<283.15 \end{aligned} \tag{B3}$$

$$\alpha_a' = k_a/(C_{p,a}\varphi_a) \tag{B4}$$

$$\beta_a' = 1/T \tag{B5}$$

μ_a=1.685731754x10^{-5}+9.151853945x10^{-8}(T-273.15)-2.16276222x10^{-9}
(T-273.15)^2 +3.413922553x10^{-11}(T-273.15)^3-2.644372665x10^{-13}(T-273.15)^4,
for ≥283.15
= 1.596x10^{-5}+5x10^{-8}(T-250), for T<283.15 (B6)

P=exp{-5800.2206/T+1.3914993-0.048640239T+4.1764768x10^{-5}T^2
-1.4452093x10^{-8}T^3+6.5459673 log(T)}, (B7)

B2. Water properties

The latent heat of vaporization of water was computed according to Belessiotis et al. (1995) while other properties of water at a temperature (T) were calculated by using correlations reported by IAPWS (1996).

k_w=(T/647.26)$^{3/2}$[0.0102811+0.0299621(T/647.26)+0.0156146(T/647.26)^2
-0.00422464(T/647.26)^3]-0.397070+0.400302φ_w/317.7
+1.06 exp[-0.171587(φ_w /317.7+2.39219)^2] +[0.0701309
/ ((T/647.26)^{10}+0.0118520](φ_w /317.7)$^{9/5}$ exp{0.642857[1-(φ_w
/317.7)$^{14/5}$]}+0.00169937Su(φ_w /317.7)^{Qu} exp{[Qu/(1+Qu)(1-(φ_w
/317.7)$^{1+Qu}$)]}-1.0200 exp{-4.11717(φ_w /317.7)$^{1.5}$ -6.17937/[(φ_w /317.7)^5]}
(B8)

where $\mathrm{Su} = \begin{cases} 1/\mathrm{DTu}, \textit{if } T \geq 647.26 \\ 1/\left(\mathrm{DTu}^{3/5}\right), \textit{otherwise} \end{cases}$

DTu= |(T/647.26)-1| +0.00308976, and Qu=2+0.0822994/(DTu$^{3/5}$).

L'=3044205.5-1679.1109T-1.14258T^2 (B9)

$$\varphi_w=322[1+1.99274064(1-T/647.096)^{1/3}+1.09965342(1-T/647.096)^{2/3}$$
$$-0.510839303(1-Ta/647.096)^{5/3}-1.75403479(1-T/647.096)^{16/3}$$
$$-45.5170352(1-T/647.096)^{43/3}-6.7469445(1-T/647.096)^{110/3}] \quad (B10)$$

$$\alpha'_w = k_w/(C_{p,w}\varphi_w) \quad (B11)$$

$$\beta'_w = -(\varphi_{w,a} - \varphi_w)/[\varphi_w(T_a - T)] \quad (B12)$$

$$\nu_w = 5.5071x10^{-5}\{(T/647.226)^{0.5}/[1+0.978197/(T/647.226)$$
$$+0.579829/(T/647.226)^2-0.202354/(T/647.226)^3]\}$$
$$\{exp[(\varphi_w/317.763)(0.5132047+0.3205656[1/(T/647.226)-1]$$
$$-0.7782567[1/(T/647.226)-1]^4 +0.1885447[1/(T/647.226)-1]^5$$
$$+ 0.2151778[\varphi_w /317.763-1] +0.7317883[1/(T/647.226)-1](\varphi_w /317.763$$
$$-1)+1.241044[1/(T/647.226)-1]^2(\varphi_w /317.763-1)+1.47683[1/(T/647.226)-1]^3$$
$$(\varphi_w /317.763-1)-0.2818107(\varphi_w /317.763-1)^2-1.070786[1/(T/647.226)-1]$$
$$(\varphi_w /317.763-1)^2-1.263184[1/(T/647.226)-1]^2(\varphi_w /317.763-1)^2+0.1778064$$
$$(\varphi_w /317.763-1)^3+0.4605040[1/(T/647.226)-1](\varphi_w /317.763-1)^3$$
$$+0.2340379[1/(T/647.226)-1]^2(\varphi_w /317.763-1)^3-0.4924179[1/(T/647.226)$$
$$-1]^3(\varphi_w /317.763-1)^3-0.04176610(\varphi_w /317.763-)^4+0.1600435$$
$$[1/(T/647.226)-1]^3(\varphi_w /317.763-1)^4-0.01578386[1/(T/647.226)-1]$$
$$(\varphi_w /317.763-1)^5-0.003629481[1/(T/647.226)-1]^3(\varphi_w /317.763-1)^6)]\}$$
$$(B13)$$

B3. References

ASHRAE, 2001. *ASHRAE Handbook Fundamentals*. SI ed. Atlanta: American Society of Heating, Refrigerating and Air-Conditioning Engineers.

Belessiotis, V., Voropoulos, E. and Delyannis, E., 1995. Experimental and theoretical method for determination of the daily output of a still: input-output method. *Desalination*, 100, pp.99-104.

Incropera, F.P., DeWitt, D.P., Bergman, T.L. and Lavine, A.S., 2007. *Fundamentals of heat and mass transfer*. 6th ed. New Jersey: John Wiley & Sons.

IAPWS, 1996. *The IAPWS Formulation 1995 for the thermodynamic properties of ordinary water substance for general and scientific use*. International Association for the Properties of Water and Steam.

Tsilingiris, P.T., 2007. The influence of binary mixture thermophysical properties in the analysis of heat and mass transfer processes in solar distillation systems. *Solar Energy*, 81, pp.1482-1492.

Appendix C

Details for construction of prototype solar stills

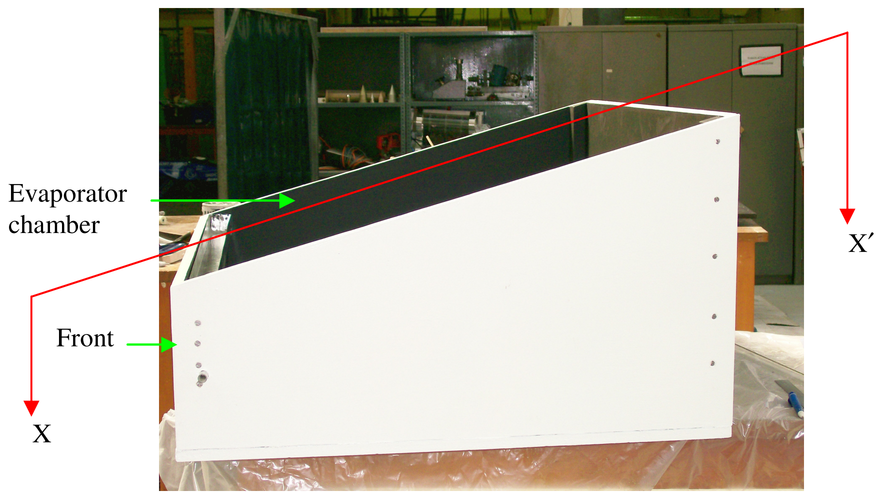

(a)

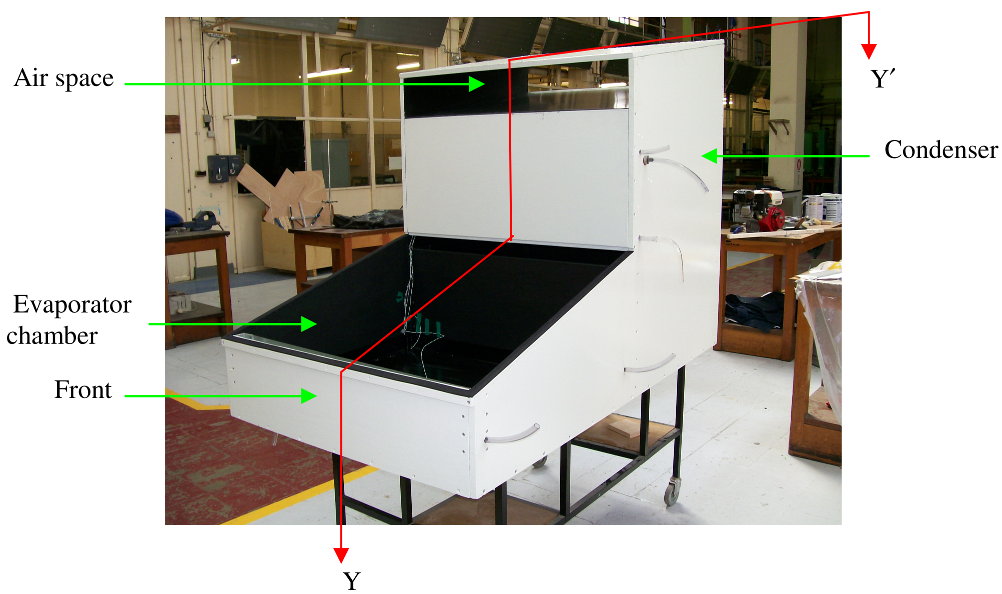

(b)

Fig.C1: Perspective view of a) conventional solar still (CSS) and b) advanced solar still (ASS) under construction in the workshop within the Department of Mechanical Engineering at the University of Strathclyde.

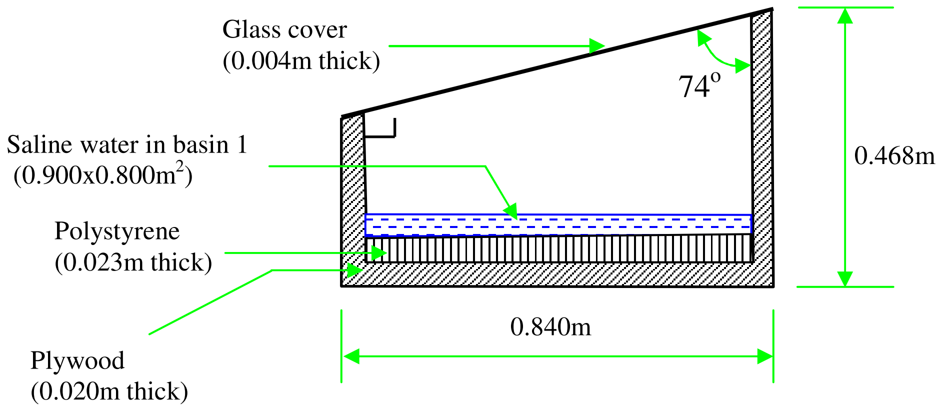

Fig.C2: Cross-section (through XX′ of Fig.C1 (a)) of the conventional solar still.

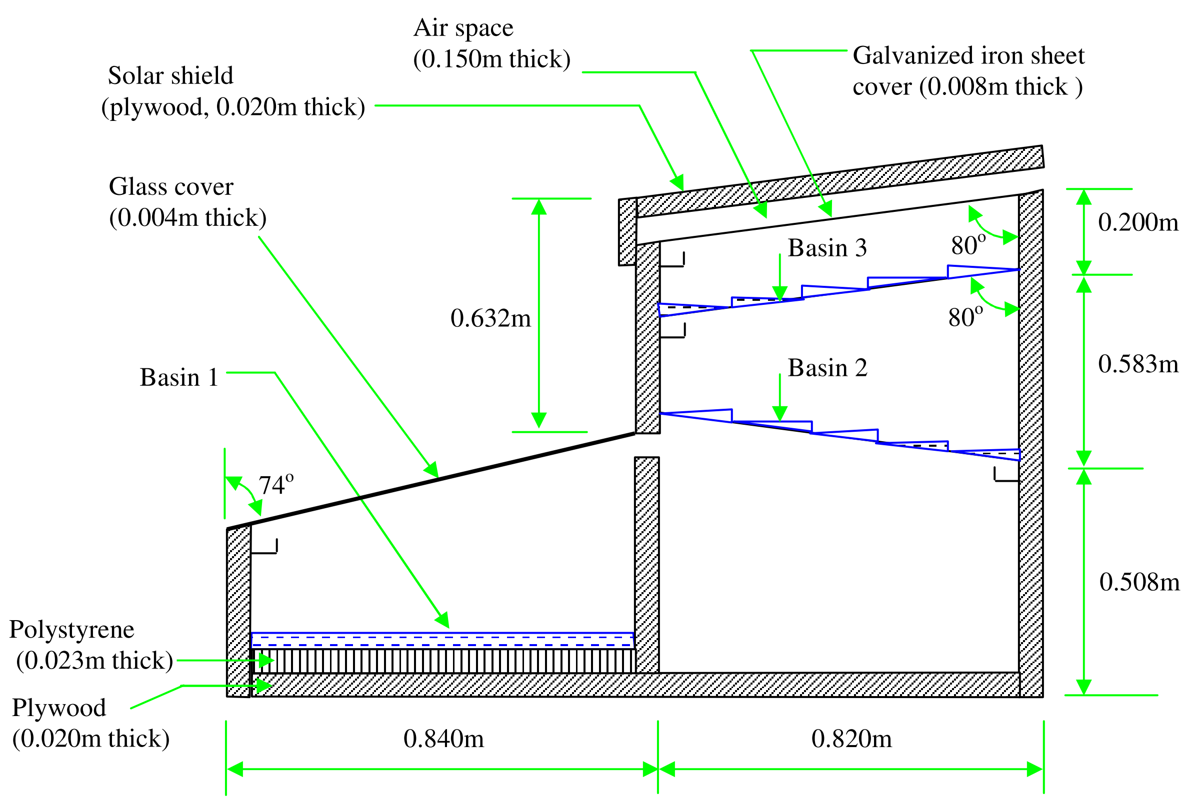

Fig.C3: Cross-section (through YY′ of Fig.C1(b)) of the ASS. The dimensions of the evaporator chambers of the CSS and ASS are similar.

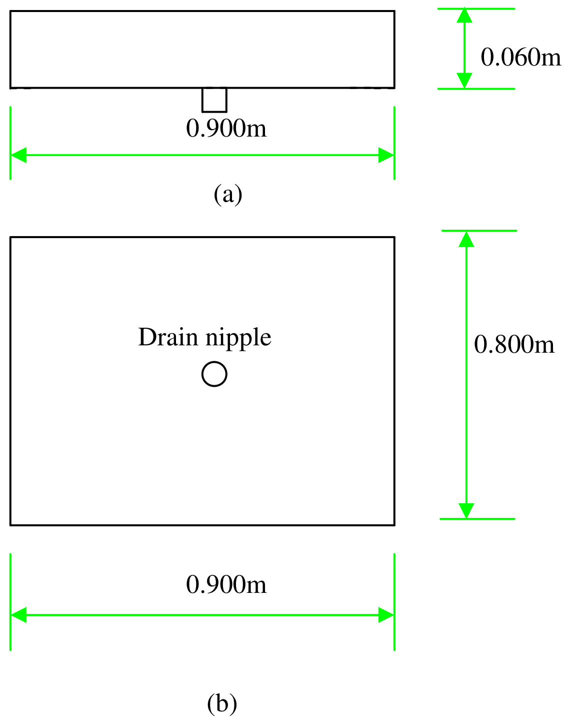

Fig.C4: Details of basin liner 1 for both the CSS and ASS, showing a) side view and b) plan. This basin is rectangular in shape, with a drain nipple in the middle of the base plate.

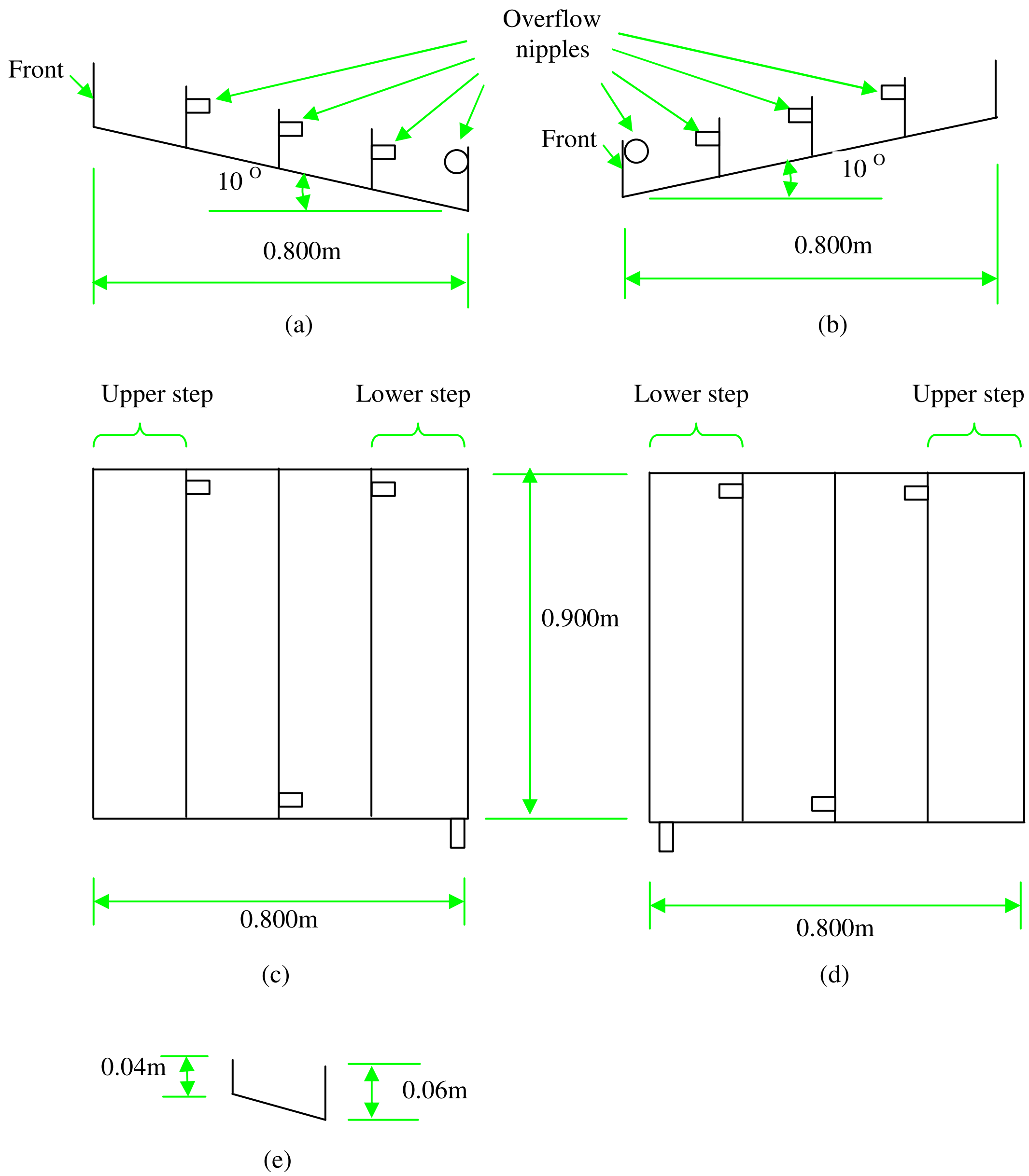

Fig.C5: Details of basins 2 and 3. a) cross-section of basin 2, b) cross-section of basin 3, c) plan of basin 2, d) plan of basin 3, and e) cross-section of each step (made of galvanized iron sheet, $8x10^{-4}$m thick). There are four steps of the same size for each basin, with overflow nipples (0.0120m ∅) to enable saline water flow from the upper step to the lower step. Saline water is fed into the upper step.

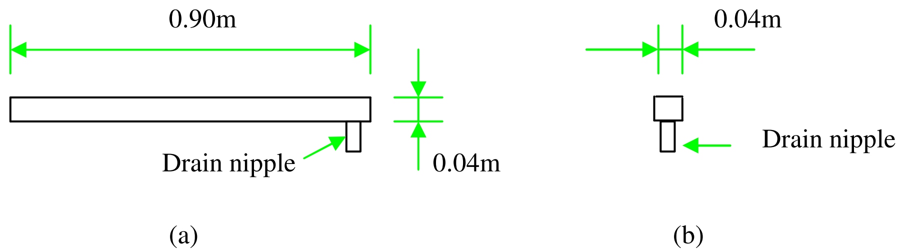

Fig.C6: a) Side-section and b) cross-section of a rectangular distillate collection channel with drain nipple (0.0120m ∅). All the channels were similar and made from galvanized iron sheet ($8x10^{-4}$m thick).

Appendix D

Cost of constructing prototype solar stills

D1. Cost

The costs of producing a conventional solar still (CSS) and advanced solar still (ASS) are presented in Tables D1 and D2. It is observed that the cost of constructing the CSS is lower that that of the ASS, due to the inclusion of a separate condenser in the latter still design. Nevertheless, the ASS produces more distilled water than the CSS. So, the extra water produced by the ASS would pay for the extra cost of the condenser

Table D1: Cost of constructing the CSS.

Item	Cost (£)
Glass (0.950x0.885 m^2)	37.60
Plywood (3.000 m^2)	26.68
Galvanized iron sheet (1.5 m^2)	5.79
Polystyrene (0.023 m thick)	5.98
Foam tape (12.5 mx0.01x0.003m)	5.90
Silicon sealant	3.98
Steel wood screws (0.051 m)	1.52
Hammerite black paint (1 litre)	12.00
Matt black paint (2.5 litres)	7.99
Pastel light green paint (2.5 litres)	7.99
PVC hose (0.012 m, bore diameter)	2.62
Labour charge for 2 days (for two artisans)	257.60
Total	375.65

Table D2: Cost of constructing the ASS.

Item	Cost (£)
Glass (0.950x0.885 m^2)	37.60
Plywood (6.000 m^2)	53.36
Galvanized iron sheet (4.000 m^2)	15.44
Polystyrene (0.023 m thick)	5.98
Foam tape (12.5 mx0.01x0.003m)	5.90
Silicon sealant	3.98
Steel wood screws (0.051 m)	3.04
Hammerite black paint (1 litre)	12.00
Matt black paint (5 litres)	15.98
Pastel light green paint (5 litres)	15.98
PVC hose (0.012 m, bore diameter)	5.24
Labour charge for 2.5 days (for two artisans)	322.00
Total	496.50

It is also seen that labour is the most expensive item (69 and 65 % of the total costs of the CSS and PSS respectively) due to the influence of wage policy. ILO (2009) reported that the minimum wage for an adult worker aged 22 years or more is £5.35 per hour, and £4.45 per hour for a worker aged between 18 and 21 years with effect from 1st October 2006 in the United Kingdom (a country with a developed economy). In addition, the ratio of minimum wage to average wage is 36.52 % (ILO, 2008). Thus the average wage is about £14.65 per hour, which is relatively high and accounts for the observed level of labour charge. Nevertheless, it is expected that the cost of labour would be low in countries with developing economies. For instance, the median wage in Malawi is MK78 (£0.34) and MK124 (£0.54) per day for women and men respectively (World Bank, 2007). Moreover, the production cost can be reduced when these stills are produced in large quantities (Mukherjee and Tiwari, 1986). It should also be noted that the cost of two units of the CSS (£751.30) is significantly higher than that for a single unit of the ASS (£496.50). However, the cost of distilled water production is a useful indicator of the economic viability of solar stills (Govin and Tiwari, 1984; Mukherjee and Tiwari, 1986). Consequently, the cost of producing distilled water was determined in this study as reported in Section 8.2.2.

D2. References

Govind and Tiwari, G.N., 1984. Economic analysis of some energy systems. Energy *Conversion and Management*, 24, pp.131-135.

ILO, 2008. *Minimum wages and collective bargaining towards policy coherence: Global wage report 2008/2009*. Geneva: International Labour Organization.

ILO, 2009. www.ilo.org/travaildatabase, accessed on 4th June 2009.

Mukherjee, K. and Tiwari, G.N., 1986. Economic analysis of various designs of conventional solar stills. *Energy Conversion and Management*, 26, pp.155-157.

World Bank, 2007. *Malawi poverty and vulnerability assessment: Investing in our Future*. Report number 36546-Mw. Washington: World Bank.